

Copyright

by

Theodore Thomas Moore

2004

This Dissertation Committee for Theodore Thomas Moore certifies that this is the approved version of the following dissertation:

**EFFECTS OF MATERIALS, PROCESSING, AND OPERATING
CONDITIONS ON THE MORPHOLOGY AND GAS
TRANSPORT PROPERTIES OF MIXED MATRIX
MEMBRANES**

Committee:

William J. Koros, Supervisor

Isaac C. Sanchez, Co-Supervisor

Sudhir Kulkarni

Michael A. Schmerling

C. Grant Willson

**EFFECTS OF MATERIALS, PROCESSING, AND OPERATING
CONDITIONS ON THE MORPHOLOGY AND GAS
TRANSPORT PROPERTIES OF MIXED MATRIX
MEMBRANES**

by

Theodore Thomas Moore, B. S.

Dissertation

Presented to the Faculty of the Graduate School of

The University of Texas at Austin

in Partial Fulfillment

of the Requirements

for the Degree of

Doctor of Philosophy

The University of Texas at Austin

December 2004

Dedication

To family and friends,

past, present, and future

without whom life would be meaningless

Acknowledgement

There are many people to thank who have shaped me to what I am today. First, my parents, whose love and support have allowed me to achieve so much. If everyone had parents such as mine, the world would be a far better place. Second, my advisor, Dr. William J. Koros, whose guidance, support, humor, and encouragement have molded me into the researcher I am now. He always seems to know when to push harder and when to pull after an especially frustrating episode. Third, friends and co-workers who are always willing to lend an ear to listen, a shoulder to cry on, or a brain to bounce ideas off of. Graduate school would have been much more difficult without friends to share in the happy and sad moments. Finally, I must thank those who have assisted in my research: Sudhir Kulkarni, Dave Hasse, and Steve Miller, collaborators at ChevronTexaco and Medal LP; John Simmons of DuPont for providing polymers; Thomas Baekmark (AFM measurements), Dr. Georges Belfort (AFM measurements), Ti Cao (light scattering), Mike McKittrick (TGA), Philip Watson (light scattering), and Dr. Mohan Srinivasarao (birefringence microscopy) for assistance with equipment and experimental techniques; Michelle Martin and Vonda Totten for administrative assistance; and remaining members of my committee: Dr. Isaac Sanchez, Dr. Grant Willson, Dr. Micheal Schmerling. Sadly, I was not always able to reciprocate kindnesses to all of these people and interactions with my committee were limited because of separation due to our group's move from the University of Texas at Austin to the Georgia Institute of Technology.

Credit is due to past group members Anshu Singh, Cathy Zimmerman, Jennifer Qin, Michael Schaefer, Trinh Vo, and especially Rajiv Mahajan and De Vu for their past work on mixed matrix membranes, teaching me the ropes in the lab, and for answering my questions, in some cases long after they had graduated. Rajiv, De, and Shilpa Damle were the source of many helpful discussions. I must also thank Alexis Hillock, Shabbir Husain, and Shu Shu, who joined the project after I did, for helpful discussions and for proofreading my manuscript. I hope that they will find it useful in their

research. Finally, to all past, present, and future group members to numerable to mention: thanks for making this such a great group to be a part of.

I will treasure many happy moments from Graduate school, but I will perhaps miss our Friday afternoon “Pickle lunches” the most. Being somewhat isolated at the UT satellite campus provided for even closer camaraderie with other students in the same situation. In particular the regulars: De, Shilpa, and Carolyn Schmit. Similar lunches shared at Georgia Tech with the group were also quite enjoyable. Shilpa, my roommate since we moved to Georgia Tech; and De, who was always willing to share a dinner while at PRC deserve special thanks. I could also count on both for very helpful technical discussions at any time as well.

I can only hope that I will be blessed with so many friends in the future. To all those who impacted and shaped me, whether mentioned here or not, all I can say is “thank you.”

**EFFECTS OF MATERIALS, PROCESSING, AND OPERATING
CONDITIONS ON THE MORPHOLOGY AND GAS
TRANSPORT PROPERTIES OF MIXED MATRIX
MEMBRANES**

Publication No. _____

Theodore Thomas Moore, Ph.D.

The University of Texas at Austin, 2004

Supervisors: William J. Koros

Isaac C. Sanchez

Gas separation membranes are currently based on polymers, which are limited by a trade-off between permeability (productivity) and selectivity. Zeolites offer significantly higher selectivities than polymers; however their properties make them prohibitively expensive to process into membranes. Organic-inorganic, or “mixed matrix”, materials may provide the basis for the next generation of economical, high

performance membranes. The topic of this research is mixed matrix materials comprising a dispersion of zeolites in a polymer matrix.

A major limitation of mixed matrix technology is the inability to prepare membranes from selected polymers and sieves with properties approaching the theoretical predictions. This difficulty is related largely to undesirable properties of the polymer-sieve interface, and this work seeks to understand and control these interfacial properties. First, an understanding of membrane formation is presented to explain how nonideal interfacial morphologies form. Factors affecting this process include: polymer flexibility, polymer – sieve affinity, and membrane preparation conditions. Membrane preparation conditions affect the propensity for stress to accumulate at the polymer-sieve interface, and depending on the severity of the stress, the likelihood that the polymer – sieve interface will fail. The next part of this work details experiments undertaken to better understand the factors affecting membrane morphology and transport properties. Factors ranging from material selection (e.g. silane coupling agent selection), dope formulation (e.g. polymer “priming”, sieve settling), and membrane preparation conditions (e.g. casting surface, temperature) were investigated. The final part of this work considers additional effects on mixed matrix properties caused by contaminants and minor feed components. A framework has been developed to account for the effects of potential impurities in the feed gas on the polymer, zeolite, and mixed matrix membrane. Based on this framework and results with model impurities, it appears that strongly sorbing components selectively displace the desired gases from the zeolite, preventing improved selectivity in mixed matrix membranes.

This work has developed a better understanding of the factors that affect mixed matrix membrane performance and identified new ones that require additional study. After further development, this technology should allow for the increased application of membranes for the separation of gases and possibly also vapors and liquids.

Table of Contents

LIST OF TABLES	XVI
LIST OF FIGURES	XIX
CHAPTER 1. INTRODUCTION, MOTIVATION, AND OVERVIEW	1
1.1. Gas Separation Membranes	1
1.1.1. Polymeric Gas Separation Membranes.....	1
1.1.2. Inorganic Gas Separation Membranes.....	3
1.1.3. Mixed Matrix Membranes	3
1.2. Gas Separation Technologies	4
1.2.1. Nitrogen and Oxygen Enrichment of Air	5
1.2.2. Natural Gas Purification	5
1.2.3. Other Separations.....	6
1.3. Research Objectives.....	8
1.3.1. Objective 1: Characterize the effect of sieve priming protocols on mixed matrix morphology and transport properties	9
1.3.2. Objective 2: Develop an engineering model to guide processing of mixed matrix membranes.....	10
1.3.3. Objective 3: Characterize the effects of sieve priming protocols on casting suspension stability.....	10
1.3.4. Objective 4: Determine the effects of potential minor components in the feed gas	11
1.4. Dissertation Overview	12
1.5. References.....	12
CHAPTER 2. THEORY AND BACKGROUND.....	14
2.1. Transport Property Theory	14
2.1.1. Permeation	14
2.1.2. Diffusion	16
2.1.2.1. Diffusion in Polymers.....	16

2.1.2.2.	Diffusion in Molecular Sieving Materials	16
2.1.3.	Sorption.....	17
2.1.3.1.	Sorption in Polymers	17
2.1.3.2.	Sorption in Molecular Sieving Materials.....	19
2.1.4.	Selective Surface Flow	19
2.2.	Modeling Strategies.....	19
2.2.1.	Selection of an Appropriate Model.....	20
2.2.2.	Modeling Mixed Matrix Materials with “Zones of Influence” Surrounding the Dispersed Phase	22
2.2.2.1.	“Matrix Rigidification”	23
2.2.2.2.	“Sieve-in-a-Cage”	24
2.2.3.	Modeling of Multicomponent Permeation in Mixed Matrix Membranes.....	27
2.2.3.1.	Modeling of Multicomponent Sorption in Polymers and Zeolites ..	27
2.2.3.2.	Modeling of Concentration Dependent Diffusion in Polymers and Zeolites	28
2.3.	Polymer-Sieve Selection Criteria	29
2.4.	A Literature Review of Mixed Matrix Membranes.....	33
2.4.1.	Mixed Matrix Membranes Prepared with Rubbery Matrices	35
2.4.2.	Mixed Matrix Membranes Prepared with Glassy Matrices.....	38
2.5.	References.....	43
CHAPTER 3.	MATERIALS AND METHODS	48
3.1.	Overview.....	48
3.2.	Materials	48
3.2.1.	Polymers	48
3.2.2.	Molecular Sieves	51
3.2.3.	Short Coupling Agents	52
3.2.4.	Gases.....	52
3.3.	Membrane Preparation.....	53
3.3.1.	Materials Selection	54

3.3.2.	Dope Preparation	55
3.3.3.	Film Preparation	57
3.4.	Membrane Testing Methods	58
3.4.1.	Gas Permeation Measurements.....	58
3.4.1.1.	Experimental Apparatus	60
3.4.1.2.	Membrane Masking Procedure.....	62
3.4.1.3.	Experimental Procedure.....	64
3.4.1.4.	Measurement of Oxygen Permeabilities in the Presence of Water Vapor	66
3.4.2.	Gas Sorption Measurements.....	67
3.4.2.1.	Gravimetric Sorption	67
3.4.2.2.	Pressure Decay Sorption.....	68
3.4.3.	Complementary Characterization Methods	69
3.5.	References.....	70
CHAPTER 4. FACTORS AFFECTING THE POLYMER – SIEVE INTERFACE IN MIXED MATRIX MEMBRANES		72
4.1.	Overview.....	72
4.2.	Polymer Flexibility and Mixed Matrix Membranes	73
4.2.1.	Characterization of Polymer Flexibility	73
4.2.2.	Effect of Low Molecular Weight Diluents on the Glass Transition Temperature.....	74
4.2.3.	Correlation of Mixed Matrix Membrane Transport Properties with Polymer Flexibility	75
4.3.	Polymer – Sieve Affinity and Mixed Matrix Membranes.....	76
4.3.1.	Characterization of Polymer-Sieve Affinity.....	76
4.3.2.	Correlation of Mixed Matrix Membrane Transport Properties with Polymer – Sieve Affinity	82
4.4.	Effect of Casting Conditions on Mixed Matrix Membranes	84
4.4.1.	Unconstrained Films; Matrix Rigidification.....	84

4.4.2.	Constrained Films; “Sieve-in-a-Cage” Formation.....	87
4.4.2.1.	Particle-Free Films.....	87
4.4.2.2.	Films Containing Particles.....	89
4.4.3.	Effect of Priming Conditions on Mixed Matrix Membranes.....	93
4.4.4.	Effect of Drying Conditions on Mixed Matrix Membranes	94
4.5.	Suggestions for the Formation of Successful Mixed Matrix Membranes	96
4.6.	References.....	98
CHAPTER 5. DEVELOPMENT METHODS TO PREPARE DESIRABLE MIXED MATRIX		
MEMBRANE MORPHOLOGIES		
		102
5.1.	Overview: Relationship Between Membrane Morphology and Transport	
	Properties	102
5.2.	Material Selection Considerations and Membrane Morphology and Transport	
	Properties	108
5.2.1.	Silanation of the Zeolite Surface for Enhanced Interfaces	109
5.2.1.1.	Effect of Silanation Method on the Transport Properties of Mixed	
	Matrix Membranes.....	109
5.2.1.2.	Effect of Selected Silane Coupling Agents on the Transport	
	Properties of Mixed Matrix Membranes.....	115
5.2.1.3.	Silane Coupling Agent Density on Silanated HSSZ-13	117
5.2.2.	Effect of Zeolite Particle Size Mixed Matrix Membranes.....	120
5.3.	Selected Dope Formulation Issues.....	121
5.3.1.	Effect of Sonicator Power on Casting Dopes and the Transport Properties	
	of Mixed Matrix Membranes	122
5.3.2.	Understanding and Removing Sieve Agglomerates from Casting	
	Suspensions for Enhanced Membrane Morphology	124
5.3.3.	Effect of Zeolite “Priming” Method on the Transport Properties of	
	Mixed Matrix Membranes	127
5.4.	Selected Membrane Preparation Issues	130
5.4.1.	Effect of Casting Substrate on Mixed Matrix Membranes	131

5.4.2.	Effect of Casting Temperature and Solvent Evaporation Rate on Mixed Matrix Membranes.....	140
5.4.3.	Effect of Drying and Annealing on Mixed Matrix Membranes	142
5.5.	Discussion.....	144
5.5.1.	Analysis of Mixed Matrix Membranes with Zeolite 4A	145
5.5.2.	Analysis of Mixed Matrix Membranes with HSSZ-13.....	149
5.5.3.	Summary and Conclusion.....	150
5.6.	References.....	152
CHAPTER 6. EFFECT OF SORBED COMPONENTS ON MIXED MATRIX MEMBRANE TRANSPORT PROPERTIES		154
6.1.	Overview.....	154
6.2.	Sorption of Gases in Polymers and Sieves	154
6.3.	Effect of Processing Conditions and Solvents on Polymers, Sieves, and Mixed Matrix Membranes	164
6.3.1.	Effect of Residual NMP in Ultem [®] on the Transport Properties of Mixed Matrix Membranes.....	165
6.3.2.	Effect of Residual Solvents in Sieves on the Transport Properties of Mixed Matrix Membranes	167
6.3.3.	Effect of Processing Equipment on Zeolite Sorption	174
6.4.	Sorption of Gases in Mixed Matrix Membranes	178
6.5.	Discussion.....	180
6.5.1.	Effect of Poorly Sorbing Zeolites on the Transport Properties of Mixed Matrix Membranes.....	180
6.5.2.	Recovery of Sorption in Poorly Sorbing Zeolites.....	184
6.5.3.	Comparison of Contaminant Effects on Zeolites and Carbon Molecular Sieves	185
6.6.	References.....	185
CHAPTER 7. EFFECT OF FEED CONTAMINANTS ON MIXED MATRIX MEMBRANE TRANSPORT PROPERTIES		187

7.1.	Overview.....	187
7.2.	Effect of Water on Mixed Matrix Membranes	188
7.2.1.	Permeation through Pure Poly(vinyl acetate) with Humidified Oxygen	188
7.2.2.	Permeation through Mixed Matrix Membranes with Humidified Oxygen	190
7.2.3.	Effect of Reactivation Conditions on Sorption in Zeolite 4A after Pre-adsorption of Water	193
7.3.	Effect of n-Butane on Mixed Matrix Membranes	195
7.3.1.	Modeling Considerations.....	195
7.3.2.	Effect of n-Butane on the CO ₂ / CH ₄ Transport Properties of Ultem [®] .	196
7.3.3.	Effect of n-Butane on the CO ₂ / CH ₄ Transport Properties of HSSZ-13	197
7.3.4.	Effect of n-Butane on the CO ₂ /CH ₄ Transport Properties of 15% HSSZ-13 Filled Ultem [®] Mixed Matrix Membranes.....	199
7.3.5.	Comparison with Permeation Data from 15% HSSZ-13 filled Ultem [®] Modules Prepared and Tested at Medal.....	202
7.4.	Discussion.....	205
7.5.	References.....	206
CHAPTER 8.	CONCLUSIONS AND RECOMMENDATIONS	208
8.1.	Summary and Conclusions	208
8.2.	Recommendations for Future Work	211
8.2.1.	Further Investigations of Mixed Matrix Membranes in the Presence of Contaminants	211
8.2.2.	Development of Methods to Repair Undesirable Mixed Matrix Membrane Morphologies.....	214
8.2.3.	Investigation of Developmental Issues Impeding Economic Feasibility of Mixed Matrix Membranes	217
8.3.	References.....	219

APPENDIX A.	ESTIMATION OF THE CO ₂ /CH ₄ TRANSPORT PROPERTIES OF ZEOLITE 4A	220
APPENDIX B.	REACTION OF SILANE COUPLING AGENTS WITH POLYMERS AND ZEOLITES	223
APPENDIX C.	COMPRESSIBILITY FACTORS OF THE GASES USED IN THIS WORK.....	228
APPENDIX D.	DISCUSSION OF A MORE RIGOROUS METHOD TO CHARACTERIZE POLYMER-SIEVE THERMODYNAMICS	229
APPENDIX E.	PROOF OF HIGHER STRESS IN THE POLYMER AT THE CENTER OF TWO VERTICAL PARTICLES AFTER SOLVENT EVAPORATION	233
APPENDIX F.	DEVELOPMENT OF MORE COMPLEX MIXED MATRIX MEMBRANE TRANSPORT PROPERTY MAPS.....	236
APPENDIX G.	POLYMERS CONTAINING DIAMINOBENZOIC ACID (DABA) FOR ENHANCED INTERACTION WITH THE ZEOLITES	248
G.1.	6FDA-6FpDA:4MPD:DABA (2:2:1) {6-64D} Based Membranes	248
G.2.	6FDA-mPDA:DABA (2:1) {6-mD} Based Membranes.....	254
G.3.	BPADA-DAPI:DABA (1:1) {B-DD} Based Membranes.....	257
G.4.	Discussion of Polymers with Reactive Groups as a General Method for Avoiding Sieve-in-a-Cage Morphology	258
APPENDIX H.	EFFECT OF N-BUTANE ON THE TRANSPORT PROPERTIES OF MIXED MATRIX MEMBRANES AT 50°C	261
	BIBLIOGRAPHY	263
	VITA	282

List of Tables

Table 1.1: Typical feed composition and sales specification ranges for natural gas streams [17, 19].	6
Table 1.2: Potential applications of molecular sieving (MS) and selective surface flow (SSF) mixed matrix membranes. Application list from [20]. (HC = Hydrocarbon)	7
Table 2.1: Other models for permeation through heterogeneous media.	21
Table 2.2: Size of the penetrants used in this work. The source is given in brackets. ...	30
Table 3.1: Selected properties of polymers. Permeation data is for 35°C and 65 psia. If no source is given, the data was measured in this work.	49
Table 3.2: Selected properties of zeolites. Permeation data is for 35°C and 65 psia. If no source is given, the data was measured for this work.....	51
Table 4.1: Glass transition temperatures and Kuhn Lengths of selected polymers.....	74
Table 4.2: Adhesion of polymer films coated on glass slides as characterized using ASTM standard D3359-97. Percent removed and standard deviation from four samples.	77
Table 4.3: Solubility parameters for selected polymers. Solubility parameters for the engineering polymers were calculated using the group contribution method of Fedors as reported by van Krevelen [28-30]. Other values taken from the source given in brackets.	80
Table 4.4: Oxygen permeabilities for mixed matrix membranes with impermeable glass spheres. The calculated permeability was determined using the Maxwell model, assuming the spheres were impermeable. Tested at 35°C and 65 psia.	83

Table 4.5: Selected physical properties for polymers and sieves used in this work.....	94
Table 5.1: Transport properties for ~15 vol% HSSZ-13 in Ultem [®] membranes prepared using zeolites silanated with different application methods. Tested at 35°C and 65 psia.....	110
Table 5.2: Transport properties for ~15 vol% HSSZ-13 in Ultem [®] membranes with sieves silanated in NMP. Tested at 35°C and 65 psia.....	114
Table 5.3: Transport properties for ~15 vol% HSSZ-13 in Ultem [®] membranes prepared with different sieve samples from ERTC. Tested at 35°C and 65 psia. The full silane names are given in the text.....	116
Table 5.4: Summary of hydroxyl and APDMES densities for unsilanated and silanated HSSZ-13 based on titration of the sites with VOCl ₃ and burn-off of the APDMES in the TGA.....	118
Table 5.5: Transport properties for ~15 vol% HSSZ-13 in Ultem [®] membranes prepared with different initial drying temperatures. Tested at 35°C and 65 psia.....	140
Table 5.6: Transport properties for ~15 vol% HSSZ-13 in Ultem [®] membranes prepared with different solvent evaporation rates. Tested at 35°C and 65 psia.....	141
Table 5.7: Transport properties for mixed matrix membranes with ~30 vol% zeolite dispersed in Ultem [®] . Tested at 35°C and 65 psia.....	152
Table 6.1: Selected data for gas sorption in selected polymers at 35°C. Literature values (where available) are given in parentheses.....	155
Table 6.2: Langmuir coefficients for regressions of penetrant sorption in zeolite 4A and HSSZ-13. Literature values (where available) are given in parentheses. Temperature is 35°C except where noted.....	157

Table 7.1: Summary of experimental data and model predictions for zeolite 4A filled PVAc membranes tested at 25°C.....	191
Table 7.2: Comparison of selectivities calculated and measured using Medal modules versus n-butane loading in an otherwise 10% CO ₂ / 90% CH ₄ feed gas at ~100 psia.....	203
Table A.1: Gas transport properties of zeolite 4A at 35°C (50/50 CO ₂ /CH ₄ and 2 atm total pressure).....	221
Table F.1: Parameters and values used to calculate the partition functions in Eq F.2 Eq F.3, and Eq F.4 [2, 4-6].....	238
Table F.2: Calculation of O ₂ /N ₂ transport properties for 15 vol% zeolite 4A in Ultem [®] containing fractions of sieves exhibiting multiple nonideal morphologies. The variables in the first 5 columns are shown in Figure F.2. ($\phi_{s1} + \phi_{s2} = 0.15$).....	246
Table G.1: Transport properties for ~15 vol% HSSZ-13 in 6FDA-6FpDA:4MPD:DABA membranes. Tested at 35°C and 65 psia.....	254
Table G.2: Transport properties for ~15 vol% zeolite 4A or HSSZ-13 in 6FDA-mPDA:DABA dried at selected temperatures. Tested at 35°C and 65 psia.....	255
Table G.3: Elemental composition obtained by XPS of the zeolite 4A samples.	256
Table G.4: Transport properties for ~15 vol% zeolite 4A in BPADA-DAPI:DABA membranes. Tested at 35°C and 65 psia feed pressure.....	258
Table H.1: Method used or assumption made to estimate the parameters necessary to model gas transport in mixed matrix membranes at 50°C with synthetic natural gas feeds contaminated with n-butane.	262

List of Figures

- Figure 1.1: Upper-bound trade-off curves (1991) for the (a) oxygen – nitrogen and (b) carbon dioxide – methane gas pairs. Adapted from [11]. Also shown are the properties for the molecular sieving materials used in this work (see section 3.2.2).
..... 2
- Figure 1.2: Schematic of a hollow fiber mixed matrix membrane. The dispersed phase exists only in the outer dense separation layer (dark) of an asymmetric membrane, while the inner support layer may be composed of a different porous polymer. 4
- Figure 2.1: Sketch demonstrating the nature of the Langmuir mode in polymers. 18
- Figure 2.2: Cartoon showing the morphology of the polymer, sieve, and “interphase” used in the three phase Maxwell model..... 23
- Figure 2.3: Zeolite 4A dispersed in Udel[®] showing “sieve-in-a-cage” morphology. 25
- Figure 2.4: O₂/N₂ diffusion selectivity as a function of pore size calculated using Eq 2.19. 31
- Figure 2.5: The use of the Maxwell model for the selection of optimal polymer – sieve combinations. The blue curve represents the calculated performance of hypothetical mixed membranes prepared with 40 vol% zeolite 4A dispersed in each of the polymers along the upper bound (black line). Red diamonds represent calculations with real polymers. The lowest diamond represents the neat polymer and subsequent diamonds represent increases of 10 vol% zeolite 4A dispersed in each polymer up to 40 vol%. 33
- Figure 2.6: (a) CO₂/CH₄ and (b) O₂/N₂ transport properties for mixed matrix membranes based on rubbery polymer matrices reported in [72, 73]. Shapes denote polymer matrix. Colors denote insert phases (black – neat polymer; blue –

silicalite; red – zeolite KY; green – one of three CMS materials). The insert loading is noted next to each data point.....	37
Figure 2.7: (a) O ₂ /N ₂ (with zeolite 4A inserts) (b) O ₂ /N ₂ (with CMS inserts) (c) O ₂ /N ₂ (with zeolite 13X inserts) and (d) CO ₂ /CH ₄ transport properties for mixed matrix membranes based on glassy polymer matrices reported in [74-76, 80, 81, 83-85]. Shapes denote polymer matrix. Colors denote insert phases (black – neat polymer; blue – silicalite; green –CMS; purple – zeolite 4A; turquoise – zeolite 13X).....	41
Figure 3.1: Structures of the polymers used in this work.....	50
Figure 3.2: Framework structures for the zeolites used in this work. Each vertex represents the center of a silica or alumina tetrahedron. Structures from International Zeolite Association http://www.iza-structure.org	52
Figure 3.3: Preparation of mixed matrix membranes. Optional dope preparation steps are highlighted in gray.....	54
Figure 3.4: Schematic of the permeation system. (1) Downstream Pressure Transducer (2), Permeate Reservoir (3) Fan, (4) Heater, (5) Rupture Device, (6) Upstream Pressure Transducer, (7) Feed Reservoir, (8) Permeation Cell, (A) Downstream Pressure Transducer Isolation Valve, (B) GC Valve, (C) Downstream Vacuum Valve, (D) Feed Valve, (E) “Middle” Valve, (F) Vent Valve, (G) Cell Isolation Valve, (H) Retentate (Metering) Valve, (I) Retentate Shutoff Valve, and (J) Vacuum Shutoff Valve.....	61
Figure 3.5: Schematic of the permeation cell {(8) in Figure 3.4}. A cross section through the cell is shown with a “sandwich” type masked membrane. The membrane assembly is composed of: membrane, yellow; filter paper, light gray; epoxy, brown; adhesive backed aluminum, checkered. Bolts, shown at left and right, and o-rings, solid black circles, assure a leak tight seal.....	62

Figure 3.6: Schematic of the Oxtran permeation device for measuring the oxygen permeability of humidified feeds.....	66
Figure 3.7: Schematic of a gravimetric “quartz spring” sorption apparatus.....	68
Figure 3.8: Schematic of a high pressure – pressure decay sorption apparatus.	69
Figure 4.1: (a) Repulsive and (b) attractive forces measured between polymer-coated slides and glass spheres glued to an AFM tip. The repulsive force, F_R , is measured as the tip is advanced toward the polymer coated surface, while the attractive force, F_A , is measured as the tip is removed from the sample as shown in the inset.....	79
Figure 4.2: (a) Amount of polymer absorbed onto an acidic surface as a function of the solvent character: acidic polymer (- - -), basic polymer (· · ·). (b) Cartoon to explain the effect of solvent on polymer adsorption. Acidic moieties (electron accepting), blue; basic moieties (electron donating), red; neutral solvent, gray. ...	81
Figure 4.3: SEM of glass spheres dispersed in (a) 40% hydrolyzed PVAc and (b) Udel [®]	82
Figure 4.4: Comparison of contraction in a material with spherical voids and rigid spherical particles. The dark gray region indicates rigidified polymer.	85
Figure 4.5: Birefringence images of (a) zeolite 4A dispersed in Ultem [®] and (b) zeolite 4A dispersed in Matrimid [®] . The largest particles in the images are ~ 5 μm	86
Figure 4.6: Simplified carton showing behavior of polymer between particles.....	91
Figure 4.7: Cartoon showing the effect of a constrained boundary on membrane morphology; delamination of the polymer – particle interface.	92
Figure 4.8: Cartoon showing likely mixed matrix morphology as a function of solvent evaporation time.	93

Figure 4.9: Cartoon showing the effect of (isotropic) expansion and contraction.	94
Figure 5.1: Transport properties (O_2/N_2) expected for various mixed matrix membrane morphologies for the Ultem [®] – zeolite 4A system at 15 vol% loading	103
Figure 5.2: Transport properties (O_2/N_2) expected for various mixed matrix membrane morphologies for the Ultem [®] – HSSZ-13 system at 15 vol% loading.	105
Figure 5.3: SEM of ~15 vol% HSSZ-13 in Matrimid [®] showing the transition from sieve-in-a-cage morphology (top) to apparently well-bonded interfaces in one sample.....	107
Figure 5.4: Comparison of membranes prepared with ~15 vol% unsilanated (red) or silanated (blue) zeolite 4A dispersed in Ultem [®] . Gray circles represent neat Ultem [®] . Tested at 35°C and 65 psia.	112
Figure 5.5: Excess weight loss compared to unsilanated HSSZ-13 for samples silanated with γ -aminopropyldimethylethoxysilane (APDMES) in 95:5 IPA : water and for a sample sonicated (without APDMES) in 95:5 IPA : water determined using the TGA. All samples were degassed at 250°C for 8 hr to determine the correct “zero” weight.	119
Figure 5.6: Comparison of membranes prepared with ~15% silanated submicron (red) or ~5 μ m (blue) zeolite 4A dispersed in Ultem [®] . Gray circles represent neat Ultem [®] . Tested at 35°C and 65 psia.	121
Figure 5.7: (a) Zeolite agglomerate in a ~15 vol% HSSZ-13 in Ultem [®] mixed matrix membrane. Sieves in the non-agglomerated regions (b) have good interfaces. ...	122
Figure 5.8: Comparison of membranes prepared with ~15% HSSZ-13 dispersed in Ultem [®] using either the 50 W (red) or 1000 W (blue) sonicators. Gray circles represent neat Ultem [®] . Tested at 35°C and 65 psia.....	124

Figure 5.9: Schematic of experiments performed to stabilize casting dopes 129

Figure 5.10: Comparison of membranes prepared with ~15 vol% HSSZ-13 dispersed in Ultem[®] using stabilized casting dopes as in Figure 5.9: (green), sieve suspension sonicated with polymer; (red), casting dope A; (blue), casting dope B1; (turquoise), casting dope B2; (yellow), casting dope C. Gray circles represent neat Ultem[®]. Tested at 35°C and 65 psia. 130

Figure 5.11: Mercury casting setup 132

Figure 5.12: Comparison of membranes prepared with ~15 vol% zeolite 4A dispersed in Ultem[®] using the following techniques: cast from NMP and remove before vitrification (blue); cast from NMP and heat to high temperature (red); cast from dichloromethane at room temperature and anneal to 250°C (green). Gray circles represent neat Ultem[®]. Tested at 35°C and 65 psia. 137

Figure 5.13: Comparison of membranes prepared with ~15 vol% HSSZ-13 dispersed in Ultem[®] using the following techniques: cast from NMP and remove before vitrification (blue); cast from dichloromethane on glass (red); cast from dichloromethane on mercury (yellow); and cast from chloroform on glass (green). Gray circles represent neat Ultem[®]. Tested at 35°C and 65 psia. 139

Figure 5.14: Comparison of membranes prepared with ~15 vol% zeolite 4A dispersed in Ultem[®] at various temperatures: (yellow) 180°C – 220°C; (red) 240°C – 260°C; (blue) 280°C – 300°C; (green) cast at room temperature and annealed at 250°C. Gray circles represent neat Ultem[®]. Tested at 35°C and 65 psia. 143

Figure 5.15: O₂/N₂ transport property maps: (a) assuming the selectivity of the nonideal morphology regions are the same as the corresponding pure material (b) allowing the selectivity of the nonideal morphology region to vary as discussed in the text (c) assuming maximum $\ell_l/r_s = 0.3$ to represent “experimentally accessible”

transport properties. The shaded area in (c) indicates transport properties indicative of multiple nonideal morphologies in sieve fractions within a single membrane. (d) shows the assumed dependence of O₂/N₂ selectivity on O₂ permeability for the matrix rigidification and stress dilated regions shown in (c).
 146

Figure 5.16: Summary of O₂/N₂ transport properties for ~15 vol% zeolite 4A in Ultem[®] on the O₂/N₂ transport property map developed in Figure 5.15c. 148

Figure 5.17: Summary of O₂/N₂ transport properties for ~15 vol% HSSZ-13 in Ultem[®] on an O₂/N₂ transport property map developed similar to that of zeolite 4A in Figure 5.15c. 150

Figure 6.1: Sorption of O₂, N₂, CO₂, and CH₄ in Ultem[®] at 35°C. Lines are fitted to the dual-mode equation (Eq 2.6) with parameters given in Table 6.1..... 156

Figure 6.2: Sorption of O₂, N₂, CO₂, and CH₄ in Matrimid[®] at 35°C. Lines are fitted to the dual-mode equation (Eq 2.6) with parameters given in Table 6.1..... 156

Figure 6.3: Sorption of O₂, N₂, CO₂, and CH₄ in zeolite 4A at 35°C. Lines are fitted to the Langmuir equation (Eq 2.6 with $k_D = 0$) with parameters given in Table 6.2.158

Figure 6.4: Sorption of O₂, N₂, CO₂, and CH₄ in HSSZ-13 at 35°C. Lines are fitted to the Langmuir equation (Eq 2.6 with $k_D = 0$) with parameters given in Table 6.2.158

Figure 6.5: Sorption of water and n-butane in zeolite 4A and HSSZ-13 at selected temperatures. Note that the pressure is given in a log scale. 160

Figure 6.6: (a) Equilibrium and (b) transient oxygen sorption in zeolite 4A from a single batch activated using different activation protocols and for a submicron zeolite 4A batch (equilibrium only). The transient curves are taken from the lowest equilibration pressure, ~2 atm. The “standard curve” is explained in the text. ... 161

Figure 6.7: Effect of equilibration pressure on the sorption rate of oxygen into zeolite 4A. Data corresponds to the sample: “285°C in new oven overnight, Sample A” from Figure 6.6a. 163

Figure 6.8: Effect of particle size distribution on the sorption rate of oxygen in zeolite 4A. The solid line is for uniform particles of 5 μm diameter. The dashed line assumes that 10% of the mass is comprised of 20 μm diameter particles. 164

Figure 6.9: Effect of residual NMP on the transport properties of neat Ultem[®]. The casting solvent and drying conditions are given for well-dried Ultem[®] membranes. 165

Figure 6.10: TGA curves for neat Ultem[®] and selected mixed matrix membranes cast on glass at 100°C and removed before vitrification, followed by drying at 75°C \times 1 night and 180°C \times 4 nights. The inset shows the FTIR spectrum of the evolved gas (top, pink) from Ultem[®] - #241 at 240°C and a standard spectrum of NMP (bottom, blue). 166

Figure 6.11: (a) Equilibrium and (b) transient oxygen sorption in activated zeolite 4A sonicated in various solvents followed by reactivation under different conditions. The transient curves are from the lowest equilibration pressure, \sim 2 atm. The maximum uptake and half time at that equilibration pressure for each transient sample are given. 168

Figure 6.12: (a) Equilibrium and (b) transient oxygen sorption in activated zeolite 4A exposed to various conditions present during silanation in 95:5 isopropanol : water. The transient curves are from the lowest equilibration pressure, \sim 2 atm. The maximum uptake and half time at that equilibration pressure for each transient sample are given. 170

Figure 6.13: (a) Equilibrium and (b) transient oxygen sorption in activated zeolite 4A exposed to various conditions present during silanation in 95:5 ethanol : water. The transient curves are from the lowest equilibration pressure, ~2 atm. The maximum uptake and half time at that equilibration pressure for each transient sample are given. 173

Figure 6.14: (a) Equilibrium and (b) transient oxygen sorption in activated zeolite 4A during and after exposure to a “sweated” copper vacuum line. The transient curves are from the lowest equilibration pressure, ~2 atm. The maximum uptake and half time at that equilibration pressure for each transient sample are given..... 175

Figure 6.15: (a) Equilibrium and (b) transient oxygen sorption in activated zeolite 4A exposed to a vacuum oven, before and after cleaning. The transient curves are from the lowest equilibration pressure, ~2 atm. The maximum uptake and half time at that equilibration pressure for each transient sample are given..... 177

Figure 6.16: Demonstration of additivity of sorption in mixed matrix membranes. O₂ and N₂ sorption in 14.6 vol% HSSZ-13 dispersed in Ultem[®]. 178

Figure 6.17: Oxygen sorption in 13.7 vol% zeolite 4A dispersed in Ultem[®] cast from dichloromethane dried under different conditions..... 180

Figure 6.18: Effect of diffusion coefficient on the theoretical uptake over maximum uptake of oxygen in zeolite 4A..... 182

Figure 6.19: Effect of decreased diffusion coefficients (cm²/s) on the theoretical transport properties of 15 vol% zeolite 4A dispersed in Ultem[®] 183

Figure 7.1: Oxygen permeability of neat poly(vinyl acetate) at 25°C and 35°C as a function of relative humidity. 189

Figure 7.2: Effect of feed humidity on the oxygen permeability of a 14.2 vol% HSSZ-13 filled poly(vinyl acetate) membrane. Experiments were performed at 35°C. ♦, Membrane 1 data; ■ Membrane 2 data..... 192

Figure 7.3: (a) Equilibrium and (b) transient oxygen sorption for activated zeolite 4A samples exposed to water and reactivated under different conditions. The “Standard Curve” on the equilibrium sorption plot is from section 6.2. The transient curves are from the lowest equilibrium pressure, ~2 atm. 194

Figure 7.4: Calculated CO₂ and CH₄ permeabilities in HSSZ-13 at 35°C as a function of feed pressure for a synthetic natural gas mixture (10% CO₂ / 90% CH₄) with selected concentrations of n-butane as a model contaminant. Calculations assume constant diffusion coefficients in the sieve..... 198

Figure 7.5: Calculated CO₂ and CH₄ permeabilities in 15 vol% HSSZ-13 filled Ultem[®] at 35°C as a function of feed pressure for a synthetic natural gas mixture (10% CO₂ / 90% CH₄) with selected concentrations of n-butane as a model contaminant. Calculations assume constant diffusion coefficients in the sieve. The permeabilities of neat Ultem[®] in the absence of n-butane are shown for comparison..... 199

Figure 7.6 Calculated CO₂/CH₄ selectivity of 15 vol% HSSZ-13 filled Ultem[®] at 35°C as a function of feed pressure for a synthetic natural gas mixture (10% CO₂ / 90% CH₄) with selected concentrations of n-butane as a model contaminant. The selectivity of neat Ultem[®] in the absence of n-butane is shown for comparison. 201

Figure 7.7: Upper-bound plot for Ultem[®] and a better-“matched” hypothetical polymer with dispersed HSSZ-13 for a 10% CO₂ / 90% CH₄ synthetic natural gas feed with and without 2% n-butane. Red markers indicate a pure feed, while green markers indicate 2% n-butane in the feed. The upper bound is given by the heavy dashed black line. The green and dashed red lines represent calculated transport properties

for 40 vol% HSSZ-13 in polymers on the upper bound with and without n-butane in the feed, respectively.	202
Figure 8.1: Scheme for the repair of mixed matrix membranes exhibiting sieve-in-a-cage morphology using a reactive intercalation scheme	217
Figure A.1: Pure gas sorption isotherms for carbon dioxide and methane in zeolite 4A at 50°C. CO ₂ isotherm is from [2] and CH ₄ isotherm is from [4].....	221
Figure B.1: Reaction of γ -aminopropyltrimethoxysilane with zeolite silanol groups and with imide groups (i.e. Ultem [®]).	223
Figure B.2: ¹ H-NMR spectrum of ~15 wt% Ultem [®] / 2 wt% APDMES in NMP.	226
Figure B.3: ¹ H-NMR spectrum of ~15 wt% Ultem [®] in deuterated NMP.	226
Figure E.1: Geometry of polymer between two vertically aligned particles before and after solvent evaporation for an initially vitrified state.	233
Figure F.1: Potential functional dependence of selectivity on the permeability of the matrix rigidification and stress dilated regions. Black, upper-bound trade-off curve; red, Park-Paul correlation; green, constant selectivity. Dashed lines were modified to go through the transport properties of neat Ultem [®]	243
Figure F.2: Cartoon shown multiple nonideal morphologies for different fractions of sieve at the polymer – sieve interface and the modeling strategy.	244
Figure G.1: Preparation procedures used for mixed matrix membranes from polymers containing diaminobenzoic acid (DABA) in their backbones.	249
Figure G.2: Summary of 6FDA-6FpDA:4MPD:DABA (2:2:1) mixed matrix membranes with 15 vol% zeolite 4A on an O ₂ /N ₂ transport property map. The membranes were prepared as shown in Figure G.1. Tested at 35°C and 65 psia.	250

Figure G.3: Summary of 6FDA-6FpDA:4MPD:DABA (2:2:1) mixed matrix membranes with 15 vol% zeolite 4A on a CO₂/CH₄ transport property map. The membranes were prepared as shown in Figure G.1. Tested at 35°C and 65 psia. 253

Figure G.4: SEM of mixed matrix membranes prepared with zeolite 4A in selected DABA containing polymers. a) 6FDA-6FpDA:4MPD:DABA b) 6FDA-mPDA:DABA c) BPADA-DAPI:DABA..... 260

Chapter 1. INTRODUCTION, MOTIVATION, AND OVERVIEW

1.1. GAS SEPARATION MEMBRANES

The separation of gases using membranes involves diffusion and sorption phenomena, as discussed in Chapter 2. The product of the diffusion and sorption coefficients gives a measure of the overall intrinsic membrane productivity, or *permeability*. This result reflects the “solution-diffusion” basis for the model used to describe permeation, which was first proposed qualitatively by Graham in 1866 [1] and quantified by von Wroblewski in 1879 [2]. John Mitchell observed that natural rubber balloons filled with different gases deflated at different rates, which demonstrated (i) that different gases permeate at different rates [3, 4], and (ii) *permselectivity* can be achieved for one gas over another. The above observations reflect the differences in sorption, diffusion, and permeation coefficients for different gases. Fick defined the diffusion coefficient as the proportionality constant between the flux and the concentration gradient [5], although the chemical potential gradient is the preferred driving force from a fundamental standpoint. Sorption in rubbery materials follows Henry’s law [6]. More recently, sorption in glassy materials has been understood as the sum of Henry’s law and Langmuir domains, using the “dual-mode” model [7]. These terms are defined more precisely in Chapter 2, but they are introduced here because they are the basic criteria that define membrane material performance.

1.1.1. Polymeric Gas Separation Membranes

Gas separation membranes are traditionally composed of synthetic polymeric materials. For separations of permanent gases, these polymers tend to be glassy because of their mechanical properties and better size-dependent separation characteristics as a class compared to rubbery polymers. Many different polymer families have been investigated as gas separation materials, including polycarbonates, polyesters, polysulfones, polyimides, and polypyrrolones [8, 9]. Polyimides and polypyrrolones,

on average, have transport properties better than other polymer families. The most common industrial-scale gas separation membrane materials are cellulose acetate, polysulfone, and the polyimide Matrimid[®] (Vantico; Brewster, NY). These polymers are used industrially because they can be spun into asymmetric hollow fiber membranes. Asymmetric hollow fiber membranes have a thin selective layer on the outside of the fiber and an inner, porous support layer [10]. This configuration maximizes the surface area-to-volume available to accomplish a separation, while simultaneously maximizing flux through the membrane. This configuration makes gas separation membrane economics competitive with those of more traditional separations.

Polymeric membranes suffer from a trade-off between their productivity, or permeability, and separation efficiency, or selectivity. This was illustrated by Robeson in 1991 where he plotted polymer selectivity versus permeability in what has become known as the “upper-bound trade-off” curves [11], illustrated in Figure 1.1. Although there was much improvement during the 1980’s, there have been few reports of *processable* polymers with properties above the 1991 upper-bound in the last decade.

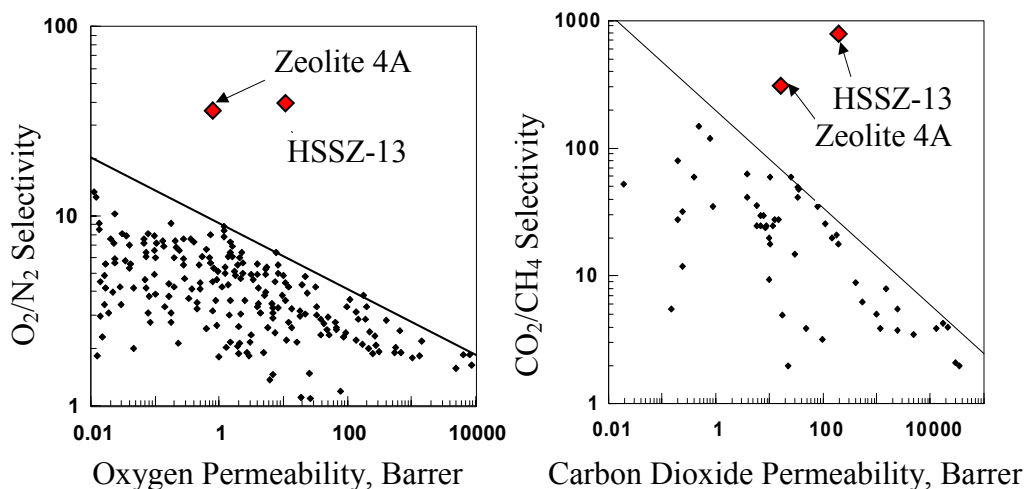


Figure 1.1: Upper-bound trade-off curves (1991) for the (a) oxygen – nitrogen and (b) carbon dioxide – methane gas pairs. Adapted from [11]. Also shown are the properties for the molecular sieving materials used in this work (see section 3.2.2).

1.1.2. Inorganic Gas Separation Membranes

Recently, research has been directed towards the development of more rigid carbons [12] and zeolites [13] as membrane materials, which have more favorable trades-off between selectivity and permeability (see Figure 1.1 for example). As discussed in Chapter 2, these inorganic materials may operate either by a molecular sieving mechanism or by *selective surface flow*. Such materials can have better transport properties than polymers, and they may act as nearly infinitely selective molecular sieves. These rigid materials are, however, characterized by poor mechanical properties and serious processing challenges. Carbons can be tailored by changing the pyrolysis protocol or by selecting polymer precursors with different properties. Although carbons have been prepared in a hollow fiber morphology, they are quite brittle [14], making it very difficult to prepare industrial-scale modules. In the case of crystalline zeolite materials, intracrystalline defects cause transport properties dramatically lower than the theoretical properties of a single crystal [13]. Zeolites are composed of silica and alumina tetrahedra joined together through oxygen atoms at each of the four vertices [15]. This work focuses on zeolites as the molecular sieving phase.

1.1.3. Mixed Matrix Membranes

Mixed matrix membranes have been proposed as a class of materials that can exceed the polymeric upper-bound trade-off curves. Mixed matrix materials are composed of an *insert* phase, such as zeolites or carbon molecular sieves, dispersed in a continuous polymer matrix. It is envisioned that mixed matrix membranes will have transport properties between those of pure polymers and the insert phases, while still being processable with conventional polymer processing techniques. A schematic of an asymmetric mixed matrix membrane is shown in Figure 1.2; however, the focus of this work is the dense skin layer shown in the enlarged area. The viability of the mixed matrix concept for gas separations has been demonstrated [16], but many challenges remain. Two of the key challenges are selecting the ideal polymer – sieve combination

to separate a given gas pair and overcoming problems occurring at polymer – sieve interfaces within the membrane. Selecting appropriate polymer – sieve combinations is complicated because the properties of each phase are potentially affected by the presence of the other and possibly by components of the feed gases. Tailoring interfacial morphology is a difficult problem frequently encountered in composites, but it is especially challenging for membranes since small changes in interfacial morphology can lead to dramatic changes in transport properties. Both challenges are addressed in this work.

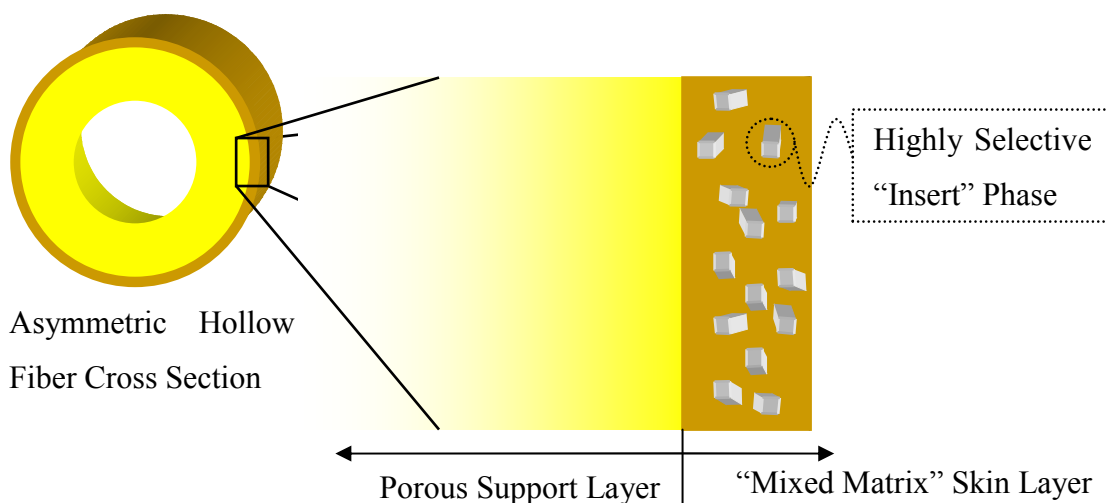


Figure 1.2: Schematic of a hollow fiber mixed matrix membrane. The dispersed phase exists only in the outer dense separation layer (dark) of an asymmetric membrane, while the inner support layer may be composed of a different porous polymer.

1.2. GAS SEPARATION TECHNOLOGIES

Membranes are one of a handful of technologies for gas separations. Other major technologies include absorption, adsorption, and distillation. In general, membranes are economical when low flowrates are required or when lower purities can be tolerated. Advances in either membrane permeability or selectivity improve the economics of membrane-based gas separations, so it is envisioned that mixed matrix membranes will increase the application of membranes. Improvements in membrane selectivity are most critical, because increased productivity can be achieved by making thinner

separation layers and increased throughput can be obtained by increasing membrane area. Increasing the application of membranes can be beneficial, as membranes tend to be more environmentally benign and require less energy for separation than the more established gas separation technologies. There are two gas pairs where mixed matrix membranes are anticipated to have the greatest immediate impact: oxygen – nitrogen and carbon dioxide – methane, and these are used as model systems in this work.

1.2.1. Nitrogen and Oxygen Enrichment of Air

There are three main technologies used for the separation of oxygen and nitrogen from air: membranes, pressure-swing adsorption, and cryogenic distillation. The later two technologies dominate high purity production or where larger flowrates are required, while membranes are used to produce relatively low purity nitrogen ($< \sim 99\%$) [10]. Nitrogen-enriched air is used for inerting applications. For example, blanketing airline fuel tanks with nitrogen can virtually eliminate the chance of a spark igniting fuel vapors. Selected applications of oxygen-enriched air include enhanced combustion efficiency or assistance to people with reduced lung capacity. Air separation membranes are typically operated at relatively low feed pressure (~ 100 psi) and at temperatures slightly above ambient. Thus, the effect of potential feed contaminants on membrane properties is of much greater concern than the ability to withstand high pressures or temperatures. Typical contaminants in an air feed include humidity and compressor oil vapors.

1.2.2. Natural Gas Purification

The methods for purifying natural gas are varied because each deposit presents a different composition. Typical feed compositions and sales specifications for natural gas streams are detailed in Table 1.1; however both vary locally. Most commonly, carbon dioxide is the major component that must be removed, since it can form carbonic acid, leading to corrosion of pipelines [17]. Hydrogen sulfide must also be removed because it is toxic and causes corrosion [17]. Membranes selectively permeate

carbon dioxide, hydrogen sulfide, and water, which can also be present. Most natural gas is currently purified using amine adsorption. This is an environmentally undesirable alternative; however, in many cases the economics for membranes are not as favorable. Studies have shown that a hybrid process where membranes remove most of the carbon dioxide and a small amine column is used for finishing have favorable economics [18]. Some natural gas deposits have so much carbon dioxide that they are economically inaccessible using available technology. Mixed matrix membranes may make recovery of methane from these deposits economical. An important factor governing the use of any membrane for natural gas purification is its ability to withstand the high feed pressures typically used. Moreover, because of the array of components encountered in natural gas feeds membranes must also tolerate contaminants in the feeds. Any potential mixed matrix membrane must also meet these two criteria.

Table 1.1: Typical feed composition and sales specification ranges for natural gas streams [17, 19].

Component	Typical Feed Composition	Sales Specification
CH ₄	70-80%	90%
CO ₂	7-40%	Less than 2%
C ₂ H ₆	3-4%	3 - 4%
C ₃ to C ₅	~3%	~3%
C ₆ and Higher	0.5 – 1%	0.5 – 1%
N ₂	Less than 4%	Less than 4%
H ₂ S	100 – 5000 ppm	Less than 4 ppm
H ₂ O	Saturated	Less than 0.1g/m ³

1.2.3. Other Separations

Mixed matrix membranes are potentially useful for many other separations. The air separation and natural gas purification are best accomplished with mixed matrix membranes having molecular sieving inserts. Other important gas pairs such as olefins

and paraffins do not have a substantial size difference, or in some cases it is desirable to remove the larger, typically more condensable component from the feed. In such cases, a *selective surface flow* insert is desirable. Selective surface flow is described in detail in section 2.1.4. Table 1.2 summarizes several separations and the type of mixed matrix membrane most suited to the particular application. It is clear that mixed matrix membranes do offer a new paradigm for gas separation technology.

Table 1.2: Potential applications of molecular sieving (MS) and selective surface flow (SSF) mixed matrix membranes. Application list from [20]. (HC = Hydrocarbon)

Category	Gases	Application	Insert Phase
Hydrogen	H ₂ /N ₂	Ammonia purge gas	MS
	H ₂ /CH ₄	Refinery hydrogen recovery	MS
	H ₂ /CO	Synthesis gas ratio adjustment	SSF
	H ₂ /O ₂	Fuel Cells	MS
Air	O ₂ /N ₂	N ₂ -enriched air for inerting	MS
		O ₂ -enriched air for combustion	
		O ₂ for respiration therapy	
Acid Gases	CO ₂ /CH ₄	Enhanced oil recovery; recover CO ₂ for reinjection	MS
		Landfill and natural gas sweetening	
	H ₂ S/CH ₄	Sour gas sweetening	SSF
	CO ₂ /N ₂	Digester gas treatment	SSF
Drying	H ₂ O/HC	Hydrocarbon drying	MS
	H ₂ O/Air	Air drying	MS/SSF ^a
Hydrocarbons	HC/Air or HC/N ₂	Pollution control; stack gas or solvent recovery	SSF
	HC/N ₂	Upgrading low-BTU gas	SSF
	HC/HC	Dew pointing of natural gas	MS/SSF ^b
Helium	He/HC	Helium recovery from gas wells	MS
	He/N ₂	Helium recovery from diving air	MS

^a An insert could potentially show both MS and SSF because water is both small and condensable.

^b If there is insufficient size difference between penetrants, they may be separable using SSF inserts.

1.3. RESEARCH OBJECTIVES

The major impediment to mixed matrix membrane technology is the inability to prepare membranes with desirable properties from “off the shelf” polymers and inserts. Criteria for selecting polymer – insert pairs have been developed, but the effect of potential feed contaminants has not been considered. A second problem is selecting a preparation procedure that gives optimal membrane morphology. The morphology of the polymer – insert interface has been found to be vitally important to membrane performance. Another issue is that sieves may agglomerate in the casting suspensions, leading to defects in the resulting membranes.

The overall objective of this work is to *develop the knowledge to allow subsequent researchers to create mixed matrix materials with desirable transport and mechanical properties for appropriate polymer – sieve combinations tailored to a specific gas pair.* The effects of materials, processing, and operating conditions on casting suspension stability, membrane interfacial properties, and overall transport performance will be investigated, as discussed in the following objectives:

1. Characterize the effect of sieve priming protocols (coupling agent size, chemical properties, and treatment conditions) on: coupling mechanism and the resulting modifications to the properties of (i) the sieve (surface and internal regions), (ii) the polymer (interfacial and matrix regions), and (iii) mixed matrix membranes
2. Develop an engineering model to guide processing of mixed matrix membranes that relates specific sieve priming protocols to observed membrane performance in terms of measurable or calculable parameters derived from the characterization work of objective one
3. Characterize the effects of sieve priming protocols on intrinsic casting suspension stability and seek general principles to guide the rational balancing of final mixed matrix membrane properties and casting suspension stability

4. Determine the effects of potential minor components in the feed gas (e.g. (a) water in air and natural gas feeds and (b) higher aliphatic and aromatic hydrocarbons in natural gas feeds) on the performance of (i) the molecular sieve, (ii) the polymer matrix, and (iii) mixed matrix membranes

Specifics for each objective are discussed sequentially below.

1.3.1. Objective 1: Characterize the effect of sieve priming protocols on mixed matrix morphology and transport properties

Several factors believed to affect mixed matrix membrane performance were investigated with a range of characterization techniques. Several polymers (detailed in Chapter 3) were used to vary the polymer – sieve affinity and the polymer flexibility, which are two factors believed to influence mixed matrix performance [16]. Two different zeolites: HSSZ-13 and zeolite 4A, each with two different particle size distributions, were used at selected loadings to further vary the polymer – sieve affinity. The different particle sizes and sieve loadings change the amount of polymer – sieve interfacial area in the membrane, potentially providing a mechanism to probe interfacial effects. Finally, different silane coupling agents were applied to the zeolites using various application methods to further vary interfacial morphology.

The desired morphology is one with no voids between the polymer and sieve phases. These voids allow bypassing of the sieves by Ångstrom-sized gas molecules. Flexible polymers with good affinity for the sieve or surface-modified sieves were thought to be necessary to achieve this goal. In many cases where voids were not observed, a rigidification of the polymer matrix near the sieves is postulated to occur [16]. This work sought to propose a mechanism for membrane formation that would explain why voids are formed in some cases and why excess rigidification is observed in others. It was hoped this understanding could be exploited to achieve desirable interfacial morphologies yielding favorable transport properties.

1.3.2. Objective 2: Develop an engineering model to guide processing of mixed matrix membranes

The goal of the second objective is to provide an engineering tool to rationalize the connection between fundamental interfacial and bulk properties and the practical performance of a given mixed matrix membrane. Previous researchers have already suggested modifications to the standard Maxwell model (see section 2.2.1) to predict the effect of interfacial voids and to model rigidification of the matrix [16]. This modified Maxwell model was used to discount an alternative sieve pore-blockage explanation for the lower-than-expected permeabilities obtained for the PVAc – zeolite 4A system. This work provided useful insights into mixed matrix properties and the nature of the interphase; however, the differences in transport properties between samples with alternatively tailored interfaces appear similar to the experimental error in transport properties measurements. Thus, formulation of an even more complex model is not justified. Instead, work focused on incorporating the effects of minor feed components in the feed gas into the model as part of objective 4. Predicting the effect of minor feed components will be even more important as mixed matrix membranes are moved toward commercialization because of the dramatic effects certain penetrants can have on their properties.

1.3.3. Objective 3: Characterize the effects of sieve priming protocols on casting suspension stability

Suspensions of large ($\sim > 1 \mu\text{m}$) particles are inherently unstable. Membranes containing large particles must be prepared from highly viscous suspensions to prevent settling before vitrification of the polymer matrix. Conversely, small ($< 1 \mu\text{m}$) particles do not settle because random Brownian motions keep them dispersed, unless particle agglomerates form. Agglomerates in casting suspensions lead to agglomerates in membranes, which may cause poor selectivity, especially in asymmetric hollow fiber membranes where the separation layer is ideally only $\sim 1000 \text{ \AA}$. Agglomerate formation

was a major concern with the small particles. Steric stabilization via attachment of polymer chains was the primary method used to stabilize the casting suspensions. Electrostatic stabilization of the casting suspensions is also possible, but was not pursued. Nonetheless, the methods used here proved sufficient to stabilize submicron zeolite suspensions.

1.3.4. Objective 4: Determine the effects of potential minor components in the feed gas

The performance of gas separation membranes can be severely affected by the presence of minor components or contaminants in the feed gases. This may cause unanticipated changes in the performance of membranes “in the field” compared to performance in the research laboratory, where they are typically tested with pure gases or simple gas mixtures. In air separation, humidity is a major concern. Natural gas consists of potentially hundreds of components (see Table 1.1) that may pose problems. It is impossible to test every potential contaminant; however, by careful selection of model contaminants, the range of effects expected of different classes of contaminants (e.g. water, aliphatic and aromatic hydrocarbons) can be established.

The effects of minor feed components on neat polymers have been studied extensively [12, 21]. Two major effects are most commonly observed: competition and plasticization. Competition causes a decrease in the permeability of lower sorbing components with small decreases in selectivity [21]. Plasticization, on the other hand, typically causes increased permeability for all components with a large drop in selectivity. In contrast, molecular sieves are rigid materials and therefore do not plasticize, but competition effects can be more important [13, 22, 23]. This work will demonstrate that the effects of minor components on mixed matrix membranes can be inferred based on their effects on the polymer matrix and sieving phase.

1.4. DISSERTATION OVERVIEW

Chapter two provides theory and background information for this work. Materials and experimental procedures used throughout this work are summarized in chapter three. Chapter four presents an understanding of membrane preparation that explains final membrane morphology and transport properties. Principles discussed in chapter four are applied to various materials and processing conditions to prepare mixed matrix membranes with favorable interfacial properties in chapter five. Chapter six reports the effects of sorbed components on the transport properties of mixed matrix membranes, while chapter seven summarizes the effects of feed contaminants. Finally, chapter eight gives conclusions and recommendations.

1.5. REFERENCES

1. Graham, T. The London, Edinburgh, and Dublin Philosophical Magazine and Journal of Science 1866, XXXII, 401-20.
2. von Wroblewski, S. Wied. Annalen der Physik 1879, 8, 29.
3. Mitchell, J.K. J. Royal Institution of Great Britain 1831, IV, 101-118.
4. Mitchell, J.K. J. Royal Institution of Great Britain 1831, V, 307-321.
5. Fick, A. Poggendorff's Annalen der Physik and Chemie 1855, 94, 59-86.
6. Kayser, H. Wied. Annalen der Physik 1891, 43, 544.
7. Paul, D.R. and W.J. Koros. J. Polym. Sci., Polym. Phys. Ed. 1976, 14, 675-85.
8. Koros, W.J.; M.R. Coleman; and D.R.B. Walker. Annu. Rev. Mater. Sci. 1992, 22, 47-89.
9. Koros, W.J.; G.K. Fleming; S.M. Jordan; T.H. Kim; and H.H. Hoehn. Prog. Polym. Sci. 1988, 13, 339-401.
10. Koros, W.J. and G.K. Fleming. J. Membr. Sci. 1993, 83, 1-80.
11. Robeson, L.M. J. Membr. Sci. 1991, 62, 165-85.
12. Ismail, A.F. and L.I.B. David. J. Membr. Sci. 2001, 193, 1-18.

13. Caro, J.; M. Noack; P. Kolsch; and R. Schafer. *Microporous and Mesoporous Matl.* 2000, 38, 3-24.
14. Vu, D.Q.; W.J. Koros; and S.J. Miller. *Ind. Engr. Chem. Res.* 2002, 41, 367-380.
15. Breck, D.W., *Zeolite molecular sieves: Structure, chemistry, and use.* 1974, Malabar, FL: Robert E. Krieger Publishing Co, Inc.
16. Mahajan, R., *Formation, characterization and modeling of mixed matrix membrane material.* Department of Chemical Engineering, University of Texas at Austin. 2000.
17. Tabe-Mohammadi, A. *Sep. Sci. Tech.* 1999, 34, 2095-2111.
18. Echt, W. *Hybrid systems; combining technologies leads to more efficient gas conditioning.* Laurance Reid gas Conditioning Conference. 2002.
19. Lee, A.L.; H.L. Feldkirchner; S.A. Stern; A.Y. Houde; J.P. Gamez; and H.S. Meyer. *Gas Sepn. Purification* 1995, 9, 35-43.
20. Lee, E.K. and W.J. Koros, *Membranes, synthetic, applications,* in *Encyclopedia of polymer science and technology.* 2002, Academic Press: New York. p. 279-344.
21. Chern, R.T.; W.J. Koros; E.S. Sanders; and R. Yui. *J. Membr. Sci.* 1983, 15, 157-69.
22. Funke, H.H.; K.R. Frender; K.M. Green; J.L. Wilwerding; B.A. Sweitzer; J.L. Falconer; and R.D. Noble. *J. Membr. Sci.* 1997, 129, 77-82.
23. Peterson, D. *Zeolites* 1981, 1, 105-12.

Chapter 2. THEORY AND BACKGROUND

The first part of this chapter introduces concepts essential to understanding gas permeation through membranes. Next, strategies for modeling the complex behavior of mixed matrix membranes are discussed. Section 2.3 builds on this discussion, showing how these models can be applied to select polymer – sieve combinations that yield improved membrane performance relative to the neat polymer matrix. The final section of this chapter provides a literature review of mixed matrix membranes.

2.1. TRANSPORT PROPERTY THEORY

2.1.1. Permeation

The permeability and selectivity of a material determine its potential as a gas separation membrane. Permeation in gas separation membranes occurs by the solution-diffusion mechanism [1]. A penetrant sorbs into the material, diffuses through it, and then desorbs at the other side. Mathematically, the permeability of penetrant A, P_A , is defined as the product of the average diffusion, \bar{D}_A , and sorption, \bar{S}_A , coefficients in the membrane:

$$P_A = \bar{D}_A \times \bar{S}_A \quad (2.1)$$

Diffusion and sorption are discussed separately in the following two subsections. The ideal selectivity, α_{AB} , or permselectivity, is the ratio of two permeabilities when the pressure on the permeate side of the membrane is zero:

$$\alpha_{AB} = \frac{P_A}{P_B} \quad (2.2)$$

Customarily, the permeability of the slower gas is used as the denominator, so selectivity is greater than or equal to one. This provides a basis to compare different

materials, since the permeabilities of a given penetrant, and hence the permselectivities, are intrinsic properties of homogeneous materials. Like other intrinsic properties of homogeneous materials, permeabilities (and permselectivities) are functions of temperature and pressure. The permselectivity is also convenient since new materials are typically first characterized with equipment that operates at essentially zero pressure on the permeate side (see section 3.4.1.)

Because sub-ambient pressure industrial operations are considered expensive, most real processes operate with a permeate pressure of at least 1 atm. Some processes are envisioned to operate at higher feed pressures with small pressure drops giving permeate pressures of a hundred or more atm to reduce recompression costs. In this case, the selectivity will typically differ from the permselectivity. In such cases, the separation factor is used in place of the permselectivity:

$$Separation\ Factor = \frac{x_{A,P} / x_{B,P}}{x_{A,F} / x_{B,F}} \quad (2.3)$$

Here x is a mole fraction, A and B refer to the gas components, and F and P indicate feed and permeate, respectively.

As stated in section 1.1.1, polymers are subject to a trade-off between permeability and selectivity. Originally developed as empirical relationships by Robeson [2], the trade-off curves have recently been given a theoretical basis by Freeman [3]. Robeson gives curves of the following form in terms of the empirical parameters k and n :

$$P_A = k \alpha_{AB}^n \quad (2.4)$$

Both Robeson and Freeman noted that the exponential parameter, n , is related to the size difference between the two penetrants A and B. The other parameter, k , depends

on the relative condensabilities of the two gases and polymer properties (e.g. interchain spacing and chain stiffness). The relative condensabilities of the two gases are fixed, leaving polymer structure as the main factor affecting transport properties that can be changed. Roughly, increasing interchain spacing will increase permeability and increasing chain stiffness will increase selectivity. However, once interchain spacing is increased beyond the point where diffusion is controlled by thermally induced motions, no additional increases in permeability can be obtained and the selectivity will decrease.

2.1.2. Diffusion

Although polymers and molecular sieving media both undergo solution-diffusion based permeation, diffusion in the two media proceeds via different mechanisms. Diffusion in each material is discussed below.

2.1.2.1. Diffusion in Polymers

Diffusion in polymers occurs via transient openings between polymer chains due to thermal fluctuations that enable small scale random displacements within the dense polymer matrix [4]. Because both the frequency and size of these fluctuations increase with temperature, the diffusion coefficient increases with temperature following an Arrhenius expression. This usually favors the larger molecule, so the diffusion selectivity typically decreases with temperature.

2.1.2.2. Diffusion in Molecular Sieving Materials

In contrast to polymers, diffusion in the type of molecular sieving media studied here (i.e. microporous, having dimensions similar to gas molecules) occurs by a pore “window” moderated mechanism [5]. In this case, however, negligible motion of the sieve is involved in the diffusion process. Between diffusional jumps, the penetrant molecules reside in the relatively open cylindrical “cages” of the zeolites. In a zeolite, the transition state occurs when the penetrant occupies the window between cages. There can be a substantial entropic selectivity when there is a size or shape difference

between two penetrants, because the number of allowed configurations in the transition state will be greater for the smaller penetrant [6]. More detailed discussions of the diffusion mechanisms for zeolites can be found elsewhere [5, 7, 8]. In contrast to zeolites, carbon molecular sieves have slit-like pores, but they still exhibit a transition state diffusion mechanism. In general, perfectly sized pore windows can provide a more selective discrimination than the random thermal fluctuations exhibited by polymers. Like polymers, molecular sieving materials exhibit increased diffusion coefficients and decreased diffusion selectivities as temperature is increased, and can be described by an Arrhenius expression.

2.1.3. Sorption

Although sorption in polymers and zeolites occur via different detailed mechanisms, both can be described with similar expressions, as demonstrated below. The sorption coefficient is defined as:

$$S = \frac{C}{p} \quad (2.5)$$

The following discussion is for pure component sorption. Multicomponent sorption is considered later in section 2.2.3.

2.1.3.1. Sorption in Polymers

According to the dual-mode model for sorption in polymers, molecules may sorb into one of two “modes” [9] comprising “dissolved”, or Henry’s Law regions, and “hole”, or Langmuir regions. The dual-mode model for penetrant “A” is expressed in terms of the Henry’s law coefficient, k_D , and the Langmuir sorption parameters: the affinity, b , and hole saturation, C_H' , constants:

$$C_A = k_{D,A} p_A + \frac{C'_{H,A} b_A p_A}{1 + b_A p_A} \quad (2.6)$$

Sorption roughly correlates with the fractional free volume of a polymer [10, 11]. The Langmuir mode occurs only in polymers below their glass transition temperatures, which have entrapped nonequilibrium “excess” free volume. The magnitude of the Langmuir saturation constant depends on the distance below the glass transition, as shown in Figure 2.1. The Henry’s law coefficient and Langmuir affinity constants both increase with penetrant condensability.

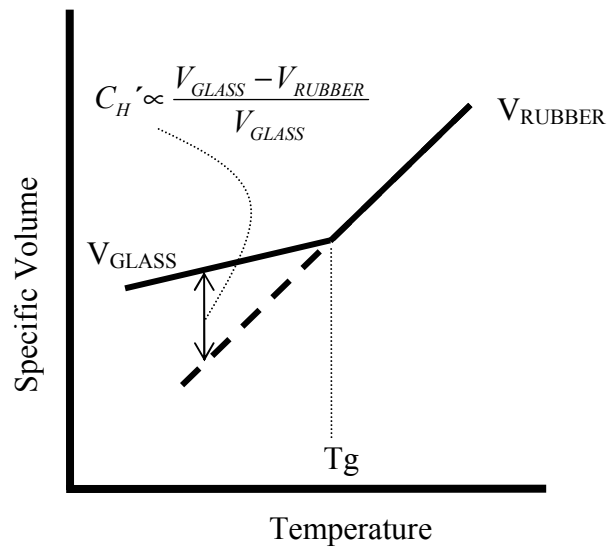


Figure 2.1: Sketch demonstrating the nature of the Langmuir mode in polymers.

Plasticization and *antiplasticization* are two other sorption-induced phenomena in polymers that merit brief mention. Swelling of a polymer occurs due to excessive sorption in the Henry’s law mode. This causes increased polymer chain mobility, leading to increased diffusion coefficients. This increase in diffusion coefficient, and hence permeability, is typically referred to as plasticization [12]. Plasticization is also accompanied by decreased selectivity. For the polymers considered here, swelling-induced plasticization is a concern for CO₂ at high pressure, although condensable contaminants may cause plasticization at lower pressures. Antiplasticization is signaled by *reduced* permeability and increased selectivity in the presence of low concentrations of plasticizing agents. The underlying cause is believed to be a stiffening of the matrix

caused by the high affinity of the plasticization agent for the matrix [13]. This may occur in polymers if a small amount of solvent remains after drying.

2.1.3.2. Sorption in Molecular Sieving Materials

Sorption in molecular sieves occurs at specific sites. Although Langmuir sorption in glassy polymers occurs at more-or-less fixed sites, these sites are randomly distributed throughout the polymer and their locations may slowly vary with time. Sorption in molecular sieves can be modeled using the same equation (Eq 2.6) as for polymers with k_D set equal to zero, since there is no “dissolved” mode in zeolites. Nonetheless, it may be necessary to account for energetic heterogeneity of the sorption sites (i.e. different sites can have different energies of adsorption). Each type of site will then have its own affinity and saturation constants. It has proven sufficient to model sieve sorption with a single site for the zeolites under the conditions used in this work.

2.1.4. Selective Surface Flow

Selective surface flow technology was first proposed and demonstrated by Rao and Sircar [14, 15]. In this phenomenon, the more condensable component of a multicomponent feed selectively adsorbs onto the surface of a microporous material. This is followed by surface diffusion of the adsorbed component. Because sorption of the more condensable (usually larger) component excludes the smaller component, a selective surface flow material is frequently selective for larger components. In contrast, molecular sieving materials are typically selective for smaller components.

2.2. MODELING STRATEGIES

Modeling the transport properties of mixed matrix membranes is important for three reasons: (i) to compare with experimental data, (ii) to better understand membrane morphology, and (iii) to serve as a predictive model for novel mixed matrix membranes. The first subsection details strategies for selecting a model that is both accurate and tractable. In section 2.2.2, this simple model is extended to encompass second-order

effects in mixed matrix membranes after Mahajan [16]. Finally, section 2.2.3 extends the model to multicomponent feeds. It is envisioned that this model will also be useful for predicting the effects of potential contaminants in real feed streams.

2.2.1. Selection of an Appropriate Model

Many of the models for transport properties of heterogeneous membranes were developed for the analogous situation of electronic conduction in heterogeneous materials. A generalized model for permeation through a heterogeneous membrane was presented by Petropoulos and later by Bouma [17, 18]:

$$\mathbf{P}_{mm} = \mathbf{P}_c \left[\frac{n \cdot \mathbf{P}_d + (1-n)\mathbf{P}_c - (1-n)\phi_d(\mathbf{P}_c - \mathbf{P}_d)}{n \cdot \mathbf{P}_d + (1-n)\mathbf{P}_c + n\phi_d(\mathbf{P}_c - \mathbf{P}_d)} \right] \quad (2.7)$$

where \mathbf{P}_{mm} is the effective permeability of a gas penetrant in a mixed matrix membrane with a volume fraction, ϕ_d , of dispersed phase (d) in a continuous matrix phase (c). \mathbf{P}_c and \mathbf{P}_d represent the permeabilities in the continuous and dispersed phases, and n is a shape factor for the dispersed phase, which varies from 0 to 1. The equation for modeling permeation through a parallel laminate is recovered by setting $n = 0$ (Eq 2.8), while $n = 1$ gives the equation for permeation through laminates in series (Eq 2.9). The series and parallel models bound the expected behavior of mixed matrix membranes.

$$\mathbf{P}_{mm} = \mathbf{P}_c(1 - \phi_d) + \phi_d\mathbf{P}_d \quad (2.8)$$

$$\mathbf{P}_{mm} = \frac{\mathbf{P}_c\mathbf{P}_d}{\mathbf{P}_d(1 - \phi_d) + \phi_d\mathbf{P}_c} \quad (2.9)$$

The equation for $n = 1/3$ corresponds to spherical particles, and is called Maxwell's equation in honor of James C. Maxwell, who first derived it in 1867 for a heterogeneous system of conducting spheres [19]. The mathematical expression is:

$$P_{mm} = P_c \left[\frac{P_d + 2P_c - 2\phi_d(P_c - P_d)}{P_d + 2P_c + \phi_d(P_c - P_d)} \right] \quad (2.10)$$

This expression appears to have first been applied to transport properties by Michaels for semicrystalline polymers [20], and it has been shown to work well for the permeability of two-phase membranes up to moderate dispersed phase loadings [17, 18, 21]. Other models were considered, but gave at best only a marginally better practical description of the results, with added mathematical complexity [17, 18]. These models are presented in Table 2.1. Thus, Maxwell's model is used in this work.

Table 2.1: Other models for permeation through heterogeneous media.		
Model	Equation	Source
Landauer Model (Effective Medium Theory)	$\sum_1^n \phi_d \left(\frac{P_{mm} - P_i}{2P_{mm} + P_i} \right) = 0$	[22, 23]
Bruggemann Model	$\left[\frac{P_{mm}/P_c - P_d/P_c}{1 - P_d/P_c} \right] \left(\frac{P_{mm}}{P_c} \right)^{-\frac{1}{3}} = 1 - \phi_d$	[24]
Higuchi Model	$P_{mm} = P_c \left[1 + \frac{3\phi_d}{\frac{P_d/P_c + 2}{P_d/P_c - 1} - \phi_d - 0.78 \frac{(1 - \phi_d)(P_d/P_c - 1)}{P_d/P_c + 2}} \right]$	[25, 26]

Maxwell's equation provides a basis for more complicated models discussed below. Nested applications of the Maxwell equation form the basis for a model of a three phase system, discussed in the next subsection, while the final subsection introduces the possibility of concentration dependent permeabilities.

2.2.2. Modeling Mixed Matrix Materials with “Zones of Influence” Surrounding the Dispersed Phase

The three-phase polymer, sieve, and potential interphase can be modeled as a pseudo two-phase system with the matrix polymer as one phase and the combined molecular sieve and interphase constituting the other, as shown in Figure 2.2. The combined sieve and interphase can be envisioned as a “pseudosieve” phase. These concepts were first proposed by Mahajan [16]. The interphase may be rigidified polymer, a void between the polymer and sieve, or a term representing surface diffusion on the sieve surface.

The Maxwell model can be used to obtain the permeability of the “pseudosieve” phase, P_{eff} , assuming the interphase is continuous and the molecular sieves are dispersed:

$$P_{eff} = P_I \left[\frac{P_d + 2P_I - 2\phi_s(P_I - P_d)}{P_d + 2P_I + \phi_s(P_I - P_d)} \right] \quad (2.11)$$

where P_d is the permeability of the sieve phase, P_I is the permeability of the interphase, and ϕ_s is the volume fraction of the sieve phase in the “pseudosieve” phase. The volume fraction ϕ_s is given by the following expression:

$$\phi_s = \frac{\phi_d}{\phi_d + \phi_I} = \frac{r_d^3}{(r_d + \ell_I)^3} \quad (2.12)$$

Here, ϕ_d and ϕ_I are the overall volume fractions in the membrane of the sieve phase and the interphase, respectively; r_d is the dispersed sieve radius; and the interphase thickness is denoted ℓ_I . As shown in Figure 2.2, the “pseudosieve” then becomes the dispersed phase in a second application of the Maxwell model, and along with the continuous polymer phase permeability, P_c , the permeability for three-phase mixed matrix membranes, P_{3MM} , is obtained:

$$P_{3MM} = P_M \left[\frac{P_{eff} + 2P_c - 2(\phi_d + \phi_I)(P_c - P_{eff})}{P_{eff} + 2P_c + (\phi_d + \phi_I)(P_c - P_{eff})} \right] \quad (2.13)$$

Thus, if the volume fraction and permeability of the interphase can be estimated, the Maxwell model can be extended to these more complicated systems.

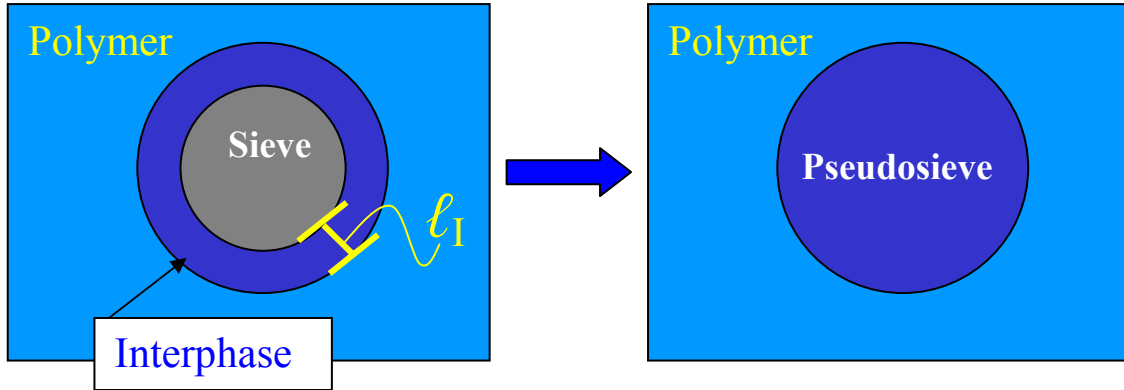


Figure 2.2: Cartoon showing the morphology of the polymer, sieve, and “interphase” used in the three phase Maxwell model.

2.2.2.1. “Matrix Rigidification”

In the “matrix rigidification” three phase Maxwell model, the interphase is assumed to be composed of rigidified polymer. Rigidification near the interface is a well documented phenomenon in organic – inorganic composites. Reduced mobility near the filler has been postulated as the cause of lower-than-predicted sorption in filled polymer systems [27], greater-than-expected increases in the modulus of filled polymer systems [28-30], and lower-than-predicted permeabilities in semicrystalline polymers [20]. Decreased mobility near the sieve would presumably lead to reduced permeability at the polymer – sieve interface. This would lead to reduced overall permeability of the mixed matrix membrane. The overall reduced permeability due to inhibited polymer mobility near the sieve surfaces would become more pronounced as the sieve loading increased, since a greater fraction of the matrix would be affected. Mahajan observed such a trend [31]. Rigidification has also been attributed to immobilization of polymer

chains due to adsorption on a surface. Similar effects occur in random ionomers [32], but these are generally limited to one persistence length, whereas the rigidified region in mixed matrix materials is believed to be up to 1 μm in some cases [27, 33].

If the permeability and the size of the rigidified region are known, the permeability of mixed matrix membranes exhibiting matrix rigidification can be calculated. The permeability of the polymer in the rigidified region near to the sieve is assumed to be decreased by a chain immobilization factor, β :

$$P_l = \frac{P_c}{\beta} \quad (2.14)$$

Permeability in the amorphous regions of semi-crystalline polymers is treated in a similar manner in the literature [20, 34, 35]. For oxygen and nitrogen, this parameter typically takes on a value of about three, although Michaels et al hypothesize that β should be a function of penetrant size [36]. Because the penetrants considered here (O_2 , N_2 , CO_2 , and CH_4) are all similarly sized, assuming a fixed value of β introduces little error. For matrix rigidification, β is greater than one, but it may be possible for “ β ” to be less than one. This corresponds to polymer near the interface that is more permeable than the bulk polymer. Potential causes of such behavior are discussed in section 5.1. The other parameter in the model, ℓ_l , is the size of the interphase, i.e., the distance from the sieve in which the polymer chains are less mobile. In practice, this parameter is varied to fit the experimental data. A more accurate determination of the interphase size can be made if membranes at multiple sieve loadings are prepared, since the interphase thickness should not vary with sieve loading provided the interphases of neighboring particles do not overlap.

2.2.2.2. “Sieve-in-a-Cage”

The term “sieve-in-a-cage” has been coined to describe polymer – sieve morphologies with voids at the interface. Figure 2.3 shows a SEM of zeolite 4A dispersed in Udel[®]

(Solvay Advanced Polymers; Alpharetta, GA) polysulfone, which has sieve-in-a-cage morphology. This morphology is undesirable, since the void is much more permeable than the zeolite. In mixed matrix membranes, this leads to permeabilities greater than and selectivities equal to or lower than the matrix polymer in a morphology that is difficult to duplicate in a hollow fiber skin layer. If the void is similar in size to the gas molecules, it is selective for the lighter gas, leading to O_2/N_2 and CO_2/CH_4 selectivities *lower* than the neat polymer [37]. Although undesirable, it is important to model sieve-in-a-cage behavior to better understand membrane morphology.

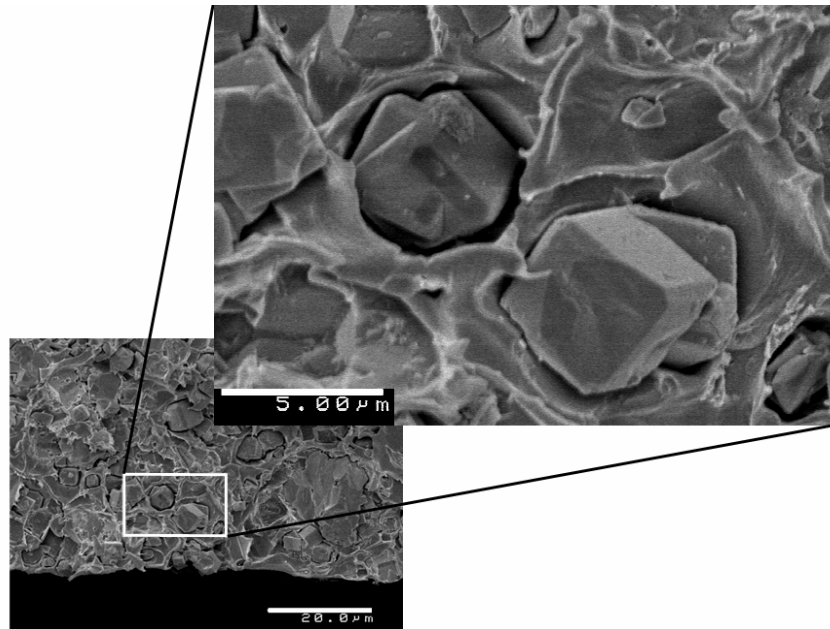


Figure 2.3: Zeolite 4A dispersed in Udel[®] showing “sieve-in-a-cage” morphology.

The permeability of the void in sieve-in-a-cage membranes is the product of effective diffusion and solubility coefficients. Assuming the penetrant in the void acts as an ideal gas, the solubility is fixed:

$$S \sim \frac{C}{p} = \frac{\frac{n}{V}}{p} = \frac{1}{RT} = 0.012 \frac{cm^3 STP}{cm^3 \cdot cmHg} \quad (2.15)$$

For very small voids, this equation must be modified to account for the finite size of the penetrant. The following equation has been suggested for the Henry's law constant for finite sized molecules of penetrant "A" in a small pore [38]:

$$S_A = \frac{C_A}{p_A} \left(1 - \frac{\sigma_A}{2r_p}\right)^2 = \frac{1}{RT} \left(1 - \frac{\sigma_A}{2\ell_I}\right)^2 \quad (2.16)$$

where σ_A is the Lennard-Jones collision diameter of penetrant "A", r_p is the radius of the pore, and ℓ_I is the thickness of the void between the two phases. The hydraulic diameter, d_H , of the void is used to relate the pore radius in Eq 2.16 to the void thickness. Assuming the void width is much greater than the void thickness ($w \gg \ell_I$):

$$2r_p = d_H = 4 \frac{\text{area}_{\text{CROSS SECTION}}}{\text{perimeter}} = 4 \frac{\ell_I w}{2\ell_I + 2w} \cong 2\ell_I \quad (2.17)$$

Diffusion through the void is assumed to fall within the Knudsen regime because of the small thickness of the void. Knudsen diffusion is given by the empirical equation [39]:

$$\begin{aligned} D &= \frac{0.97 \times 10^{-5} \text{ cm}^2 \cdot (\text{g/mol})^{1/2}}{s \cdot \text{\AA} \cdot \text{K}^{1/2}} \sqrt{\frac{T}{M_p}} r_p \\ &= \frac{0.97 \times 10^{-5} \text{ cm}^2 \cdot (\text{g/mol})^{1/2}}{s \cdot \text{\AA} \cdot \text{K}^{1/2}} \sqrt{\frac{T}{M_p}} \ell_I \end{aligned} \quad (2.18)$$

where M_p is the molecular weight of the penetrant (g/mol), T is the absolute temperature (K), and the pore radius (\AA) has again been replaced by $1/2$ the hydraulic diameter. This expression must also be modified to account for the finite size of the penetrant [40]:

$$\begin{aligned} D &= \frac{0.97 \times 10^{-5} \text{ cm}^2 \cdot (\text{g/mol})^{1/2}}{s \cdot \text{\AA} \cdot \text{K}^{1/2}} \sqrt{\frac{T}{M_p}} r_p \left(1 - \frac{\sigma_p}{2r_p}\right) \\ &= \frac{0.97 \times 10^{-5} \text{ cm}^2 \cdot (\text{g/mol})^{1/2}}{s \cdot \text{\AA} \cdot \text{K}^{1/2}} \sqrt{\frac{T}{M_p}} \ell_I \left(1 - \frac{\sigma_p}{2\ell_I}\right) \end{aligned} \quad (2.19)$$

In addition to the permeability of the void, the other parameter in the three-phase Maxwell model for “sieve-in-a-cage” is the void thickness. In practice, the model is usually fit to the permeation results with void thickness as an adjustable parameter. For mixed matrix membranes with voids larger than a few nanometers, scanning electron microscopy can give an estimate of the size of the average void. However, Ångstrom-sized voids are below the resolution of the SEM, so TEM must be used to independently determine void size. Ångstrom sized voids turn out to be an important case of sieve-in-a-cage morphology since such voids can actually lead to mixed matrix selectivities lower than the neat polymer. In practice, it is difficult to get an accurate representation of the average void thickness using either SEM or TEM because of sample preparation artifacts and the difficulty of averaging from just a few images.

2.2.3. Modeling of Multicomponent Permeation in Mixed Matrix Membranes

More complex effects (e.g. competition [41], frame-of-reference effects [42], plasticization [43]) may be present with multicomponent feeds, and appropriate models can be developed to account for them. Such models can be used with one of the equations discussed in section 2.2.1 to calculate the permeability and selectivity of multicomponent feeds through mixed matrix membranes.

2.2.3.1. Modeling of Multicomponent Sorption in Polymers and Zeolites

The dual-mode model (Eq 2.20) provides a convenient framework to describe sorption of multicomponent mixtures in polymers and zeolites. In zeolites, the Henry’s law term (k_{D,AP_A}) is zero. Sorption in the Henry’s law mode of the polymer is assumed to be unaffected by the presence of other components. Mathematically, these ideas are embodied by the following expression:

$$C_A = k_{D,A} p_A + \frac{C'_{H,A} b_A p_A}{1 + \sum_i^N b_i p_i} \quad (2.20)$$

The only difference between this and the pure component dual-mode expression (Eq 2.6) is the term accounting for the affinities and partial pressures of other components in the denominator of the Langmuir isotherm. Eq 2.20 assumes the pure gas and multicomponent affinity and saturation constants are the same. A more general treatment would require that these constants be determined either from mixed gas permeation or sorption experiments, which can be difficult.

2.2.3.2. Modeling of Concentration Dependent Diffusion in Polymers and Zeolites

The concentration dependence of the diffusion coefficient in polymers can be determined from permeation and sorption measurements. Diffusion in polymers is assumed to occur either through the dissolved mode, D_D , or through the hole mode, D_H . Local equilibrium is assumed due to exchange ability between the two populations. In this case, the dual-mode expression for permeation of penetrant “A” is:

$$P_A = k_{D,A} D_{D,A} \left(1 + \frac{\frac{D_{H,A} C'_{H,A} b_A}{D_{D,A} k_{D,A}}}{1 + b_A p_A + b_B p_B} \right) \quad (2.21)$$

In zeolites, the diffusion coefficient is a function of pressure, frequently modeled as:

$$D_A = D_{0,A} \frac{\partial \ln p_A}{\partial \ln C_A} \quad (2.22)$$

where $D_{0,A}$ is the diffusion coefficient of penetrant “A” at infinite dilution. In order to estimate the transport properties of multicomponent feeds in mixed matrix membranes,

the infinite dilution diffusion coefficient of each penetrant can be assumed equal to that of a pure gas. The pure gas Langmuir equation is used for the concentration in the denominator of Eq 2.22. The average diffusion coefficient using Eq 2.22 is:

$$\bar{D}_A = \frac{D_{0,A}}{\frac{C_A}{C'_{H,A}}} \text{Ln} \left(\frac{C'_{H,A}}{C'_{H,A} - C_A} \right) = \frac{D_{0,A}(1+b_A p_A)}{b_A p_A} \text{Ln}(1+b_A p_A) \quad (2.23)$$

More complex equations to better describe diffusion in zeolites with multicomponent feeds have been developed [8, 44-46]; however, at present, sufficient data to determine the parameters in these equations do not exist.

Once the sorption and diffusion coefficients for both the polymer and zeolite have been calculated, the permeability of each is determined using Eq 2.1 and then Maxwell's equation is used to calculate the permeability of the mixed matrix membrane. Of course, the accuracy of this calculation depends on the validity of the assumptions behind Eq 2.20 through Eq 2.23. The modeling strategies developed in this section are useful for selecting polymer – sieve pairs that are expected to show improved transport properties. More fundamental selection criteria are discussed in the following section.

2.3. POLYMER-SIEVE SELECTION CRITERIA

Three properties of a zeolite should be considered when selecting an insert phase. The most obvious property is the pore size of the zeolite. The IUPAC breaks porous materials into three classes: macroporous ($r_p > 200 \text{ \AA}$), mesoporous ($20 \text{ \AA} < r_p < 200 \text{ \AA}$), and microporous ($r_p < 20 \text{ \AA}$). Clearly for gases of the dimensions shown in Table 2.2, a microporous zeolite is required to achieve transport properties beyond the Knudsen regime (Eq 2.18). Several representations of molecular size have been given in Table 2.2, since the dimensions are dependent on how the space occupied by a molecule is defined. The effect of zeolite pore size is illustrated in Figure 2.4, which shows the expected O_2/N_2 diffusion selectivity as a function of pore size after

accounting for the finite size of the penetrants (Eq 2.19). Note that for pore radii greater than about 5 Å, the pore shows essentially Knudsen selectivity, where nitrogen diffusion is *faster* than oxygen. Furthermore, in order to achieve high selectivities, it is necessary to select a material that acts as a molecular sieve for the gas pair to be separated. For example, silicalite is a poor choice for separating O₂ and N₂ since it has a minimum pore diameter of 5.2 Å [47], greater than the size of all the molecules in Table 2.2. Zeolite 4A is a good choice because it has a pore size through which oxygen can diffuse unabated, while nitrogen must forgo a degree of freedom to transit the pore. A second, less obvious criterion is that the dimensionality of the pore system must be considered. For zeolites with one-dimensional pore systems, such as AlPO₄-5, only pores parallel to the direction of gas flow are expected to contribute to the flux [48, 49]. One-dimensional zeolites can also undergo single file diffusion mechanisms in their pores, meaning diffusion occurs only as fast as the slowest gas [48, 49]. Similarly, zeolites with two-dimensional pore systems, such as silicalite and ZSM-5, can also display anisotropic effects [50]. Three-dimensional zeolites are ideally suited to mixed matrix membranes, since it is unnecessary to orient the pores to achieve enhanced transport properties. A third property of zeolites that may affect transport behavior is the porosity. Zeolites with more open structures are expected to have higher permeabilities. A proper pore size and a three dimensional pore structure are probably more important than porosity, however.

Table 2.2: Size of the penetrants used in this work. The source is given in brackets.

		CH ₄	CO ₂	N ₂	O ₂
Collision Diameter, Å		3.8 [5]	3.3 [5]	3.64 [5]	3.46 [5]
Spherocylindrical Potential	Length, Å			4.07 [51]	3.75 [52]
	Width, Å			3.09 [51]	2.68 [52]
95% Charge Density	Length, Å			3.87 [53]	3.72 [53]
	Width, Å			3.01 [53]	2.82 [53]

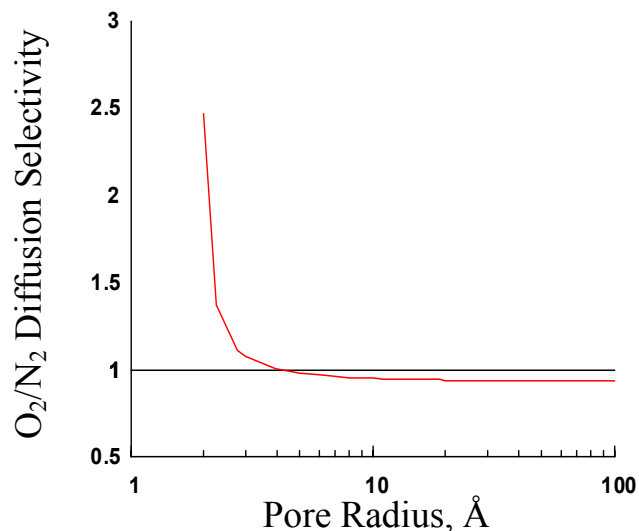


Figure 2.4: O₂/N₂ diffusion selectivity as a function of pore size calculated using Eq 2.19.

The three zeolite structural parameters discussed in the preceding paragraph relate to diffusive properties, but the permeability is also affected by sorption. There are some basic “rules of thumb” to consider that influence sorption. In addition to the properties of the penetrant such as condensability, the affinity to the sorbent is an important parameter affecting sorption. There is evidence of specific affinities for sorbates to polymers, (e.g. CO₂ to basic polymers such as PMMA [54]), and such effects can be even more pronounced in zeolites. Polar molecules such as water have very high affinities for certain molecular sieves. For example, molecular sieves that have substantial aluminum content tend to have greater affinities for polar sorbates because aluminum requires a counterion to balance charge. Although not as strongly held as water, carbon dioxide also has a high affinity for zeolites. Even molecules such as nitrogen can have significant affinities because of their quadrupole moments. This is why N₂ has a higher sorption coefficient than O₂ in zeolites, in contrast to polymers.

With this understanding of these qualitative concepts, a more rigorous treatment using models presented in the previous section can be applied to optimize polymer – sieve

combinations. Figure 2.5 illustrates the use of Maxwell's equation (Eq 2.10) to calculate the properties of potential mixed matrix membranes. It is apparent that a maximum exists in the expected selectivity increase when the polymer permeability is slightly less than the sieve permeability. Other models from Table 2.1 also predict this maximum. This maximum roughly corresponds to matching the permeability of the fast gas (oxygen) in the two phases, so it can permeate through either phase without impairment. The slow gas experiences a longer path length because it is more likely to permeate around the zeolite. Thus, it is unwise to select a polymer far more permeable than the zeolite. This situation corresponds to the right hand side of Figure 2.5. In this case, zeolite 4A is two orders of magnitude less permeable than the polymer, resulting in a *decrease* in permeability relative to the neat polymer with no discernable increase in selectivity. This is indicated by the arrow extending from 100 Barrer on the figure. On the other hand, choosing a polymer on the left side of Figure 2.5 needlessly limits the overall permeability of the mixed matrix membrane. This concept of matching the fast-gas permeabilities of the polymer and sieve was first qualitatively identified by Kulprathipanja [55] and later explained by Zimmerman [56].

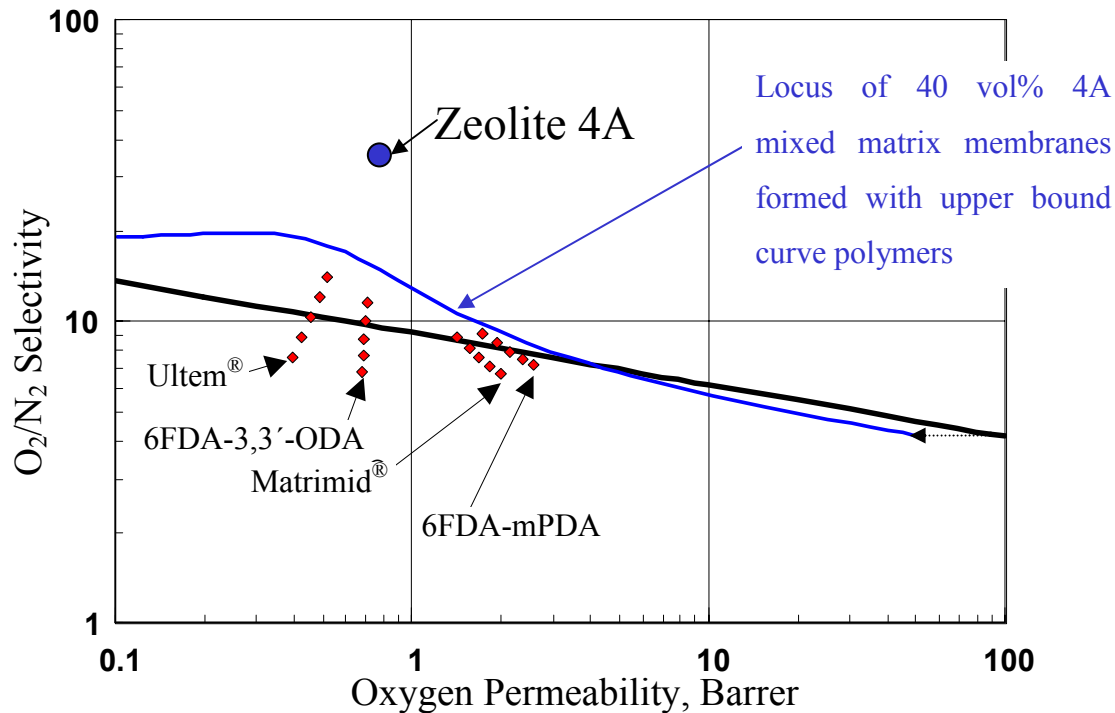


Figure 2.5: The use of the Maxwell model for the selection of optimal polymer – sieve combinations. The blue curve represents the calculated performance of hypothetical mixed membranes prepared with 40 vol% zeolite 4A dispersed in each of the polymers along the upper bound (black line). Red diamonds represent calculations with real polymers. The lowest diamond represents the neat polymer and subsequent diamonds represent increases of 10 vol% zeolite 4A dispersed in each polymer up to 40 vol%.

2.4. A LITERATURE REVIEW OF MIXED MATRIX MEMBRANES

Organic – inorganic materials have been studied for some time; however, their application to membranes is a more recent development with most work occurring in the past 10-15 years. The first known application of mixed matrix materials to transport was reported in 1960 by Barrer and James [57, 58]. They dispersed zeolites in polymeric binders for use as cation exchange membranes. They noted that voids formed between the two phases, which filled with electrolyte solutions causing reduced performance. This problem could be temporarily resolved by filling the voids with an inert liquid or by preparing the membranes via in situ polymerization, but performance

suffered over time, presumably due to degradation of the interface [57]. The interface is still the limiting factor in mixed matrix technology.

Paul and Kemp prepared membranes comprised of zeolite 5A dispersed in silicone rubber to demonstrate the effect of immobilizing sorption on permeation [59]. Using both sorption and permeation experiments, they found the time lag increased dramatically upon addition of the zeolites, but the steady state permeability changed little. The lack of improved permeability can probably be attributed the pore size of zeolite 5A, which is too large to discriminate between the gases used by Paul and Kemp. This work was done before the importance of proper pore size was understood.

There have been many attempts to add impermeable fillers into polymers to affect their transport properties. Typically, impermeable fillers are only useful in barrier applications, since they cause permeabilities lower than the neat polymer, in the case of good polymer – filler interfaces, or introduce non-selective voids in the case of poor polymer – filler interfaces. The barrier application has been known for some time [60, 61] and it is not discussed further here. However, there are some ways impermeable fillers could positively affect membrane performance:

1. by acting as crosslinking sites for the polymer matrix to inhibit plasticization of the membrane under challenging feed conditions [62, 63]
2. by introducing voids at the interface, a highly condensable feed should condense into the pores, causing increased permeability through the membrane [64]
3. by introducing a nanoscopic insert that modifies the free volume distribution of the polymer to change its intrinsic transport properties [63-65]

The focus of this review will be on membranes with *permeable* inserts. Furthermore, this review is broken into two parts. The first will discuss membranes prepared with rubbery polymers, where improvements in transport properties are frequently observed,

provided the polymer and insert have matched transport properties. The next subsection will discuss mixed matrix membranes prepared with glassy polymers. Only recently have successful membranes lacking voids at the polymer – sieve interface been demonstrated with glassy polymers.

2.4.1. Mixed Matrix Membranes Prepared with Rubbery Matrices

Membranes prepared with rubbery matrices or tested under conditions where the matrix is rubbery have been more successful than their glassy polymer counterparts. This is because rubbery polymers, in general, lead to better (void – free) interfaces. The reason for this is explained in Chapter 4. Poly(dimethyl siloxane) (PDMS) was a common matrix. Silicalite, with its hydrophobic interior, was added to PDMS to improve the alcohol – water selectivity [66, 67]. Bartels-Caspers et al reported that it may be possible to separate alcohol – water mixtures using PDMS filled with ZSM-5 zeolite, which also has a hydrophobic interior [68]. This conclusion was based on sorption data, as they reported no transport data. Zeolites with hydrophilic interiors did not demonstrate increased alcohol – water selectivity in PDMS. Dotremont et al studied pervaporation of halogenated hydrocarbon – water mixtures through PDMS filled with various zeolites [69]. They found that silicalite improved the selectivity, while more hydrophilic zeolites did not. Vankelecom et al investigated carbon molecular sieve filled PDMS for the separation of alcohol – water and aromatic hydrocarbon – water separations [70]. No selectivity improvement in the alcohol – water system was observed because of excess swelling of the matrix. This is in contrast to the results for zeolite filled PDMS, where it was thought that the zeolites provide crosslinking sites for the matrix [71]. On the other hand, the carbons did improve selectivity relative to neat PDMS for the aromatic hydrocarbon – water system where swelling is less of a concern.

Fewer papers have reported gas separation properties of zeolite filled rubbery polymers. Jia et al reported improved O₂/N₂ selectivities for silicalite filled PDMS [72]. Duval et al found no improvement with zeolite 5A filled materials, and they attributed this to

either adsorbed water in the pores of zeolite 5A or strong adsorption in 5A such that permeation is very slow [73]. However, they found improvement in the CO₂/CH₄ selectivity for silicalite and zeolite Y filled membranes. Larger improvements were observed for zeolite Y, with the highest selectivity of ~35 observed for a 50% zeolite Y filled nitrile-butadiene rubber. Modest improvements in O₂/N₂ selectivity from 2.1 to 2.6 and from 3 to 4.7 were reported for ~50% silicalite filled PDMS and EPDM rubber membranes, respectively. Duval et al also reported improvements in O₂/N₂ selectivity for CMS filled materials.

Selected results from references [72] and [73] are plotted in Figure 2.6 on the O₂/N₂ and CO₂/CH₄ upper-bounds. While the improvements relative to the respective neat polymers are impressive, the transport properties are in many cases not as good as commercially available glassy polymers. Except at the highest loadings, the membranes are well below the upper-bound. Furthermore, glassy polymers can be spun into hollow fiber morphologies to achieve favorable economics, whereas this is much more difficult with a rubbery polymer. Thus, researchers have focused on a way to prepare mixed matrix membranes with glassy polymers, and that is discussed next.

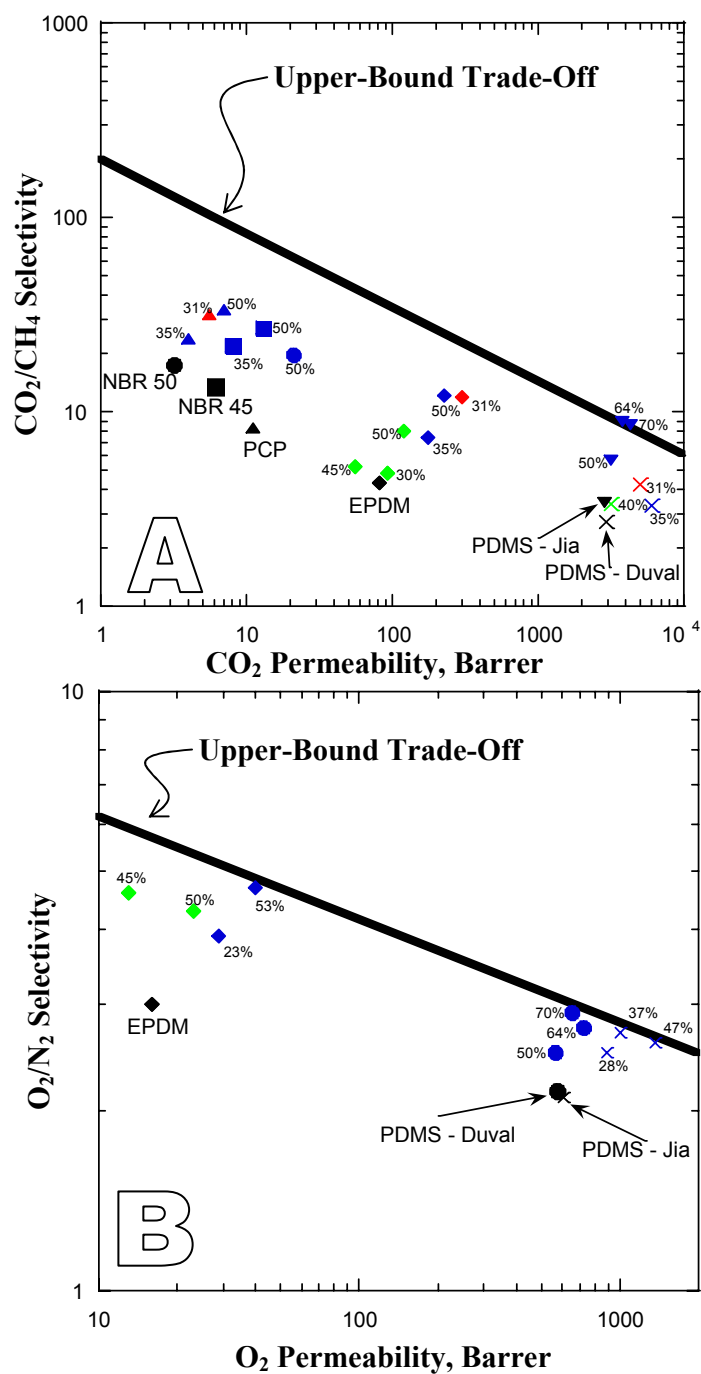


Figure 2.6: (a) CO₂/CH₄ and (b) O₂/N₂ transport properties for mixed matrix membranes based on rubbery polymer matrices reported in [72, 73]. Shapes denote polymer matrix. Colors denote insert phases (black – neat polymer; blue – silicalite; red – zeolite KY; green – one of three CMS materials). The insert loading is noted next to each data point.

2.4.2. Mixed Matrix Membranes Prepared with Glassy Matrices

The incorporation of inserts into glassy polymer membranes has proven much more difficult than for the rubbery counterparts. The first glassy polymer reference is a patent from UOP showing selectivity improvement over neat cellulose acetate by inclusion of silicalite [55]. However, Duval et al reported no improvement in transport properties upon inclusion of silicalite into cellulose acetate ($T_g = 80^\circ\text{C}$), Ultem[®] ($T_g = 210^\circ\text{C}$), or poly(4-methyl-1-pentene) ($T_g=36^\circ\text{C}$) [74]. These poor results were attributed to voids at polymer – sieve interfaces. A number of innovative techniques were attempted to improve properties, without success, including: silanation of the zeolites to improve adhesion with the polymer, preparation of the membranes above the T_g of the polymer matrix (poly(4-methyl-1-pentene) matrix), extended sub- T_g annealing (Ultem[®] at 150°C for 4 weeks), and compression of the membranes above the T_g [74]. Improvements in interfacial morphology were noted in the latter case, although the membranes were reported “damaged” after heat treatment so transport properties were not measured. The authors postulated that successful mixed matrix membranes can be prepared using silane treated zeolites to promote adhesion and casting at high temperatures where the polymer is flexible. Unfortunately, no additional work on this subject has appeared by these authors since this publication. Gür prepared membranes of zeolite 13X dispersed in polysulfone with good morphologies using melt processing [75]. Zeolite 13X has a pore size larger than the gases studied, so no improvement in properties relative to the neat polymer could be expected and none was observed. Sür reported modest improvements in selectivity with polyethersulfone ($T_g = 225^\circ\text{C}$) filled with zeolites 13X and 4A, especially at higher loadings [76]. Vankelecom reported that polyimide-based mixed matrix membranes filled with borosilicate, silicalite, or zeolite Y exhibited voids at the polymer – sieve interfaces [77]. No gas permeation data were given, although modest improvements in the selectivities for xylene isomers were reported in pervaporation experiments. However, xylenes may condense in the voids at polymer – sieve interfaces, limiting the effect of

sieve bypassing. Vankelecom also suggested silanation to improve the morphology of the polymer – zeolite interface [78], however, no gas permeation data were reported and this is the most recent work in the area by this group.

In 1997, a significant development was the application of models for the transport properties of heterogeneous systems to mixed matrix membranes allowing performance with a given filler to be predicted [56]. Without a model to predict these properties, researchers had no way to know whether lack of improvement was the result of poor morphologies or a fundamental incompatibility between the transport properties of the two phases. Soon thereafter, Zimmerman et al also published criteria for selecting molecular sieves and suitably compatible polymers for a given separation to yield a substantial mixed matrix effect [79] (see section 2.3). In 2000, improvements in transport properties relative to the neat polymer consistent with predicted behavior were demonstrated, and a new phenomenon dubbed “matrix rigidification” was identified [16] (see section 2.2.2.1). Subsequently, a number of approaches to successfully prepare mixed matrix membranes with glassy matrices have been applied, including: addition of a plasticizer to the matrix [80], preparation at high temperature with silanated zeolites [81], the use of matrices with specific groups that react with the zeolites [81], and the use of inserts that are more compatible with the polymer matrices (e.g. carbon molecular sieves) [82, 83].

Yong et al used 2,4,6-triaminopyrimidine to induce crosslinking of the matrix, demonstrating a small improvement in selectivity [84]. However, so much crosslinker was added that the matrix permeability decreased by a factor of over 40. Wang et al reported increased selectivity upon inclusion of nanocrystals of zeolite 4A into Udel[®] [85], however the authors also suggested that the nanocrystals may have altered polymer chain packing, affecting the base properties of the polymer matrix.

Figure 2.7 shows selected data reported for mixed matrix membranes prepared with glassy polymer matrices. Substantial improvements in transport properties relative to

the polymer matrices are evident, especially for carefully prepared membranes with zeolite 4A inserts (Figure 2.7a). Some membranes show only increased permeabilities relative to the polymer matrix, indicative of sieve-in-a-cage morphology, including zeolite 4A dispersed in Matrimid[®] (Figure 2.7a) and silicalite or zeolite Y dispersed in Ultem[®] (not shown). In other cases, little or no improvement is observed relative to the polymer matrix because of the poor choice of zeolite (Figure 2.7c).

Despite these advances, a continuing problem is the inability to *reproducibly* prepare membranes from polymer – sieve combinations that should show improved transport properties. It is unclear whether fundamental incompatibilities between the two phases exist or whether membrane preparation conditions cause the poor performance. This work seeks to address this problem.

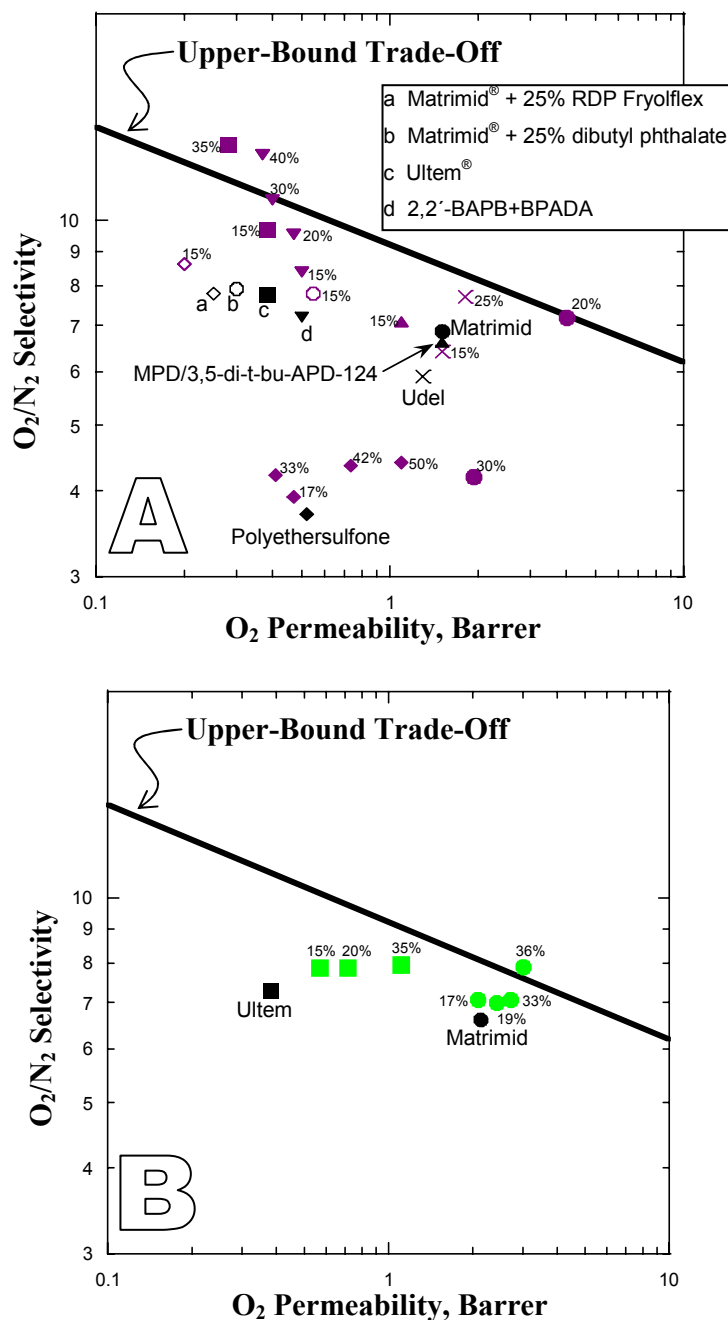


Figure 2.7: (a) O_2/N_2 (with zeolite 4A inserts) (b) O_2/N_2 (with CMS inserts) (c) O_2/N_2 (with zeolite 13X inserts) and (d) CO_2/CH_4 transport properties for mixed matrix membranes based on glassy polymer matrices reported in [74-76, 80, 81, 83-85]. Shapes denote polymer matrix. Colors denote insert phases (black – neat polymer; blue – silicalite; green – CMS; purple – zeolite 4A; turquoise – zeolite 13X).

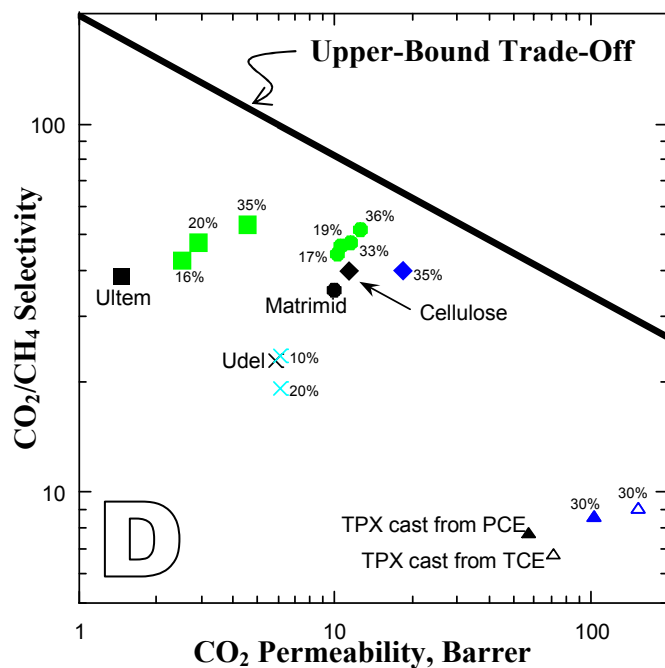
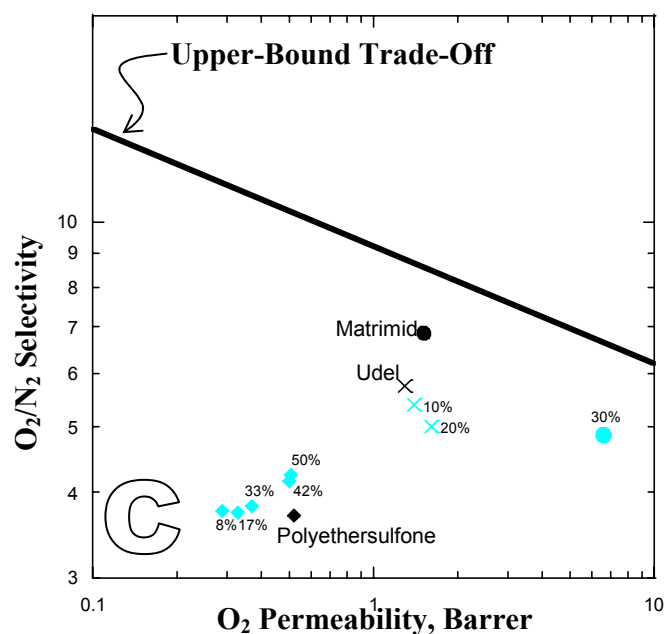


Figure 2.7: (a) O_2/N_2 (with zeolite 4A inserts) (b) O_2/N_2 (with CMS inserts) (c) O_2/N_2 (with zeolite 13X inserts) and (d) CO_2/CH_4 transport properties for mixed matrix membranes based on glassy polymer matrices reported in [74-76, 80, 81, 83-85]. Shapes denote polymer matrix. Colors denote insert phases (black – neat polymer; blue – silicalite; green – CMS; purple – zeolite 4A; turquoise – zeolite 13X).

2.5. REFERENCES

1. Wijmans, J.G. and R.W. Baker. *J. Membr. Sci.* 1995, 107, 1-21.
2. Robeson, L.M. *J. Membr. Sci.* 1991, 62, 165-85.
3. Freeman, B.D. *Macromolecules* 1999, 32, 375-380.
4. Koros, W.J. and G.K. Fleming. *J. Membr. Sci.* 1993, 83, 1-80.
5. Breck, D.W., *Zeolite molecular sieves: Structure, chemistry, and use.* 1974, Malabar, FL: Robert E. Krieger Publishing Co, Inc.
6. Singh, A. and W.J. Koros. *Ind. Eng. Chem. Res.* 1996, 35, 1231-4.
7. Shelekhin, A.B.; A.G. Dixon; and Y.H. Ma. *AIChE J.* 1995, 41, 58-67.
8. Karger, J. and D. Ruthven, *Diffusion in zeolites.* 1992, New York: John Wiley and Sons.
9. Paul, D.R. and W.J. Koros. *J. Polym. Sci., Polym. Phys. Ed.* 1976, 14, 675-85.
10. Ganesh, K.; R. Nagarajan; and J.L. Duda. *Ind. Eng. Chem. Res.* 1992, 31, 746-55.
11. Jordan, S.S. and W.J. Koros. *Macromolecules* 1995, 28, 2228-35.
12. Petropoulos, J.H. *J. Membr. Sci.* 1992, 75, 47-59.
13. Maeda, Y. and D.R. Paul. *J. Membr. Sci.* 1987, 30, 1-9.
14. Rao, M.B. and S. Sircar. *J. Membr. Sci.* 1993, 85, 253-64.
15. Sircar, S.; M.B. Rao; and C.M.A. Thaeron. *Sepn. Sci. and Tech.* 1999, 34, 2081-2093.
16. Mahajan, R. and W.J. Koros. *Ind. Eng. Chem. Res.* 2000, 39, 2692-2696.
17. Bouma, R.H.B.; A. Checchetti; G. Chidichimo; and E. Drioli. *J. Membr. Sci.* 1997, 128, 141-149.
18. Petropoulos, J.H. *J. Polym. Sci., Polym. Phys. Ed.* 1985, 23, 1309-24.
19. Maxwell, J.C., *A treatise on electricity and magnetism. Vol. 1.* 1873, Oxford: Clarendon press.

20. Michaels, A.S. and R.B. Parker, Jr. *J. Polym. Sci.* 1959, 41, 53-71.
21. Fricke, H. *Physica (The Hague)* 1931, 1, 106-15.
22. Landauer, R. *J. Appl. Phys.* 1952, 23, 779-84.
23. Davis, H.T. *J. Am. Ceram. Soc.* 1977, 60, 499-501.
24. Bruggemann, D.A.G. *Annalen der Physik V* 1935, 24, 636.
25. Higuchi, W.I. *J. Phys. Chem.* 1958, 62, 649-53.
26. Higuchi, W.I. and T. Higuchi. *J. Am. Pharm. Assoc., Sci. Ed.* 1960, 49, 598-606.
27. Manson, J.A. and E.H. Chiu. *J. Polym. Sci., Polym. Symp.* 1973, No. 41, 95-108.
28. Galperin, I. and T.K. Kwei. *J. Appl. Polym. Sci.* 1966, 10, 673-80.
29. Kwei, T.K. and C.A. Kumins. *J. Appl. Polymer Sci.* 1964, 8, 1483-90.
30. Manson, J.A. and L.H. Sperling, *Polymer blends and composites.* 1976, New York: Plenum Press.
31. Mahajan, R., *Formation, characterization and modeling of mixed matrix membrane materials.* Department of Chemical Engineering, University of Texas at Austin. 2000.
32. Eisenberg, A.; B. Hird; and R.B. Moore. *Macromolecules* 1990, 23, 4098-107.
33. Moore, T.T.; R. Mahajan; D.Q. Vu; and W.J. Koros. *AIChE J.* 2004, 50, 311-21.
34. Michaels, A.S. and H.J. Bixler. *J. Polym. Sci.* 1961, 50, 393-412.
35. Michaels, A.S.; W.R. Vieth; and J.A. Barrie. *J. Appl. Phys.* 1963, 34, 13-20.
36. Michaels, A.S. and H.J. Bixler. *J. Polym. Sci.* 1961, 50, 413-39.
37. Mahajan, R. and W.J. Koros. *Polym. Engr. and Sci.* 2002, 42, 1420-1431.
38. Ferry, J.D. *Journal of General Physiology* 1936, 20, 95-104.
39. Knudsen, M. *Annalen der Physik* 1909, 28, 75-130.

40. Suh, S.H. and J.M.D. MacElroy. *Mol. Phys.* 1986, 58, 445-73.
41. Costello, L.M. and W.J. Koros. *Ind. Eng. Chem. Res.* 1993, 32, 2277-80.
42. Kamaruddin, H.D. and W.J. Koros. *J. Membr. Sci.* 1997, 135, 147-159.
43. Ismail, A.F. and W. Lorna. *Sepn. Purification Tech.* 2002, 27, 173-194.
44. Krishna, R. and D. Paschek. *Sepn. Purification Tech.* 2000, 21, 111-136.
45. Krishna, R. *Intl. Comm. in Heat and Mass Transfer* 2001, 28, 337-346.
46. Chen, Y.D.; R.T. Yang; and L.M. Sun. *Chem. Engr. Sci.* 1993, 48, 2815-16.
47. Flanigen, E.M.; J.M. Bennett; R.W. Grose; J.P. Cohen; R.L. Patton; R.M. Kirchner; and J.V. Smith. *Nature* 1978, 271, 512-16.
48. Hahn, K.; J. Kaerger; and V. Kukla. *Phys. Rev. Lett.* 1996, 76, 2762-5.
49. Sholl, D.S. and K.A. Fichthorn. *J. Chem. Phys.* 1997, 107, 4384-4389.
50. Caro, J.; M. Noack; P. Kolsch; and R. Schafer. *Microporous and Mesoporous Matl.* 2000, 38, 3-24.
51. Hirschfelder, J.O.; C.F. Curtiss; and R.B. Bird, *Molecular theory of gases and liquids.* 1954, New York: John Wiley & Sons, Inc.
52. Bussery, B. and M. Aubert-Frecon. *Chem. Phys. Lett.* 1991, 179, 393-7.
53. Bader, R.F.W.; W.H. Henneker; and P.E. Cade. *J. Chem. Phys.* 1967, 46, 3341-63.
54. Kazarian, S.G.; M.F. Vincent; F.V. Bright; C.L. Liotta; and C.A. Eckert. *J. Am. Chem. Soc.* 1996, 118, 1729-36.
55. Kulprathipanja, S.; R.W. Neuzil; and N.N. Li, Separation of fluids by means of mixed matrix membranes. US Patent No. 697,990. 1988.
56. Zimmerman, C.M.; A. Singh; and W.J. Koros. *J. Membr. Sci.* 1997, 137, 145-154.
57. Barrer, R.M. and S.D. James. *J. Phys. Chem.* 1960, 64, 421-7.
58. Barrer, R.M. and S.D. James. *J. Phys. Chem.* 1960, 64, 417-21.

59. Paul, D.R. and D.R. Kemp. *J. Polym. Sci., Polym. Symp.* 1973, No. 41, 79-93.
60. Nielsen, L.E. *J. Macromol. Sci., Part A* 1967, 1, 929-42.
61. Cussler, E.L.; S.E. Hughes; W.J. Ward, III; and R. Aris. *J. Membr. Sci.* 1988, 38, 161-74.
62. Nunes, S.P.; J. Schultz; and K.V. Peinemann. *J. Matl. Sci. Lett.* 1996, 15, 1139-1141.
63. Marand, E.; C.J. Cornelius; P. Meakin; and A.J. Hill. *Polym. Matl. Sci. and Engr.* 2001, 85, 297-298.
64. Merkel, T.C.; B.D. Freeman; R.J. Spontak; Z. He; I. Pinnau; P. Meakin; and A.J. Hill. *Science* 2002, 296, 519-522.
65. Kraus, G. and J.T. Gruver. *J. Polym. Sci., Part A-2* 1970, 8, 571-81.
66. Vankelecom, I.F.J.; S. De Beukelaer; and J.B. Uytterhoeven. *J. Phys. Chem. B* 1997, 101, 5186-5190.
67. Te Hennepe, H.J.C.; C.A. Smolders; D. Bargeman; and M.H.V. Mulder. *Sep. Sci. Tech.* 1991, 26, 585-96.
68. Bartels-Caspers, C.; E. Tusel-Langer; and R.N. Lichtenthaler. *J. Membr. Sci.* 1992, 70, 75-83.
69. Dotremont, C.; I.F.J. Vankelecom; M. Morobe; J.B. Uytterhoeven; and C. Vandecasteele. *J. Phys. Chem. B* 1997, 101, 2160-2163.
70. Vankelecom, I.F.J.; J. De Kinderen; B.M. Dewitte; and J.B. Uytterhoeven. *J. Phys. Chem. B* 1997, 101, 5182-5185.
71. Vankelecom, I.F.J.; E. Scheppers; R. Heus; and J.B. Uytterhoeven. *J. Phys. Chem.* 1994, 98, 12390-6.
72. Jia, M.; K.V. Peinemann; and R.D. Behling. *J. Membr. Sci.* 1991, 57, 289-96.
73. Duval, J.M.; B. Folkers; M.H.V. Mulder; G. Desgrandchamps; and C.A. Smolders. *J. Membr. Sci.* 1993, 80, 189-98.
74. Duval, J.M.; A.J.B. Kemperman; B. Folkers; M.H.V. Mulder; G. Desgrandchamps; and C.A. Smolders. *J. Appl. Polym. Sci.* 1994, 54, 409-18.
75. Gür, T.M. *J. Membr. Sci.* 1994, 93, 283-9.

76. Süer, M.G.; N. Ba; and L. Yilmaz. *J. Membr. Sci.* 1994, 91, 77-86.
77. Vankelecom, I.F.J.; E. Merckx; M. Luts; and J.B. Uytterhoeven. *J. Phys. Chem.* 1995, 99, 13187-92.
78. Vankelecom, I.F.J.; S. Van den Broeck; E. Merckx; H. Geerts; P. Grobet; and J.B. Uytterhoeven. *J. Phys. Chem.* 1996, 100, 3753-8.
79. Zimmerman, C.M.; R. Mahajan; and W.J. Koros. *Polym. Mater. Sci. Engr.* 1997, 77, 328-329.
80. Mahajan, R.; R. Burns; M. Schaeffer; and W.J. Koros. *J. Appl. Polym. Sci.* 2002, 86, 881-890.
81. Mahajan, R. and W.J. Koros. *Polym. Engr. and Sci.* 2002, 42, 1432-1441.
82. Vu, D.Q.; W.J. Koros; and S.J. Miller. *J. Membr. Sci.* 2003, 211, 335-348.
83. Vu, D.Q.; W.J. Koros; and S.J. Miller. *J. Membr. Sci.* 2003, 211, 311-334.
84. Yong, H.H.; H.C. Park; Y.S. Kang; J. Won; and W.N. Kim. *J. Membr. Sci.* 2001, 188, 151-163.
85. Wang, H.; B.A. Holmberg; and Y. Yan. *J. Matl. Chem.* 2002, 12, 3640-3643.

Chapter 3. MATERIALS AND METHODS

3.1. OVERVIEW

The focus of this research is on mixed matrix membranes with molecular sieving zeolites as inserts. Section 3.2 discusses the neat polymers, sieves, and coupling agents used to prepare these membranes as well as the gases used for characterizing them. Section 3.3 details basic procedures and processes for preparing mixed matrix membranes. The equipment and methods for measuring permeabilities and selectivities are well described in the literature, but a brief description of each is provided in section 3.4. Section 3.4 also mentions complementary characterization techniques used here.

3.2. MATERIALS

One of the goals of this research was to further develop a simple method for preparing successful mixed matrix membranes. Thus, most materials were used as received or with minimal processing. Solvents were filtered through 0.2 μm PTFE filters to remove any potential dust particles before incorporating them into casting dopes. Solvents used in this study include dichloromethane (MeCl_2), N-methyl pyrrolidinone (NMP), dimethylacetamide (DMAc), toluene, isopropanol (IPA), and ethanol (EtOH) from Aldrich (Milwaukee, WI); dichloromethane and tetrahydrofuran (THF) from EM Sciences (Gibbstown, NJ); and dichloromethane, chloroform (CHCl_3), isopropanol, and tetrahydrofuran from FisherChemicals (Fair Lawn, NJ). When using zeolites, new solvents or solvents from “Sure-Seal” bottles were used to prevent contamination from water in the solvent.

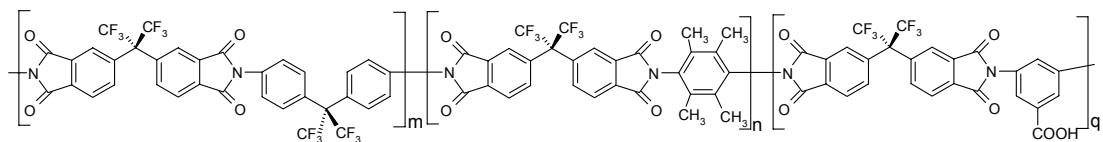
3.2.1. Polymers

The polymers used in this research were obtained commercially or from collaborators. PVAc and 40% hydrolyzed PVAc (Aldrich; Milwaukee, WI), Ultem[®] (GE Plastics; Pittsfield, MA), Udel[®] (Solvay Advanced Polymers; Alpharetta, GA), Matrimid[®] (Vantico; Brewster, NY), and epichlorohydrin (Zeon Chemicals Inc.; Louisville, KY)

were all obtained commercially. Several polymers, including 6FDA-mPDA, 6FDA-mPDA:DABA (2:1), 6FDA-6FpDA:4MPD:DABA (2:2:1), and BPADA-DAPI:DABA (1:1) were kindly provided by Medal LP (Newport, DE). Most of these polymers are prepared by condensation polymerizations of dianhydrides and diamines. When a polymer is comprised of multiple diamines, the ratio of diamines is indicated as m:n:q. Selected properties for these polymers are reported in Table 3.1 and structures are given in Figure 3.1.

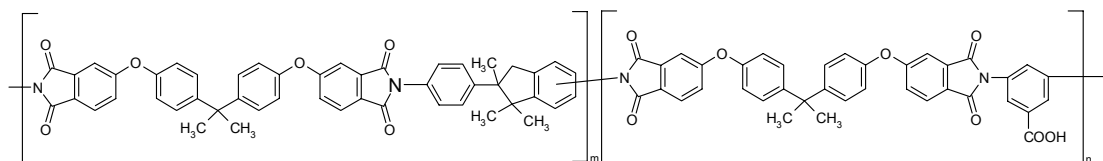
Table 3.1: Selected properties of polymers. Permeation data is for 35°C and 65 psia. If no source is given, the data was measured in this work.

	Permeability, Barrer		Selectivity		Density g/cm ³	Tg °C	Source
	O ₂	CO ₂	O ₂ /N ₂	CO ₂ /CH ₄			
6FDA-6FpDA:4MPD:DABA (2:2:1)	22	100	4.2	33		367	
BPADA-DAPI:DABA (1:1)	0.65	2.7	6.8	33			
6FDA-mPDA	2.6	9.4	6.9	66	1.47	295	
6FDA-mPDA:DABA (2:1)	2.1	7.6	7.0	74			
Matrimid [®]	2	10	6.9	35.5	1.2	305	
Ultem [®]	0.4	1.4	7.6	38	1.28	215	[1]
Udel [®]	1.4	5.6	5.6	22	1.24	186	[1, 2]
Poly(vinyl acetate)	0.5		6		1.19		[3]
40% Hydrolyzed PVAc	0.28		6.7				



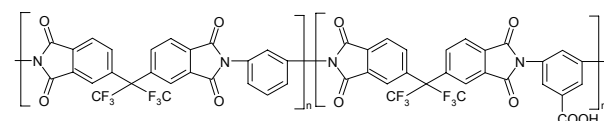
6FDA-6FpDA:4MPD:DABA (2:2:1)

4,4'-(hexafluoroisopropylidene) diphthalic anhydride – 4,4'-(hexafluoroisopropylidene) dianiline :
2,3,5,6-tetramethyl-p-phenylenediamine : 3,5-diaminobenzoic acid



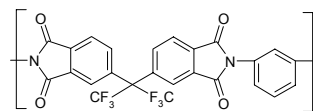
BPADA-DAPI:DABA (1:1)

2,2-bis[4-(3,4-dicarboxyphenoxy)phenyl] propane dianhydride – 5(6)-amino-1-(4'aminophenyl)-1,3,3-trimethylindane : 3,5-diaminobenzoic acid



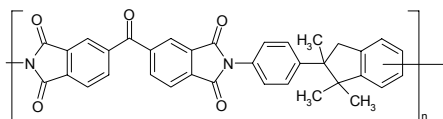
6FDA-mPDA:DABA (2:1)

4,4'-(hexafluoroisopropylidene) diphthalic anhydride –
1,3-phenylenediamine : 3,5-diaminobenzoic acid



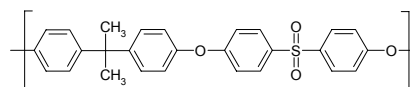
6FDA-mPDA

4,4'-(hexafluoroisopropylidene)
diphthalic anhydride - 1,3-
phenylenediamine



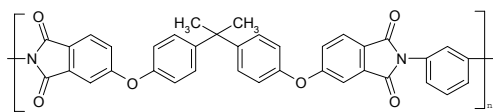
BTDA-DAPI (Matrimid®)

3,3',4,4'-benzophenonetetracarboxylic acid dianhydride -
5(6)-amino-1-(4'aminophenyl)-1,3,3-trimethylindane



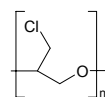
Udel®

Sodium 4,4'-Isopropylidenediphenolate -
4,4'-dichlorodiphenylsulfone

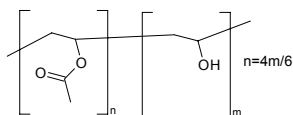


BPADA-mPDA (Ultem®)

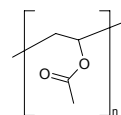
2,2-bis[4-(3,4-dicarboxyphenoxy)phenyl] propane
dianhydride - 1,3-phenylenediamine



Epichlorohydrin



40% Hydrolyzed Poly(vinyl acetate)



Poly(vinyl acetate)

Figure 3.1: Structures of the polymers used in this work

3.2.2. Molecular Sieves

This work concentrated on zeolite molecular sieves as the dispersed phase. Zeolite 4A was purchased from Advanced Specialty Gas Equipment (Middlesex, NJ). Zeolite 4A has an LTA (Linde Type A) type structure, which has a 3-dimensional pore network of interconnected cages that is ideally suited to the separation of O₂/N₂ and CO₂/CH₄. A second molecular sieve, HSSZ-13, was provided by ChevronTexaco Energy Technology Company (ETC) (Richmond, CA). This zeolite has a chabazite (CHA) type structure, which is also well suited to the separation of O₂/N₂ and CO₂/CH₄. Table 3.2 gives selected properties of these zeolites. The CO₂/CH₄ properties of zeolite 4A were estimated as discussed in Appendix A. Figure 3.2 shows the framework structure of both zeolites. Each vertex in the figure represents either a silica or an alumina tetrahedron. Zeolite 4A has a Si:Al ratio of one, while that of HSSZ-13 is typically around 25, but varies somewhat by batch.

Table 3.2: Selected properties of zeolites. Permeation data is for 35°C and 65 psia. If no source is given, the data was measured for this work.

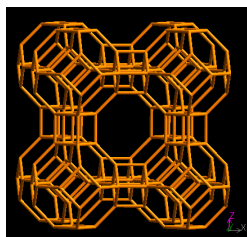
	Permeability, Barrer		Selectivity		Density	Pore Size
	O ₂	CO ₂	O ₂ /N ₂	CO ₂ /CH ₄	g/cm ³	Å
Zeolite 4A	0.77 [4]	15 [†]	37 [4]	340 [†]	1.52 ^{††}	3.8
HSSZ-13	10 [‡]	200 [‡]	40 [‡]	>400 [‡]	1.51 ^{††}	3.8 ^{**}

[†] See Appendix A

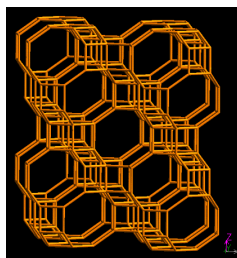
^{††} Estimated from: zeolite 4A, x-ray diffraction data [5]; HSSZ-13, neutron diffraction data [6]

[‡] Estimated by fitting mixed matrix membrane transport properties to the Maxwell model with sieve permeability as a parameter.

^{**} Assumed the same as for a chabazite, which has the same structure [5].



Zeolite 4A (LTA)



HSSZ-13 (CHA)

Figure 3.2: Framework structures for the zeolites used in this work. Each vertex represents the center of a silica or alumina tetrahedron. Structures from International Zeolite Association <http://www.iza-structure.org>.

3.2.3. Short Coupling Agents

Zeolites were commonly treated with γ -aminopropyltrimethoxysilane (United Chemical Technologies; Bristol, PA) or (Gelest; Morrisville, PA) to enhance adhesion to the polymer matrix prior to incorporation into mixed matrix membranes. Silane coupling agents are used extensively to modify the surfaces of inorganic materials to enhance adhesion to polymers [7]. The ethoxy group undergoes a hydrolysis in solution before the silane reacts with hydroxyl groups that are ubiquitous on zeolite surfaces [7]. An aminosilane was chosen since it reacts with imide groups in polyimides [8-11]. The reaction between the silane and the sieve and between the silane and the polymer is discussed more extensively in Appendix B. The effect of other silane coupling agents on mixed matrix membranes is discussed in section 5.2.1.2. Zeolite 4A was also modified with the amino acid glycine, which has a carboxylic acid functionality and an amine functionality, but membranes prepared with these modified zeolites did not show enhanced performance.

3.2.4. Gases

Pure gases (O_2 , N_2 , CO_2 , CH_4 , Ar, and He) of 99.999% purity (99.99% CH_4) were obtained from either the local Air Liquide or Air Products/Airgas vendor. Synthetic natural gas (10% CO_2 / 90% CH_4) was used to check for competition effects. Humidified oxygen was prepared by bubbling O_2 through distilled water.

3.3. MEMBRANE PREPARATION

The basic procedure for preparation of a mixed matrix membrane is outlined in Figure 3.3. The first major step is material selection. Criteria for selecting polymers and sieves with compatible transport properties are outlined in section 2.3. The criterion that the polymer – sieve combination form a favorable mixed matrix morphology should be added. It may be possible to accomplish this by modifying the surface of the sieve with a silane coupling agent. A solvent compatible with both polymer and sieve must also be selected. Dope preparation is the next major step. While it may seem simple to mix the polymer solution and sieve suspension, there are a number of optional unit operations that can stabilize the dope, resulting in a better membrane. The final major step is membrane formation. In this work, films have been prepared to simplify characterization, but if this technology is to be industrially relevant hollow fibers must be prepared. The dope requirements depend on which membrane formation method is applied, and there are many variables in the two membrane formation methods that may affect the final product. Knowledge of whether the properties of membranes prepared as films can be duplicated in hollow fibers is also desirable. Selected issues from each of these three major steps are discussed in detail in Chapter 5. The following subsections give a generic procedure for preparation of both pure polymer and mixed matrix membranes. Optional procedures and their relative merits are also discussed.

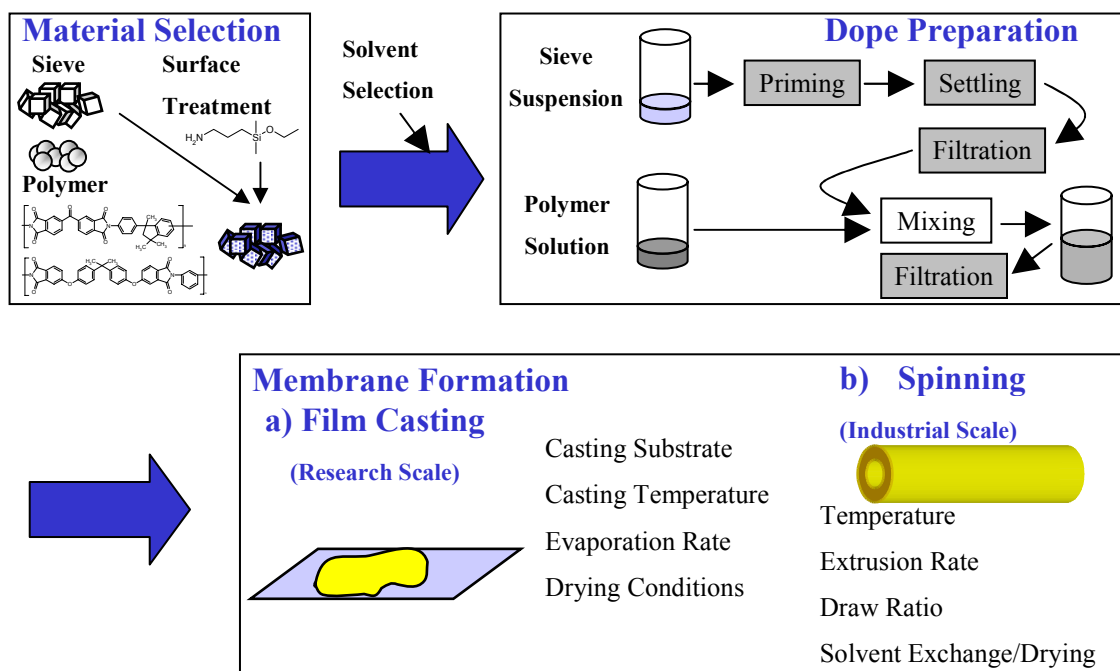


Figure 3.3: Preparation of mixed matrix membranes. Optional dope preparation steps are highlighted in gray.

3.3.1. Materials Selection

Once a polymer – sieve combination has been selected, the biggest consideration is whether to modify the zeolites to enhance adhesion between the polymer and the sieve. Thus, silanation is a materials selection issue. If silanation is desired, the silane is added directly to the dried zeolites in a plastic container, followed by addition of a suitable solvent. EtOH, IPA, and NMP were all used as silanation solvents (see section 5.2.1.1). Plastic is used because the silane could react with glass. The plastic dish is put in a water bath to moderate the temperature increase. The reaction is performed with one of two sonicators, both operating at 20000 Hz. A sonicator capable of delivering either 25 or 50 W *maximum* of power from Sonics & Materials Inc. (Danbury, CT) is typically used for smaller batches (~1 g). For larger batches, a more powerful model from Dukane (Leesburg, VA) capable of delivering 1000 W *maximum* is used. The 50 W sonicator has a 6 mm microtip, while the 1000 W sonicator has a ½''

tip. For an identical silanation container, the 50 W sonicator requires ~15 W of power to drive the tip at 20000 Hz, while the larger tip requires ~100 W. Typically 2-7 g of zeolite is sonicated in 200 mL of a 95:5 mixture of the desired solvent with water. Enough silane is added to the zeolites to give a ~2% solution. Even for larger batch sizes, this is a swamping excess of silane coupling agent based on the particle size and surface density of the reactive hydroxyl groups on the zeolite. The silanation suspensions are sonicated for 30 minutes total in 5 minute increments punctuated with 5 minute “rest” periods. The rest periods prevent the temperature of the sieve suspension from increasing too much. The maximum temperature reached is around 55°C.

3.3.2. Dope Preparation

Depending on the desired film casting method, one of two types of casting “dopes” is required. Films can be cast either by dropping the dope onto the substrate through a syringe or by pouring the dope onto a substrate and drawing it into a thin film with a casting knife. These techniques are discussed further in the following subsection. Only dilute dopes (less than about 5% solids) can be dropped through a syringe, while more concentrated, highly viscous dopes must be drawn with a knife. More viscous dopes are required to prevent settling of zeolites having particle size greater than one micron. Most membranes with submicron zeolites were also prepared using concentrated casting dopes to facilitate comparison to membranes prepared with larger zeolites.

Regardless of whether a dilute or concentrated casting dope is desired, the first step is to dry the materials in a vacuum oven overnight. Polymers are dried between 100°C and 140°C unless otherwise noted in the text. Zeolite 4A must be dried at about 300°C under nitrogen to obtain a fully active zeolite, as shown in section 6.2. Initially, the more hydrophobic HSSZ-13 sieves were not dried before use; however, it was subsequently found that drying the sieves gave better results, so they are also dried between 100°C and 140°C.

To prepare a dilute polymer solution, the desired amount of polymer is placed in a clean glass bottle, an appropriate filtered solvent is added to give a 1 – 2% polymer solution, and the solution is allowed to dissolve. Dissolution usually occurs within a few minutes. When casting films, an approximately 20% polymer solution is required to give the desired film thickness of 1-2 mils using the casting knife of 8-16 mil clearance. Concentrated polymer solutions are placed on a mechanical roller to dissolve without entraining excess air. This polymer solution is generally rolled overnight to assure complete dissolution.

Mixed matrix casting dopes are prepared as two parts: a sieve suspension and a polymer solution, which are then mixed together. The sieve suspension is typically of low viscosity, whereas the polymer solution is concentrated and highly viscous. This is necessary so the resulting casting dope is approximately 15% – 25% total solids. To prepare the sieve suspension, dried sieves are put in a bottle with a sufficient amount of an appropriate solvent (usually ~0.3 g sieve in ~3 mL solvent). The amount of sieves is dictated by the desired sieve loading in the membrane. This mixture is then sonicated for one or two minutes, usually with the 50 W sonicator mentioned in the previous subsection. When sonicating for two minutes, the suspension is mixed gently by hand between the first and second minutes to wash sieves from the side of the bottle. After the sieve suspension is sonicated, it was sometimes set aside to allow any larger particles or particle agglomerates to settle out, or alternatively, they were filtered out. Neither settling nor filtration was performed regularly, however. At this time, the sieves could be “primed” with a small amount of the matrix polymer to facilitate adhesion between the two phases. Priming is discussed in more detail in section 5.3.3. When the settling procedure is used, the sieve suspension is added to the polymer solution, being careful to keep the settled material in the sieve container. This could also be done by carefully decanting the dispersed phase with a pipette. Otherwise, the previously prepared polymer solution is poured into the sieve suspension. In some cases, the resulting polymer-sieve-solvent mixture was stirred with a spatula to break up

the highly viscous polymer solution, and in rare cases the sonicator was used for this purpose. In most cases the resulting polymer-sieve-solvent mixture is simply allowed to mix on the roller for several hours until a homogeneous casting dope is obtained. Regardless of whether the sieve suspension is poured into the polymer solution or vice versa, some of the material remains behind in the other bottle. It is therefore necessary to record the weights of all the bottles used to prepare the solutions/suspensions so the actual fraction of sieves in the membrane can be determined. The fraction of sieves in the membrane could be independently determined by burning the polymer off the sieves in the TGA. The sieve fractions determined from these two methods were generally in good agreement.

3.3.3. Film Preparation

Once the casting dope is ready, films are cast using one of two methods. These two methods are discussed in the following two paragraphs, but first some general considerations are first given. Casting is done within a fume hood because of the nature of the solvents. Some membranes were cast in a glove bag, which could be purged with dry nitrogen before casting to drive out humidity. When it is desired to dramatically slow down the evaporation rate, the bag is pre-saturated with the solvent used in the casting dope. Several different casting substrates were used, as discussed in section 5.4.1, but a glass plate is most commonly used. After casting in a glove bag, the nascent film is covered with an inverted funnel. The spout of the funnel is further covered with aluminum foil or a Kimwipe[®] (Kimberly-Clark Corp.; Roswell, GA) to control the solvent evaporation rate. It is necessary to cast solutions with low volatility solvents on glass in the vacuum oven or on a hotplate to remove the solvent. These films are covered with an inverted pan to keep dust from settling on the nascent films.

To cast a pure polymer film from a dilute solution, the solution is first poured into a glass syringe with a 0.2 μm PTFE filter attached to the tip. A filter should not be used when casting mixed matrix dopes since it will likely entrap zeolites. The casting dope

is dropped onto the substrate into a circular stainless steel mold. The amount of dope required is determined by the desired film thickness, the area of the stainless steel casting mold, the dope concentration, and the density of the resulting membrane. Should any air bubbles develop in the nascent film, they can be pushed up against the edge of the stainless steel casting ring with the tip of the syringe.

Viscous dopes are cast by first pouring them onto the desired casting substrate. A casting knife (Paul N. Gardner & Co.; Pompano Beach, FL) with an 8, 10, 12, or 16 mil clearance is then used to draw the dope into a film of uniform thickness.

3.4. MEMBRANE TESTING METHODS

This section details the standard methods used to test membranes. The permeability is most easily obtained from a gas permeation measurement, which can also provide the diffusion coefficient. The sorption coefficient is directly measured from a gas sorption measurement, although the diffusion coefficient can also be determined from the data using kinetic analysis. Several complementary characterization techniques were also used to probe membrane morphology, and these are discussed in the final subsection.

3.4.1. Gas Permeation Measurements

The permeability of a given gas and the selectivities for gas pairs were determined using the standard isochoric (constant-volume, variable pressure) technique [12-14], where the steady state increase in the permeate pressure, $\left[\frac{dp}{dt} \left(\frac{\text{Torr}}{s} \right) \right]$, is directly proportional to the permeability:

$$\begin{aligned}
\text{Permeability (Barrer)} = & \left[\frac{dp}{dt} \left(\frac{\text{Torr}}{s} \right) \right] \times \frac{\left(\frac{101325 \text{ Pa}}{760 \text{ Torr}} \right) [V_D (\text{m}^3)]}{\left(8.314 \frac{\text{Pa} \cdot \text{m}^3}{\text{mol} \cdot \text{K}} \right) [T (\text{K})]} \times \\
& \left\{ \frac{\left(8.314 \times 10^6 \frac{\text{Pa} \cdot \text{cm}^3 \text{ STP}}{\text{mol} \cdot \text{K}} \right) (273.15 \text{ K})}{(1 \text{ atm}) \left(\frac{101325 \text{ Pa}}{\text{atm}} \right)} \right\} \times \quad (3.1) \\
& \frac{[\ell (\text{cm})] \left(\frac{14.696 \text{ psia}}{76 \text{ cmHg}} \right)}{[A (\text{cm}^2)] [p_F (\text{psia})]} \times \frac{1 \times 10^{10} \text{ Barrer}}{\frac{\text{cm}^3 \text{ STP} \cdot \text{cm}}{\text{cm}^2 \cdot \text{s} \cdot \text{cmHg}}}
\end{aligned}$$

The terms in brackets are known, with units given in parentheses: permeate reservoir volume, V_D (m^3); temperature, T (K); membrane thickness, ℓ (cm); membrane area, A (cm^2); and feed pressure, p_F (psia). The term in braces converts from moles to $\text{cm}^3 \text{ STP}$.

The *time lag*, θ_A , is the time at which the initial permeate pressure (essentially zero) intersects the line formed by extrapolating dp/dt backwards. The time lag is related to the thickness of the membrane, and the diffusion coefficient of penetrant “A”, D_A , through the membrane (cm^2/s) via the following expression:

$$\theta_A = \frac{\ell^2}{6D_A} \quad (3.2)$$

Steady state permeation data (typically $t > 4\theta$) is used to calculate dp/dt . If the membrane is too thin, no time lag will be observed. The following two subsections describe the equipment in detail and outline basic experimental procedures.

3.4.1.1. Experimental Apparatus

The experimental apparatus is shown in Figure 3.4. The system is enclosed in an insulated box to regulate temperature at 35°C. A heating tape or light bulb is used as the heat source (4) and a fan (3) is used to assure temperature uniformity in the box. All fittings are stainless steel Swagelok[®] (Solon, OH) or Swagelok[®] VCR[®] fittings.

The upstream pressure is measured with a 0-1000 psia gauge (6) from either Ashcroft or Heise. Both were obtained from Dresser Instruments (Stratford, CT). The downstream transducer (1) is a 10 Torr Baratron[®] 622 capacitance manometer supplied by MKS instruments (Andover, MA). Older systems have a type 122A Baratron[®], which has similar operating parameters. These transducers are connected to a PDR-5-B, also from MKS, which provides power and a digital readout of the voltage output. This voltage output can easily be converted to pressure. This voltage is recorded with a Keithley KCPI-3107 data acquisition board installed in a computer running Labview[®] software from National Instruments (Austin, TX). Initially, data was recorded with a model 1241 or 1242 strip chart recorder from Soltec (Sun Valley, CA), but both data acquisition systems give identical results.

The permeation cell (8) was manufactured from stainless steel components. This cell consists of two faces, upstream and downstream as shown in cross section in Figure 3.5. The downstream face is flat, with the exception of a groove for a Viton[®] (Dupont; Wilmington, DE) o-ring, which has appropriate temperature and chemical resistance. A piece of porous grade D sintered metal (Metron Technology; Austin, TX) is inserted into the downstream face to support the membrane. The membrane is usually masked onto the cell as described in the next subsection. There is one outlet from the downstream face, connected to the permeate reservoir. In contrast, the upstream face of the permeation cell has two tubing connections. One is an inlet for the feed; the other an outlet for the retentate. The upstream face has a bored out area to prevent crushing the membrane. In some cells, there is a groove for a second Viton[®] o-ring in the

upstream face, whereas in others, there is just a larger bored out area. In cells lacking the second o-ring, the membranes are masked directly onto the cell, and the “sandwich” masking method can not be used (see following subsection). As with any high vacuum application, leakage of atmospheric air is a concern, but any leakage into the permeate reservoir is accounted for in all experiments. Furthermore, only data from experiments with acceptable leak rates ($\sim 10\%$ of the total dp/dt) were used.

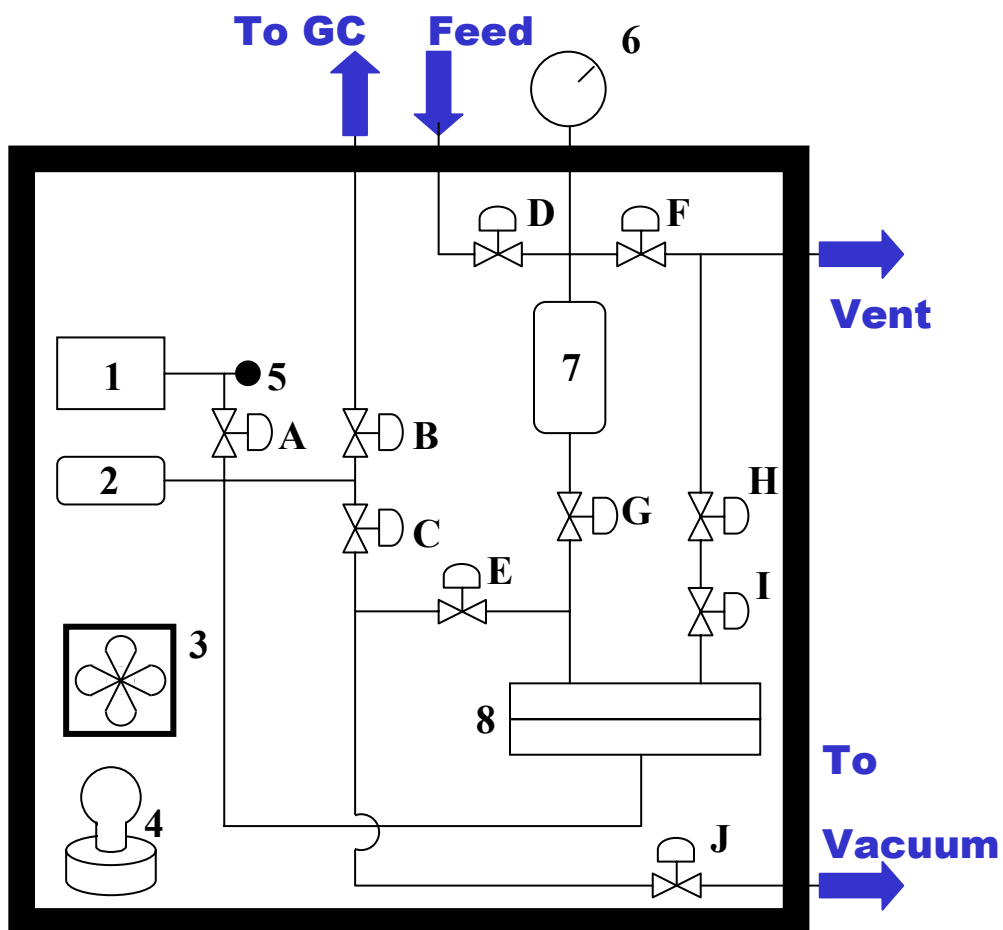


Figure 3.4: Schematic of the permeation system. (1) Downstream Pressure Transducer (2), Permeate Reservoir (3) Fan, (4) Heater, (5) Rupture Device, (6) Upstream Pressure Transducer, (7) Feed Reservoir, (8) Permeation Cell, (A) Downstream Pressure Transducer Isolation Valve, (B) GC Valve, (C) Downstream Vacuum Valve, (D) Feed Valve, (E) “Middle” Valve, (F) Vent Valve, (G) Cell Isolation Valve, (H) Retentate (Metering) Valve, (I) Retentate Shutoff Valve, and (J) Vacuum Shutoff Valve.

After the pressure in the permeate reservoir has risen above 5 torr, mixed gas analysis can be performed with a HP 5890 Series II gas chromatograph (Agilent Technologies; Palo Alto, CA). This is done by allowing the permeate to expand into the GC sample loop by opening valve B. After a sufficient equilibration time, usually 3 minutes, valve B is closed and the contents of the sample loop are injected onto the GC column. For O₂/N₂ analysis, the column is 6' of zeolite T followed by 3' of zeolite 13X molecular sieve, and for CO₂/CH₄ analysis, the column is 8' of HayeSep Q 80/100 mesh. The column temperatures are ambient and 90°C, respectively. The thermal conductivity detector (TCD) is maintained at 150°C. Typically 3-4 aliquots of the permeate gas are sampled with the GC at 15 minute intervals.

3.4.1.2. Membrane Masking Procedure

Unless a large, defect-free area (~10 cm diameter) can be prepared, the membranes must be masked with Fasson[®] 802 adhesive backed aluminum tape (Avery Denison Specialty Tape Division; Pasadena, CA) so a smaller membrane area can be used. Typically, smaller areas are also preferred to conserve materials. There are two basic masking procedures; (i) preparing a “sandwich” type mask and (ii) masking directly onto the cell. These two procedures are described in the next two paragraphs. Note that a cross section of the cell is shown in Figure 3.5 with a “sandwich” type mask.

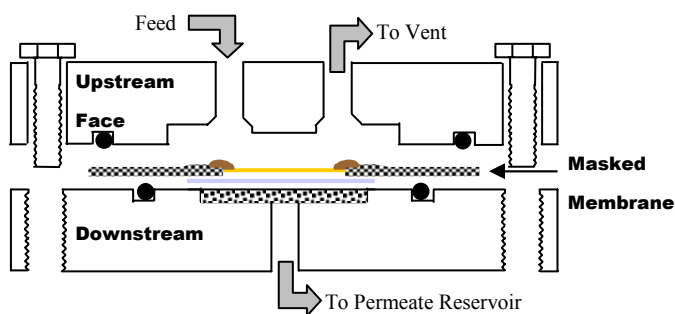


Figure 3.5: Schematic of the permeation cell {(8) in Figure 3.4}. A cross section through the cell is shown with a “sandwich” type masked membrane. The membrane assembly is composed of: membrane, yellow; filter paper, light gray; epoxy, brown; adhesive backed aluminum, checkered. Bolts, shown at left and right, and o-rings, solid black circles, assure a leak tight seal.

The “sandwich” method was originally used to prepare small areas for testing. A hole is cut into the center of two pieces of adhesive backed aluminum tape. A piece of the membrane slightly larger than the hole in the aluminum mask is then sandwiched between these two pieces of adhesive backed aluminum with the adhesive layers facing in. A layer of Devcon[®] 5-minute epoxy (Danvers, MA) is placed on the top face of the sandwich at the aluminum – membrane interface, as depicted in Figure 3.5. This layer of epoxy prevents the formation of a small, direct gas pathway between the feed and permeate reservoirs caused by potential poor bonding of the adhesive backed aluminum to the membrane. At this time, epoxy can also be used to cover any pinhole or other defects that might be in the membrane. Once the epoxy has dried overnight in the atmosphere, the average membrane thickness is determined with an Ames micrometer (Watham, MA). Epoxy should not be dried in the atmosphere when used with membranes containing components, such as zeolites, that are sensitive to humidity. Alternatively, it is possible to dry the epoxy in the permeation cell with an upstream gas purge. The membrane area is measured by placing the epoxied sandwich assembly on a Microtek flatbed scanner (Redondo Beach, CA). The sandwich is scanned at 300 dpi resolution, and then Scion Image software (Scion Corporation; Frederick, MD) is used to determine the exposed area of the membrane. The sandwich is then sealed into the cell with a Zitex Teflon[®] filter having 1-3 μm pores (Cole Parmer; Vernon Hills, IL) or 3 pieces of Whatman[®] #1 medium porosity filter paper (Fisher; Pittsburg, PA) placed between the membrane and the sintered metal disk. This prevents the sintered metal from damaging the membrane.

The second masking method is based on a scheme developed by Zimmerman [15] for extremely fragile membranes. It was found to give the lowest leakage of gas into the permeate reservoir, so it is the preferred masking method. The first step is to make a sandwich as in the earlier method, without applying epoxy. A third aluminum mask is prepared with an outer diameter larger than the sandwich but smaller than the o-ring groove in the permeation cell bottom. This third mask should have an inner diameter the

same or slightly larger than that of the sandwich. The sandwich, together with the underlying filter paper, is placed on the cell downstream face, and then this third mask is used to tape the sandwich to the cell downstream face. In this case, the adhesive layer of the third mask forms the seal, preventing leakage into the permeate reservoir. If no epoxy is desired, the cell is assembled immediately after taping the sandwich assembly to the cell bottom and then placed in the system.

If epoxy is desired for a membrane masked directly onto the cell, the following procedure is used. After the third mask is applied, the cell downstream face is placed in the system and the permeate reservoir is evacuated. Adding the epoxy while applying vacuum to the membrane pulls the epoxy into any defects, forming a better seal. This was found to reduce the occurrence of epoxy delamination from the membrane, which could be a problem when the sandwich method was used. The epoxy is then allowed to cure in the system overnight, with vacuum applied on the permeate reservoir. When the epoxy is dry, the cell downstream face is removed and placed on the flatbed scanner to determine the permeation area. After that, the cell is bolted together and placed in the permeation system. If it is necessary to epoxy a membrane containing zeolites, it is dried in the fully assembled cell with vacuum on the downstream and a nitrogen purge on the upstream. The membrane area is then determined after testing is complete.

3.4.1.3. Experimental Procedure

This section refers to valves shown on permeation apparatus in Figure 3.4. After the cell is inserted, the “middle” and GC valves are closed and vacuum is drawn on the downstream side of the membrane until the pressure is ~0.05 torr or less. Next, the downstream vacuum valve is closed to isolate the permeate reservoir while vacuum is drawn on the feed side, including parts of the feed line that were exposed to the atmosphere. Vacuum is drawn on the feed side for a short time, and then the downstream vacuum valve is reopened to evacuate the entire system. This procedure is necessary to ensure that the pressure on the downstream side of the membrane is always

less than or equal to that on the upstream. If the downstream pressure exceeds the upstream pressure, the membrane can be damaged. The entire system is then evacuated at least overnight to ensure that all gases sorbed into the membrane or onto the system internals are removed. Once the system has been thoroughly evacuated, the leak rate of atmospheric gases into the permeate reservoir is measured by closing valves B, C, E, G, and I to isolate the cell. Although care is taken in assembling the systems and inserting the cell each time, there is always a finite leak into the permeate reservoir from the atmosphere. This leak must be quantified so it can be accounted for in the data analysis.

Gases are first introduced into the feed side with the cell isolation valve closed. This feed is then rapidly purged through the vent valve three times to further flush out any contaminants. After that, the system is allowed to reach thermal equilibrium for at least one hour, since the gas will have cooled during expansion into the feed reservoir. The membrane remains under dynamic vacuum during equilibration of the feed gas. After equilibration, the middle valve is closed and the cell isolation valve is opened to allow the feed gas to contact the membrane. Then, the downstream vacuum valve is quickly closed and the pressure rise in the permeate reservoir due to permeation through the membrane is initiated. After the first gas has been tested, the system is again evacuated overnight before testing the second gas. Typically, the first one or two gases in the cycle were retested near the end of the experiment to verify repeatability.

When feeding a mixed gas, the retentate flow rate must also be set using valves I and H with a bubble flow meter on the vent. This flow rate is set so that the “stage cut” is less than 1% so the feed concentration does not change appreciably. The stage cut is the fraction of the feed gas that permeates through the membrane. Another stipulation is that the flow rate is low enough to avoid a pressure drop in the feed gas. The retentate is typically set at a few mL/min, satisfying both conditions. The (mixed) gas is then allowed to permeate sufficiently long to reach steady state before closing the downstream valve to start gas collection.

3.4.1.4. Measurement of Oxygen Permeabilities in the Presence of Water Vapor

The measurement of the oxygen permeability with humidified oxygen is performed with an Oxtran 100A permeation device (Mocon; Minneapolis, MN). This device, shown schematically in Figure 3.6, differs from the standard permeation apparatus. In this device, a 2% hydrogen in nitrogen sweep stream carries the oxygen permeate to a nickel-cadmium fuel cell, which accurately determines the oxygen content in the sweep stream. The output voltage from the fuel cell can be converted into an oxygen permeability. Both the oxygen and nitrogen/hydrogen sweep streams are humidified in separate bubblers filled with DI water. Salt solutions were initially used to regulate the relative humidity in the feeds; however, this corroded the fuel cell. After obtaining a new fuel cell, the relative humidity was regulated by controlling the bubbler temperature with water baths. The relative humidity was also monitored using a RH-30-2 humidity sensor (Omega; Stamford, CT). The sensor tip was enclosed in a plastic fitting with a small holdup volume attached to the outlet of the Oxtran with a short tube. The humidities measured by the sensor were in good agreement with those expected based on the bubbler temperatures.

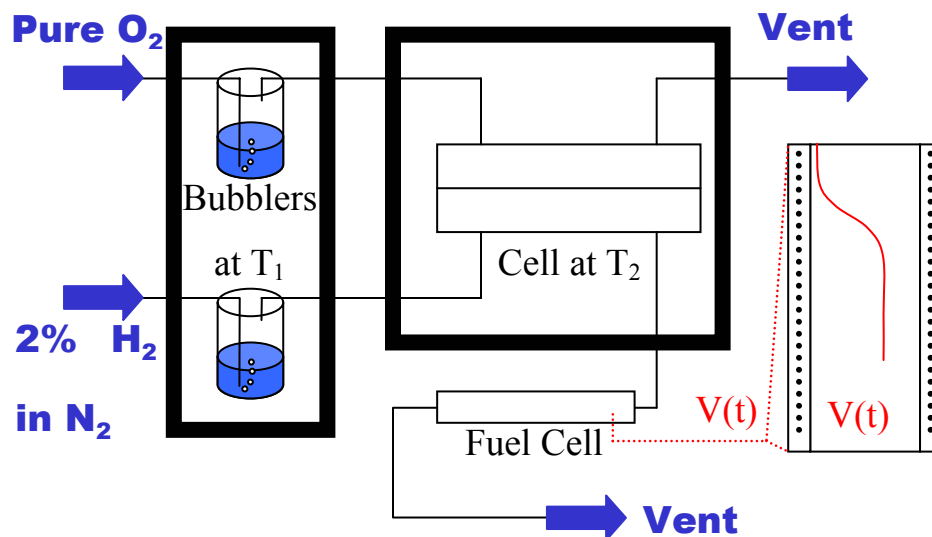


Figure 3.6: Schematic of the Oxtran permeation device for measuring the oxygen permeability of humidified feeds.

3.4.2. Gas Sorption Measurements

Gas sorption can be measured several ways. Perhaps the two most common are gravimetric sorption and pressure decay sorption. Gravimetric sorption is typically used for highly sorbing gases (i.e. at low pressure). Pressure decay sorption is used for the remaining applications. The principle data obtained using sorption measurements is the sorption coefficient in the membrane. Provided sorption is not too fast and the sample is of uniform thickness, it is also possible to obtain the diffusion coefficient. This is done by fitting the experimental sorption curve with an appropriate theoretical expression that is a function of the diffusion coefficient.

3.4.2.1. Gravimetric Sorption

Gravimetric sorption is measured in a McBain balance [16, 17]. Figure 3.7 shows a schematic of a typical apparatus. After the sample and pressure transducer completely evacuated, they are closed off and the headspace in the solvent vial is evacuated for a short time. Next, the vacuum valve is closed and the pressure transducer valve is opened, allowing a small amount of vapor into the manifold. Finally, the valve is opened to slowly introduce gas into the temperature regulated sample compartment. Equilibrium sorption can be determined based on the extension of a quartz spring with known spring constant. This is measured with a cathetometer (not shown) by noting the change in position of the quartz spring reference line relative to the reference scale inside the sample compartment. Then, pressure may be increased incrementally or the sample may be evacuated completely to determine sorption at a different equilibration pressure. By making measurements at several equilibration pressures, the entire sorption curve can be determined. Since the apparatus is usually glass, measurements are limited to below atmospheric pressure, so this method is favored for highly sorbing vapors. This method was used to measure water sorption in HSSZ-13 and zeolite 4A.

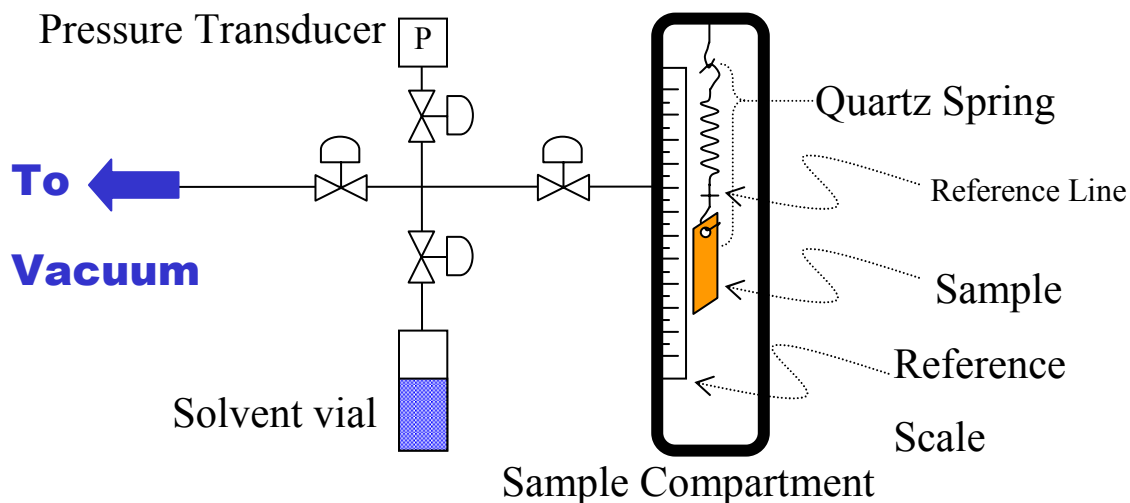


Figure 3.7: Schematic of a gravimetric “quartz spring” sorption apparatus.

3.4.2.2. Pressure Decay Sorption

Pressure decay sorption is useful for measuring the sorption of gases at pressures greater than 1 atm in polymers, sieves, and mixed matrix membranes. Equipment and operating techniques are well documented in the literature [18, 19]. A schematic of the necessary apparatus is shown in Figure 3.8. Gas is introduced into a feed reservoir of known volume after complete evacuation of both reservoirs. After allowing the pressure in the feed reservoir to equilibrate for a few minutes, the valve between the sample and feed reservoirs is opened for 3 seconds to allow gas into the sample reservoir. Then the valve is closed and the pressure in both reservoirs is monitored. The feed reservoir pressure should stabilize immediately, while the sample reservoir pressure will decrease a small amount due to sorption into the sample. Once the sample reaches equilibrium with the gas in the sample reservoir, a mole balance before and after the expansion gives the amount sorbed into the sample. Compressibility factors, given in Appendix C, must be used to account for the non-ideality of the gas phase. Finally, the pressure in the feed reservoir is changed and the whole cycle is repeated to derive the whole sorption curve. Data was recorded using a PC running Labview[®] data acquisition software interfaced with a Keithley Instruments 2700 Multimeter.

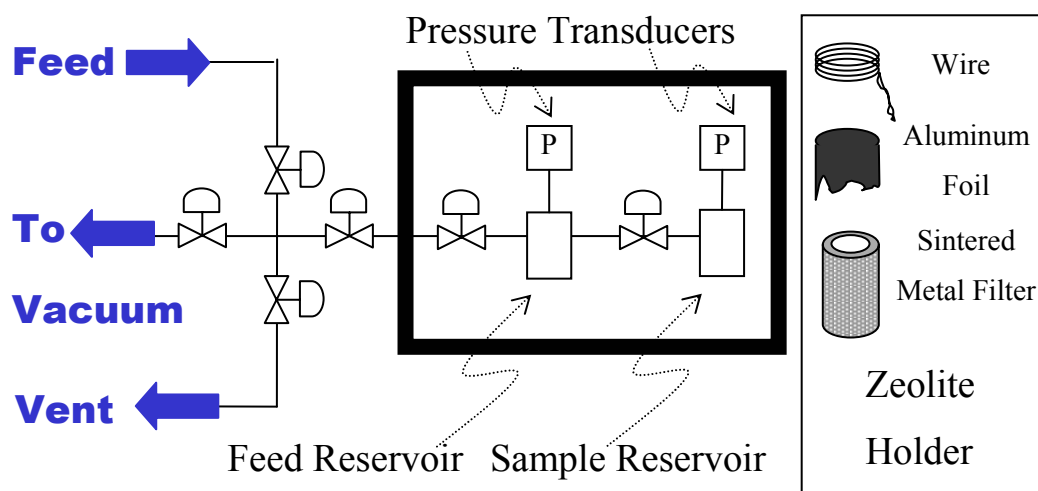


Figure 3.8: Schematic of a high pressure – pressure decay sorption apparatus.

Sorption in zeolites had not previously been measured with the pressure decay technique in this equipment. Zeolite powder is enclosed in a $0.5 \mu\text{m}$ sintered metal filter element (Swagelok[®] part number SS-2FK4-05), which is cylindrically shaped with one open end (see inset in Figure 3.8). After putting the sample into the filter element, the open end is covered with a piece of aluminum foil. Finally, a wire is wrapped around the filter element to hold the aluminum foil in place. The volume of each filter element, aluminum cover, and wire wrap was carefully calibrated since the unoccupied volume in the sample reservoir is an important parameter in the mole balance.

3.4.3. Complementary Characterization Methods

Several complementary techniques were used to examine these materials. Frequently used complementary techniques are discussed here. Other complementary techniques that were used infrequently are discussed at the appropriate place in the text. More detailed discussions of each of these techniques can be found in the literature.

The T_g of selected neat polymers and mixed matrix materials was determined using differential scanning calorimetry. It was hypothesized that the polymer phase of mixed matrix materials should show an elevated T_g or even a second, higher T_g relative to the neat polymer, especially as the specific surface area of polymer – sieve contact is

increased. Usual heating rates are 10°C/min. Two heating cycles are typically done so that the thermal history of the sample is “erased” in the first heating cycle.

The scanning electron microscope can sometimes be used to directly observe membrane morphology. Although the SEM could not resolve Ångstrom-sized voids believed to exist in some samples, larger voids between the polymer and sieve can be clearly discerned using the SEM. Cross sections are prepared by fracturing film samples in liquid nitrogen after submersion for 2 minutes. Fractured films are then mounted onto metal sample holders with carbon tape. Next, a conductive layer of gold, gold/palladium, or chromium is sputtered onto the samples for about 60 seconds in an argon plasma. Finally, samples are examined using either a Hitachi S-800 or S-4500 field emission scanning electron microscope (Hitachi High-Technologies Corporation; Tokyo, Japan), typically with an accelerating voltage of 15kV.

Another useful complementary characterization technique is thermogravimetric analysis with infrared analysis of the evolved gas. Thermogravimetric analysis was performed in a Netzsch STA 409 PC TGA (Burlington, MA). Samples can be heated to a maximum of 1600°C in nitrogen or 1500°C in air at rates from about 1°C to 20°C per minute. Infrared analysis is performed with a Bruker Optics Tensor27 infrared spectrometer (Manning Park, MA) with an attached gas module. A transfer line heated to 200°C between the TGA and the IR prevented condensation of the evolved gases.

3.5. REFERENCES

1. Kesting, R. and A. Fritzsche, Polymeric gas separation membranes. 1993, New York: John Wiley & Sons.
2. McHattie, J.S.; W.J. Koros; and D.R. Paul. Polymer 1991, 32, 840-50.
3. Daniels, W.A., Vinyl ester polymers, in Concise encyclopedia of polymer science and engineering, J.I. Kroschwitz, Editor. 1990, John Wiley & Sons: New York. p. 1264-7.

4. Zimmerman, C.M.; A. Singh; and W.J. Koros. *J. Membr. Sci.* 1997, 137, 145-154.
5. Baerlocher, C.; W.M. Meier; and D.H. Olson, *Atlas of zeolite framework types*. 5 ed. 2001, New York: Elsevier.
6. Smith, L.J.; A. Davidson; and A.K. Cheetham. *Catal. Lett.* 1998, 49, 143-146.
7. Plueddemann, E.P., *Silane coupling agents*. 1982, New York: Plenum Press.
8. Greenblatt, J.; C.J. Araps; and H.R. Anderson, Jr., Aminosilane-polyimide interactions and their implications in adhesion, in *Polyimides: Synthesis, characterization, and applications [Proceedings of the technical conference on polyimides]*. 1984. p. 573-88.
9. Shang, X.-y.; Z.-k. Zhu; J. Yin; and X.-d. Ma. *Chem. Matr.* 2002, 14, 71-77.
10. Linde, H.G. *J. Polym. Sci., Polym. Chem. Ed.* 1982, 20, 1031-41.
11. Ansel, M. and P.D. Murphy. *J. Adhesion Sci. Tech.* 1994, 8, 787-806.
12. O'Brien, K.C.; W.J. Koros; T.A. Barbari; and E.S. Sanders. *J. Membr. Sci.* 1986, 29, 229-38.
13. Pye, D.G.; H.H. Hoehn; and M. Panar. *J. Appl. Polym. Sci.* 1976, 20, 1921-31.
14. Moore, T.T.; S. Damle; J. Williams; and W.J. Koros. *J. Membr. Sci.* 2004, Accepted.
15. Zimmerman, C.M., *Advanced gas separation membrane materials: Hyper rigid polymers and molecular sieve-polymer mixed matrixes*. Department of Chemical Engineering, University of Texas at Austin. 1998.
16. Jacques, C.H.M. and H.B. Hopfenberg. *Polym. Eng. Sci.* 1974, 14, 441-8.
17. McBain, J.W., *The sorption of gases and vapours by solids*. Twentieth-century chemistry, ed. J.C. Philip. 1932, London: George Routledge & Sons, Ltd.
18. Costello, L.M. and W.J. Koros. *Ind. Eng. Chem. Res.* 1992, 31, 2708-14.
19. Koros, W.J. and D.R. Paul. *J. Polym. Sci., Polym. Phys. Ed.* 1976, 14, 1903-7.

Chapter 4. FACTORS AFFECTING THE POLYMER – SIEVE INTERFACE IN MIXED MATRIX MEMBRANES

4.1. OVERVIEW

The preparation of mixed matrix membranes is a complex process. Knowledge of the factors affecting the final morphology is needed to create membranes with desirable properties. The interface is frequently found to be the critical factor determining the performance of organic – inorganic hybrid materials, including mixed matrix membranes. Mahajan identified two factors that significantly impact the morphology of mixed matrix membranes: polymer flexibility and the affinity of the polymer and molecular sieve [1]. Several additional factors affecting morphology and performance are presented and discussed in this chapter. These include the thermal expansion coefficients and temperature history, internal stress formation and drying conditions, and the presence or absence of specific interactions between the polymer and sieve. These interactions may be covalent bonds (e.g. silane coupling agents), strong affinity (e.g. acid-base interactions between polymer and sieve), or merely dispersive van der Waals interactions. This chapter seeks to demonstrate a more fundamental understanding of why polymer flexibility and polymer – sieve affinity are important and how they are related. A major goal of this work is to allow *a priori* predictions of membrane performance, and an understanding of these factors is essential for the realization of this goal. The importance of polymer flexibility in the formation of successful mixed matrix membranes is reviewed in section 4.2. Section 4.3 discusses polymer – sieve affinity, which impacts the strength of the interface. In section 4.4, a discussion of stresses encountered during membrane preparation is given. These stresses significantly affect membrane morphology and transport properties. A final section lists suggestions for the preparation of successful mixed matrix membranes.

4.2. POLYMER FLEXIBILITY AND MIXED MATRIX MEMBRANES

The inherent flexibility of polymers distinguishes them from other classes of materials and makes them desirable for membrane applications, since it allows easier processing than with other materials. In this section, methods to characterize polymer flexibility are first mentioned, followed by a brief discussion of the effect of various diluents on flexibility. Finally, the transport properties of mixed matrix membranes are correlated with the flexibility of the polymer matrix.

4.2.1. Characterization of Polymer Flexibility

Simha and Boyer suggested that the glass transition temperature (T_g) could be correlated with the inherent flexibility of a polymer chain [2]. The glass transition is a nonequilibrium phenomenon related to the entrapment of excess “free volume” in a sample as it is cooled from a “rubbery” state to a “glassy” state. Many polymer properties change abruptly at the T_g . An example is the change in slope of specific volume shown in Figure 2.1. Although the T_g is affected by many other factors, it has since become a popular measure of polymer flexibility. Other factors which affect the observed T_g include: molecular weight, intramolecular interactions, the thermal history of the sample, and such experimental considerations as the rate of measurement and the measurement method used. The most common method for the determination of the T_g is differential scanning calorimetry. Glass transition temperatures for several of the polymers used in this work are reported in Table 4.1.

A more fundamental measure of the flexibility of a polymer chain is the statistical chain segment length, embodied as either the Kuhn length [3] or the persistence length [4]. The Kuhn length is traditionally used to characterize more flexible materials, while the persistence length has been used to describe so-called “worm-like” semirigid and highly rigid materials such as DNA [4]. The Kuhn length is the length of a hypothetical monomer unit necessary to fit the random coil model of a polymer chain. In general, a polymer with a contour length of greater than 10 Kuhn lengths can be approximated as

a random coil [5]. Several researchers have noted that polyimides behave more like random coils than rigid rods, unless the chains are very short [6-8]. Kuhn lengths from the literature are given in Table 4.1. When determining the Kuhn length, a solvent that gives the unperturbed dimensions of the chain should be used, at the “theta” condition. A theta solvent is a somewhat poor solvent, which tends to contract a chain, to balance the expanding effect of excluded volume [9]. In this work, the glass transition is used predominantly as a measure of polymer flexibility, since it is more experimentally accessible and easily related to actual formation conditions, as discussed later.

Table 4.1: Glass transition temperatures and Kuhn Lengths of selected polymers.

Polymer	Glass Transition Temperature		Kuhn Length	
	T _g , °C	Source	L _K , Å	Source
Matrimid [®]	305°C	[10]	42 Å	††
Ultem [®]	208°C	[10]	23.1 Å, 18.9Å	[11], [12]
Udel [®]	187°C	[13]	16.3 Å, 17.3 Å	[11], [14]
PVAc	30°C	[15]	16.0Å	[14]
40% Hydrolyzed PVAc	52°C	†		

† Extrapolated based on T_g of poly(vinyl alcohol) (85°C) and PVAc from [16].

†† This was determined via light scattering in chloroform. It is consistent with other reported Kuhn lengths for polyimides [6].

4.2.2. Effect of Low Molecular Weight Diluents on the Glass Transition Temperature

Low molecular weight diluents, such as solvents or highly swelling penetrants, tend to decrease the glass transition temperature of a polymer (i.e. increase flexibility) [17-20]. Nonetheless, at low concentrations they can actually decrease the flexibility of polymer chains [21]. The nature of the interaction between the diluent and polymer determines the magnitude of the decrease (or increase) in the T_g. This is important as remaining

solvent can increase the flexibility of the matrix during the critical stages of membrane formation, giving mixed matrix membranes with favorable morphologies. Intuitively, a smaller amount of a stronger solvent should be required to achieve the same Tg depression as weaker solvent. Theories exist to predict the Tg depression by diluents. Chow proposed the following equation [22]:

$$Ln\left(\frac{Tg}{Tg_0}\right) = \frac{zR}{M_p\Delta C_{PP}} [(1-\theta)\ln(1-\theta) + \theta\ln\theta] \quad (4.1)$$

where Tg_0 is the glass transition temperature of the neat polymer, z is a lattice coordinate number, R is the gas constant, M_p is the molecular weight of a monomer, and ΔC_{PP} is the excess transition isobaric specific heat of the polymer. The lattice coordinate number has been taken as 1 [18] or 2 [22], to fit the experimental data. The parameter θ is given by:

$$\theta = \frac{V_P}{zV_D} \frac{\phi_D}{1-\phi_D} \quad (4.2)$$

where ϕ_D is the volume fraction of diluent, and V_P and V_D are the molar volumes of the polymer and diluent, respectively. This equation has been successfully used to model the decreases in Tg with increasing CO₂ pressure [18, 22, 23].

4.2.3. Correlation of Mixed Matrix Membrane Transport Properties with Polymer Flexibility

An examination of past work reveals that polymer flexibility is a very important parameter affecting mixed matrix membrane transport properties. A quick review of section 2.4.1 shows that mixed matrix membranes prepared with many rubbery matrices display enhanced selectivity over the neat polymer. Among the mixed matrix membranes based on glassy polymers (see section 2.4.2), most successful membranes were prepared under conditions where the polymer matrix was at or above its Tg. Some

membranes were prepared at elevated temperatures, while others were prepared by adding a plasticizer to enhance the flexibility of the matrix. Few successful examples exist of glassy polymer-based mixed matrix membranes for gas separations prepared below their T_g . A notable exception is zeolite 4A dispersed in 6FDA-6FpDA:4MPD:DABA (2:2:1) prepared by Mahajan [24]. As discussed in the following section, this may be the result of a specific interaction between carboxylic acid pendant groups on the polymer and the surface of zeolite 4A. The reasons for the importance of flexibility of the polymer matrix and the apparent exception of the polymer with specific interactions should become clear in section 4.4.

4.3. POLYMER – SIEVE AFFINITY AND MIXED MATRIX MEMBRANES

Another important factor governing the properties of the interface is the affinity of the polymer for the sieve. If the polymer is incompatible with the sieve, a void between the two phases will form, which is detrimental to mixed matrix membrane performance. Subsection 4.3.1 details work to qualitatively characterize polymer – sieve affinity. The second subsection discusses mixed matrix membrane transport properties relative to polymer – sieve affinity. Model mixed matrix membranes were prepared using impermeable glass spheres. The affinity of these spheres for polymers was directly characterized using a novel atomic force microscopy technique.

4.3.1. Characterization of Polymer-Sieve Affinity

Perhaps the simplest measure of polymer – sieve affinity is to measure the force required to remove a polymer from the surface. Because the sieves are microscopic, this is not possible in practice. Nevertheless, a glass surface may provide a reasonable “surrogate” for the zeolites. Because the predominant active group on both is silanol ($-\text{Si}-\text{OH}$), it was thought they may exhibit similar surface properties. Thus, polymers were deposited from a dilute MeCl_2 solution onto glass slides in a ring covered with plastic wrap. Evaporated solvent quickly saturated the headspace, dramatically slowing the evaporation rate. Uncontrolled evaporation leads to “orange peel” in polymer films.

Initially, adhesion was characterized using the ASTM standard D3359-97, developed for coatings on metal substrates [25]. This is a “peel” test, wherein a 10×10 grid of 1 mm squares is cut into a coating adhered to a substrate using a razor. Regular office tape is then placed over the grid and removed by pulling it back at a 180° angle. The tape used was Highland 6200 Invisible Scotch Tape (3M; St. Paul, MN). According to the ASTM standard, the adhesion is then classified on a scale of 0 - 5 based on the fraction of the coating remaining on the substrate. This classification is presented in Table 4.2 along with the average percent removed and standard deviation for four test specimens. The “B” after the classification indicates that the test was performed according to method B of standard D3359-97. These polymers were selected because mixed matrix membranes had previously been prepared from them, so these results could be compared with membrane performance.

Table 4.2: Adhesion of polymer films coated on glass slides as characterized using ASTM standard D3359-97. Percent removed and standard deviation from four samples.

	ASTM Grade	Percent Removed
PVAc	5B	0
40% Hydrolyzed PVAc	3B	5.8 ± 4.8
Epichlorohydrin	0B	79 ± 18
Udel [®]	3B	6.7 ± 10.7
Ultem [®]	4B	1.7 ± 3.0
Matrimid [®]	4B	1.7 ± 2.0

The results of this test did not correlate well with membrane performance. Membranes with well adhered interfaces had been prepared with the flexible materials PVAc (highest adhesion in Table 4.2), 40% hydrolyzed PVAc, and epichlorohydrin (lowest adhesion in Table 4.2). The three rigid engineering thermoplastics all displayed sieve-in-a-cage morphology. The reason for the poor correlation with membrane performance

may be related to the principle of the test. This test essentially determines whether the adhesion between polymer and substrate or between tape and polymer is stronger, which both vary for each polymer. This test is typically used to characterize the adhesion of coatings onto different substrates. In this case, the tape – coating adhesion is constant and coating – substrate results can be compared.

A more fundamental method was desired to characterize polymer – sieve affinity, so the adhesive force between a glass sphere and a polymer film cast onto a glass slide was measured with atomic force microscopy (AFM). These measurements were performed by Thomas Baekmark and Georges Belfort of Rensselaer Polytechnic Institute. Borosilicate glass spheres of 2.5 μm diameter (Duke Scientific; Palo Alto, CA) were used as a surrogate for zeolite 4A since a method for gluing glass spheres onto an AFM tip was already known [26]. Figure 4.1a shows the repulsive force, measured as the AFM cantilever is moved toward the surface and Figure 4.1b shows the attractive force, measured as the cantilever is moved away from the surface. Since it is believed that the polymer is being pulled away from the sieve during film formation, the attractive force may be expected to better correlate with mixed matrix membrane properties. Figure 4.1 shows that Udel[®] interacts least favorably with glass, and Matrimid[®] and Ultem[®] are intermediate between Udel[®] and the PVAc. The hydrolyzed PVAc attractive force has a high standard deviation, and could match the attractive forces most of the other polymers. PVAc appears to have the best compatibility with glass. Nonetheless, the high standard deviations on the adhesive forces for these later four materials make it difficult to say with certainty that one polymer has a significantly better interaction with glass than the others. Not surprisingly, glass is most attractive toward itself.

A second set of adhesive force experiments between the polymer coated glass slides and a Matrimid[®] coated glass sphere was performed. These results show that Matrimid[®] has a greater affinity for itself than for glass, as expected. This is a critical observation, since if the Matrimid[®] – Matrimid[®] interaction was weaker than the Matrimid[®] – glass

interaction, delamination would be expected in the polymer matrix (cohesive) and not at the polymer-glass interface (adhesive), where it is observed.

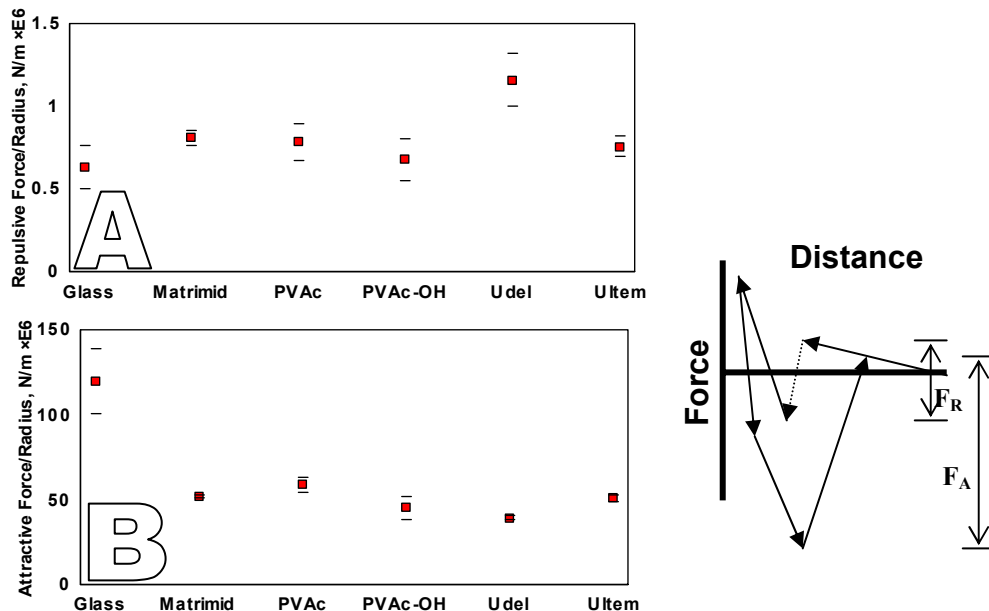


Figure 4.1: (a) Repulsive and (b) attractive forces measured between polymer-coated slides and glass spheres glued to an AFM tip. The repulsive force, F_R , is measured as the tip is advanced toward the polymer coated surface, while the attractive force, F_A , is measured as the tip is removed from the sample as shown in the inset.

Clearly the AFM results above do not provide a basis to predict membrane performance with zeolite 4A. More rigorous thermodynamics can better account for both dispersive and specific (e.g. hydrogen bonding or acid-base) interactions, allowing better prediction of polymer – sieve affinity. A discussion of the types of *specific* interactions expected between polymers and sieves and potential methods to quantify them follows.

Initially, polymer – sieve interactions were quantified using the liquid-solid-solvent strength parameter, ϵ° , which correlates the elution time of solvents through packed chromatographic columns [27]. Equations are given for calculating ϵ° :

$$\epsilon^\circ_{SILICA} = -0.519 + \frac{0.043\delta_s}{MPa^{1/2}} \quad (4.3)$$

$$\varepsilon^{\circ}_{ALUMINA} = -0.786 + \frac{0.0611\delta_s}{MPa^{1/2}} \quad (4.4)$$

where δ_s is the solubility parameter of the solvent in $MPa^{1/2}$. The liquid-solid-solvent strength parameter, ε° , varies from 0 to 1, with 0 corresponding to pentane, which has only dispersive interactions. Of course, this method has the disadvantage that liquid-solid-solvent strength parameters are not known for zeolite 4A, but it seems reasonable to assume that it will have parameters similar to alumina and silica. These relations can also be used with solubility parameters (Table 4.3) of polymers, either measured or calculated by group contribution methods [28-30], to estimate polymer – sieve affinity. An increasing ε° indicates increasing specific interactions with the polymer or solvent, so polymers with higher solubility parameters are expected to have more favorable specific interactions with zeolite 4A. Thus, PVAc would be expected to have a weaker interaction with zeolite 4A than Matrimid[®], which was not found to be the case based on mixed matrix membrane morphology and transport properties.

Table 4.3: Solubility parameters for selected polymers. Solubility parameters for the engineering polymers were calculated using the group contribution method of Fedors as reported by van Krevelen [28-30]. Other values taken from the source given in brackets.

Material	Solubility Parameter (MPa) ^{1/2}
Matrimid [®]	27.8
Ultem [®]	26.3
Udel [®]	†
PVAc	18.6-19.9 [15]
40% Hydrolyzed PVAc	25.8-29.1 [28]

† The solubility parameter for Udel[®] could not be estimated as there is no provision for sulfur in the method.

Acid-base interactions have been shown to be an important factor determining adsorption of polymers onto surfaces [31, 32]. Fowkes has shown that basic polymers will adsorb onto acidic surfaces, but not basic ones [31]. This is illustrated in Figure 4.2. Similarly, acidic polymers will adsorb onto basic surfaces. The solvent from which the polymer is adsorbed also plays an important role, since it may be able to displace the polymer if it interacts more strongly than the polymer. The mechanical properties of polymer – filler systems are improved when they are prepared from solvents that are more amenable to polymer adsorption [33]. Simply coating the sieve with a compatible polymer may not guarantee good interfaces, since the coating layer must be compatible with the bulk polymer. Dilsiz reports that Ultem[®] and polyurethane sized carbon fibers show decreased adhesion due to masking of adsorption sites on a fiber and the inability of the bulk epoxy matrix and sizing polymer to interweave [32].

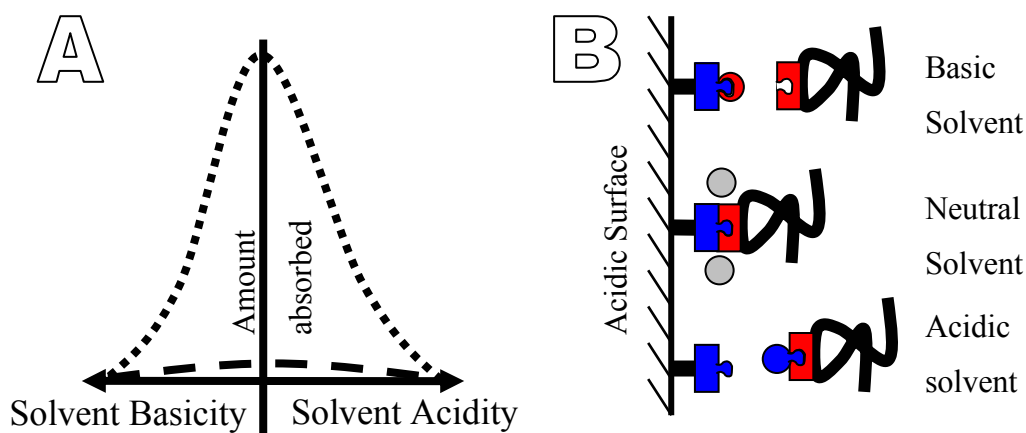


Figure 4.2: (a) Amount of polymer absorbed onto an acidic surface as a function of the solvent character: acidic polymer (- - -), basic polymer (· · ·). (b) Cartoon to explain the effect of solvent on polymer adsorption. Acidic moieties (electron accepting), blue; basic moieties (electron donating), red; neutral solvent, gray.

Appendix D contains a discussion of more detailed relationships to quantify acid-base interactions. These relationships were not used because obtaining the parameters for these relationships is in many cases more difficult than preparing membranes. Therefore, these more detailed relationships can not serve as a basis to predict mixed matrix membrane transport properties.

4.3.2. Correlation of Mixed Matrix Membrane Transport Properties with Polymer – Sieve Affinity

Concurrent with the AFM measurements, membranes were prepared and characterized using the same glass spheres. The oxygen permeabilities of the sphere filled membranes are compared with permeabilities predicted using the Maxwell model in Table 4.4. The higher permeabilities for all but hydrolyzed PVAc indicate that all these membranes have voids between the polymer and sieve. This was verified with the SEM. Figure 4.3 shows glass spheres dispersed in hydrolyzed PVAc and Udel[®], as examples of good and bad polymer – sieve adhesion, respectively. SEMs for Matrimid[®], Ultem[®], and PVAc show voids similar to those in Udel[®]. The hydrolyzed PVAc displays a permeability lower than the prediction, which is consistent with earlier observations for zeolite 4A filled mixed matrix membranes attributed to matrix rigidification [1, 34]. Curiously, PVAc does not form void-free mixed matrix membranes with these spheres, even though PVAc – zeolite 4A does. This was a repeatable phenomenon as several membranes were prepared with spheres dispersed in PVAc and they all gave similar behavior. This may be due to a lower silanol concentration on the surface of the borosilicate glass spheres than on zeolite 4A, since it is believed that the PVAc undergoes strong interactions with the silanol groups. In section 5.4.1, significant differences in the affinity of Ultem[®] for various glass types will be discussed. It is also believed that differing silanol content on the surface of these various glass types plays an important role in adhesion.

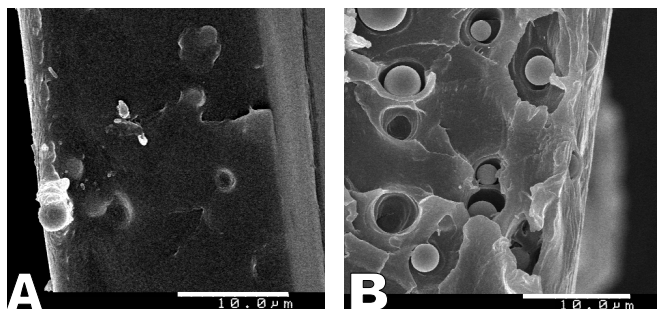


Figure 4.3: SEM of glass spheres dispersed in (a) 40% hydrolyzed PVAc and (b) Udel[®].

Table 4.4: Oxygen permeabilities for mixed matrix membranes with impermeable glass spheres. The calculated permeability was determined using the Maxwell model, assuming the spheres were impermeable. Tested at 35°C and 65 psia.

Polymer	Permeability, Barrer		Percent Difference
	Experimental	Calculated	
Matrimid [®]	1.85	1.80	2.7%
Ultem [®]	0.50	0.34	47%
Udel [®]	1.65	1.2	38%
PVAc	0.61	0.43	42%
40% hydrolyzed PVAc	0.23	0.24	-4.2%

Dispersive forces may be inadequate to withstand the stresses occurring during membrane formation. These stresses may cause delamination of the polymer matrix from the sieve surface, as discussed in the following section. Indeed, only four polymers were previously known that can form void-free mixed matrix membranes with unsilanated zeolite 4A: PVAc, hydrolyzed PVAc, epichlorohydrin, and 6FDA-6FpDA:4MPD:DABA. However, closer examination of these materials reveals the potential for specific interactions with the surface. The carbonyl groups in PVAc and hydrolyzed PVAc are basic and can form acid-base complexes with acidic silanol groups found on the sieve surface [35]. Similarly, DABA group of 6FDA-6FpDA:4MPD:DABA may actually react with silanol groups on the zeolite, but if not it is certainly capable of hydrogen bonding with silanols on the zeolite surface. This would make polymer – sieve delamination unlikely. Epichlorohydrin may also be able to form hydrogen bonds sieve silanol groups and its ether group. Silanation of zeolites is one method to improve polymer – sieve affinity by adding specific interactions. Void-free mixed matrix membranes have been prepared with several additional polymers, including Ultem[®], using silanated zeolites.

4.4. EFFECT OF CASTING CONDITIONS ON MIXED MATRIX MEMBRANES

An understanding of how preparation conditions lead to different morphologies is vital for generating mixed matrix membranes with desirable transport properties. Individual polymer chains occupy less volume as more solvent is removed, whereas the volume of the inorganic materials considered here is unaffected by solvents. As the solvent evaporates from the polymer chains, the polymer chains must relax on *the same timescale* to reach their new equilibrium conformation; otherwise stresses will arise in the material. Once a polymer vitrifies, the timescale for relaxation via polymer diffusion becomes very long, so polymer chains can not diffuse relative to one another over experimentally accessible timescales to relieve stresses. Clearly, this is more likely to be a serious factor for higher T_g polymers. Depending on the magnitude and direction of these stresses, which themselves depend on material and formation considerations, either a void (sieve-in-a-cage) or a rigidified region (matrix rigidification) may develop at the polymer – sieve interface. These may initially appear to be contradictory effects, but the analysis below will show how these effects are caused by the same phenomenon. Both solvent evaporation and cooling from an elevated temperature may cause a rigidified region near the particles, because both cause contraction of the matrix. Thermal effects are considered in section 4.4.4.

4.4.1. Unconstrained Films; Matrix Rigidification

The formation of rigidified/compressed interfaces caused by stresses arising during solvent evaporation is discussed first. Figure 4.4 (top left) shows a polymer matrix with spherical voids at the vitrification point (i.e. stresses can no longer relax as they are formed). This essentially prevents the centers of mass of each chain from moving relative to the centers of mass of other chains, but does not prevent overall contraction of the membrane. Because each chain occupies less volume with incremental solvent loss and no additional chains can diffuse to the polymer – void interface, the diameter of the encapsulated void will decrease. This will allow the polymer chains to maintain a

random-coil-like conformation. Because the distances between the centers of mass of each set of polymer chains decrease by the same factor, the resulting polymer matrix exists in a stress free, although smaller, configuration (top right of Figure 4.4).

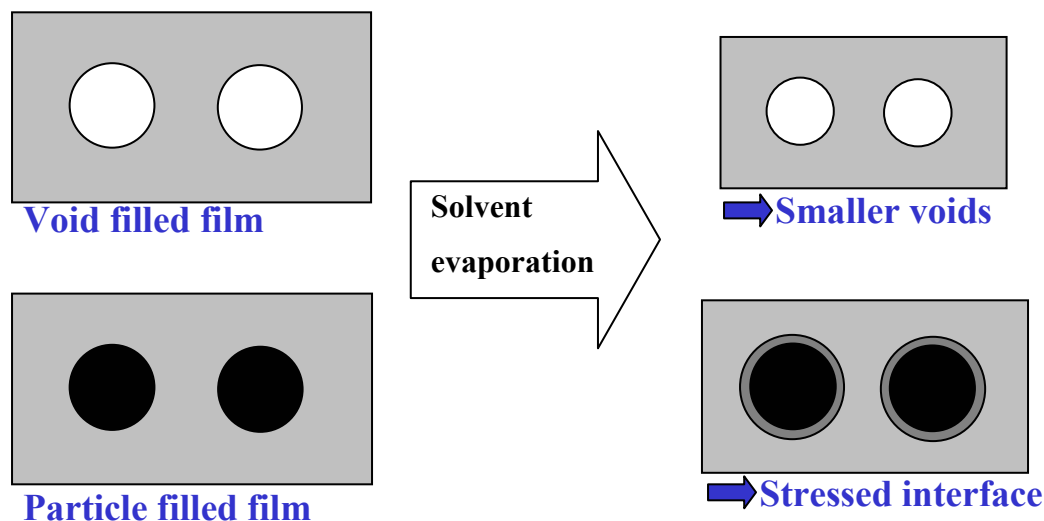


Figure 4.4: Comparison of contraction in a material with spherical voids and rigid spherical particles. The dark gray region indicates rigidified polymer.

If the voids in the polymer matrix at its vitrification point are replaced with particles, the result is quite different. Because each polymer chain must occupy the same surface area on the particle with incremental solvent loss, the chains at the surface lose their volume only in the direction normal to the particle surface. This gives chains with a distorted, flattened morphology on the surface rather than a random coil conformation. Because of this *inhibited contraction* by the particle surface, the polymer ends up stretched over the surface, causing a compressive stress on the particle. This effect could extend many polymer layers from the particle into the bulk polymer. Modeling of several mixed matrix systems suggests affected regions of 0.5 to 0.7 μm for 5 μm zeolites [34, 36].

Because polymer near the particle exists in a non-equilibrium, somewhat compressed conformation, it is reasonable to assume its transport properties differ from the bulk polymer. Because the chains are stressed, their segmental mobility is likely lower, so

polymer within the affected region would likely display a lower permeability. In fact, modeling of several mixed matrix systems suggests the permeability in the affected region is reduced by a factor of 3 or 4 compared to the bulk polymer [34]. Similar effects occur in the amorphous phase near crystallites in semicrystalline polymers [37, 38]. The permeability reduction may be more pronounced for larger penetrants, as found in semicrystalline polymers [37, 39], but the data are inconclusive.

If this *inhibited contraction* hypothesis is correct, there should be higher stresses in the polymer matrix near the particles. The stress field in mixed matrix materials was analyzed using birefringence microscopy. Birefringence is caused by differences in refractive index, which are indicative of oriented polymer chains. Stresses at the interface could lead to orientation of polymers near the particles. Figure 4.5 shows birefringence microscopy images of two mixed matrix membranes taken through the plane of the membranes. Neither membrane has visible sieve-in-a-cage morphology with the SEM. Both polymer matrices exhibit light areas indicating higher stresses near particles. As expected, the Matrimid[®]-based membrane shows higher stresses (birefringence) at the interface, presumably caused by its higher T_g.

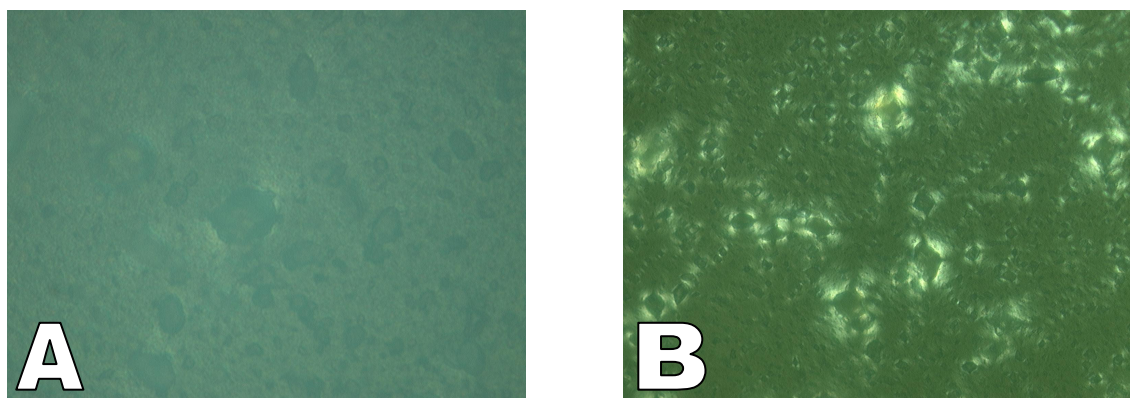


Figure 4.5: Birefringence images of (a) zeolite 4A dispersed in Ultem[®] and (b) zeolite 4A dispersed in Matrimid[®]. The largest particles in the images are $\sim 5 \mu\text{m}$.

4.4.2. Constrained Films; “Sieve-in-a-Cage” Formation

Void formation in mixed matrix membranes has been attributed to many factors [1]:

- A fundamental incompatibility between the polymer and sieve phases
- Inability of the polymer to conform to the sieve surface due to low flexibility
- Stresses developed during membrane formation due to solvent evaporation

The stress that develops seems to be the underlying cause of sieve-in-a-cage morphology. Depending on the magnitude of the stress developed during membrane formation, poorer polymer – particle interactions or less flexible polymers can be tolerated. Allowing the film to contract in only one dimension (e.g. if adhered to a casting substrate) leaves the film in biaxial tension. If the stress is great enough, voids may form at polymer – particle interfaces as discussed below.

When a film is prepared on a substrate, most of the contraction due to solvent evaporation must occur perpendicular to the substrate (z-direction). For a film of finite size, a small amount of lateral contraction can occur in the plane of the film (x- and y-directions) since only the top edge is unconstrained. First, contraction in a neat polymer film is considered and then the effect of particles suspended in a matrix is addressed.

4.4.2.1. Particle-Free Films

Stress development due to solvent evaporation from films adhered to a substrate has been studied directly using an overhanging-beam method [40] or a parallel-plate capacitor method [41]. A brief review of two models for residual stresses in solvent cast films follows. One assumption, frequently implicit, made by these researchers is that the film can contract only perpendicular to the substrate.

Croll assumed that relaxation processes (e.g. polymer diffusion) prevent stress accumulation in a rubbery material. Thus, *stresses do not accumulate until enough*

solvent has evaporated to make the nascent film glassy. Based on this assumption, Croll presents the following expression for the stress that develops during solvent evaporation in a neat polymer film adhered to a substrate [42]:

$$\sigma_R = \frac{E}{3(1-\nu)} \frac{\phi_S - \phi_R}{(1-\phi_R)} \quad (4.5)$$

where σ_R is the residual stress in the plane of the film, E is the tensile modulus, ν is Poisson's ratio, ϕ is the volume fraction, and the subscripts S and R refer to the solvent present at the "solidification" point and in a "dry" film, respectively. The solidification point occurs when the Tg of the nascent film is equal to the preparation temperature. The factor $(3(1-\nu))^{-1}$ arises because the film is in biaxial tension. A calculation shows that for neat Ultem[®], ($E = 3309$ MPa, $\nu = 0.36$ [43]), assuming 10% residual solvent at the solidification point, a stress of ~170 MPa develops, well below the failure strength of neat Ultem[®]. This probably represents a conservative estimate because higher percentages of residual solvent were measured in Ultem[®]-based mixed matrix films believed near their solidification point.

Monk modeled the stresses generated during the formation of polyimide films cast on a substrate [44]. A substantially similar model of this process was subsequently presented by Lee [45]. This analysis accounted for three sources of stress: curing of the polyimide from the poly(amic acid), solvent evaporation from the nascent film, and stresses induced by the difference in thermal expansion between the film and substrate. For simplicity, parameters in the model were assumed functions of temperature and concentration only. Thus, it would be difficult to adapt this model to the fixed temperature profile encountered during membrane casting. The model includes numerous equations and is not duplicated here for brevity. Nonetheless, solvent evaporation was found to be a significant source of the total stress.

4.4.2.2. Films Containing Particles

Filled polymer films as coatings were studied by both Croll and Perera. In general, these researchers were interested in the overall in-plane stress, since it governs film integrity and film – substrate delamination. This work is summarized below.

As in neat polymer films, Croll assumed that stresses begin to accumulate in a particle filled film only after enough solvent has evaporated to raise its Tg to the preparation temperature [46]. The following expression was derived for the strain in the film:

$$\varepsilon = \frac{\left(\frac{\phi_S}{1-\phi_S} - \frac{\phi_R}{1-\phi_R} \right)}{3 \left(1 + \frac{\phi_S}{1-\phi_S} + \frac{\phi_P}{1-\phi_P} \right)} \quad (4.6)$$

where ε is the strain, ϕ is a volume fraction, and the subscripts S and R are the same as before and P refers to the particle, which were pigments in Croll's work. Here, ϕ 's are defined relative to the amount of polymer. The residual stress in the plane of the film should then be:

$$\sigma_R = \frac{E_C}{3(1-\nu_C)} \frac{\left(\frac{\phi_S}{1-\phi_S} - \frac{\phi_R}{1-\phi_R} \right)}{\left(1 + \frac{\phi_S}{1-\phi_S} + \frac{\phi_P}{1-\phi_P} \right)} \quad (4.7)$$

where the subscript C refers to the composite material. The modulus of the composite will generally increase, while the Poisson's ratio will generally decrease. This tends to increase the residual stress in particle filled composites compared to the corresponding neat polymer. The filler also tends to increase the Tg of the surrounding polymer matrix, so the onset of stress formation is earlier than in the corresponding neat polymer film (i.e. ϕ_S is higher in a filled polymer than the corresponding neat polymer). The net

effect is to make the residual stress in a particle filled composite higher than the corresponding neat polymer, unless the stress is high enough to initiate a relief mechanism. Relief mechanisms include delamination from the substrate, cracking of the polymer matrix, and debonding of the polymer – particle interface. Croll noted films that adhered to the substrate tended to display voids between the polymer and particle, while those that delaminated from the substrate typically had good polymer – particle adhesion. The later outcome is desirable for mixed matrix membranes.

Perera provided a brief review of adhesion and stress in organic coatings [47], including the effects of solvent evaporation, thermal expansion, and environmental swelling (e.g. humidity) on the residual stress. He introduced the concept of a critical pigment (particle) volume concentration (CPVC) [48]. The residual stress increases to the CPVC and then rapidly decreases once it is exceeded. Below the CPVC, relaxation processes dominate, while relief mechanisms dominate above the CPVC. Perera found that the onset of stress accumulation roughly coincided with the transition from external mass transfer controlled to diffusion limited solvent evaporation from the nascent film [49]. In the same work, he also showed that the materials prepared from solvents with higher plasticizing effectiveness produced films with less residual stress. He also identified polymer – particle interactions as important in determining the maximum residual stress [50]. Stronger interactions lead to higher maximum residual stresses because polymer – particle debonding requires a higher stress to initiate. Many of these concepts have been observed or hypothesized for mixed matrix membranes.

The models for the neat and particle filled polymers are for the *overall* stress in the film, which will likely differ from the local stress at the polymer – particle interface. The stress at the polymer – particle interface is likely the controlling factor in void formation. Next, the effect of particles in a constrained polymer film on the local polymer – particle stress is qualitatively considered.

The stress field in a particle filled film is complex, so the behavior of polymer between two sets of particles will first be analyzed before behavior in a mixed matrix film is considered. Figure 4.6 shows hypothesized behavior for polymer between two sets of particles that are aligned either vertically or horizontally. For both sets of particles, it is assumed that all movement must occur in the z-direction, corresponding to the expected behavior in a mixed matrix membrane. The vertically aligned particles will move toward each other, and this will result in a more compressive stress in the z-direction at the center of the polymer ($x = 0$) than at the edge ($x = r_p$). This is proven in detail in Appendix E. In the horizontally aligned particles, the polymer will tend to contract toward the center of the polymer matrix. This will cause a substantial stress in the x-direction because the particles can not move closer together to alleviate it. However, if the tensile stress in the polymer between the horizontally aligned particles is greater than the interfacial strength, the interface between the polymer and the particle will fail. Thus, for vertically aligned particles, the stress is relieved by particle movement. Conversely, the only relief mechanisms available to polymer between horizontally aligned particles are cohesive or adhesive failure.

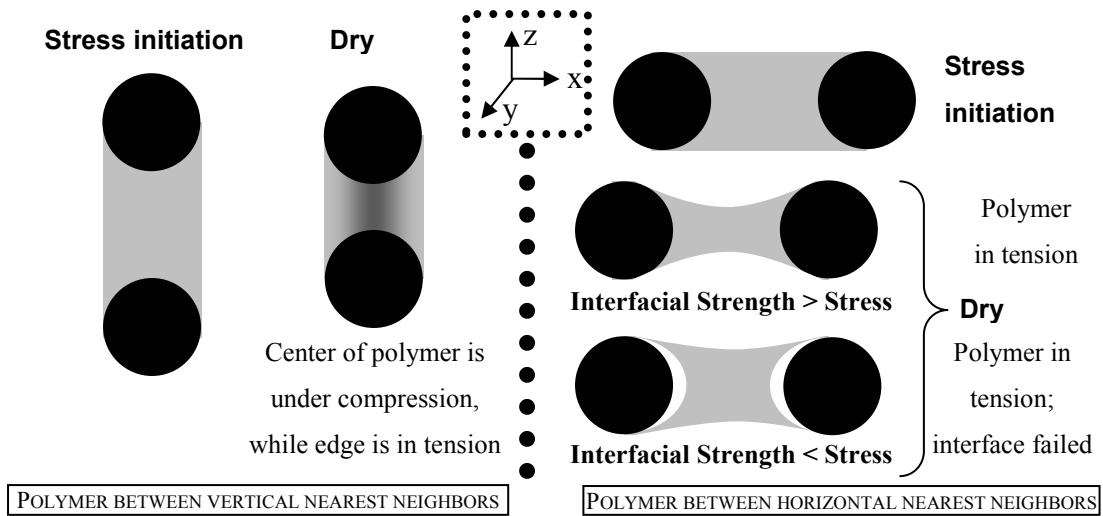


Figure 4.6: Simplified cartoon showing behavior of polymer between particles.

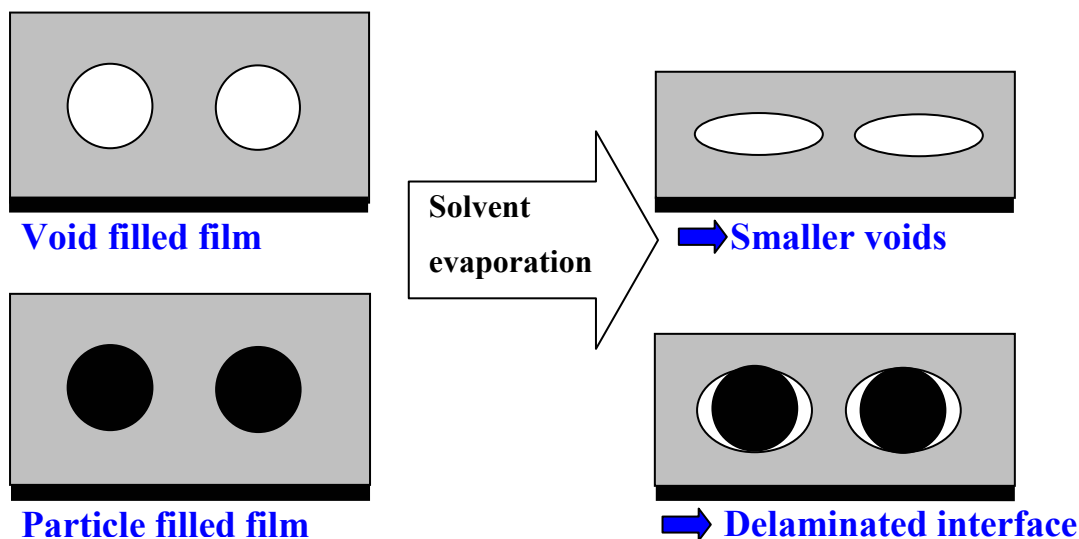


Figure 4.7: Cartoon showing the effect of a constrained boundary on membrane morphology; delamination of the polymer – particle interface.

Figure 4.7 shows a simplistic cartoon contrasting the hypothesized behavior for a constrained film containing particles with a particle free film. In the particle free film, the voids deform in response to the large stress that develops in the plane of the film. In a constrained particle filled film, the polymer can only move in the z-dimension (neglecting edge effects), so the same is true of the particles. Since the particles do not change shape as the solvent evaporates, there will be a stress distribution on the particle surface. Polymer – particle affinity is typically much weaker than polymer – polymer affinity, so any failure is expected at the polymer – particle interface. In particular, it appears that substantial stresses in the plane of the film cause tensile stresses on the particle parallel to the plane of the film. The polymer – particle interface will fail if the interfacial strength is less than the stress developed at any point on the surface. The most likely point of failure is at the particle poles with normal parallel to the substrate, as shown in Figure 4.7.

The strength of the interface is determined by the affinity between the polymer and the particle. Therefore, specific polymer – particle interactions (e.g. acid-base) will be helpful in overcoming stresses that arise during membrane formation. Modification of

the particle surface may be necessary to enhance polymer – particle affinity so larger stress can be tolerated. However, even silane modified zeolite 4A exhibits relatively weak interfaces with polymer matrices. The interfacial strength for silane modified interfaces are reported to be at most 30 MPa for a poly(vinyl butyral) matrix [51-54]. Recall that the calculated stress for an Ultem[®] film was 170 MPa. This is much greater than the strength of the interface, explaining why failure is observed at the interface.

4.4.3. Effect of Priming Conditions on Mixed Matrix Membranes

Priming of the sieves may lead to even more complex effects, illustrated in Figure 4.8. The most important criteria for selection of a priming polymer are (i) compatibility with the sieve surface and (ii) miscibility with the matrix polymer. These should be considered when developing membrane priming procedures. Miscibility can be assured by using the matrix polymer for priming, but if insufficient time is allowed for the priming layer and the matrix to interdiffuse, a poor matrix – priming polymer interface may result. Alternatively, if the priming polymer is held too tightly by the sieve, the matrix polymer may be unable to interdiffuse with it. This problem was reportedly encountered with Ultem[®] and polyurethane primed glass fibers in an epoxy matrix [32].

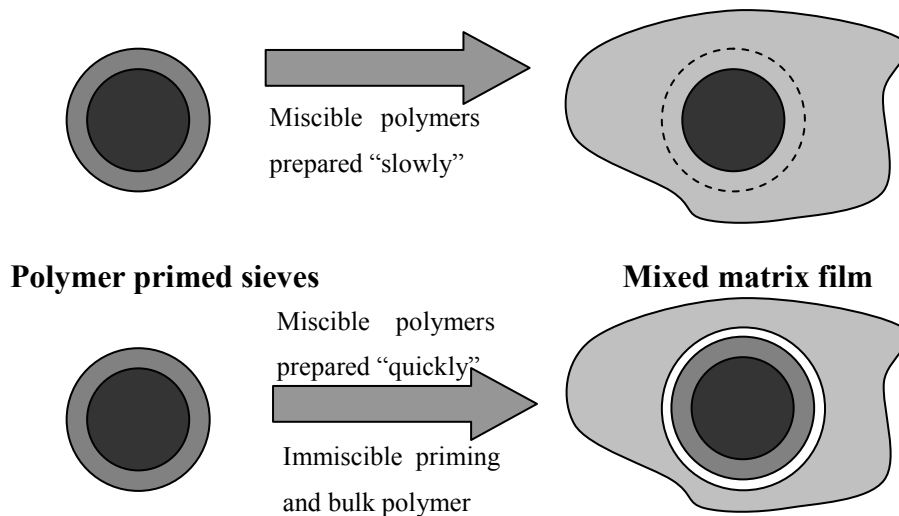


Figure 4.8: Cartoon showing likely mixed matrix morphology as a function of solvent evaporation time.

4.4.4. Effect of Drying Conditions on Mixed Matrix Membranes

A mismatch in the thermal expansion coefficients between matrix and filler is frequently cited as a cause of interfacial failure in composites [55, 56]. The thermal expansion coefficients of polymers are generally greater than those of sieves, as shown in Table 4.5. As the matrix expands with an increase in temperature, polymer at the interface is pulled *away* from the sieve, rather than toward it, which one might initially expect. Conversely, cooling a film causes a compressive stress on the interface. The arguments explaining this observation are outlined in Figure 4.9. If the matrix expands isotropically, the dimensions of the shell of polymer encasing the sieve must increase during heating. Since the volume of the sieve increases less with temperature, this will cause either a tensile stress or a void at the polymer – sieve interface.

Table 4.5: Selected physical properties for polymers and sieves used in this work.

Polymer	Thermal Expansion Coefficient, °C ⁻¹	Young's modulus, MPa (tensile)	Poisson's Ratio
Matrimid [®]	2.8×10^{-5} [57]	2689 [57]	
Ultem [®]	5.4×10^{-5} [43]	3309 [43]	0.36 [43]
Udel [®]	5.6×10^{-5} [58]	2452 [58]	
Poly(vinyl acetate)	22×10^{-5} [15]	600 [15]	
Zeolite 4A	6.9×10^{-6} [59]	$6.9 \times 10^4 - 8.7 \times 10^4$ † [60]	0.22 † [61]

† Data is for glass. This probably gives a lower bound for the modulus of zeolite 4A as glass is amorphous whereas zeolite 4A is crystalline.

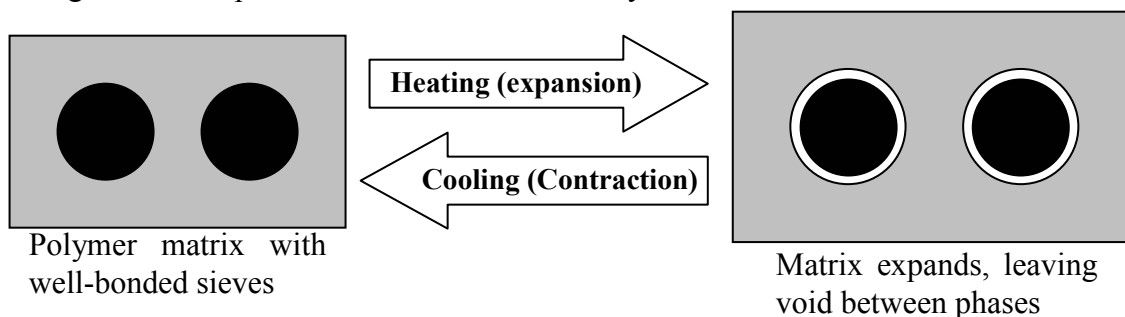


Figure 4.9: Cartoon showing the effect of (isotropic) expansion and contraction.

Thermal expansion in particle filled composites has been analyzed by Nielsen [61] and Kraus [62]. The stress due to thermal expansion/contraction is given by:

$$\sigma = EK(\alpha_1 - \alpha_2)(T_0 - T) \quad (4.8)$$

where σ is the tangential tensile stress at the interface, E is the Young's modulus of the polymer, α_1 and α_2 are the thermal expansion coefficients of the polymer and filler, respectively, and T_0 is the glass transition temperature. K is a shape factor given by the following equation (for a single sphere embedded in a matrix):

$$K = \frac{1}{2 \left(\frac{1 + \nu_1}{2} + \frac{1 - 2\nu_2}{E_2 / E_1} \right)} \quad (4.9)$$

where ν_1 and ν_2 are the Poisson's ratios of the polymer and filler, respectively, and E_1 and E_2 are the Young's moduli for the polymer and filler, respectively.

A quick calculation using Eq 4.8 and Eq 4.9 reveals that a tensile stress of 20 MPa arises in Ultem[®] heated from 25°C to its Tg of 215°C. This calculation depends little on the modulus used for zeolite 4A (E_2) since it is an order of magnitude larger than that of Ultem[®]. These stresses are similar to the strength of silane modified interfaces (see section 4.4.2.2), so delamination is a possibility. Accordingly, heating of mixed matrix membranes prepared with high Tg polymers may cause failure of the polymer – sieve interface. Furthermore, drying above the Tg should relieve any stresses, but *the stress-free state at such temperatures may be with a void between polymer and sieve*, as in the right side of Figure 4.9. Then, as the material is cooled below its Tg, the polymer should contract back to its original dimensions, which should be near the sieve. Nonetheless, if the polymer – sieve interface has failed during heating, a favorable interface may not re-form during cooling. Also, annealing above Tg should not

eliminate matrix rigidification completely since the matrix will contract during cooling whether or not the matrix exists in a stress free state at the higher temperature.

4.5. SUGGESTIONS FOR THE FORMATION OF SUCCESSFUL MIXED MATRIX MEMBRANES

This chapter presented an understanding of membrane formation that explains how different mixed matrix membrane morphologies are formed. It explains the importance of polymer flexibility and polymer – sieve affinity identified by Mahajan. Based on this analysis, it appears that the polymer – sieve affinity may be less important than selecting membrane preparation conditions that either (i) avoid in-plane stresses in nascent films, or (ii) maintain flexibility during membrane preparation so that any stresses that do arise can relax. Enhanced polymer – sieve affinity may mitigate stresses that form, but the ability of the interface to tolerate the stress seems quite limited even for a zeolite modified with a silane coupling agent. Recall that the strength of silane modified interfaces was only reported to be ~ 30 MPa. Several methods to circumvent void formation due to stresses induced during membrane preparation can be inferred based on the previous section. The relative merits of each are discussed below, and several are investigated further in the following chapter. These include:

1. Using a high flexibility polymer so that the stresses do not accumulate until residual solvent levels are very low
2. Using a solvent with a better plasticizing effectiveness so that less solvent remains at the onset of stress development
3. Using a silane coupling agent to modify the zeolites to improve polymer – zeolite affinity
4. Casting at higher temperatures where the onset of stress development occurs with less solvent remaining

5. Casting on a nonstick surface to prevent tensile stresses from forming in the plane of the nascent film
6. Removing the nascent film from the substrate before or soon after it vitrifies to prevent stress accumulation
7. Using melt processing to prepare membranes to eliminate stresses associated with solvent evaporation

Inherently less flexible glassy polymers make better gas separation membranes than rubbery polymers so the first solution is not relevant. A polyimide is the preferred polymer matrix but they typically have high T_gs. There are very few good solvents for polyimides, so the second option is also limited. Void free films were prepared with silane coupling agent modified sieves in Ultem[®] (T_g = 215°C) but not Matrimid[®] (T_g = 305°C) when prepared at ~200°C on a glass plate. At this temperature, Ultem[®] would have little or no residual solvent when it vitrifies, while substantial solvent would remain in Matrimid[®] when it vitrifies. Void-free Ultem[®] – silane-coupling-agent-modified sieve films have been prepared at 100°C by removing the nascent film from the glass plate before or soon after it vitrifies. Suggestions 3 through 6 will be investigated in more detail in the following chapter. Researchers were able to prepare apparently void-free membranes (determined via SEM) comprised of zeolite 13X in Udel[®] using melt processing [63]. However, zeolite 13X was not suitable to separate the gas penetrants used, so increased selectivity was not observed.

If the understanding of membrane formation presented here is correct, it may be easier to prepare a mixed matrix membranes in hollow fiber form than in film form. Since the hollow fiber support layer is either the same polymer or a similar polymer, there is no underlying substrate to limit contraction to one dimension. However, an excessive draw ratio in the fiber could potentially lead to polymer – sieve debonding, since it would put the fiber in tension.

4.6. REFERENCES

1. Mahajan, R., Formation, characterization and modeling of mixed matrix membrane materials. Department of Chemical Engineering, University of Texas at Austin. 2000.
2. Simha, R. and R.F. Bayer. *J. Chem. Phys.* 1962, 37, 1003-7.
3. Kuhn, W. *Angew. Chem.* 1936, 49, 858-62.
4. Porod, G. *Monatshefte fuer Chemie* 1949, 80, 251-5.
5. Denkinger, P. and W. Burchard. *J. Polym. Sci., Part B: Polym. Phys.* 1991, 29, 589-600.
6. Ohya, H.; V.V. Kudryavtsev; and S.I. Semenova, *Polyimide membranes: Applications, fabrications, and properties.* 1996, Tokyo, Japan: Gordon and Breach Publishers.
7. Cotts, P.M.; T.M. Swager; and Q. Zhou. *Macromolecules* 1996, 29, 7323-7328.
8. Schmitz, L. and M. Ballauff. *Polymer* 1995, 36, 879-82.
9. Flory, P.J., *Principles of polymer chemistry.* 1953, Ithaca, NY: Cornell University Press.
10. Vu, D.Q., Formation and characterization of asymmetric carbon molecular sieve and mixed matrix membranes for natural gas purification. Department of Chemical Engineering, University of Texas at Austin. 2001.
11. Inoue, T. and K. Osaki. *Macromolecules* 1996, 29, 1595-9.
12. Pavlov, A.V.; O.M. Karanyan; A.G. Morozov; G.S. Matvelashvili; G.V. Kazakova; and N.A. Anissimova, *Molecular properties of poly(ether imide) in solution, in Polyimides and other high temperature polymers; proceedings of the 2nd. European technical symposium.* 1991. p. 173-7.
13. Affolter, S.; A. Ritter; and M. Schmid. *Macro.Matl. Engr.* 2001, 286, 605-610.
14. Aharoni, S.M. *Macromolecules* 1983, 16, 1722-8.
15. Lindemann, M.K., *Physical constants of poly(vinyl acetate), in Polymer handbook, J. Brandrup and E.H. Immergut, Editors.* 1989, John Wiley & Sons: New York. p. V/71-5.

16. Peyser, P., Glass transition temperatures of polymers, in Polymer handbook, J. Brandrup and E. Immergut, Editors. 1989, John Wiley & Sons: New York. p. VI209-VI212.
17. Ismail, A.F. and W. Lorna. *Sepr. Purification Tech.* 2002, 27, 173-194.
18. Chiou, J.S.; J.W. Barlow; and D.R. Paul. *J. Appl. Polym. Sci.* 1985, 30, 2633-42.
19. Wessling, M.; S. Schoeman; T. Van der Boomgaard; and C.A. Smolders. *Gas Sep. Purification.* 1991, 5, 222-8.
20. Di Marzio, E.A.; C. Castellano; and A. Yang. *J. Polym. Sci., Part B: Polym. Phys.* 1996, 34, 535-43.
21. Maeda, Y. and D.R. Paul. *J. Membr. Sci.* 1987, 30, 1-9.
22. Chow, T.S. *Macromolecules* 1980, 13, 362-4.
23. Vrentas, J.S. and C.M. Vrentas. *Macromolecules* 1991, 24, 2404-12.
24. Mahajan, R. and W.J. Koros. *Polym. Engr. and Sci.* 2002, 42, 1432-1441.
25. Standard test methods for measuring adhesion by tape test (d 3359-97). 1997, American Society for Testing and Materials: West Conshohocken, PA.
26. Frank, B.P. and G. Belfort. *Langmuir* 1997, 13, 6234-6240.
27. Barton, A.F.M., *Crc handbook of solubility parameters and other cohesion parameters.* 1983, Boca Raton, FL: CRC Press Inc.
28. van Krevelen, D., *Properties of polymers; their correlation with chemical structure, their numerical estimation and prediction from additive group contributions.* 3 ed. 1990, New York: Elsevier.
29. Fedors, R.F. *Polym. Engr. Sci.* 1974, 14, 147-54.
30. Fedors, R.F. *Polym. Engr. Sci.* 1974, 14, 472.
31. Fowkes, F.M. and M.A. Mostafa. *Ind. Eng. Chem. Prod. Res. Dev.* 1978, 17, 3-7.
32. Dilsiz, N. and J.P. Wightman. *Colloids and Surfaces, A: Physicochemical and Engineering Aspects* 2000, 164, 325-336.

33. Marmo, M.J.; M.A. Mostafa; H. Jinnai; F.M. Fowkes; and J.A. Manson. *Ind. Eng. Chem., Prod. Res. Dev.* 1976, 15, 206-11.
34. Moore, T.T.; R. Mahajan; D.Q. Vu; and W.J. Koros. *AIChE J.* 2004, 50, 311-21.
35. Fontana, B.J. and J.R. Thomas. *J. Phys. Chem.* 1961, 65, 480-7.
36. Manson, J.A. and E.H. Chiu. *J. Polym. Sci., Polym. Symp.* 1973, No. 41, 95-108.
37. Michaels, A.S. and R.B. Parker, Jr. *J. Polym. Sci.* 1959, 41, 53-71.
38. Michaels, A.S.; W.R. Vieth; and J.A. Barrie. *J. Appl. Phys.* 1963, 34, 13-20.
39. Michaels, A.S. and H.J. Bixler. *J. Polym. Sci.* 1961, 50, 413-39.
40. Croll, S.G. *J. Oil Colour Chem. Assoc.* 1980, 63, 271-5.
41. Patel, K.S.; P.A. Kohl; and S.A.B. Allen. *J. Polym. Sci., Part B: Polym. Phys.* 2000, 38, 1634-1644.
42. Croll, S.G. *J. Appl. Polym. Sci.* 1979, 23, 847-58.
43. Ultem product data sheet. 1997, GE Plastics: Pittsfield, MA.
44. Monk, D.J.; Y. He; and D.S. Soane, Stresses in polyimide films during cure and thermal cycling, in *Manufacturing processes and materials challenges in microelectronic packaging*. 1991, ASME: New York. p. 87-93.
45. Lee, S.H. and Y.C. Bae. *Macromolecular Theory and Simulations* 2000, 9, 281-286.
46. Croll, S.G. *Polymer* 1979, 20, 1423-30.
47. Perera, D.Y. *Prog. Organic Coatings* 1996, 28, 21-23.
48. Perera, D.Y. and D. Vanden Eynde. *J. Coatings Tech.* 1981, 53, 40-5.
49. Perera, D.Y. *J. Oil Colour Chem. Assn.* 1985, 68, 275-81.
50. Perera, D.Y. and D. Vanden Eynde. *J. Coatings Tech.* 1984, 56, 47-53.
51. Miller, A.C. and J.C. Berg. *J. Adhesion Sci. Tech.* 2002, 16, 495-507.
52. Harding, P.H. and J.C. Berg. *J. Appl. Polym. Sci.* 1998, 67, 1025-1033.

53. Harding, P.H. and J.C. Berg. *J. Adhesion Sci. Tech.* 1997, 11, 1063-1076.
54. Harding, P.H.; S.A. Page; J.A.E. Maanson; and J.C. Berg. *J. Adhesion Sci. Technol.* 1998, 12, 497-506.
55. Manson, J.A. and L.H. Sperling, *Polymer blends and composites.* 1976, New York: Plenum Press.
56. Kang, S.; S.I. Hong; C.R. Choe; M. Park; S. Rim; and J. Kim. *Polymer* 2000, 42, 879-887.
57. Matrimid product data sheet. 2000, Vantico, Inc.: Brewster, NY.
58. Udel product data sheet. 1993, Amoco Performance Products, Inc.: Alpharetta, GA.
59. Barrer, R.M. and W.M. Meier. *Trans. Faraday Soc.* 1958, 54, 1074-85.
60. Ko, F.K. and P. Fang, Inorganic fibers, in *Concise encyclopedia of polymer science and engineering*, J.I. Kroschwitz, Editor. 1990, John Wiley & Sons: New York. p. 472-7.
61. Nielsen, L.E. and T.B. Lewis. *J. Polym. Sci., Part A-2* 1969, 7, 1705-19.
62. Kraus, G. and J.T. Gruver. *J. Polym. Sci., Part A-2* 1970, 8, 571-81.
63. Gür, T.M. *J. Membr. Sci.* 1994, 93, 283-9.

Chapter 5. DEVELOPMENT METHODS TO PREPARE DESIRABLE MIXED MATRIX MEMBRANE MORPHOLOGIES

5.1. OVERVIEW: RELATIONSHIP BETWEEN MEMBRANE MORPHOLOGY AND TRANSPORT PROPERTIES

This chapter seeks to use the understanding of membrane formation developed in the previous chapter to prepare mixed matrix membranes having desirable morphologies and exhibiting favorable transport properties. The relationship between membrane morphology and membrane transport properties is well developed. Figure 5.1 reviews the O_2/N_2 transport properties expected for various mixed matrix membrane morphologies using the Ultem[®] – zeolite 4A system as an example. Figure 5.2 shows a similar plot for the Ultem[®] – HSSZ-13 system. Measured transport properties for several neat Ultem[®] membranes are shown on both figures to illustrate repeatability. The Maxwell model predicts a significant improvement in selectivity compared to neat Ultem[®] for both zeolites. Nonetheless, nonideal morphologies can cause the transport properties to vary from the Maxwell prediction. Many of these nonideal morphologies occur at the interface of the dispersed phase with the polymer matrix. These nonideal morphologies are discussed in the following paragraphs.

The first of these nonideal morphologies is a rigidified region of polymer at the interface (matrix rigidification), discussed in section 2.2.2.1. Membranes with matrix rigidification morphology have properties within the diagonal crosshatched region of Figure 5.1 and Figure 5.2. Lines of constant chain immobilization factor, β , and of constant relative rigidified region thickness, ℓ_I/r_S , are shown to illustrate the effects of these parameters (defined in section 2.2.2.1). Even for infinite rigidification, ($\beta = \infty$), the selectivity is not lower than that of the neat polymer (within experimental error). The top left boundary at $\ell_I/r_S = 0.88$ corresponds to rigidification of the entire matrix.

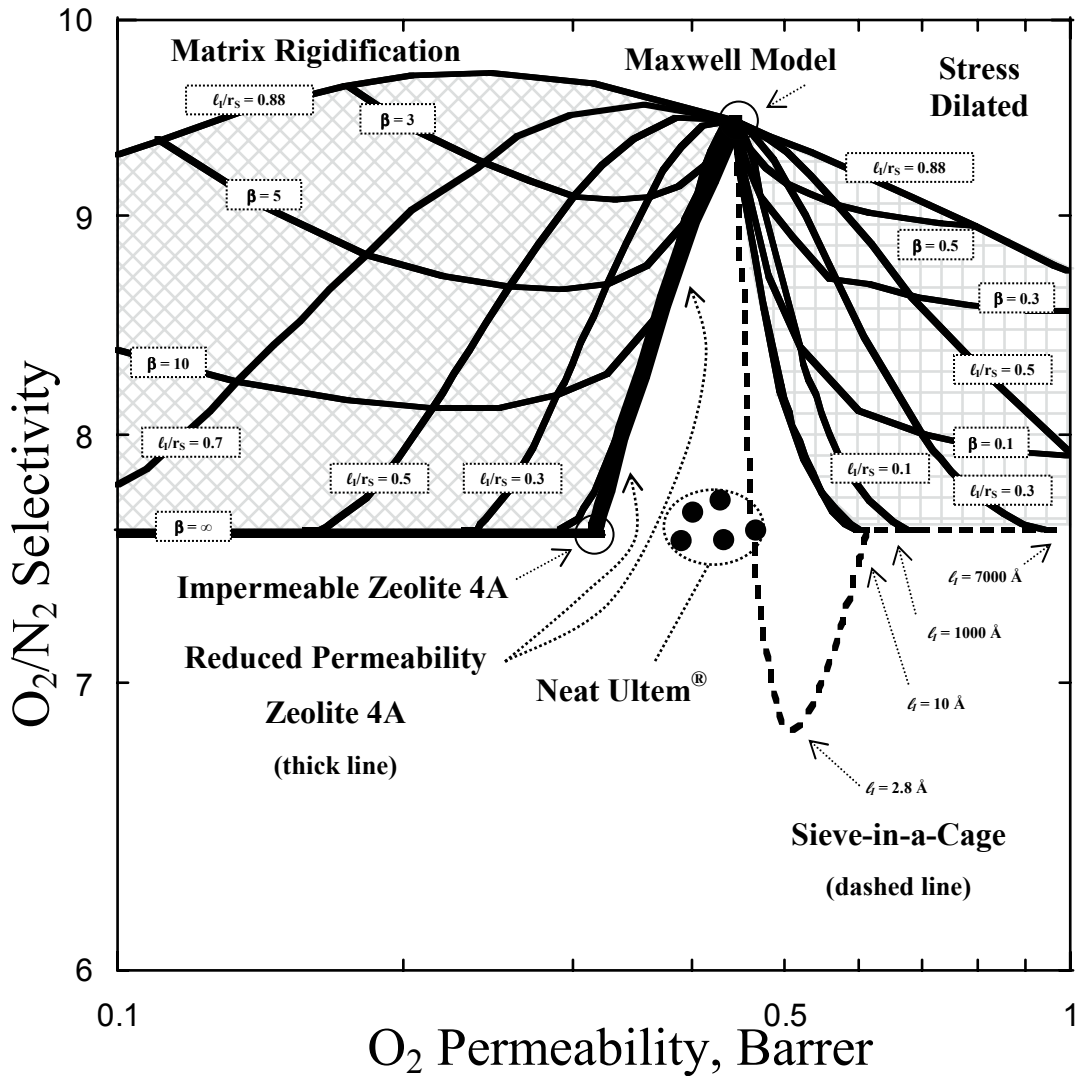


Figure 5.1: Transport properties (O_2/N_2) expected for various mixed matrix membrane morphologies for the Ultem[®] – zeolite 4A system at 15 vol% loading.

Another nonideal morphology is a zeolite that exhibits a permeability lower than normal. The effect of reduced zeolite permeability depends on the relative permeabilities of the matrix and zeolite. For zeolite 4A, which is only slightly more permeable than Ultem[®], reductions in zeolite permeability cause reduced mixed matrix selectivity. Reductions in the permeability of zeolite 4A cause decreased selectivity, following the trajectory of the thick line originating at the Maxwell model prediction in

Figure 5.1. An impermeable zeolite gives a mixed matrix membrane permeability lower than the neat polymer with the same selectivity, as shown for the circle labeled “Impermeable Zeolite 4A” on Figure 5.1. Conversely, HSSZ-13 is much more permeable than Ultem[®], so a reduction in the permeability of HSSZ-13 initially gives mixed matrix membranes with *higher* selectivity, following the thick line on Figure 5.2. The maximum mixed matrix selectivity occurs when the HSSZ-13 permeability is decreased to about 1 Barrer (from its initial value of 10 Barrer). As the permeability decreases beyond 1 Barrer, the Ultem[®] – HSSZ-13 mixed matrix membrane exhibits the behavior of completely impermeable zeolites, which is indicated by the circle labeled “Impermeable HSSZ-13” on Figure 5.2. Membranes with reduced permeability zeolites can have transport properties in the diagonal crosshatched region because they may also exhibit matrix rigidification. This was the case for the impermeable zeolite 3A in PVAc [1] and for impermeable spheres in hydrolyzed PVAc (section 4.3.2). Sorption experiments detailed in Chapter 6 have shown that reduced permeability zeolites are a significant problem, especially with zeolite 4A, and this is reflected in the transport properties reported in this chapter.

Sieve-in-a-cage is another nonideal mixed matrix membrane morphology, where a void exists at the polymer – sieve interface. As the void size increases, the permeability increases. The transport properties expected for this morphology are indicated on Figure 5.1 and Figure 5.2 as dashed lines, with selected void sizes identified. Regardless of the sieving phase, the mixed matrix selectivity first goes through a minimum, below that of neat Ultem[®], but quickly recovers to that of the neat polymer. The high permeability of HSSZ-13 makes the selectivity minimum for Ångstrom-scale void sizes less pronounced than for zeolite 4A. If the cages of neighboring zeolites overlap such that there is a continuous void pathway through the membrane, it will have a very high permeability with selectivity near one. This is increasingly likely as membrane thickness decreases, and that is why sieve-in-a-cage morphology is especially undesirable in the ultra-thin separation layers of hollow fibers.

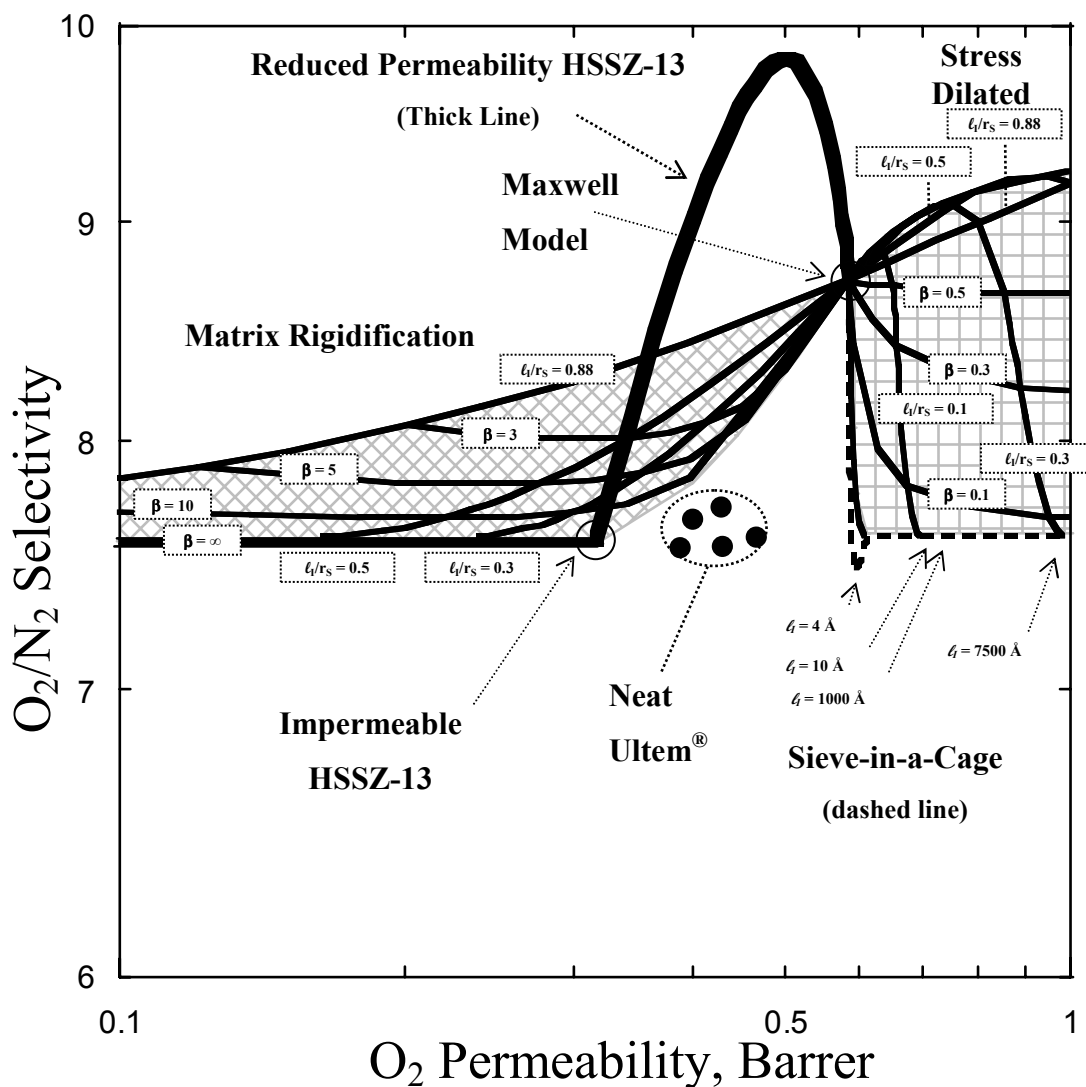


Figure 5.2: Transport properties (O_2/N_2) expected for various mixed matrix membrane morphologies for the Ultem[®] – HSSZ-13 system at 15 vol% loading.

A fourth nonideal morphology, *stress dilated interfaces*, is also speculated, although this morphology is less well understood. In a stress dilated interface, the permeability of the matrix near the zeolite is assumed to have permeability *higher* than the bulk matrix. This corresponds to a β of less than one in the analysis of section 2.2.2.1. This region is shown on Figure 5.1 and Figure 5.2 with a checkered background, and lines of constant β and l_1/r_s are given to illustrate the effects of these parameters. For

simplicity, the matrix selectivity was assumed unchanged. This assumption is relaxed in the analysis presented in section 5.5 and Appendix F. While matrix rigidification is likely to increase the selectivity because the free volume of the polymer is lowered, stress dilation raises the free volume, so it probably causes decreased selectivity. Potential causes of stress dilated morphology are: (i) addition of free volume to the polymer matrix near the interface prior to complete interfacial failure (i.e. prior to sieve-in-a-cage formation), (ii) disruption of the normal packing of bulk polymer, for example by nanoparticles, and (iii) increased free volume near the interface because of poor polymer – sieve affinity [2]. A maximum is predicted for HSSZ-13 filled Ultem[®] in the stress dilated region, because raising the matrix permeability leads to a better matched polymer – sieve system.

The analysis above requires a single dominant nonideal morphology, but it is also possible that a single membrane could exhibit *multiple* nonideal morphologies. This possibility is also addressed in Appendix F. Figure 5.3 shows a composite SEM of ~15 vol% HSSZ-13 dispersed in Matrimid[®]. The sieves in the top half of the membrane have distinct cages; whereas the cages appear absent in the bottom half. While it is possible that the cages have simply become too small to resolve with the SEM, it is also possible the sieves in this region exhibit matrix rigidification or stress dilated morphology. Similar effects could lead to significant sample-to-sample variation within the *same film*, which has been observed in this work. Membranes with multiple nonideal morphologies could have transport properties overlapping the crosshatched and checkered regions of Figure 5.1 and Figure 5.2. They could also have transport properties in the triangular region between the matrix rigidification and stress dilated regions. Many membranes prepared in this work have transport properties within this triangular region, indicating the likely presence of multiple nonideal morphologies near different zeolites within the membranes. Potential causes of this behavior are mentioned in the text.

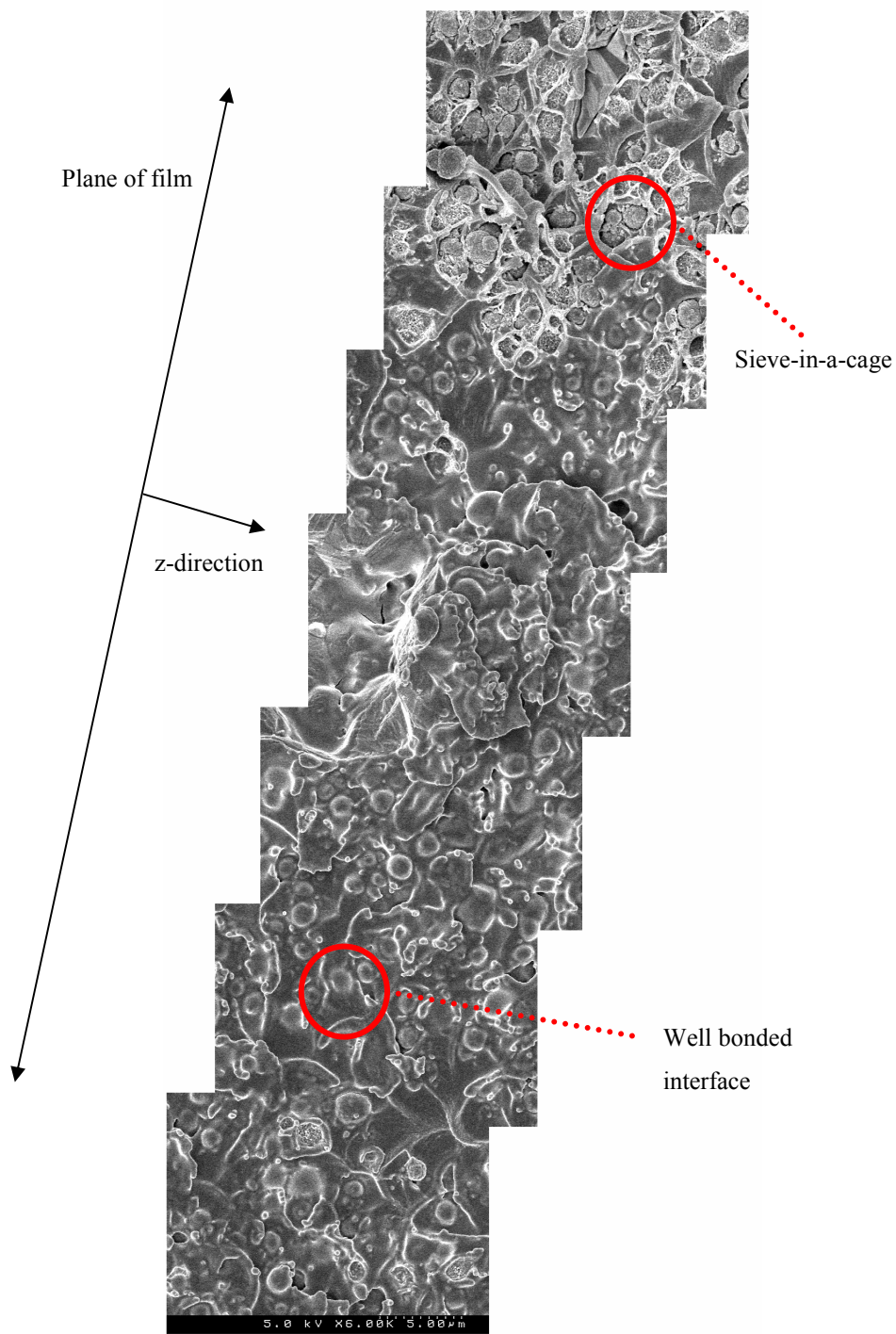


Figure 5.3: SEM of ~15 vol% HSSZ-13 in Matrimid[®] showing the transition from sieve-in-a-cage morphology (top) to apparently well-bonded interfaces in one sample.

The only morphology that can be independently observed using the SEM is sieve-in-a-cage morphology with large voids. Ångstrom-sized voids are too small to resolve with the SEM. Similarly, effects akin to matrix rigidification are frequently postulated in organic – inorganic hybrids (see section 2.2.2.1), but rigidification is also difficult to directly observe. Evidence of stresses at the interface, which are believed to cause matrix rigidification, is shown in the birefringence microscopy images of Figure 4.5. Gas permeation provides a basis to infer membrane morphology. Thus, this chapter uses permeation measurements, coupled with appropriate transport property maps similar to Figure 5.1 and Figure 5.2, to diagnose the effects of various material selection, dope formulation, and membrane casting considerations on the morphology and transport properties of mixed matrix membranes.

The following section considers material selection issues, such as whether and how to silanate the sieve surface, and which silane to use. Polymers with groups capable of favorable interactions directly with the zeolite are an alternative to silanating the zeolite surface. Work with such polymers, containing diaminobenzoic acid (DABA), is detailed in Appendix G. Selecting a zeolite particle size is also briefly considered in subsection 5.2.2. Section 5.3 considers dope formulation procedures. These include initial dispersal of the sieve suspension and priming of the zeolite surface with a small amount of polymer. These steps are necessary to stabilize the casting dopes to prevent the formation of zeolite agglomerates that would appear in the resulting membranes. Membrane casting techniques designed to minimize the stress on the zeolite surface to prevent sieve-in-a-cage morphology are considered in section 5.4. Finally, this chapter is closed with a discussion section to summarize important conclusions.

5.2. MATERIAL SELECTION CONSIDERATIONS AND MEMBRANE MORPHOLOGY AND TRANSPORT PROPERTIES

Material selection is a critical factor affecting mixed matrix membrane morphology and transport properties. Section 2.3 discussed matching of the polymer matrix to a given

sieve. Polymers with identical transport properties may still lead to mixed matrix membranes with different nonideal morphologies and transport properties because their chemical and physical properties are not the same. The first subsection considers modification of the zeolite surfaces with silane coupling agents. Silane coupling agents modify the apparent chemical and physical properties of the zeolite surface, and this may significantly affect the polymer – sieve interface. The final subsection presents a brief study of zeolite particle size. This physical property of the zeolites may affect the degree of matrix rigidification in mixed matrix membranes.

5.2.1. Silanation of the Zeolite Surface for Enhanced Interfaces

Successfully engineering the polymer – sieve interface is the key to mixed matrix membranes with desirable morphologies and transport properties. The silane used to modify the zeolite surface may significantly affect the properties of the interface. The optimal silanation method is developed and then various silanes are considered in subsection 5.2.1.2. While it is possible to prepare mixed matrix membranes with favorable morphologies without silane coupling agents using some polymers, silanating the surface appears essential for submicron zeolites. The surface density of the silane coupling agent is determined for the preferred silanation method in the final subsection.

5.2.1.1. Effect of Silanation Method on the Transport Properties of Mixed Matrix Membranes

Several silanation techniques were investigated using the base silane, γ -aminopropyldimethylethoxysilane, to see if there is an optimal method for application of the silane to the zeolite surface. All samples were silanated in a high shear mixer at ChevronTexaco, except for the sonicated sample, which was done following the procedure in section 3.3.1. Three base batches of submicron HSSZ-13 were used for these experiments; the base batch used is indicated in the results table. A common solvent for silanations is toluene [3-5], so it was included in this study as a nonpolar medium. Pure isopropanol, instead of the standard 95:5 IPA : H₂O mixture, was also

tried to ascertain whether lack of water has any effect. There is a report in the literature that aminosilanes can orient with the amine toward the zeolite surface under the wrong pH conditions, blocking a hydroxyl group from becoming silanated [6]. Thus, a sample was prepared in a solution with pH adjusted to the isoelectric point of HSSZ-13 (pH = 5.6), which is reported to be the optimal condition for attachment of the silane [6]. As shown in Table 5.1, there is no significant difference in the transport properties of the membranes prepared from most of the silanated sieves compared to the variability within a single (sonicated) sample. One possible exception is the sample silanated in toluene, but even its selectivity is similar to the others. Because there is little difference among the various silanation methods, the sonication method is the preferred procedure.

Table 5.1: Transport properties for ~15 vol% HSSZ-13 in Ultem[®] membranes prepared using zeolites silanated with different application methods. Tested at 35°C and 65 psia.

Description	O ₂ Permeability, Barrer	O ₂ /N ₂ Selectivity	CO ₂ Permeability, Barrer	CO ₂ /CH ₄ Selectivity
Neat Ultem [®]	0.40	7.6	1.4	38
Maxwell Model	0.59	8.7	2.2	44
16402.72.52.90 silanated via sonication	0.55 ± 0.07	7.8 ± 0.1	2.0 ± 0.2	38 ± 3
	Average of 5 membranes		Average of 4 membranes	
16402.72.52.90 unsilanated	31	0.84	Not tested	
16327.61.92 silanated in IPA : H ₂ O	0.58	8.2	2.0	41
16327.61.92 silanated in toluene	0.78	8.0	2.8	40
16402.71 silanated in IPA : H ₂ O	0.55	7.8	1.9	38
16402.71 silanated after adjusting pH to 5.6	0.49	8.0	Not tested	
16402.71 silanated in IPA	0.51	8.1	1.8	40

The unsilanated sample gives transport properties significantly worse than the others, and the surface of this membrane is covered with large sieve agglomerates. The quality of this membrane is so poor that the selectivity is near one, indicating some of the agglomerates must extend through the membrane. The high permeability of this membrane confirms this. Conversely, membranes prepared with the various silanation methods have smaller agglomerates visible upon close inspection, but these are typically much thinner than the membrane thickness. While such smaller agglomerates would not catastrophically affect mixed matrix membranes, sieves that exist as agglomerates may not contribute to enhanced selectivity if their interstitial spaces are poorly coated with polymer. These agglomerates likely cause increased permeability because of the encapsulated void space. This may explain why the selectivity enhancement is lower than predicted by the Maxwell model.

Indeed, large sieve agglomerates have been encountered in other membranes prepared with unsilanated *submicron* zeolites, so it appears that surface modification is necessary to prevent agglomeration of submicron zeolites. The only exception is unsilanated submicron HSSZ-13 dispersed in 6FDA-6FpDA:4MPD:DABA (discussed in section G.1), but even this was carefully primed with polymer before the main casting dope was formulated. Agglomeration is not encountered with unsilanated larger zeolites. HSSZ-13 with a larger particle size was not available, so $\sim 5 \mu\text{m}$ zeolite 4A was used for this study. Figure 5.4 contrasts the results for $\sim 15 \text{ vol}\%$ zeolite 4A in Ultem[®] membranes prepared with unsilanated and silanated $\sim 5 \mu\text{m}$ zeolite 4A. Both sets of membranes have properties that fall within the same range. Some samples exhibit transport properties in the triangular region between the matrix rigidification and stress dilated regions, indicating both morphologies may be present. Nonetheless, the average properties for membranes prepared from both the silanated and unsilanated zeolites lie near the region of the transport property map indicative of nearly impermeable zeolite 4A. This problem was common to membranes prepared from zeolite 4A, and it is discussed in more detail in Chapter 6.

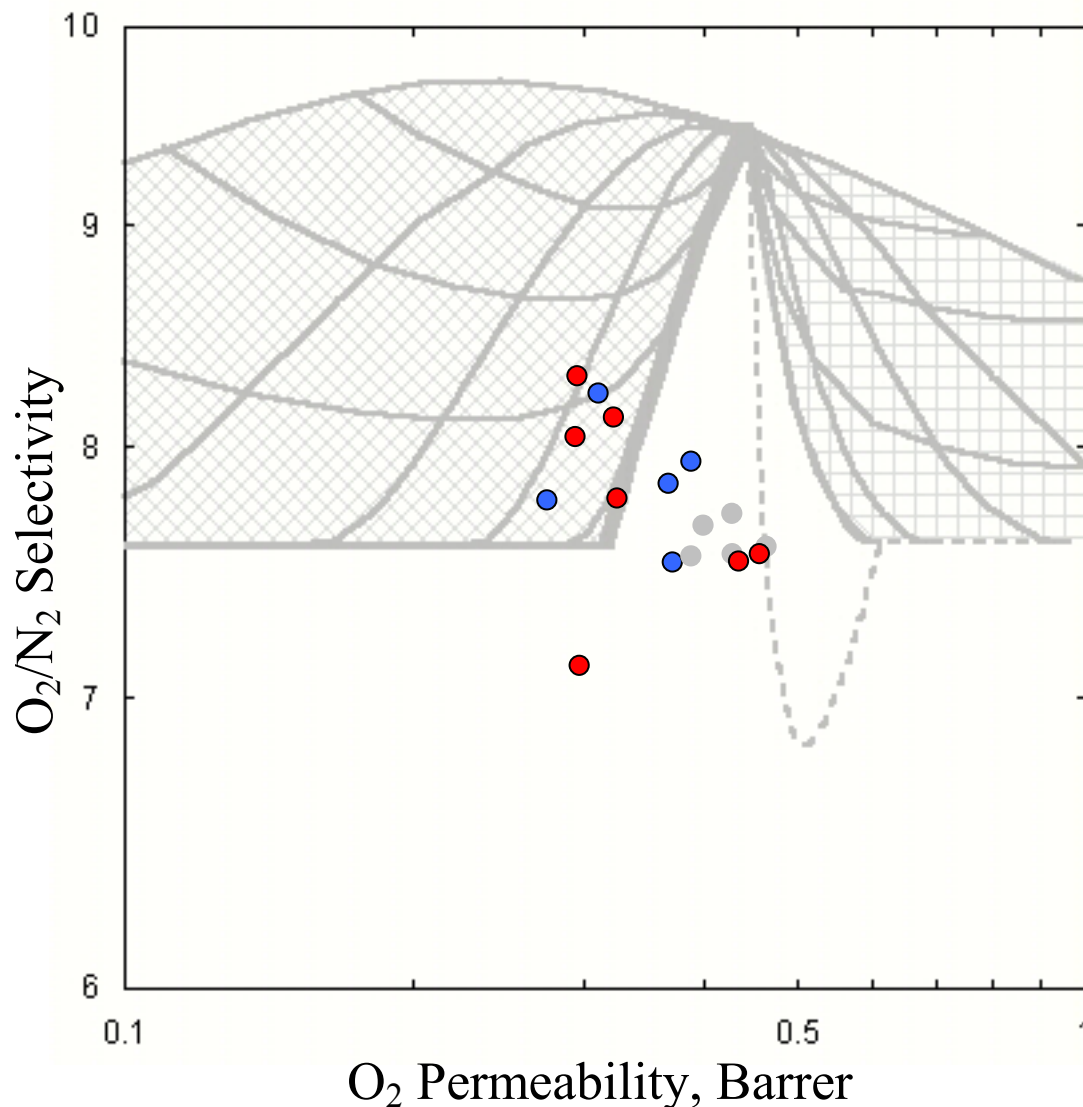


Figure 5.4: Comparison of membranes prepared with ~15 vol% unsilanated (red) or silanated (blue) zeolite 4A dispersed in Ultem[®]. Gray circles represent neat Ultem[®]. Tested at 35°C and 65 psia.

The favorable properties of membranes prepared with unsilanated zeolite 4A are also significant since it was previously believed that a silane was needed to prevent delamination of Ultem[®] – zeolite 4A interfaces. This is not surprising in light of section 4.3.1, where many indicators of polymer affinity for unmodified zeolite 4A suggested little difference among the polymers. This result also signifies the triumph of proper casting conditions, which were chosen to reduce the likelihood of sieve-in-a-cage

morphology, as discussed in more detail in section 5.4.1. Nevertheless, membranes prepared with unsilanated zeolites may be more prone to failure during casting or during long-term use, so it may be advisable to silanate the surface anyway.

In a separate study, NMP was also considered as a silanation solvent. After silanation, it is necessary to recover the zeolites from the silanation solvent, which can be somewhat difficult with submicron zeolites. Filtration of 5 g of submicron zeolites requires several hours per solvent wash, making this process difficult to scale up. Also, as discussed later (section 6.3.2), it proved difficult to completely remove isopropanol from the zeolites, so an alternative solvent is desirable. One way to potentially solve both problems is to silanate in a solvent that will dissolve the polymer. It is possible to silanate materials in NMP with a small amount of water added to hydrolyze the silane [7]. One potential problem with silanating in NMP is the removal of excess silane and water prior to casting dope formulation. It may be possible to drive off these more volatile components simply by heating the suspension. The following paragraph explores possible post-silanation processing to remove water and excess silane.

Three casting dopes were prepared from zeolites silanated in NMP to determine the best method to manage the residual silane and water. All three casting dopes were primed using a “solution priming” procedure, which is discussed in section 5.3.3. Solution priming is done by heating the sieves with ~10% of the matrix polymer in NMP to ~140°C for 4 hours. Casting dope “A” was prepared using the standard solution priming technique after recovering the sieves via filtration, which should have removed residual silane and water. Casting dope “B” was prepared by heating the suspension obtained after silanation to ~140°C for 1 hour to drive off residual silane and water before adding the polymer for solution priming. A third casting dope was prepared by solution priming the suspension obtained immediately after silanation (i.e. containing residual silane and water). This dope gelled and could not be cast, probably because of a reaction between residual APDMES and Ultem[®] (see Appendix B), so no further work

was attempted with this sample. The transport properties for membranes prepared from the first two casting dopes are given in Table 5.2. The membrane prepared from casting dope A has a somewhat lower permeability than Ultem[®] – HSSZ-13 membranes prepared from conventionally silanated HSSZ-13. The membrane prepared from casting dope B is darker (brown) than any of the other Ultem[®] – HSSZ-13 membranes (white – tan). Perhaps the heating protocol did not completely remove residual APDMES, which then reacted with Ultem[®] during solution priming. The O₂/N₂ transport properties of this membrane are somewhat worse than Ultem[®] – HSSZ-13 prepared from conventionally silanated HSSZ-13.

Table 5.2: Transport properties for ~15 vol% HSSZ-13 in Ultem[®] membranes with sieves silanated in NMP. Tested at 35°C and 65 psia.

Membrane	O ₂ Permeability, Barrer	O ₂ /N ₂ Selectivity
Neat Ultem [®]	0.40	7.6
Maxwell Model	0.59	8.7
Casting Dope A	0.40	8.0
Casting Dope B	0.91	6.9

Although the membrane prepared from casting dope A has somewhat favorable transport properties, it did not represent a significant advance compared to the conventional silanation in 95:5 IPA : water followed by filtration. Thus, it was not pursued further. This technique may still be promising if a method to remove unreacted APDMES without having to recover the zeolites via filtration can be developed. This would be easier if a lower silane to HSSZ-13 ratio was used. This study used a swamping excess (~2g APDMES per 3-5g HSSZ-13) of silane, since the same swamping excess is used when silanating in IPA : H₂O. Thus, a reduction of this ratio is quite permissible.

5.2.1.2. Effect of Selected Silane Coupling Agents on the Transport Properties of Mixed Matrix Membranes

The various nonideal morphologies discussed in section 5.1 mostly arise at the polymer – sieve interface. Silane coupling agents significantly alter the chemical and physical properties of that interface. Thus, it is reasonable to expect that the particular silane used may significantly alter the type and degree of nonideal morphology formed. Several different coupling agents that may potentially affect interfacial properties were considered. These agents, and the motivation for each, are discussed next.

The first sample was silanated with γ -aminopropyldimethylethoxysilane (APDMES) as a “control” to compare other samples with. The pH adjusted sample from the previous study was also repeated using sonication as the silanation method with the base APDMES silane. The third case studied was to preadsorb ethylene diamine onto the zeolite surface before the standard APDMES silanation. There is a report that preadsorption of EDA onto the surface prevents the free amine end of APDMES from interacting with surface hydroxyls, yielding a higher surface coverage of APDMES [8]. A fourth sample was γ -aminopropylmethyldiethoxysilane (APMDMES), which has two groups capable of reacting with the zeolite. It was thought this may yield better attachment to the zeolite, possibly leading to *increased* matrix rigidification. The final case was γ -aminobutyldimethylmethoxysilane (ABDMMS). The increased flexibility of the longer tether of ABDMMS, compared to APDMES, may have facilitated better access to the polymer. On the other hand, the increased length of this tether may hold the polymer matrix farther from the sieve, leading to a more open interface.

Membranes were prepared at ~15 vol% loading in Ultem[®] with each of the five silanated samples mentioned above. All of the silanations were done at ChevronTexaco using the standard sonication silanation method with a single batch of HSSZ-13. The results for these membranes are given in Table 5.3. The results of the pH adjusted sample were not significantly different than for those in Table 5.1, further supporting

the relative unimportance of the particular silanation method. The sample silanated after EDA preadsorption was significantly worse than the others. APDMES is supposed to displace EDA as it reacts with the zeolite surface; however, analysis with the TGA revealed a significant amount of EDA evolved from the zeolite after the silanation procedure. This EDA likely prevented the formation of favorable polymer – sieve interactions since Ultem[®] is probably even less likely to displace EDA than APDMES is. APMDMES- and ABDMMMS- silanated HSSZ-13 both gave membranes with properties similar to APDMES silanated HSSZ-13, perhaps indicating that the particular silane has little effect on the overall transport properties. This could be because the small size of the silanes makes their effect highly localized. Indeed, the previous subsection suggests that the main role of the silane is to prevent agglomerate formation in submicron zeolites, since unsilanated and silanated $\sim 5 \mu\text{m}$ zeolites gave membranes with similar properties. None of the samples are significantly better than the base APDMES, so it was used as the primary silane for this work.

Table 5.3: Transport properties for $\sim 15 \text{ vol}\%$ HSSZ-13 in Ultem[®] membranes prepared with different sieve samples from ERTC. Tested at 35°C and 65 psia. The full silane names are given in the text.

Silane	O ₂ Permeability, Barrer	O ₂ /N ₂ Selectivity	CO ₂ Permeability, Barrer	CO ₂ /CH ₄ Selectivity
Neat Ultem [®]	0.40	7.6	1.4	38
Maxwell Model	0.59	8.7	2.2	44
APDMES	0.64 ± 0.13	7.9 ± 0.1	2.2 ± 0.4	40 ± 2
	Average of 4 membranes		Average of 4 membranes	
APDMES at pH = 5.6	0.59	7.9	2.1	38
APDMES after EDA adsorption	5.3	1.2	Not tested	
APMDMES	0.53	8.1	1.8	41
ABDMMS [†]	0.60	8.0	2.2	41

[†] Membrane prepared using solution priming (discussed in section 5.3.3).

5.2.1.3. Silane Coupling Agent Density on Silanated HSSZ-13

The density of the silane coupling agent on the sieve surface was determined for the standard silanation technique (APDMES using the sonication procedure). Poorly silanated zeolites could cause agglomeration. Furthermore, a monolayer of silane is desirable so the polymer will bond with a silane that is directly attached to a zeolite. Two techniques were considered to determine the surface silane density. The first was to react the residual surface hydroxyl groups with VOCl_3 , followed by elemental analysis. The second technique was to burn the silane off the zeolite in the TGA.

HSSZ-13 samples were allowed to react under vacuum with VOCl_3 , which undergoes a 1:1 reaction with hydroxyl groups, leaving VOCl_2 on the surface and evolving HCl [9, 10]. APDMES-silanated and unsilanated HSSZ-13 from a single zeolite batch were tested. After several freeze-pump-thaw cycles, the VOCl_3 liquid is transferred into the flask containing the zeolites via a common vacuum line by heating the flask with the VOCl_3 and cooling the flask containing the zeolites. The reaction is then allowed to proceed overnight at room temperature, with the reaction flask closed off but under vacuum. The zeolites are pale yellow after the reaction because of attached VOCl_2 groups. Unreacted VOCl_3 is then evacuated from the zeolite flask. Finally, the zeolites are recovered and submitted for elemental analysis (Galbraith Laboratories; Knoxville, TN) to determine the vanadium content. Using the vanadium per unit weight and the known HSSZ-13 density and surface area per unit volume, the hydroxyl density on the zeolite surface can be calculated. The surface area per unit volume was measured at ChevronTexaco ($21.2 \text{ m}^2/\text{g}$). The hydroxyl content of both samples determined in this manner is reported in Table 5.4. The density of silane coupling agent on the surface is derived by subtracting the hydroxyl density of the silanated sample from the unsilanated sample; it is also reported in Table 5.4.

The second technique was to burn the silane off the surface and to follow the weight loss with the TGA. HSSZ-13 samples, (unsilanated and silanated with APDMES in

95:5 isopropanol : water), were heated to 1000°C at 5 K/min in air to burn off the silane coupling agent. Samples were held for 8 hr at 250°C to degas the zeolite before continuing at 5 K/min to 1000°C. Both samples show significant weight loss in the first hour due to adsorbed gases and vapors. Holding the zeolite at 100°C for 8 hr was also tried, but it does not completely degas the sample. Figure 5.5 shows the difference (excess weight loss) between two samples of silanated HSSZ-13 and unsilanated HSSZ-13. This excess weight loss can be attributed to the silane coupling agent. As shown in Table 5.4, the weight loss corresponds to 2.4 - 2.9 APDMES molecules per square nanometer of sieve surface. HSSZ-13 was also sonicated without APDMES in 95:5 IPA : water with the same procedure used to silanate the zeolites. It gave ~0.2% weight loss. Subtracting this weight loss from that measured with APDMES present gives an APDMES surface density of between 1.8 and 2.3 molecules per square nanometer. The 0.2% weight loss in the IPA sonicated sample is probably due to residual IPA. This residual IPA was unexpected at this temperature, and as shown in section 6.3.2, it causes reduced sorption of gases in the zeolites.

Table 5.4: Summary of hydroxyl and APDMES densities for unsilanated and silanated HSSZ-13 based on titration of the sites with VOCl_3 and burn-off of the APDMES in the TGA.

	Hydroxyl density, number/nm ²	Hydroxyl density <i>after silanation</i> , number/nm ²	APDMES density, number/nm ²
VOCl_3 titration	3.2, 4.5	2.6, 2.7	0.6 – 2.0
TGA burn-off			2.4 – 2.9
TGA burn-off (corrected for IPA loss)			1.8 – 2.3

After correction for this weight loss, the APDMES surface densities measured using these two techniques are indistinguishable compared to the error in the measurements.

They agree qualitatively with the typical value of 2 silanes/nm² reported by Plueddemann [6]. The hydroxyl densities determined using the VOCl₃ titration are also similar to that reported for amorphous silica dried at ~150°C [11]. The presence of a significant silane density, coupled with the observed poor performance of membranes prepared with unsilanated HSSZ-13 demonstrate the significant effect of the silane on submicron zeolites.

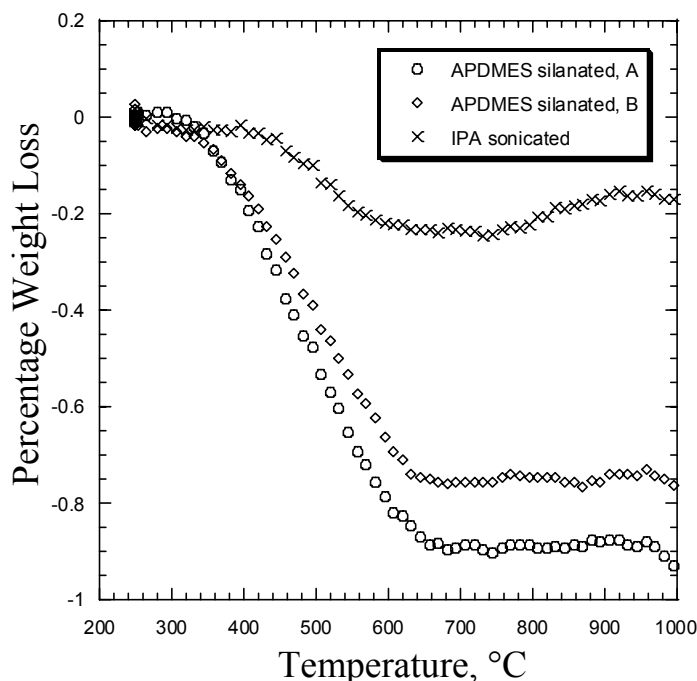


Figure 5.5: Excess weight loss compared to unsilanated HSSZ-13 for samples silanated with γ -aminopropyltrimethylethoxysilane (APDMES) in 95:5 IPA : water and for a sample sonicated (without APDMES) in 95:5 IPA : water determined using the TGA. All samples were degassed at 250°C for 8 hr to determine the correct “zero” weight.

The evolved gases from other APDMES silanated HSSZ-13 were also monitored with infrared spectroscopy. In air, the silane decomposes to ethylene at about 250°C. However, no decomposition products could be identified below 400°C in a nitrogen atmosphere. Thus, it appears that drying up to 250°C is acceptable, although higher temperatures may be tolerated in an inert atmosphere.

5.2.2. Effect of Zeolite Particle Size Mixed Matrix Membranes

Although the Maxwell model predicts no particle size effect, the particle size of the dispersed phase may affect the transport properties of mixed matrix membranes exhibiting nonideal morphologies. Smaller particles have a larger surface area-to-volume ratio, so surface effects such as matrix rigidification and sieve-in-a-cage morphology may be amplified. On the other hand, the thickness of the rigidified polymer region or of the interfacial void could be reduced because the particles are smaller. Membranes were prepared and tested with silanated submicron (0.1 – 0.2 μm) and $\sim 5 \mu\text{m}$ zeolite 4A dispersed in Ultem[®] to determine whether particle size affects the nonideal morphology formed. O_2/N_2 transport properties are summarized on Figure 5.6. CO_2/CH_4 transport properties (not shown) confirm the behavior diagnosed with the O_2/N_2 transport properties. There does not seem to be a significant difference for the two particle sizes given the scatter within the data. The average transport properties for the submicron samples are similar to the average properties for the $\sim 5 \mu\text{m}$ samples. The lower-than-expected permeabilities and selectivities of these membranes may indicate the zeolites suffer from reduced permeability. Nonetheless, impermeable zeolites would not affect the formation of matrix rigidification or sieve-in-a-cage domains, so any potential effect of particle size must be secondary in nature. Thus, it appears the relative interphase thickness, ℓ_I/r_S , is more reasonable measure of the scale of the nonideal morphology than the absolute interphase thickness, ℓ_I (i.e. larger particles have larger ℓ_I , but the effect is offset by their lower surface area-to-volume ratio).

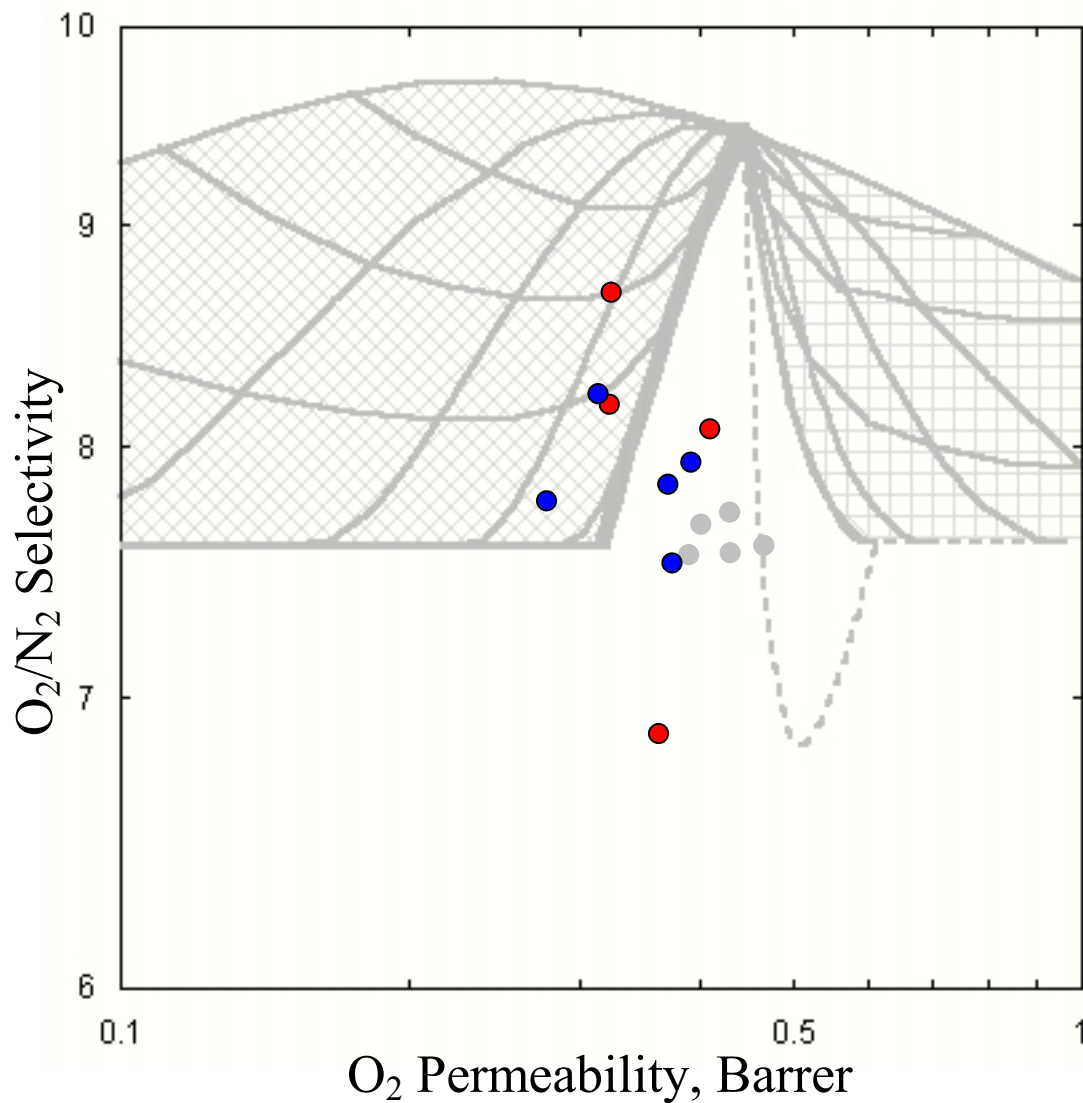


Figure 5.6: Comparison of membranes prepared with ~15% silanated submicron (red) or ~5 μm (blue) zeolite 4A dispersed in Ultem[®]. Gray circles represent neat Ultem[®]. Tested at 35°C and 65 psia.

5.3. SELECTED DOPE FORMULATION ISSUES

The importance of proper dope formulation increases with the incorporation of submicron zeolites into mixed matrix membranes. Submicron zeolites were found to have a propensity to form agglomerates (see Figure 5.7). Such agglomerates, consisting of sieve particles uncoated with polymer, allow nonselective permeation of gases

through their interstitial spaces. The first subsection considers the effect of sonicator power on both silanation and initial sieve dispersal. Subsection 5.3.2 studies the causes of these agglomerates and methods to remove them from the casting dopes. The final subsection develops an optimal polymer “priming” method to stabilize casting dopes.

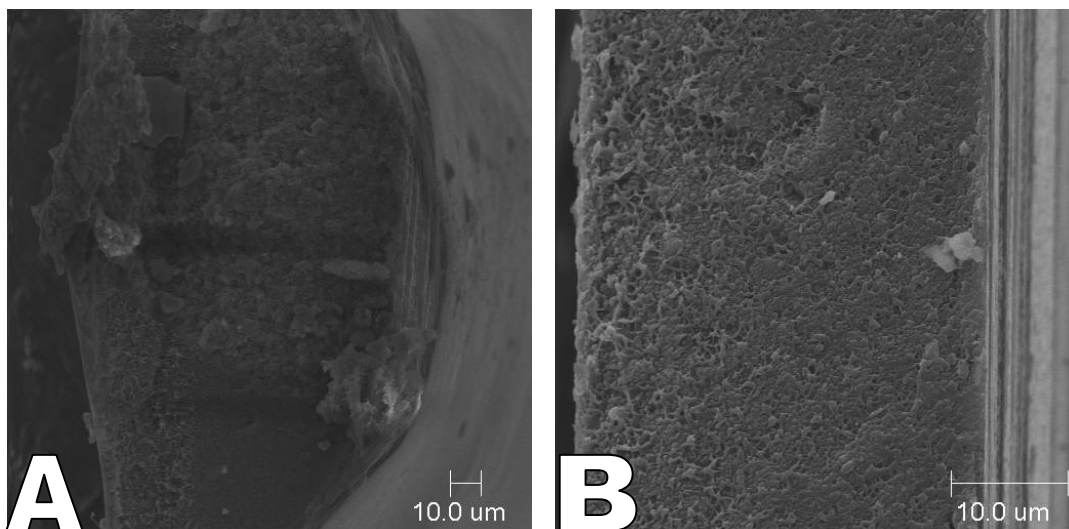


Figure 5.7: (a) Zeolite agglomerate in a ~15 vol% HSSZ-13 in Ultem[®] mixed matrix membrane. Sieves in the non-agglomerated regions (b) have good interfaces.

5.3.1. Effect of Sonicator Power on Casting Dopes and the Transport Properties of Mixed Matrix Membranes

The sonicator power used for silanation and initial dispersal of the sieve suspension may be an important variable, since sonication is the primary method used to disperse the sieves. Mahajan had used a sonicator with a low *maximum* power output of 50 W and a 6 mm diameter horn [12], while collaborators use a sonicator that is capable of delivering 1000 W of power with a ½” horn. Both sonicators operate at 20000 Hz. Initially, this work used the 50 W sonicator, but membranes were also prepared using the larger model. Submicron HSSZ-13 from a single batch was silanated with APDMES using each sonicator. There is a significant difference in the ability of the two sonicators to agitate the silanation suspension in a ~7 cm diameter plastic container.

The 1000 W sonicator easily disperses all the sieves and the surface of the liquid is not quiescent. Conversely, the 50 W sonicator does not completely disperse the particles, and the surface of the liquid in the container is quiescent except for the area nearest the ultrasonic horn tip. When the silanation is complete, sieves from the 1000 W sonicator are well dispersed, whereas about half of those from the 50 W sonicator exist in millimeter-sized agglomerates. These agglomerates were not retained for use in the membranes since it was possible they were poorly silanated. The 50 W (maximum) sonicator requires ~16 W of power to drive the horn, whereas the 1000 W (maximum) sonicator requires ~100 W. Another difference is the maximum temperature in the bulk silanation suspension during sonication. The 50 W sonicator gives a bulk silanation suspension temperature of ~35°C, while the 1000 W sonicator gives a maximum of ~55°C. The local temperature near the ultrasonic horn is likely higher, but it could not be probed. When a smaller plastic container (diameter ~ 2.5 cm) is used, the 50 W sonicator is able to vigorously agitate the entire silanation suspension. Thus, no millimeter-sized agglomerates form, but fewer sieves can be silanated in this container.

Membranes comprised of ~15 vol% HSSZ-13 dispersed in Ultem[®] were prepared from the sieves silanated using each sonicator. The sieves were also dispersed in the casting solvent using the same sonicator with which they were silanated. There is no noticeable difference in the agglomerate density of membranes prepared using the two sonicators. More agglomerates may have been present if the millimeter-sized agglomerates from the 50 W sonicator were used in membranes. As shown in Figure 5.8, both sonicators lead to similar membrane transport properties. Using the 1000 W sonicator did not lead to a significant improvement in morphology or transport properties, so the difference in power output does not appear to affect the reaction of the silane. Nonetheless, it is important that the sonicator can break-up agglomerates so the chemistry can occur. Therefore, the 1000 W sonicator was used for larger (~ 5 g) silanation batches. The less powerful sonicator was used for smaller (< 0.5 g) batches with the smaller reaction container, and for initial sieve dispersal in the sieve suspension.

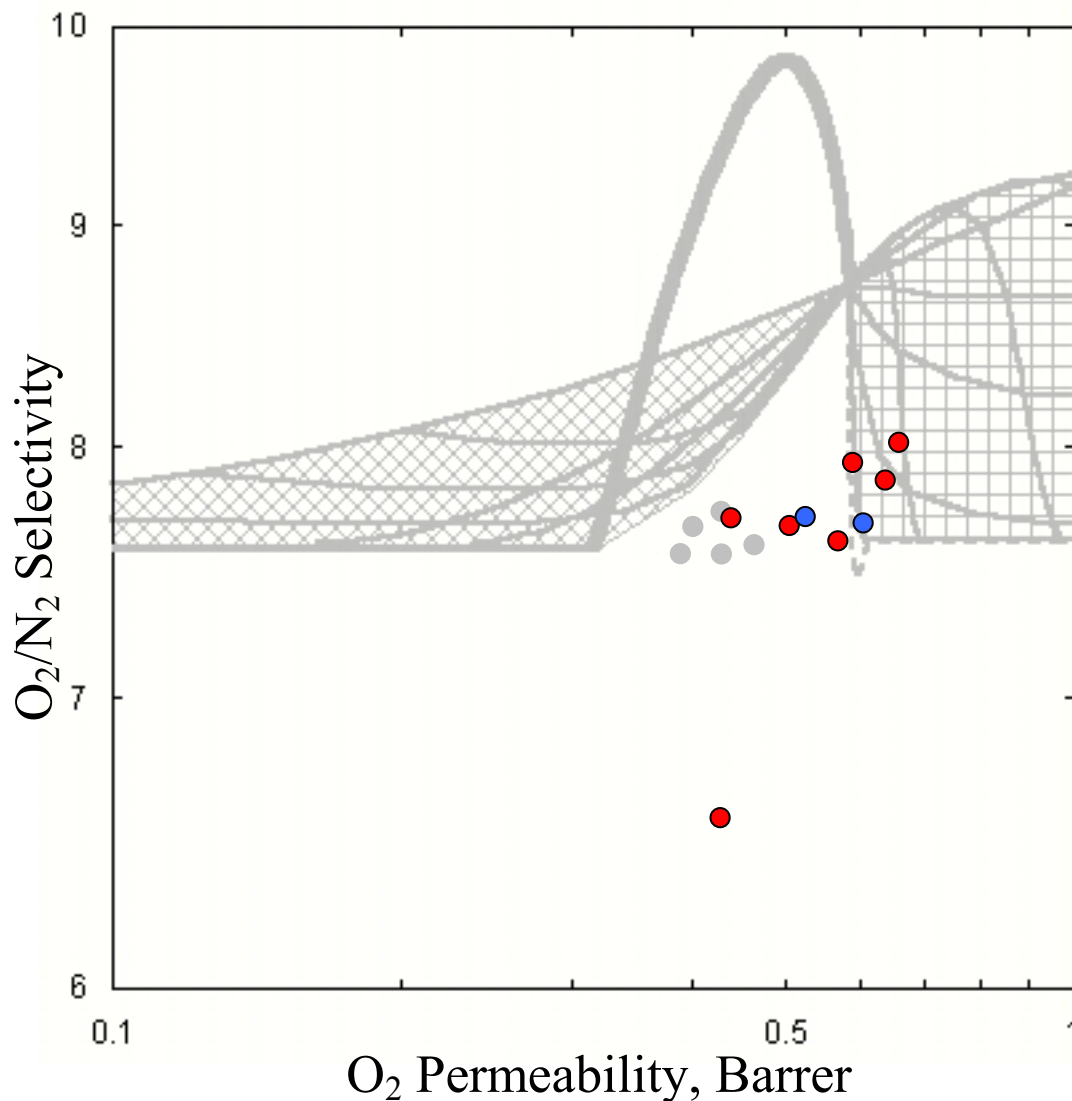


Figure 5.8: Comparison of membranes prepared with ~15% HSSZ-13 dispersed in Ultem[®] using either the 50 W (red) or 1000 W (blue) sonicators. Gray circles represent neat Ultem[®]. Tested at 35°C and 65 psia.

5.3.2. Understanding and Removing Sieve Agglomerates from Casting Suspensions for Enhanced Membrane Morphology

A number of experiments were undertaken to understand when sieve agglomerates are formed and how best to eliminate them from mixed matrix membranes. It was hypothesized that small amounts of water present in the casting dope due to ambient

humidity may have caused the agglomerates. The *external* surface of HSSZ-13 is very hydrophilic, so water may accumulate near it. If the water layers of neighboring HSSZ-13 particles overlap, it is possible they will form a separate phase, even though water is miscible with NMP. The particles would then tend to segregate in this phase, forming agglomerates. To test this, a sieve suspension was prepared in a solvent comprised of ~10% water in NMP instead of pure NMP. The membrane prepared from this casting dope does not have significantly more agglomerates than other membranes, so humidity does not appear to cause them. Another hypothesis was that the agglomerates form after initial dispersal of the sieves, but before the polymer solution is added. To test this, a membrane was prepared after allowing the sieve suspension to settle for 10 minutes before adding the polymer solution. A slight increase in agglomerate density was noted upon visual inspection. After sitting overnight, a suspension of the same ~0.1 μm sieve solution had formed a floc (i.e. the top of the solution had clarified, but shaking the solution easily redispersed most of the sieves. Nonetheless, the sieves likely existed as smaller agglomerates after breakup of the floc. While silanation resulted in a significant reduction in agglomerate size, it does not completely stabilize the casting suspensions. Thus, it is important to further stabilize suspensions of submicron zeolites.

One possibility studied to better stabilize sieve suspensions is to add about 10% of the polymer solution to the sieve suspension halfway through the initial dispersal of the sieves with the sonicator. Adding all of the polymer solution makes the resulting polymer – sieve suspension very viscous and difficult to mix with the sonicator. With only 10% of the polymer solution, the sieve suspension is relatively dilute and mixing is much more complete. Sonicating with a small amount of polymer in the sieve suspension appears to significantly reduce the number of agglomerates present in the membranes, but it does not eliminate them. Adsorption of polymer onto the sieve surface likely reduces the formation of sieve agglomerates through steric stabilization [13]. The transport properties of several membranes prepared in this manner are shown

later on Figure 5.10. One of these membranes had the highest selectivity ($O_2/N_2 = 8.6$) of all similar membranes, but the permeability was greater than the Maxwell prediction (0.82 versus 0.58 Barrer). This line of experiments led to the development of “solution priming” discussed in the next subsection.

The fact that agglomerates are reduced by adding a small amount of polymer to the sieve suspension during initial dispersal suggests that agglomerates form in casting dopes rather than during membrane casting. Once it became clear that agglomerates form in the casting dopes, attempts were made to remove them before casting so they will not be present in the resulting membranes. One of the casting dopes with the worst agglomerates was filtered through a 7 μm sintered metal filter to try to remove the agglomerates. A 1000 psi nitrogen blanket was necessary to force the dope through the filter. Despite the high pressure, only a few mL of purified dope were obtained before the filter became clogged. The filter may have removed a significant fraction of the zeolites, but some clearly remained in the recovered filtrate, which was cast into an essentially agglomerate free membrane. Unfortunately, the membrane formed was too small to test. Nonetheless, this demonstrates that filtration is an effective method to remove sieve agglomerates. In another experiment, the sieve suspension was filtered after the initial dispersal, but before adding the polymer to see if this affected the number of agglomerates in the resulting mixed matrix membranes. Membranes prepared from this solution still suffer from small agglomerates, and this is further evidence that polymer is necessary to fully stabilize the casting dopes.

While a carefully devised study of aged solutions was not performed in this work, one final observation regarding casting dope stability is noted since it may provide an avenue for future research. In casting dopes containing submicron zeolites that have been aged for several months, some of the sieves have clearly settled to the bottom of the container. The suspension above the settled matter remains opaque, indicating that most of the sieves remain suspended. Lesser aged (~ 1 week) casting dopes seem to

produce better looking membranes with fewer agglomerates, so longer settling times may be more beneficial. Gravitational settling is very slow because of the high viscosity of the casting dopes, but this process could be accelerated using centrifugation. Since settling and filtration remove a portion of the sieves, the amount of sieves in the resulting membranes could be determined in the TGA. Thus, settling may provide an additional technique to remove agglomerates from casting dopes.

5.3.3. Effect of Zeolite “Priming” Method on the Transport Properties of Mixed Matrix Membranes

Mixed matrix membrane quality has been improved by replacing *film priming* with *solution priming*. Priming and silanation of the sieves are the primary stabilization methods. For solution priming, the sieve suspension is heated to 140°C in the presence of a fraction of the desired matrix polymer (typically ~10% of the total). The alternative film priming procedure is to cast a film, dry it at 180°C to react the silanated sieves to Ultem[®], and then redissolve it to make a second film. Film priming was implemented because it is easier to perform on single membranes, whereas solution priming is easier with larger amounts of sieves, typically used for several membranes. In addition to more consistent transport properties, membranes prepared via solution priming have fewer sieve agglomerates than those prepared via film priming.

The experiments undertaken to demonstrate improvements realizable using solution priming (cases A, B1, B2, and C) are detailed in Figure 5.9, with corresponding permeation data in Figure 5.10. Figure 5.10 also shows the results for membranes prepared by adding polymer during initial sieve dispersal discussed in the previous subsection (green points). Sieves primed using solution priming method “C” were provided by Shabbir Husain of the research group. Membranes prepared using this method demonstrate the most consistent improvement in transport properties of any membranes tested. Solution priming gives better results when the priming suspension is heated (method “B1”), rather than just allowed to stand at room temperature (method

“B2”). Figure 5.10 shows that membranes prepared with solution primed (method B1, or C) casting dopes are more likely to display higher selectivities than membranes prepared with film primed casting dopes. While high selectivities are possible using film priming, the results are inconsistent, occasionally varying significantly within the same sample (for example, red and green points on Figure 5.10).

The improvement in transport properties may be strongly related to the conditions under which Ultem[®] reacts with the silanated sieves, discussed in Appendix B. The reaction between the imide group of the polymer and amine tail of the silanated zeolites is expected to proceed faster at higher temperatures (if at all at room temperature). This explains the difference between solution priming methods “B1” and “B2”. Any reaction between the silanated surface and the polymer is also expected to proceed more rapidly in a suspension than in a film, because of the increased mobility in the suspension. Membranes prepared via film priming frequently have agglomerates. It would be difficult for a glassy polymer to diffuse into their interstitial spaces, causing selectivities lower than the Maxwell model prediction. Conversely, if any agglomerates form during solution priming, they should be broken up by stirring, allowing easy polymer access.

The difference in the properties obtained from the two high temperature primed membranes, (“C” and “B1”; yellow versus blue on Figure 5.10), could be due to the slightly different silanation methods used. In particular, the use of the sonication bath instead of the ultrasonic horn is novel and requires additional study. It may also be desirable to consider dialysis to recover sieves after silanation because of: (i) the difficulty of filtration and (ii) the ability to recover the sieves in suspension as opposed to as a powder where handling and agglomeration may be a concern. The scatter within the data make it difficult to conclude that silanation with the bath (blue points on Figure 5.10) is superior to silanation with the sonicator (yellow points). While solution priming significantly reduces agglomerates, it may not completely eliminate them.

Even a few agglomerates could increase the permeability of an otherwise matrix rigidified membrane without significantly lowering the selectivity. This could be the case for the two yellow points that fall on the sieve-in-a-cage line in Figure 5.10.

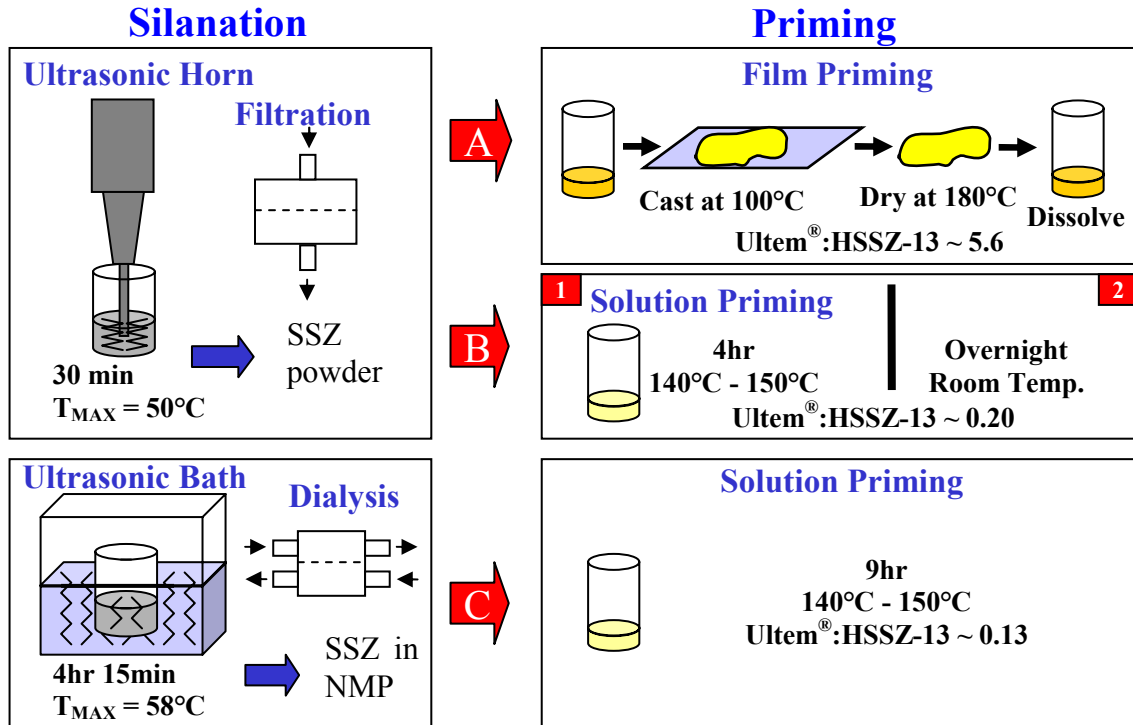


Figure 5.9: Schematic of experiments performed to stabilize casting dopes

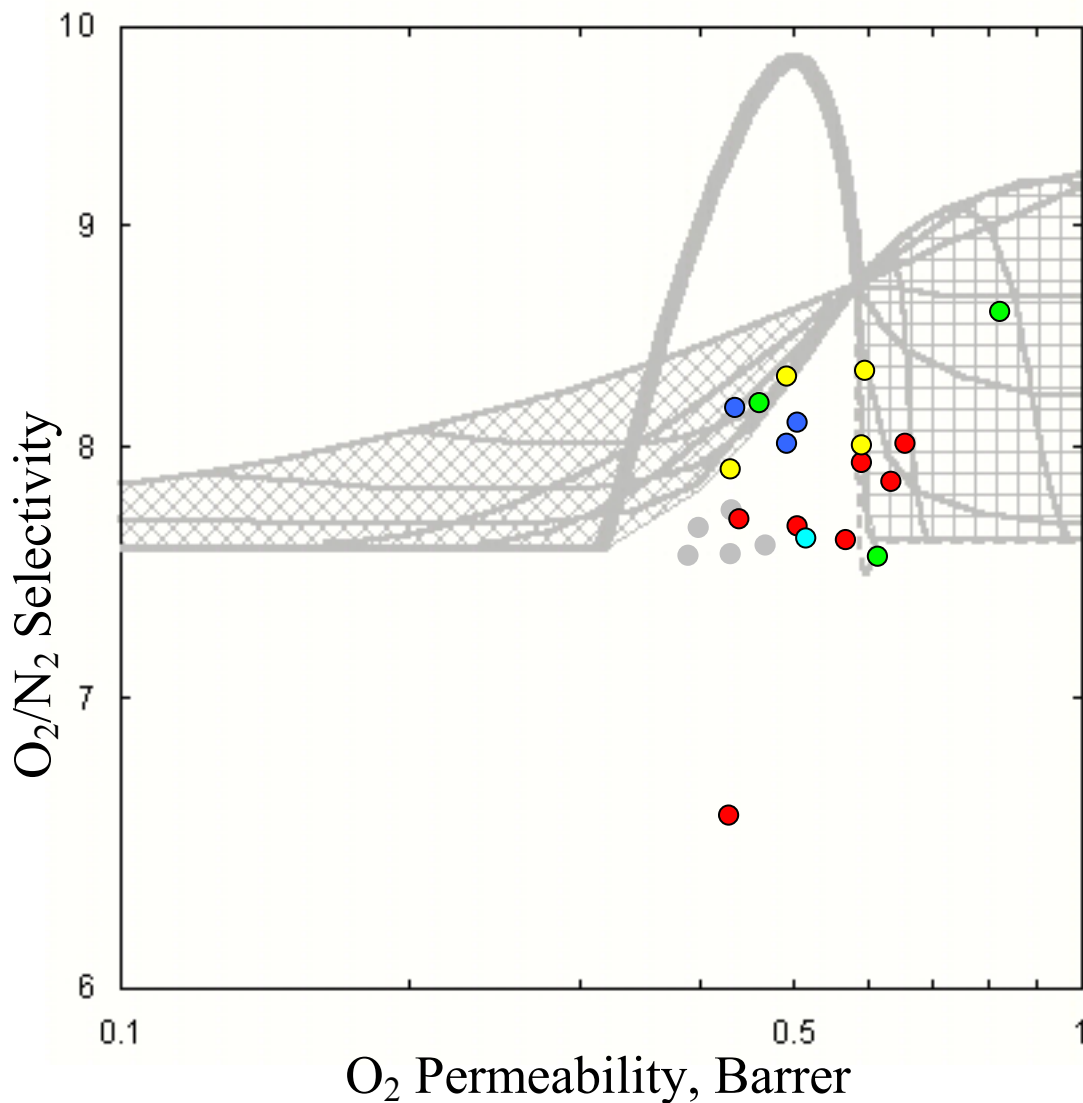


Figure 5.10: Comparison of membranes prepared with ~15 vol% HSSZ-13 dispersed in Ultem[®] using stabilized casting dopes as in Figure 5.9: (green), sieve suspension sonicated with polymer; (red), casting dope A; (blue), casting dope B1; (turquoise), casting dope B2; (yellow), casting dope C. Gray circles represent neat Ultem[®]. Tested at 35°C and 65 psia.

5.4. SELECTED MEMBRANE PREPARATION ISSUES

The stresses that are believed to cause the key nonideal mixed matrix morphologies of sieve-in-a-cage and matrix rigidification arise during preparation of the membrane. Thus, membrane preparation techniques should be selected to minimize stresses in the

membrane. The first subsection discusses several casting techniques that were investigated and their advantages and disadvantages. The effects of casting temperature and membrane drying and annealing conditions are also considered in short subsections.

5.4.1. Effect of Casting Substrate on Mixed Matrix Membranes

A number of casting techniques were considered to prevent sieve-in-a-cage morphology caused by adhesion to the casting substrate (see section 4.5). The ideal casting substrate should have several properties: (i) it should allow free contraction of any polymer or mixed matrix membranes cast on it, (ii) it should have a high surface energy so nascent membrane films will not bead up, (iii) it should be immiscible with the casting dope, and (iv) it should be more dense than the nascent membrane if it is not a solid. The most common casting substrate is probably glass, but many of the polymers used in this work adhere strongly to it. Modification of glass surfaces to reduce adhesion is discussed later. Another alternative is Teflon[®] or Teflon[®]-coated glass, but it fails criterion (ii) above. This problem can be reduced by using a high viscosity casting dope based on a volatile solvent, but beading will occur if the viscosity is low or if the evaporation rate is slow. Liquids are good candidates for fulfilling criterion (i), but many fail criterion (iii) or (iv). Fluorinert (3M; Minneapolis, MN), a perfluorinated liquid, was tried as a casting substrate, but flat films could not be obtained. A variation on this method is to cast at the interface of two immiscible liquids to promote spreading of the casting dope, but this proved complex and flat films could not be obtained.

One liquid that meets all four criteria is mercury. The setup used for casting on mercury is shown in Figure 5.11. Mercury is kept in a petri dish inside a desiccator because of its toxicity. The desiccator body is covered with plastic wrap. Before casting, the desiccator is saturated with the solvent used in the casting dope (typically dichloromethane) by placing ~20 mL in the bottom of the desiccator. Saturation within the desiccator is verified by placing an ice cube against the side of the desiccator prior to casting. Condensation on the cooled glass indicates saturation. The lid of the

desiccator is then removed and a very dilute (~2% solids) casting dope is dropped onto the mercury with a pipette through a hole in the plastic wrap. The desiccator lid is then replaced. As the solvent evaporates, the nascent membrane becomes opaque, indicating that most of the solvent has left, but it will not dry completely in the sealed desiccator. Therefore, once most of the solvent has left the nascent membrane (after several hours), the desiccator lid is removed so remaining solvent can evaporate. After several more hours, the membrane is removed and placed in a vacuum oven to complete drying.

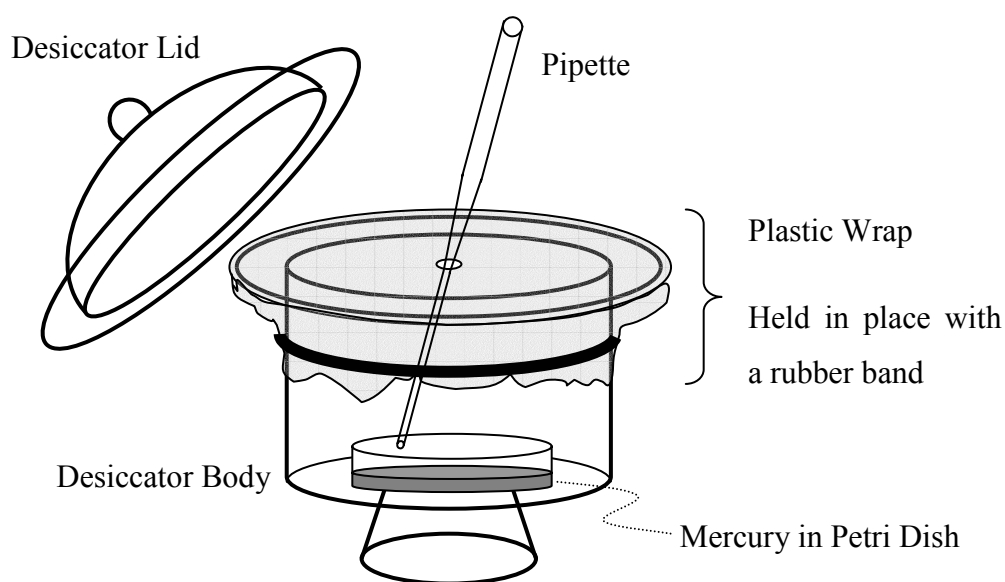


Figure 5.11: Mercury casting setup

The best membrane (~15 vol% HSSZ-13 in Ultem[®]) cast using this procedure had O₂ permeability of 0.4 Barrer, and O₂/N₂ selectivity of 8.4. This data is compared to membranes cast using other methods later on Figure 5.13. Conversely, membranes cast on glass from similar casting dopes under ambient conditions typically had selectivities comparable to neat Ultem[®] (7.4-7.6) with higher permeabilities (0.6-0.8), indicating sieve-in-a-cage morphology. Several Matrimid[®] – HSSZ-13 membranes were also cast. Two of these membranes had oxygen permeabilities *lower* than neat Matrimid[®] (1.9 and 1.8), eliminating the possibility of *large* voids at the polymer – sieve interface.

Unfortunately, both membranes had O₂/N₂ selectivity somewhat below neat Matrimid[®] (5.6 and 5.3). These and the CO₂/CH₄ results (not shown) seem to indicate an Ångstrom-scale sieve-in-a-cage morphology. The apparent Ångstrom-scale sieve-in-a-cage morphology may indicate that Matrimid[®] has a fundamental packing difficulty at the sieve surface.

Two casting techniques were found useful for casting on glass substrates. The first is to cast the membrane on glass from a low volatility solvent (NMP) at elevated temperature (~100°C). The nascent membrane is removed from the substrate once it forms a film with sufficient mechanical strength, but *before* vitrification (usually about 15-45 minutes). This procedure was adopted to prevent stress accumulation in the plane of the membrane that could cause sieve-in-a-cage morphology. Membranes are then dried vertically in a vacuum oven, with rods at the top and bottom to keep the membrane planar. Most of the Ultem[®] – HSSZ-13 membranes discussed in this chapter were prepared in this manner. The other technique, first developed by Mahajan [14], is to cast in a vacuum oven on a “treated” glass plate preheated to 70°C. Immediately following casting, the oven temperature is increased to ~200°C, and dynamic vacuum is drawn to -10 to -3 in Hg with a nitrogen purge. When membranes were allowed to dry completely at this temperature (or higher), they were very difficult to remove from the treated glass substrate. Reasons for this difficulty are discussed in the following paragraph. Therefore, many of these membranes were removed from the substrate after only a few hours and then drying was completed in an aluminum foil envelope at the desired conditions. By casting near the T_g of the polymer, the matrix remains flexible as the solvent evaporates, minimizing stresses in the membrane.

Mahajan did not encounter such difficulties in removing membranes from treated glass plates, so this phenomenon was investigated further [12]. Glass plates were treated with Glasclad[®]-18 (United Chemical Technologies; Bristol, PA), an octadecylsilane derivative, to reduce polymer adhesion. For this work, a *tempered* glass plate was used,

because tempered glass is better able to withstand the stresses caused by temperature cycling. On the other hand, Mahajan reported only that a Glassclad[®]-treated glass plate was used [12], so he may have used a regular glass plate. These various treated and untreated, regular and tempered glass plates were probed by viewing the contact angles of water on them. A proper goniometer setup was unavailable, but in many cases the differences could be easily observed with the naked eye. Before treatment with Glassclad[®], the contact angle of water on regular glass was much smaller than on tempered glass. The contact angle of water on tempered glass was slightly smaller than that on polyethylene, which was smaller than that on Teflon[®], as expected. On the other hand, after treatment of both glasses with Glassclad[®] thrice using the procedure recommended by the manufacturer, the contact angles of water on the two treated glasses were similar. Thus, adding Glassclad[®] to the *regular* glass surface reduced the contact angle, but there was no discernable difference in the contact angle of water on treated and untreated *tempered* glass. Therefore, it appears there is a significant difference in treated-regular and treated-tempered glass. Mahajan may have used Glassclad[®]-treated *regular* glass, and this could explain why it was difficult to remove membranes heated to high temperatures on Glassclad[®]-treated *tempered* glass. This hypothesis was tested by casting a small amount of Ultem[®] – zeolite 4A mixed matrix dope on a glass slide treated with Glassclad[®]. The resulting film was easy to remove from the surface after extended heating at high temperature. This was verified by a Shu Shu of the research group using a Glassclad[®]-treated regular glass casting plate. This demonstrates the subtle effects the casting substrate may have on mixed matrix membranes. Unfortunately, this discovery was made late in this research.

When casting at elevated temperature, it can be difficult to gauge when enough solvent has evaporated to give a nascent membrane with sufficient mechanical strength to remove, while retaining enough solvent to keep the polymer matrix rubbery. This is complicated by uneven solvent evaporation from the membranes. These factors may have contributed to the large scatter observed in the transport properties of membranes

prepared with this technique. An alternative that should be investigated in more detail is to cast from a two solvent system; one volatile (e.g. dichloromethane) and one of low volatility (e.g. NMP). Enough low volatility solvent is added to keep the nascent membrane rubbery once the volatile solvent has evaporated, leaving a membrane with suitable mechanical strength for handling. Such a membrane can be prepared at room temperature, whereas other procedures for casting from NMP require higher temperatures. Because the low volatility solvent slowly evaporates at room temperature, it should be easier to control the amount of solvent remaining when the film is removed. These membranes can then be dried in the vacuum oven in the conventional manner.

Pattern formation on the surface (sieve segregation caused by surface tension gradient driven Marangoni flows) has also been a problem for sieve filled membranes prepared on mercury or using the high temperature casting technique. This phenomenon was first observed by Mahajan [15]. In membranes cast on mercury, faster evaporation occurs when the desiccator is presaturated with only the plastic wrap on the desiccator body, causing pattern formation. This is eliminated by slowing the solvent evaporation rate using the saturated atmosphere casting technique described earlier. In the high temperature casting technique, Mahajan demonstrated that pattern formation can be avoided by heating the film from above. This is accomplished by casting the dope on a glass plate placed on a lab jack. After the casting dope is drawn into a film, the lab jack is raised until the nascent membrane is about ½ inch from the top of the heated oven.

Figure 5.12 summarizes transport properties of membranes prepared with ~15 vol% zeolite 4A dispersed in Ultem[®]. Most of the membranes have permeabilities lower than neat Ultem[®], indicating the absence of sieve-in-a-cage morphology for most or all of the sieves in the membrane. Nevertheless, the selectivities are lower than expected. This is believed to be due to zeolites exhibiting reduced permeability as discussed in the following chapter. Most membranes were prepared from NMP either by casting and

immediately heating to $\sim 200^{\circ}\text{C}$ or by removing the film from the surface before the matrix vitrified when casting at a lower temperature. These procedures prevent accumulation of tensile stresses at polymer – sieve interfaces that could lead to sieve-in-a-cage morphology. The membranes prepared by casting and immediately heating to high temperature (red points on Figure 5.12) exhibit less scatter. Most have transport properties within or very near the matrix rigidification region of the transport property map. On the other hand, membranes prepared by removing the nascent membrane before vitrification (blue points) have more scatter. Many have transport properties within the matrix rigidification region, but some lie in the triangular region between the matrix rigidification and stress dilated regions. These transport properties can only be described by assuming some of the zeolites within the membranes exhibit different nonideal morphologies. Membranes cast and removed before vitrification dried unevenly, so there could be variation within the membranes. Membranes prepared from dichloromethane at lower temperature have high permeabilities and selectivities equal to or worse than neat Ultem[®], with one important exception. After annealing such membranes to 250°C for 12 hr in nitrogen, transport properties similar to membranes prepared with the other two techniques are obtained (green points on Figure 5.12). This is discussed in more detail in section 5.4.3.

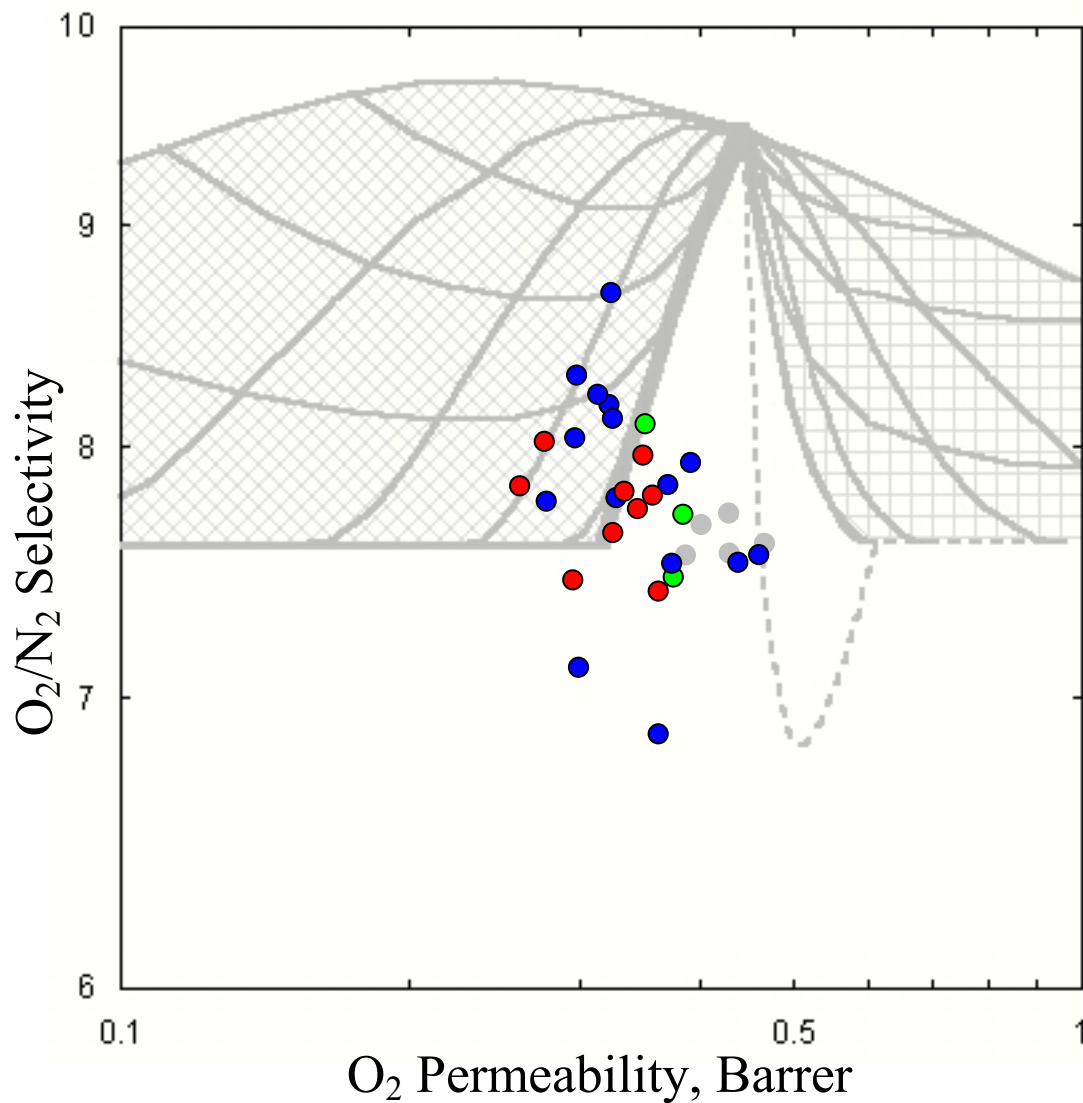


Figure 5.12: Comparison of membranes prepared with ~15 vol% zeolite 4A dispersed in Ultem[®] using the following techniques: cast from NMP and remove before vitrification (blue); cast from NMP and heat to high temperature (red); cast from dichloromethane at room temperature and anneal to 250°C (green). Gray circles represent neat Ultem[®]. Tested at 35°C and 65 psia.

A number of different casting techniques were also used to prepare Ultem[®] – HSSZ-13 membranes. Figure 5.13 presents a summary of these membranes, all at ~15 vol% loading. Most of the membranes with the highest selectivities were prepared from NMP by casting at ~100°C and removing the nascent membrane before vitrification.

However, not all membranes cast in this manner exhibit increased selectivity. The scatter in these results is discussed in the following paragraph. Membranes prepared from the more volatile solvents, dichloromethane and chloroform, must be cast near ambient temperature because of their low boiling points. Evaporation of these volatile solvents typically occurs too fast to remove the nascent membrane before vitrification, so these membranes were allowed to dry on the substrate. Figure 5.13 shows that these membranes (red and green) display transport properties consistent with sieve-in-a-cage morphology. Several membranes were also prepared from dichloromethane on mercury, which allows contraction in response to any in-plane stresses that arise, preventing tensile stresses on the sieve surface. One of these mercury-cast membranes had transport properties in the matrix rigidification region. Thus it appears possible to prepare membranes that do not exhibit sieve-in-a-cage morphology from glassy matrices at room temperature, *provided appropriate measures are taken to prevent tensile stresses on the sieve surfaces.*

The transport properties of membranes prepared from NMP are widely scattered. Figure 5.13 represents membranes prepared from different silanes and application methods, including film-and solution-primed sieves. The point of this figure is that *all membranes with significant improvement in selectivity were prepared using casting methods designed to eliminate tensile stresses on the polymer – sieve interface,* regardless of the materials selection or dope formulation issues. This is not a sufficient condition for successful mixed matrix membranes, but it is necessary. Some of the scatter can undoubtedly be explained by differences in material selection and dope formulation. In particular, many of these membranes exhibit sieve agglomerates, since they were prepared before the optimal priming procedure was developed. As discussed previously, such agglomerates may not contribute to enhanced selectivity, but may cause increased permeability. Thus, a fraction of the sieves in such membranes exhibit sieve-in-a-cage morphology, while the remainder exhibit matrix rigidification, and this explains the difficulty in realistically modeling their results by assuming a *single*

nonideal morphology. Such membranes where a portion of the sieves exist as agglomerates with the remainder exhibiting matrix rigidification should have transport properties to the right of the matrix rigidification region. This is precisely where a number of membranes fall.

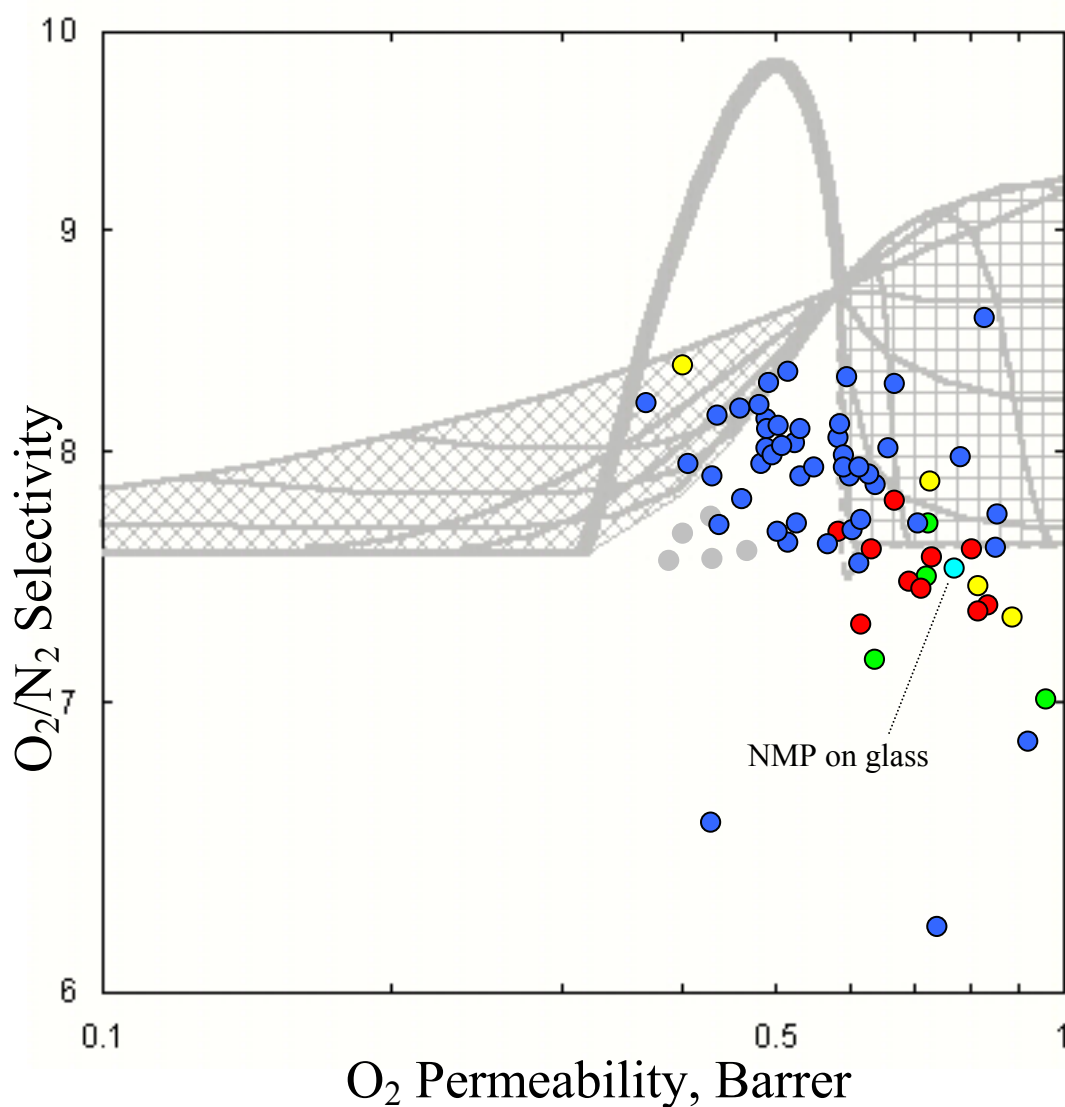


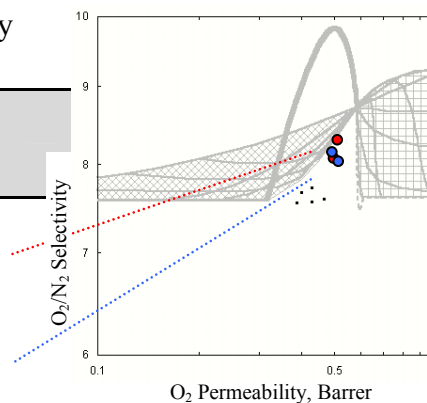
Figure 5.13: Comparison of membranes prepared with ~15 vol% HSSZ-13 dispersed in Ultem[®] using the following techniques: cast from NMP and remove before vitrification (blue); cast from dichloromethane on glass (red); cast from dichloromethane on mercury (yellow); and cast from chloroform on glass (green). Gray circles represent neat Ultem[®]. Tested at 35°C and 65 psia.

5.4.2. Effect of Casting Temperature and Solvent Evaporation Rate on Mixed Matrix Membranes

It is difficult to change the casting temperature without changing another important variable, such as the solvent or evaporation rate. Nonetheless, this can be done within limited ranges. Ultem[®] – HSSZ-13 membranes were prepared from the same casting dope by casting from NMP on glass at 70°C and 100°C and then removing the nascent membranes before the polymer matrix vitrified. Transport properties for these membranes are summarized in Table 5.5. The differences in permeation properties in these membranes are negligible compared to the expected variability within individual membranes, so the casting temperature seems unimportant as long as vitrification on the casting plate is avoided. Although the transport properties of membranes in Table 5.5 may appear more consistent than others in this chapter, no special measures were taken to achieve these properties. In fact, they were prepared with film priming rather than solution priming, so those cast at 100°C should be equivalent to samples sonicated with APDMES in Table 5.1 and Table 5.3. One conceivable explanation is that these membranes were prepared well into this work, so more experience with the preparation technique likely led to the more consistent properties in Table 5.5.

Table 5.5: Transport properties for ~15 vol% HSSZ-13 in Ultem[®] membranes prepared with different initial drying temperatures. Tested at 35°C and 65 psia.

Initial Drying Temperature	O ₂ Permeability, Barrer	O ₂ /N ₂ Selectivity
Neat Ultem [®]	0.4	7.6
Maxwell Model	0.59	8.7
70°C	0.49	8.1
	0.51	8.4
100°C	0.48	8.2
	0.50	8.0



The effect of solvent evaporation rate on mixed matrix membranes was also considered. If the evaporation rate could be slowed enough, it is possible that stresses will relax before causing failure of the polymer – sieve interface. Ultem[®] – HSSZ-13 membranes prepared from dichloromethane were used in this study. This is a very volatile solvent, so it evaporates quickly (~minutes) unless the headspace above the membrane is carefully presaturated with solvent. Membranes that dried in minutes were adhered to the glass casting plate, although slipping a razor under the surface of the membrane caused the entire membrane to “jump” off the surface. This indicates the stresses induced in the film during rapid solvent evaporation. Conversely, membranes that were slowly dried delaminated from the surface during solvent evaporation. These membranes are expected to have lower stresses, and may be less likely to exhibit sieve-in-a-cage morphology. Nonetheless, as shown in Table 5.6, even membranes prepared in carefully presaturated atmospheres had transport properties consistent with sieve-in-a-cage morphology. These dichloromethane-cast membranes from Table 5.6 appear as red samples on Figure 5.13. Because stress relaxation in glassy polymers occurs very slowly it may be impossible to slow the evaporation rate enough to prevent sieve-in-a-cage formation for glassy polymer-based membranes adhered to a substrate.

Table 5.6: Transport properties for ~15 vol% HSSZ-13 in Ultem[®] membranes prepared with different solvent evaporation rates. Tested at 35°C and 65 psia.

Membrane	O ₂ Permeability, Barrer	O ₂ /N ₂ Selectivity	CO ₂ Permeability, Barrer	CO ₂ /CH ₄ Selectivity
Neat Ultem [®]	0.4	7.6	1.4	38
Maxwell Model	0.59	8.7	2.2	44
Fast solvent evaporation	0.80	7.6	3.0	40
	0.73	7.6	2.8	37
Slow solvent evaporation	0.83	7.4	3.1	37
	0.71	7.4	2.7	38

The solvent from the successful Ultem[®] – HSSZ-13 membrane cast on mercury was slowly evaporated. The edges of membranes prepared on mercury with fast evaporation curled under. This could have been caused by the vitrified top half of the nascent membrane acting as a constraining substrate for the more slowly evaporating bottom half of the nascent membrane. This may have caused tensile stresses and sieve-in-a-cage morphology in the bottom portion of the membrane. Favorable transport properties were not observed for fast-evaporated mercury-cast membranes. Fast evaporation also causes patterning, so it is not recommended.

5.4.3. Effect of Drying and Annealing on Mixed Matrix Membranes

Section 4.4.4 discusses the potential effects of elevated drying temperatures on mixed matrix membranes. They offer the appealing possibility of reducing the matrix rigidification effect, repairing sieve-in-a-cage morphology, and removing potential sorbed molecules that may cause reduced permeability in the zeolites. On the other hand, it is also possible that the delicate morphology of the interface could be damaged during thermal cycling. Figure 5.14 plots the transport properties for several ~15 vol% zeolite 4A in Ultem[®] mixed matrix membranes dried at various temperatures. Most of these membranes were prepared using either the high temperature casting technique or by casting and removing before vitrification as discussed in section 5.4.1. When drying at 260°C or below, the membranes tend to exhibit permeability less than neat Ultem[®]. The selectivity improvement in these membranes was typically smaller than expected indicating either excess rigidification, ($\beta > 10$), or reduced permeability zeolites. Based on analysis the following chapter, it appears that reduced permeability zeolites are the cause. Again, a many membranes have transport properties in the region between the matrix rigidification and stress dilated regions, indicating the possible presence of multiple nonideal morphologies within individual samples. Nonetheless, the ability to prepare mixed matrix membranes from glassy polymers that do not exhibit exclusively sieve-in-a-cage morphology is important.

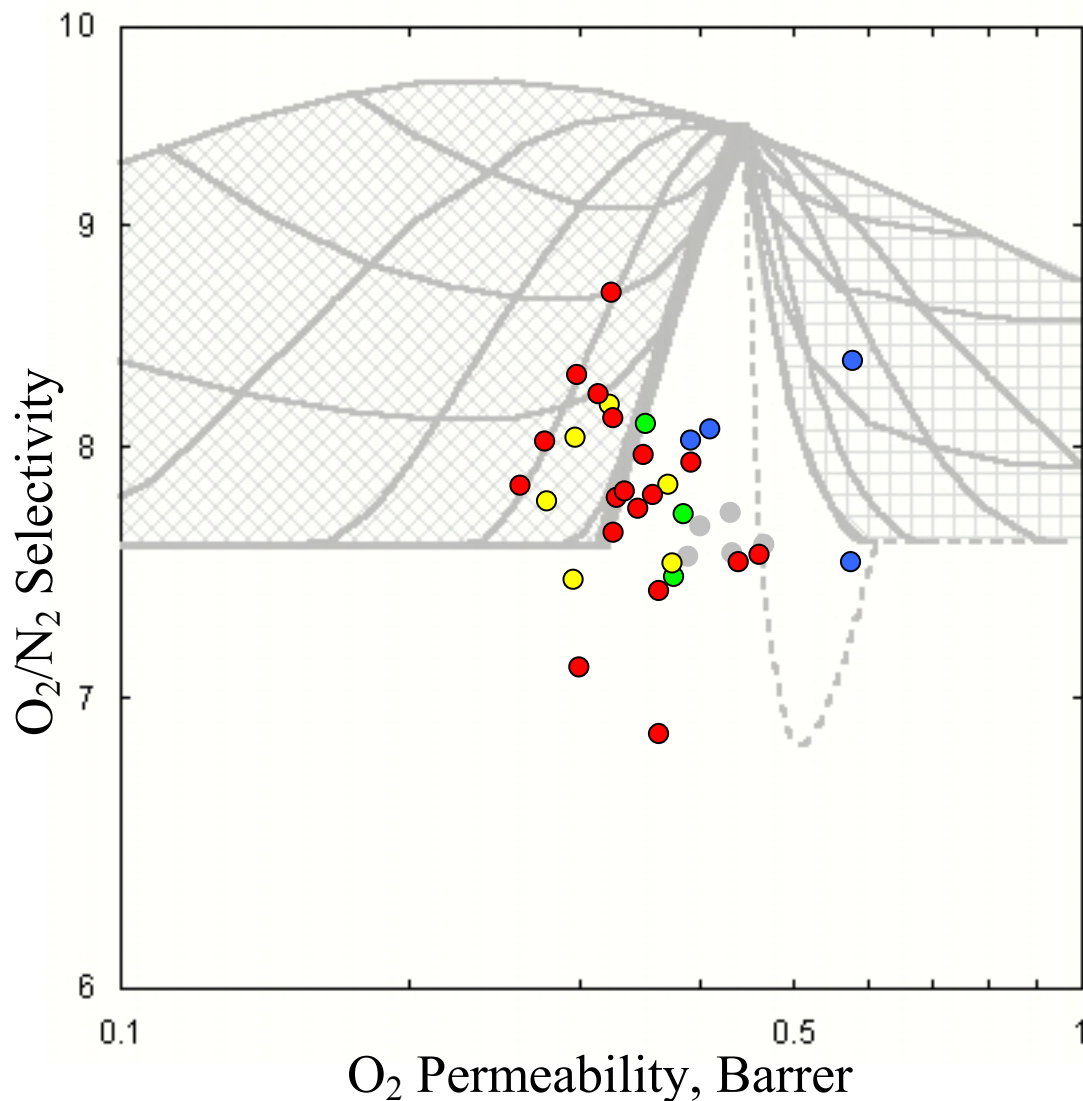


Figure 5.14: Comparison of membranes prepared with ~15 vol% zeolite 4A dispersed in Ultem[®] at various temperatures: (yellow) 180°C – 220°C; (red) 240°C – 260°C; (blue) 280°C – 300°C; (green) cast at room temperature and annealed at 250°C. Gray circles represent neat Ultem[®]. Tested at 35°C and 65 psia.

Three of the samples (in green) on Figure 5.14 were prepared by annealing at 250°C in nitrogen a membrane that was cast on glass from dichloromethane. After drying this same membrane at 100°C, transport properties consistent with sieve-in-a-cage morphology were observed, as expected for a membrane cast on glass well below the T_g of the matrix. Thus, it appears that annealing the membrane well above the matrix

T_g (208°C) was able to *repair* sieve-in-a-cage morphology. While these annealed membranes have improved properties relative to unannealed membranes, annealing may not completely repair the interfaces of all the sieves in the membrane. These annealed membranes exhibit transport properties between the matrix rigidification and stress dilated regions, indicating the possible presence of both morphologies. Conversely, drying of 6-mD based membranes (discussed in section G.2) at 250°C does not seem to have repaired the sieve-in-a-cage morphology, but this was ~50°C below the T_g.

Figure 5.14 also shows several membranes that were annealed at 300°C. These samples exhibit higher permeabilities, on average, than the others, which may indicate that some of the polymer – sieve interfaces within these membranes have been damaged. In particular, one of the samples exhibits the speculated stress dilated morphology, which may be a precursor to full interfacial failure. Another of these 300°C annealed membranes appears to display full sieve-in-a-cage morphology. Bonds between polyimides and γ -aminopropyltriethoxysilane, which has an amine functionality similar to APDMES, reportedly are broken at 300°C, but then reform upon cooling [7]. Further heating to 350°C removes the silane from the surface. This same reference indicates that most silane – polyimide failures result in cohesive failure of the interface [7]. 6-mD membranes heated to 350°C (section G.2) also exhibit higher permeabilities than the corresponding samples dried at lower temperature. Thus, drying of mixed matrix membranes at elevated temperatures is not recommended.

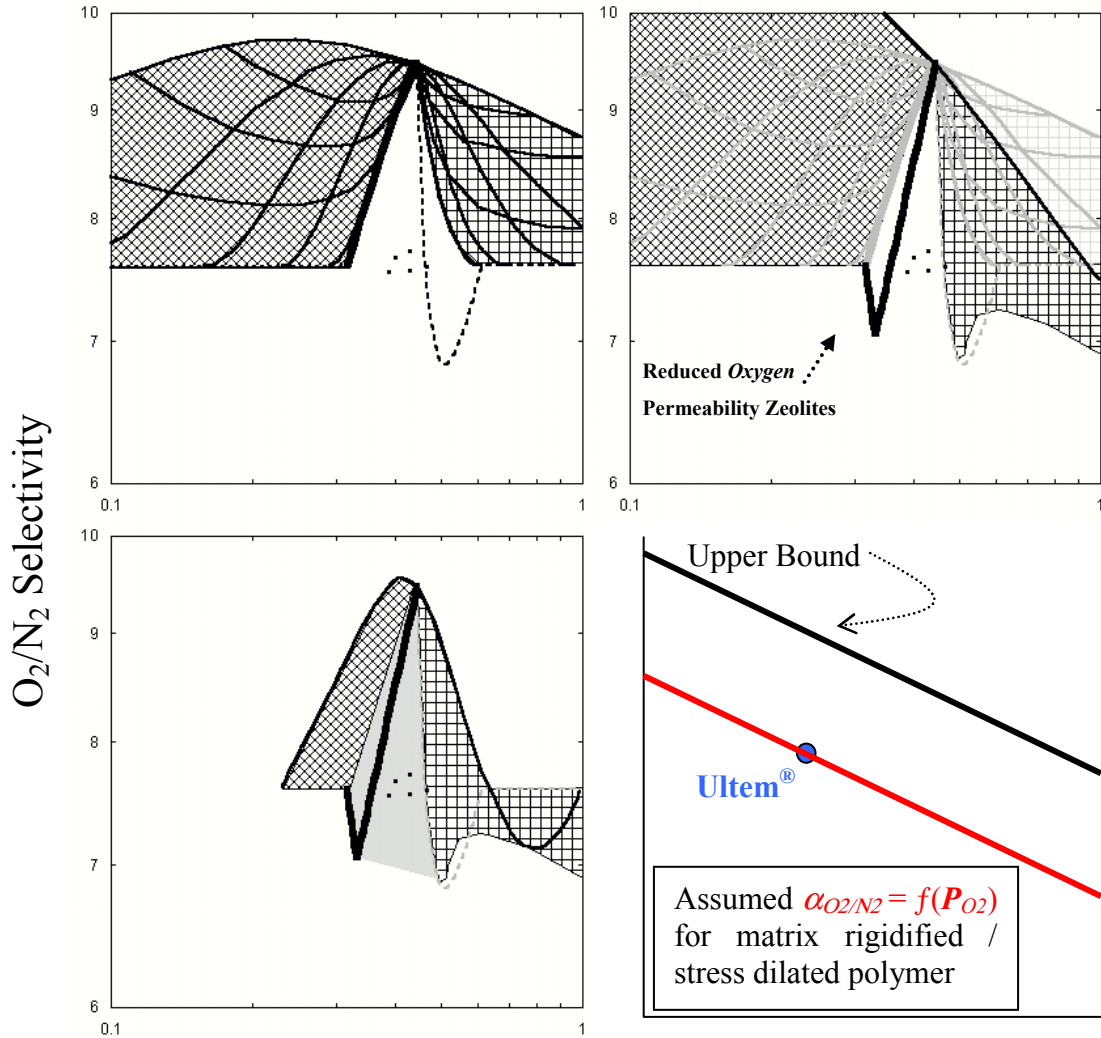
5.5. DISCUSSION

Many of the membranes presented in this chapter do not fall in regions of the transport property map that are characteristic of a single nonideal morphology. The following two subsections discuss how the properties of these membranes can potentially be explained. The Ultem[®] – zeolite 4A and Ultem[®] – HSSZ-13 systems are considered sequentially. The final subsection presents results and conclusions from this chapter.

5.5.1. Analysis of Mixed Matrix Membranes with Zeolite 4A

As mentioned throughout the text, zeolite 4A used in this work is believed to suffer from reduced permeability. In the following chapter, a number of potential causes of this behavior are elucidated. Many contaminants or processing solvents were discovered to slow sorption of oxygen into zeolite 4A, without significantly impacting the equilibrium sorption. Thus, a small amount of contaminant has a large effect on zeolite diffusion and permeation. This could occur if the contaminant covers pore entrances to the zeolite. This could also occur if the contaminant partially blocks the pores between neighboring cages. In section 7.2.3, this is suggested as the cause of reduced sorption kinetics in the presence of small amounts of water. If the pore size is only partially blocked, the diffusion selectivity through the pore could also be altered. In particular, it is possible that oxygen would lose rotational degrees of freedom in the transition state, whereas nitrogen does not have any to lose, in even pristine zeolite 4A. This would considerably depress the zeolite selectivity, as rotational degrees of freedom contribute significantly to the faster diffusion and permeation of oxygen compared to nitrogen. The transport property map used throughout this chapter (Figure 5.15a) shows a simple calculation for “reduced permeability zeolites” that assumes the zeolite selectivity is unchanged. If the oxygen permeability and O_2/N_2 selectivity both decrease (because oxygen loses rotational degrees of freedom), the alternative curve on Figure 5.15b labeled “Reduced *Oxygen* Permeability Zeolites” is obtained. The minimum in this curve occurs because the permeability is nonzero when oxygen has lost all its rotational degrees of freedom, but the selectivity (2.5) is lower than neat Ultem[®]. The details behind this calculation are discussed in Appendix F. In this calculation, the nitrogen permeability through the zeolite is assumed constant because only oxygen loses rotational degrees of freedom. This assumption may not fully capture the behavior the real system, since it is likely that vibrational degrees of freedom are also impacted. This would reduce the nitrogen permeability as well, and may lead to a smaller decrease in O_2/N_2 selectivity with decreasing oxygen

permeability. Nonetheless, this may represent a more realistic case than assuming the O_2/N_2 selectivity is unchanged as zeolite permeability decreases.



Oxygen Permeability, Barrer

Figure 5.15: O_2/N_2 transport property maps: (a) assuming the selectivity of the nonideal morphology regions are the same as the corresponding pure material (b) allowing the selectivity of the nonideal morphology region to vary as discussed in the text (c) assuming maximum $\ell_V/r_S = 0.3$ to represent “experimentally accessible” transport properties. The shaded area in (c) indicates transport properties indicative of multiple nonideal morphologies in sieve fractions within a single membrane. (d) shows the assumed dependence of O_2/N_2 selectivity on O_2 permeability for the matrix rigidification and stress dilated regions shown in (c).

The matrix rigidification and stress dilated regions shown in Figure 5.15a were both calculated assuming the selectivity of the rigidified and dilated regions are unchanged. It is believed that these nonideal morphologies are caused by changes in the fractional free volume of the polymer matrix near the sieves. Permeability and selectivity are functions of fractional free volume. Thus, the fractions of the polymer matrix exhibiting these nonideal morphologies likely have different selectivities than the bulk matrix. Matrix rigidification and stress dilated regions allowing for variable selectivity are also plotted on Figure 5.15b. The selectivity dependence of the matrix rigidified or stress dilated polymer region as a function of the permeability of this region was assumed parallel to the upper bound, as shown in Figure 5.15d. At $\beta = 1$, the “affected” polymer region should have the properties of neat Ultem[®], so this line ($\alpha_{O_2/N_2} = f(P_{O_2})$) must pass through its transport properties. More details behind this calculation can also be found in Appendix F. Allowing the selectivity to vary can significantly change the transport property map. Nonetheless, the added region for matrix rigidification with selectivities significantly above the Maxwell model calculation ($\sim > 9.5$) may be experimentally inaccessible because it requires rigidification of most or all of the matrix. The highlighted regions in Figure 5.15c, corresponding to $\ell_l/r_s < 0.3$, may represent a more reasonable boundary for experimentally accessible transport properties.

Another possibility is that fractions of the sieves within individual membranes may display different nonideal morphologies. An infinite number of combinations of matrix rigidified, stress dilated, and sieve-in-a-cage fractions, β 's, and ℓ_l/r_s 's are possible. Membranes having sieve fractions exhibiting multiple nonideal morphologies could have transport properties in the gray shaded region of Figure 5.15c. They could also have transport properties overlapping the single morphology regions of the transport property map. Case studies for potential multiple nonideal morphology membranes are also given in Appendix F.

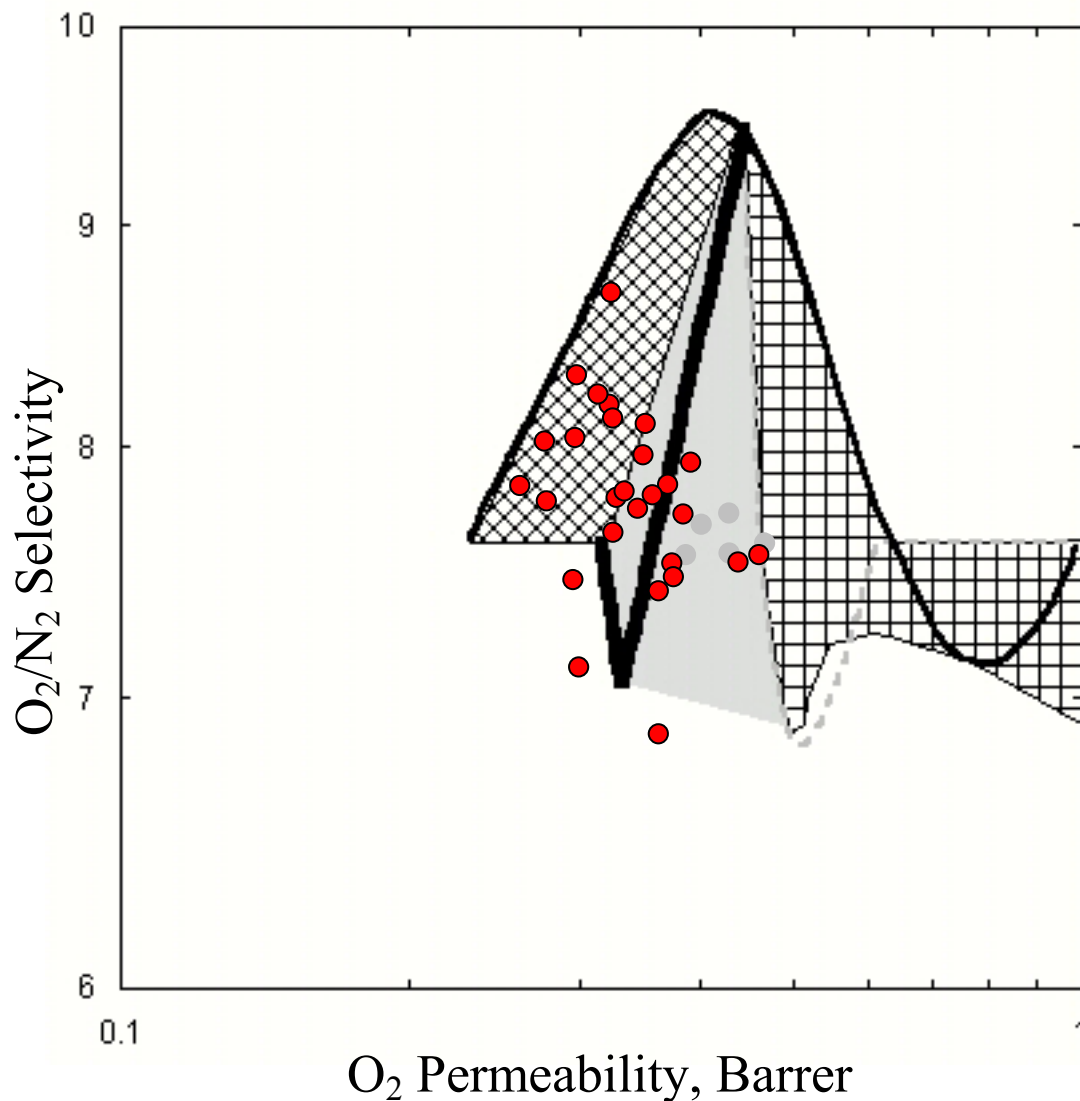


Figure 5.16: Summary of O_2/N_2 transport properties for ~15 vol% zeolite 4A in Ultem[®] on the O_2/N_2 transport property map developed in Figure 5.15c.

Figure 5.16 summarizes the O_2/N_2 transport properties for 15 vol% zeolite 4A in Ultem[®]. Based on these experimental transport properties, modeling calculations, and the results of sorption experiments in the following chapter, **it appears that the primary reason many of the zeolite 4A-based membranes exhibit transport properties below the Maxwell prediction is because of *reduced permeability in the zeolite phase*.** This permeability reduction likely also causes reduced selectivity in the

zeolite phase, and therefore, within the overall mixed matrix membrane. Matrix rigidification may be superimposed on these membranes with reduced permeability zeolites, accounting to points left of the “Reduced *Oxygen* Permeability Curve”.

5.5.2. Analysis of Mixed Matrix Membranes with HSSZ-13

Figure 5.17 summarizes the O₂/N₂ transport properties for ~15 vol% HSSZ-13 in Ultem[®] on a transport property map equivalent to Figure 5.15c. There are a number of membranes that have transport properties outside the regions covered by the simple transport property map of Figure 5.2. These more complicated models can account for a greater fraction of the experimental data.

In zeolite 4A-based membranes, the lower-than-expected transport properties were attributed primarily to reduced zeolite permeability. This may also be true for HSSZ-13. Nonetheless, reduced permeability in HSSZ-13 could not be independently observed using sorption experiments discussed in Chapter 6 because sorption occurs too quickly in the available samples. Furthermore, it is difficult to say with certainty in this system whether reduced zeolite permeability is the dominant factor because there is visual evidence that multiple nonideal morphologies may exist in many membranes prepared with HSSZ-13. Sieves that exist as sieve agglomerates in mixed matrix membranes have properties consistent with sieve-in-a-cage morphology even if the underlying cause of this morphology is different. The remaining well dispersed, well-bonded sieve fraction may exhibit Maxwellian, matrix rigidification, or reduced permeability zeolite behavior. It appears **many Ultem[®] – HSSZ-13 membranes have lower-than-expected transport properties because of *multiple nonideal morphologies*, in particular sieve-in-a-cage morphology due to agglomerates.** This illustrates the importance of working with a polymer – zeolite system that will give rise to a single nonideal morphology to facilitate better understanding mixed matrix membrane morphology and transport properties. These problems with HSSZ-13 were not envisioned at the onset of this work.

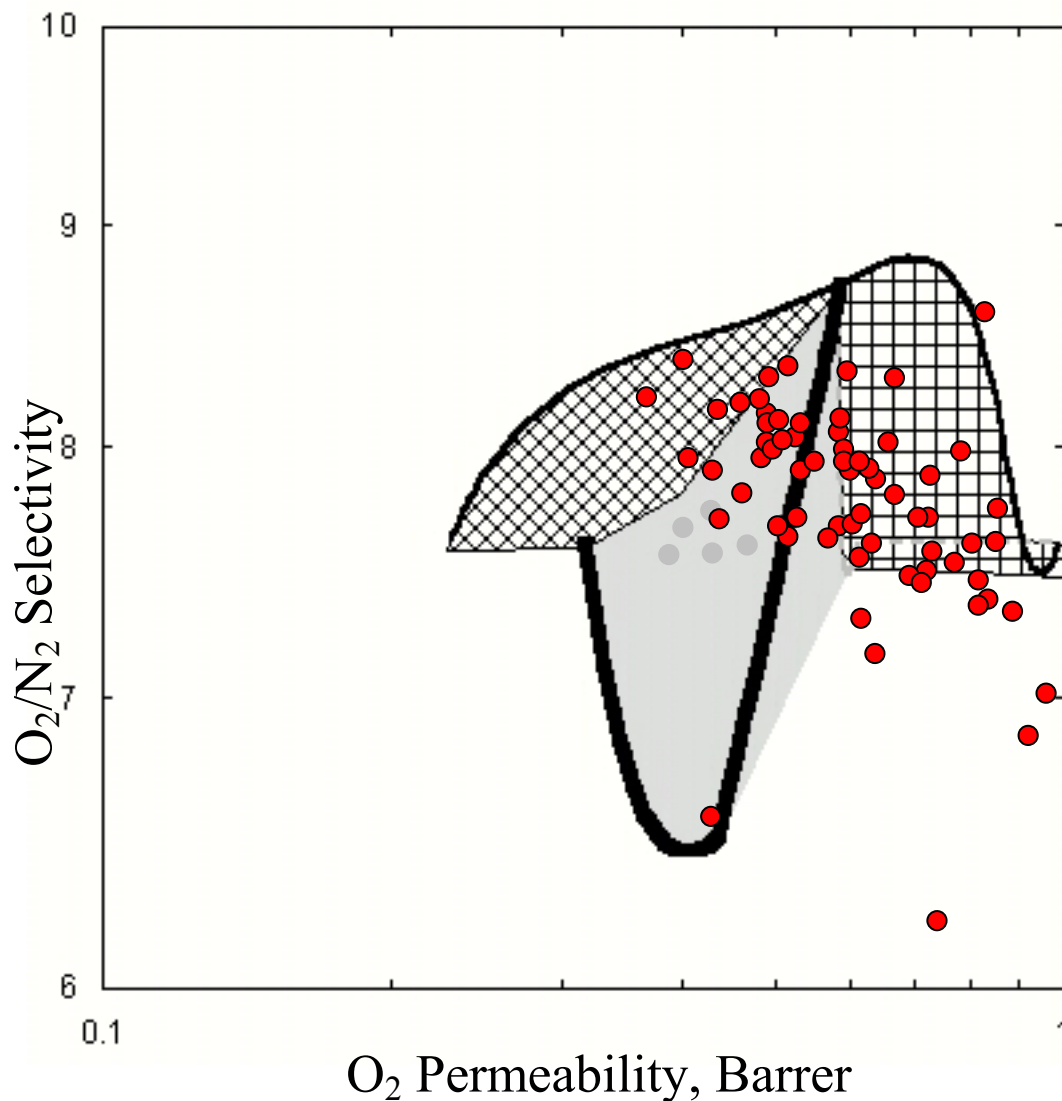


Figure 5.17: Summary of O₂/N₂ transport properties for ~15 vol% HSSZ-13 in Ultem[®] on an O₂/N₂ transport property map developed similar to that of zeolite 4A in Figure 5.15c.

5.5.3. Summary and Conclusion

This chapter has illustrated the importance of eliminating tensile stresses that may form on sieve surfaces during membrane casting. Several techniques were presented that make this possible, including: (i) casting at a temperature near or above the T_g of the matrix, (ii) casting at intermediate temperature and removing the nascent membrane

before the matrix vitrifies, or (iii) casting on a substrate (e.g. mercury) that allows free contraction of the nascent membrane. These methods should eliminate sieve-in-a-cage morphology, but they can not eliminate the matrix rigidification. Nonetheless, sieve agglomerates within membranes may have transport properties similar to sieve-in-a-cage morphology, but this is caused by poor sieve stabilization. Sieve agglomerates are much more of a problem with submicron zeolites. However, it was shown that by appropriate priming of a suitably silanated zeolite, successful mixed matrix membranes with minimal agglomerates can be prepared. Mixed matrix membranes can also be prepared from some polymers (e.g. 6-64D in section G.1) on glass because the membranes delaminate from the glass, preventing in plane stresses from arising. Nonetheless, delamination from the substrate during casting does not appear to prevent sieve-in-a-cage morphology in all cases (e.g. Ultem[®] – HSSZ-13 from dichloromethane). Finally, if the zeolites exhibit reduced permeability due to some other artifact, the casting technique is unlikely to increase the zeolite permeability.

In some cases, it appears that sieve-in-a-cage morphology can be repaired by annealing the membranes above the T_g of the matrix (e.g. Ultem[®] – zeolite 4A), although perhaps incompletely. This approach appears limited with higher T_g polymers, since higher temperatures (300°C+) are believed to damage the polymer – sieve interfaces. This damage may have been caused by increased thermal expansion at higher temperature. Clearly, attempts to repair mixed matrix membranes exhibiting nonideal morphologies using high temperature annealing have given mixed results. A more substantial study of the variables, including heating and cooling rates and thermal hold times, is merited.

Although all of the membranes previously presented in this chapter were prepared at approximately 15 vol% zeolite loading, membranes prepared at 30 vol% zeolite loading verify the conclusions drawn based on the lower loading membranes. Transport properties for these membranes are given in Table 5.7. The ~30 vol% HSSZ-13 in Ultem[®] membrane had among the highest selectivity of any Ultem[®] – HSSZ-13

membrane tested. Thus the selectivity increases as more zeolite is added, even if it does not reach the value predicted by the Maxwell model at a given loading. The permeability of the ~30 vol% zeolite 4A in Ultem[®] membrane is lower than almost all of the other Ultem[®] – zeolite 4A membranes prepared. This is consistent with mixed matrix membranes that suffer from reduced permeability zeolites. The causes of reduced permeability zeolites are investigated in the following chapter.

Table 5.7: Transport properties for mixed matrix membranes with ~30 vol% zeolite dispersed in Ultem[®]. Tested at 35°C and 65 psia.

Zeolite	O ₂ Permeability, Barrer	O ₂ /N ₂ Selectivity	CO ₂ Permeability, Barrer	CO ₂ /CH ₄ Selectivity
Neat Ultem [®]	0.4	7.6	1.4	38
HSSZ-13	0.51	8.5	1.7	44
Zeolite 4A	0.28	7.9	1.0	45

5.6. REFERENCES

1. Moore, T.T.; R. Mahajan; D.Q. Vu; and W.J. Koros. *AICHE J.* 2004, 50, 311-21.
2. Zhang, J.; H. Chen; Y. Li; R. Suzuki; T. Ohdaira; and Y.C. Jean. *Polym. Preprints* 2004, 45, 9-10.
3. Cauvel, A.; D. Brunel; F. Di Renzo; P. Moreau; and F. Fajula, *Functionalization of γ zeolites with organosilane reagents*, in *Catalysis by microporous materials*. 1995, Elsevier. p. 286-93.
4. Jaroniec, C.P.; R.K. Gilpin; and M. Jaroniec. *J. Phys. Chem. B* 1997, 101, 6861-6866.
5. Vrancken, K.C.; P. Van Der Voort; K. Possemiers; and E.F. Vansant. *J. Colloid Interface Sci.* 1995, 174, 86-91.
6. Plueddemann, E.P., *Silane coupling agents*. 1982, New York: Plenum Press.
7. Ansel, M. and P.D. Murphy. *J. Adhesion Sci. Tech.* 1994, 8, 787-806.
8. Kanan, S.M.; W.T.Y. Tze; and C.P. Tripp. *Langmuir* 2002, 18, 6623-6627.

9. Rice, G.L. and S.L. Scott. *Langmuir* 1997, 13, 1545-1551.
10. Rice, G.L. and S.L. Scott. *J. Molecular Catalysis A: Chem.* 1997, 125, 73-79.
11. Iler, R.K., *The chemistry of silica: Solubility, polymerization, colloid and surface properties and biochemistry.* 1979, New York: John Wiley & Sons.
12. Mahajan, R., *Formation, characterization and modeling of mixed matrix membrane materials.* Department of Chemical Engineering, University of Texas at Austin. 2000.
13. Piirma, I., *Polymeric surfactants. Surfactant science series. Vol. 42.* 1992, New York, NY: Marcel Dekker, Inc.
14. Mahajan, R. and W.J. Koros. *Polym. Engr. and Sci.* 2002, 42, 1432-1441.
15. Mahajan, R.; R. Burns; M. Schaeffer; and W.J. Koros. *J. Appl. Polym. Sci.* 2002, 86, 881-890.

Chapter 6. EFFECT OF SORBED COMPONENTS ON MIXED MATRIX MEMBRANE TRANSPORT PROPERTIES

6.1. OVERVIEW

Sorption is a powerful technique for analyzing the behavior of polymers, zeolites, and mixed matrix membranes. Both equilibrium and transient sorption give useful information about materials. If a processing condition causes sorption below equilibrium, it will reduce the transport rate through the material because it can accommodate less gas. Similarly, the sorption rate into the material is a function of the diffusion coefficient through the material, and if sorption is slow, permeation will be reduced.

The next section discusses sorption in the pure materials comprising mixed matrix membranes (i.e. polymers and zeolites). Section 6.3 discusses reduced equilibrium sorption or sorption rates caused by processing conditions. The next section demonstrates that sorption in mixed matrix membranes is approximately additive, provided there are no processing related artifacts affecting sorption in either or both phases of the membrane. The final section gives a discussion of the implications of the results presented in this chapter on mixed matrix membrane technology.

6.2. SORPTION OF GASES IN POLYMERS AND SIEVES

It was necessary to measure sorption of the neat polymer and pure sieve for later comparison with mixed matrix membranes. Equilibrium sorption of O₂, N₂, CO₂, and CH₄ in Ultem[®] (Figure 6.1) and Matrimid[®] (Figure 6.2) were measured. Oxygen sorption was not measured above 10 atm for safety reasons. Experimental equilibrium sorption curves are similar to those reported in the literature (see references in Table 6.1). The experimental and literature regressed dual-mode parameters in Table 6.1 do not match well in some cases, because small curvatures or few data make an accurate fit

difficult. The regressed parameters are quite dependent on the initial guesses used for the curve fit, but the resulting sets of parameters fit the data well. Kinetic sorption in these materials is best characterized in terms of diffusion coefficients. However, in many cases, sorption occurred too quickly to accurately determine the diffusion coefficients, because the samples were too thin. Instead, dual-mode parameters from the literature are reported in Table 6.1. These parameters are required for the multicomponent modeling work discussed in the following chapter.

Table 6.1: Selected data for gas sorption in selected polymers at 35°C. Literature values (where available) are given in parentheses.

Polymer	Gas	k_D cm ³ STP/cm ³ /atm	b 1/atm	C'_H cm ³ STP/cm ³	D_D cm ² /s ×10 ⁸	D_H/D_D	Source
Ultem [®]	O ₂	0.185	0.082	2.04			
	N ₂	0.050 (0.063)	0.034 (0.045)	5.20 (4.15)	(0.572)	(0.042)	[1, 2]
	CO ₂	1.04 (0.758)	0.355 (0.366)	17.3 (25.02)	(1.14)	(0.063)	[1, 2]
	CH ₄	0.17 (0.207)	0.21 (0.136)	5.83 (7.31)	(0.113)	(0.073)	[1, 2]
Matrimid [®]	O ₂	0.245	0.054	5.31			
	N ₂	0.120	0.087	3.94			
	CO ₂	1.44	0.367	25.5			
	CH ₄	0.136	0.105	14.3			

[†]Diffusion coefficient at 30°C

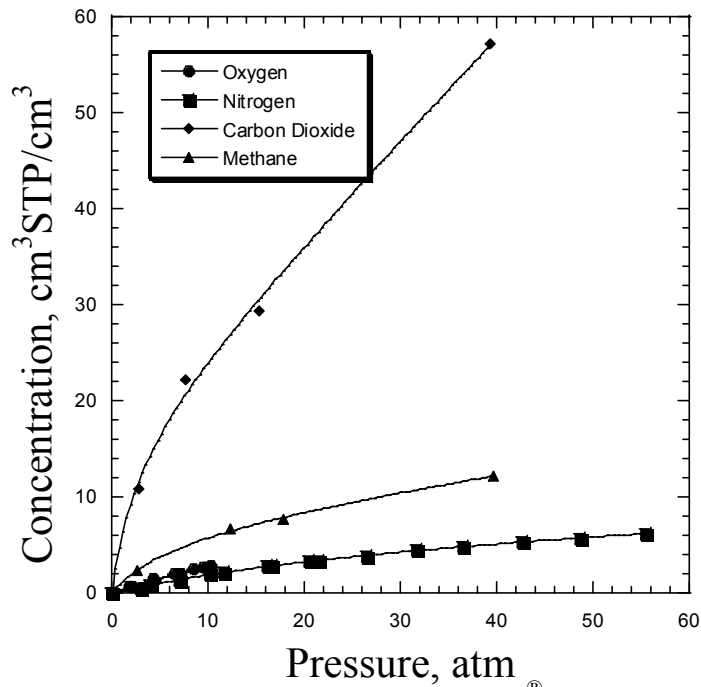


Figure 6.1: Sorption of O₂, N₂, CO₂, and CH₄ in Ultem[®] at 35°C. Lines are fitted to the dual-mode equation (Eq 2.6) with parameters given in Table 6.1.

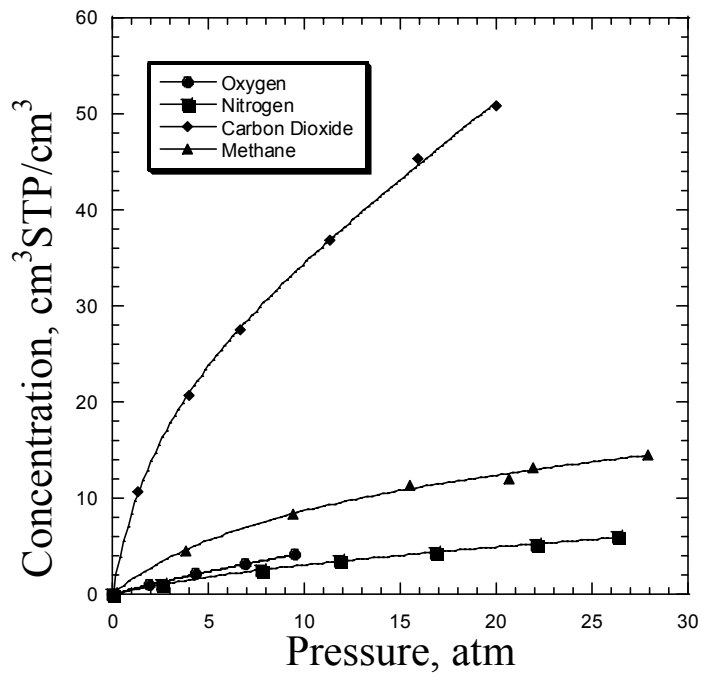


Figure 6.2: Sorption of O₂, N₂, CO₂, and CH₄ in Matrimid[®] at 35°C. Lines are fitted to the dual-mode equation (Eq 2.6) with parameters given in Table 6.1.

Measuring “normal” sorption in the zeolites was not as straightforward. First, a method to contain the zeolites in the sorption cell had to be devised, as discussed in section 3.4.2.2. Second, samples from the same batch of zeolite 4A initially appeared to give different sorption characteristics, even after the same activation treatment. Eventually, this was attributed to contamination in zeolite processing equipment. This insight explains why poorer transport properties than expected were observed for many of the membranes in Chapter 5. Equilibrium sorption in zeolite 4A and HSSZ-13 for selected gases is shown in Figure 6.3 and Figure 6.4, respectively. The parameters for fitting these curves are given in Table 6.2.

Table 6.2: Langmuir coefficients for regressions of penetrant sorption in zeolite 4A and HSSZ-13. Literature values (where available) are given in parentheses. Temperature is 35°C except where noted.

Sieve	Penetrant	b 1/atm	C'_H cm ³ STP/cm ³	Source
Zeolite 4A	Water, 25°C	(2510)	(537)	[3]
	Oxygen	0.041	98.8	
	Nitrogen	0.076	116	
	Carbon Dioxide	4.27	158	
	Methane	0.164	107	
HSSZ-13	Water	47.0	432	
	n-Butane	615	66.7	
	Oxygen	0.056	89.4	
	Nitrogen	0.144	50.5	
	Carbon Dioxide	0.607	194	
	Methane	0.340	77.6	

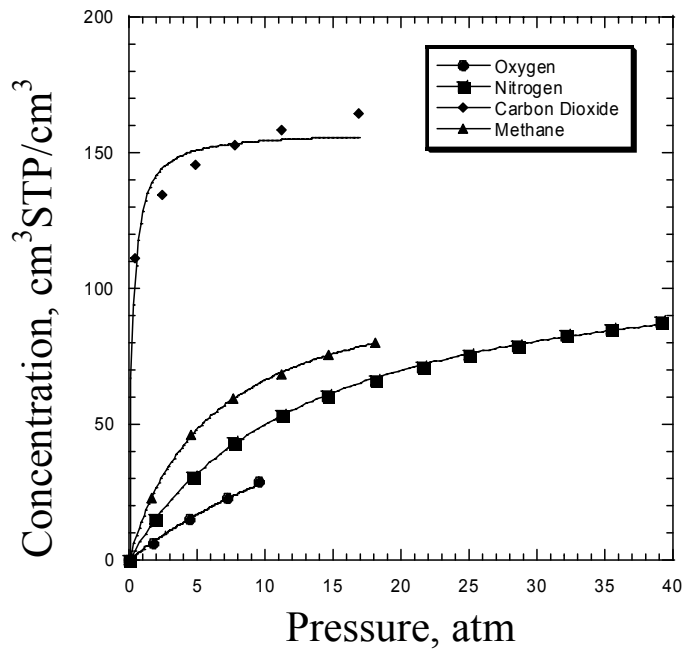


Figure 6.3: Sorption of O_2 , N_2 , CO_2 , and CH_4 in zeolite 4A at $35^\circ C$. Lines are fitted to the Langmuir equation (Eq 2.6 with $k_D = 0$) with parameters given in Table 6.2.

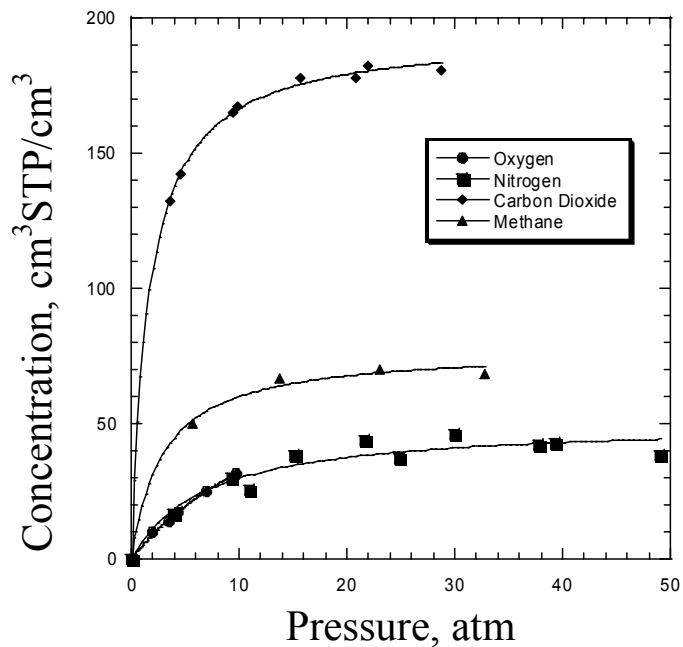


Figure 6.4: Sorption of O_2 , N_2 , CO_2 , and CH_4 in HSSZ-13 at $35^\circ C$. Lines are fitted to the Langmuir equation (Eq 2.6 with $k_D = 0$) with parameters given in Table 6.2.

Equilibrium sorption for water and n-butane was also needed for the modeling work presented in the next chapter. These data are shown in Figure 6.5. A log scale is used on the pressure axis so the low pressure data can be distinguished. When plotted in this manner, a sigmoidal shape is typically observed instead of the classical Langmuir shape. Water sorption at 25°C was measured by Breck [3]. Water sorption in HSSZ-13 was measured using the gravimetric sorption technique in section 3.4.2.1. Data from two samples are shown to indicate the reproducibility of these measurements. Finally, n-butane sorption data in HSSZ-13 was provided by ChevronTexaco ETC. Increasing the temperature by 15°C causes an order of magnitude increase in the saturation pressure of n-butane. There is a dramatic difference between gas sorption (O₂, N₂, CO₂, CH₄) and sorption of the condensable components (i.e. water and n-butane). Sorption is governed by the condensability of the penetrant and the affinity of the penetrant for the sieve. This explains why the order of Langmuir *affinity* constants (*b* in Table 6.2) in both zeolites is H₂O > CO₂ > CH₄ > N₂ > O₂, with the more hydrophobic HSSZ-13 having a higher affinity for n-butane than water. The order of affinity constants in zeolites for nitrogen and oxygen is *opposite* that for polymers. Although nitrogen is less condensable, it has a higher affinity for the sieve than oxygen because its higher quadrupole moment allows for increased intermolecular interactions with the zeolite.

It is more difficult to determine the diffusion coefficient for gases in zeolites for two reasons: (i) in some cases, sorption occurs so quickly that it is impossible to accurately fit the data as a function of the diffusion coefficient and (ii) all the zeolite samples are polydisperse making it difficult to determine the characteristic length-scale. Nonetheless, for slower gases in zeolite 4A, such as oxygen, it is possible to determine *relative* diffusion coefficients in the same large (~5 μm) sample activated or processed under different conditions. This has provided important insights into the nature of zeolites and the effects of various solvents and processing conditions.

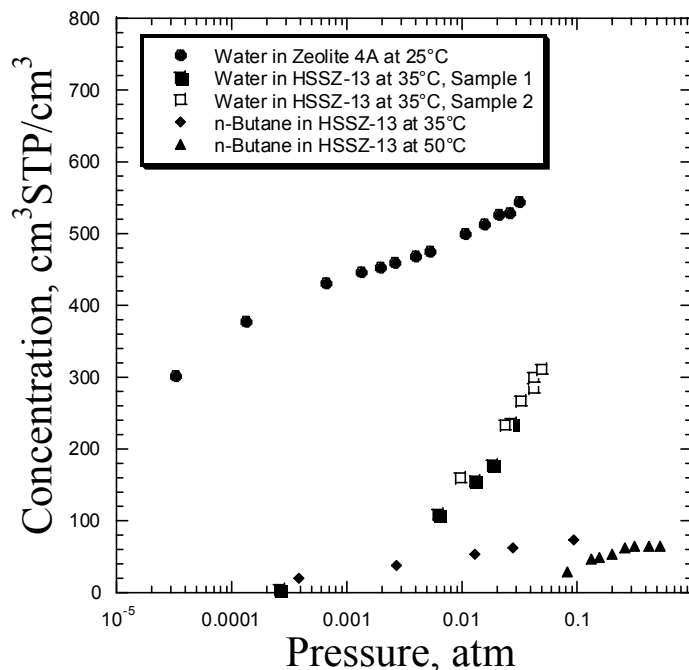


Figure 6.5: Sorption of water and n-butane in zeolite 4A and HSSZ-13 at selected temperatures. Note that the pressure is given in a log scale.

It is necessary to “activate” zeolite 4A after exposure to ambient humidity or extended storage because of its extreme hydrophilicity. Several activation methods were considered for zeolite 4A: (a) drying in an oven under a nitrogen purge at 300°C for 12 hr, (b) calcination (in air) in the TGA at 590°C for 30 min, (c) drying in the TGA under a nitrogen purge at 280°C for 12 hr, and (d) drying in a new vacuum oven at ~285°C overnight. Activation in a well-used general-purpose vacuum oven resulted in poor sorption characteristics as discussed in section 6.3.3. Equilibrium oxygen sorption for samples from a single batch activated using the four protocols above is shown in Figure 6.6a. Figure 6.6a also shows sorption in a submicron zeolite 4A sample (activated at 250°C vacuum) to illustrate that particle size does not affect equilibrium sorption. Each sample exhibits the same sorption within the error expected from these measurements. Thus, all of the data were fit to a single “standard” sorption curve for oxygen in zeolite 4A to use as a baseline for future samples.

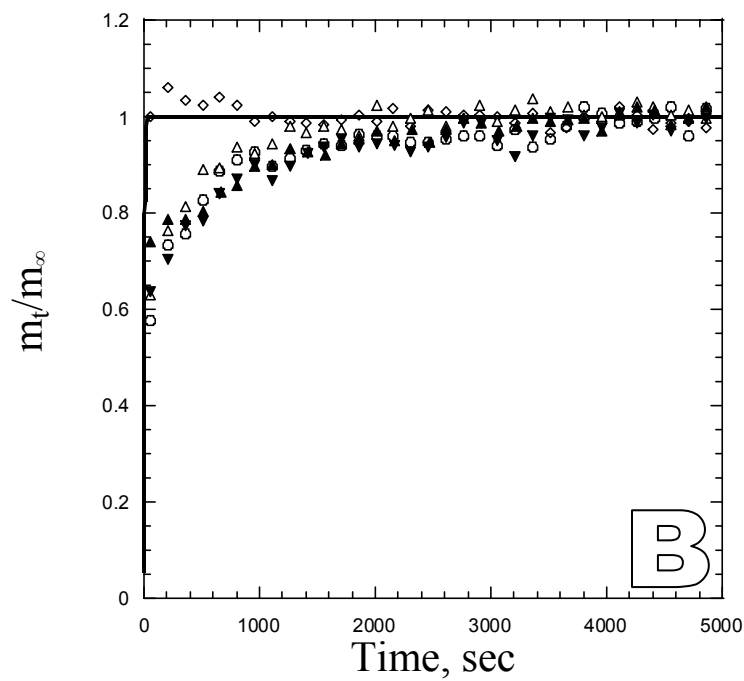
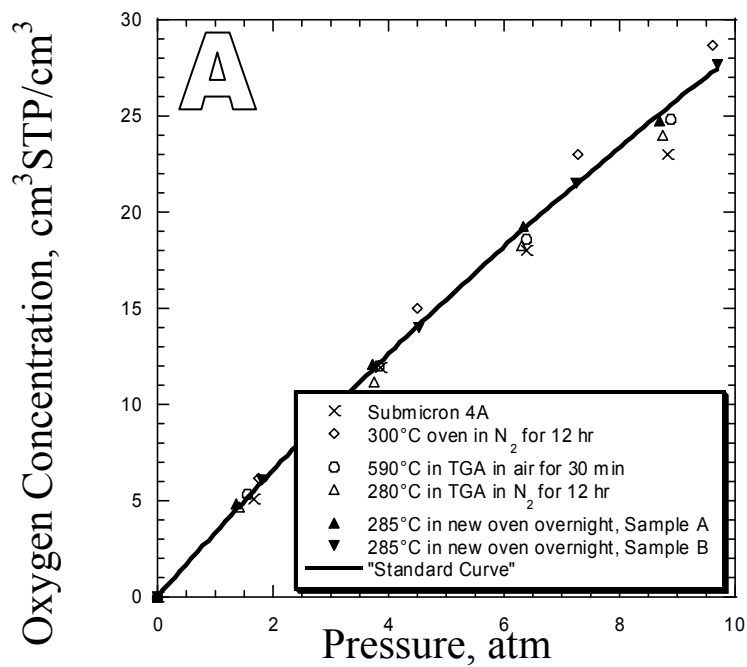


Figure 6.6: (a) Equilibrium and (b) transient oxygen sorption in zeolite 4A from a single batch activated using different activation protocols and for a submicron zeolite 4A batch (equilibrium only). The transient curves are taken from the lowest equilibration pressure, ~2 atm. The “standard curve” is explained in the text.

Kinetic sorption for the $\sim 5 \mu\text{m}$ samples is shown in Figure 6.6b. The submicron sample has faster kinetics because of its smaller size, so it is meaningless to compare this sample with the others. The remaining $5 \mu\text{m}$ samples in Figure 6.6b all reach equilibrium within ~ 2000 seconds. Most exhibit a tail (i.e. $\sim 2/3$ of sorption occurs in the first minute but remaining sorption is slower). The sample activated in 300°C flowing nitrogen does not exhibit such a tail. In Figure 6.6b, the transient curve is for the lowest equilibration pressure, which varied between 1.3 and 2 atm for the five samples. Drying method “d”, activation in the vacuum oven overnight at 285°C , was repeated, and the results for both are similar as shown in Figure 6.6b. Using the diffusion coefficient of oxygen reported in the literature, $4.0 \times 10^{-9} \text{ cm}^2/\text{s}$ [4], a “standard curve” for the theoretical sorption kinetics was also plotted in Figure 6.6b, assuming spherical particles of $5 \mu\text{m}$ radius. The zeolites are actually cubic, but assuming a spherical shape makes little difference because the aspect ratio of both is unity. This diffusion coefficient suggests extremely fast sorption, and only the sample dried in 300°C flowing nitrogen approaches this rate. This theoretical curve will be used later as a baseline for future samples.

The diffusion coefficient in the zeolite may be a function of the sorbed concentration, or equivalently, the equilibration pressure. In order to check this, a plot (Figure 6.7) of the relative uptake, (m_t/m_∞) , was prepared for one of the zeolite 4A samples (“ 285°C in new oven overnight, sample A” of Figure 6.6). Plotting the relative uptake normalizes the transient sorption curve. If the data for each equilibration pressure fall on the same curve, then the diffusion coefficient must be identical for each. This is the case in Figure 6.7, indicating that the diffusion coefficient of oxygen is not a function of sorbed concentration in zeolite 4A over the pressure-range studied. Oxygen does not approach capacity saturation in zeolite 4A, where the diffusion coefficient is expected to display the greatest deviation from linearity, even at the highest pressure studied. Thus, it is not surprising that the diffusion coefficient was not a function of sorbed concentration.

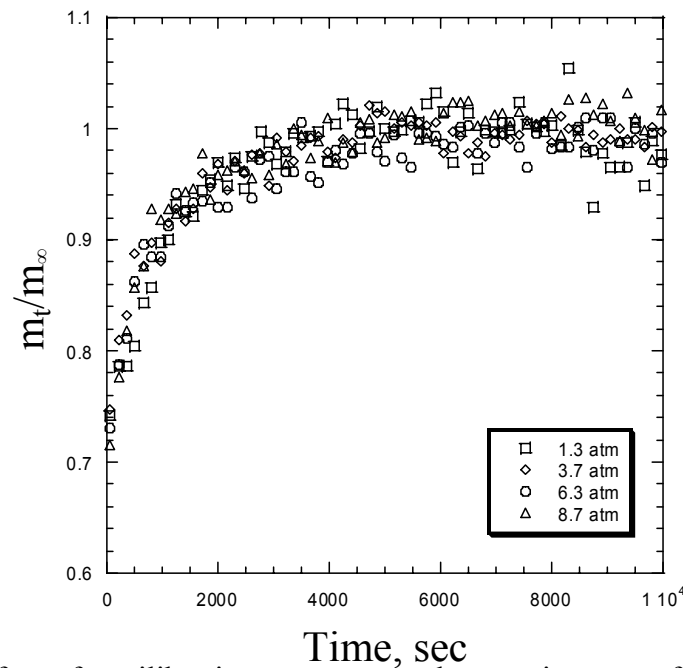


Figure 6.7: Effect of equilibration pressure on the sorption rate of oxygen into zeolite 4A. Data corresponds to the sample: “285°C in new oven overnight, Sample A” from Figure 6.6a.

Another potential complication with the transient sorption data is the polydispersity of the zeolite 4A sample. The assumed 5 μm particle radius for the theoretical transient curve in Figure 6.6b probably represents a conservative estimate, since most of the particles have side lengths of less than 5 μm when observed with the SEM. Nevertheless, some larger particles are observed. The effect of larger particles was modeled by repeating the calculation for the theoretical uptake rate assuming that 10% of the mass of the zeolite 4A was comprised of particles with a 20 μm diameter. This corresponds to approximately 0.7% of the total number if the remaining particles are all of 5 μm diameter. The calculated transient sorption curves for these two “particle size distributions” are contrasted in Figure 6.8. The larger particles cause tailing. Most of the sorption still occurs within the first few seconds because of the large fraction of smaller particles. Thus, the particle size distribution probably makes little difference in the observed half times, although it may cause the “tailing” phenomenon.

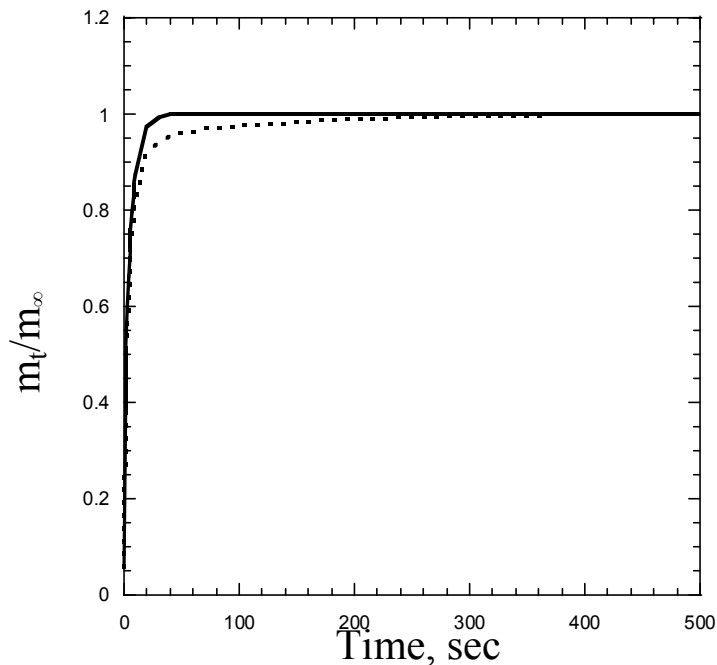


Figure 6.8: Effect of particle size distribution on the sorption rate of oxygen in zeolite 4A. The solid line is for uniform particles of 5 μm diameter. The dashed line assumes that 10% of the mass is comprised of 20 μm diameter particles.

6.3. EFFECT OF PROCESSING CONDITIONS AND SOLVENTS ON POLYMERS, SIEVES, AND MIXED MATRIX MEMBRANES

Mixed matrix membranes, and zeolites in particular, have proven very sensitive to the particular processing conditions and equipment used in their preparation. Here, several challenges that caused poor transport properties in polymers, zeolites, and/or mixed matrix membranes are discussed. Completely removing solvents from zeolites has proven especially difficult. Zeolite 4A was exposed to various solvents and processing conditions to verify they did not affect zeolite sorption. The maximum drying temperature for silanated zeolites is limited by the stability of the silane (see section 5.2.1.3). Once the silanated zeolites have been incorporated into mixed matrix membranes, the stability of the polymer – sieve interface must also be considered when selecting drying conditions. If a mixed matrix membrane is treated above the stability limit of the silane but the transport properties are still favorable, the stability of the silane is irrelevant. Nonetheless, 250°C was used as an upper limit for practical drying.

6.3.1. Effect of Residual NMP in Ultem[®] on the Transport Properties of Mixed Matrix Membranes

Low levels of residual solvents can reduce the mobility of polymer chains. This *antiplasticization* effect typically results in permeabilities lower than the solvent-free polymer with slightly increased selectivities. In the presence of higher solvent concentrations, the membrane may plasticize as the polymer chains loosen, allowing faster permeation and lower selectivities. One of the drying procedures (75°C overnight, followed by 180°C-200°C for four nights) used for Ultem[®]-based membranes was found to leave ~2-3 percent residual NMP in neat Ultem[®]. This was determined using the method in the following paragraph. As shown below in Figure 6.9, this gives lower permeability and higher selectivity expected of a polymer exhibiting antiplasticization. After additional drying at 300°C to remove residual solvent, the transport properties of solvent-free Ultem[®] were recovered.

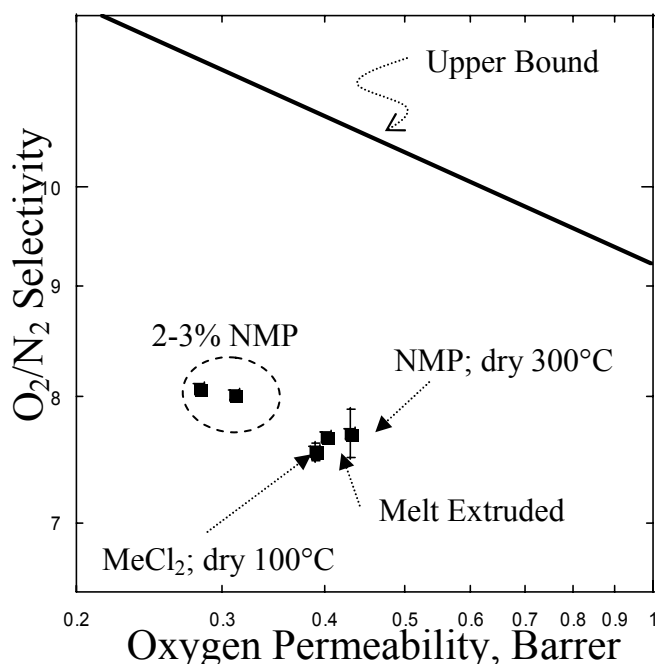


Figure 6.9: Effect of residual NMP on the transport properties of neat Ultem[®]. The casting solvent and drying conditions are given for well-dried Ultem[®] membranes.

Thermogravimetry with IR analysis of the evolved gas was performed to measure residual solvent in several membranes. Samples were heated at 20K/min in nitrogen. Heating one sample (#192) at 2K/min gave a similar weight loss curve. Results are compared in Figure 6.10. In neat Ultem[®], the weight loss initiates at about 200°C and is nearly finished at 250°C. Conversely, in the mixed matrix samples, most of the weight loss occurs below 200°C, indicating the presence of adsorbed water. Nevertheless, some weight loss does occur in the mixed matrix samples above 200°C (see #192), which can be attributed to NMP. Thus, this drying procedure appears to incompletely remove NMP. Residual NMP would not completely devastate mixed matrix membrane performance, but it could lead to apparently increased selectivities that may wrongly be attributed to the presence of the sieves. Thus, subsequent membranes prepared using NMP were dried at 250°C or higher overnight before testing to avoid this complication.

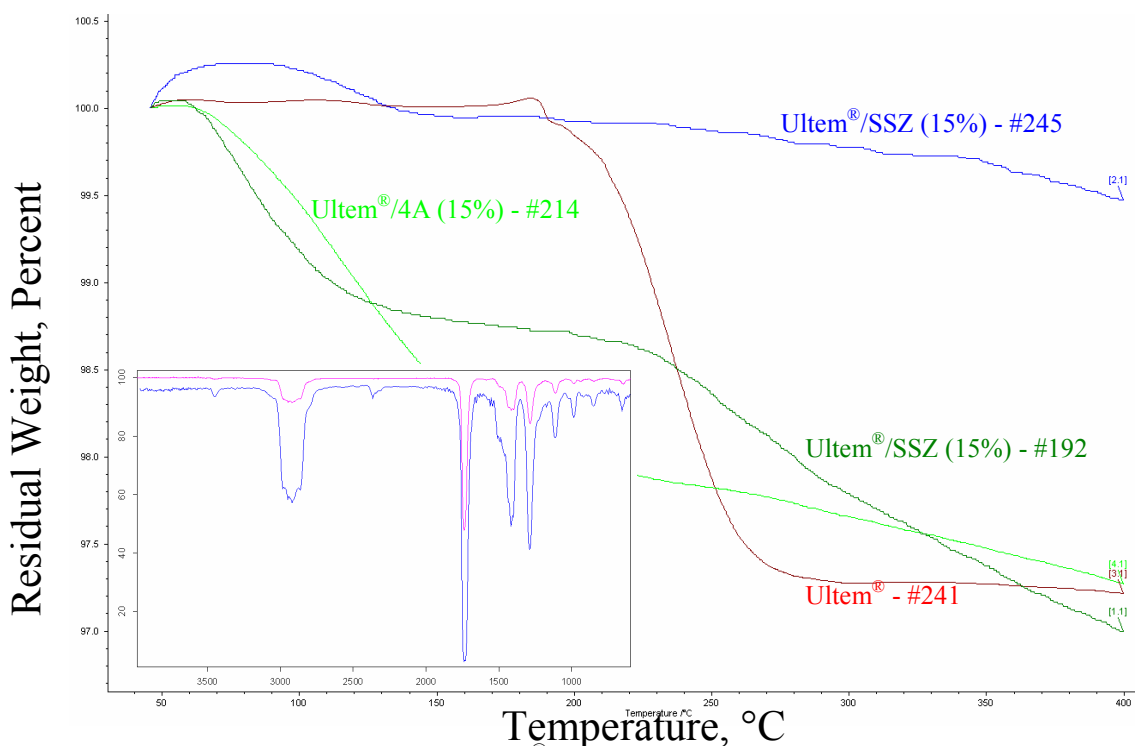


Figure 6.10: TGA curves for neat Ultem[®] and selected mixed matrix membranes cast on glass at 100°C and removed before vitrification, followed by drying at 75°C × 1 night and 180°C × 4 nights. The inset shows the FTIR spectrum of the evolved gas (top, pink) from Ultem[®] - #241 at 240°C and a standard spectrum of NMP (bottom, blue).

6.3.2. Effect of Residual Solvents in Sieves on the Transport Properties of Mixed Matrix Membranes

Work by Qin demonstrated residual solvent (methanol) the zeolites in PVAc – zeolite 4A mixed matrix membranes impermeable [5]. Dichloromethane was subsequently used in that work, but no drying conditions for the membranes were given. Qin diagnosed the clogged behavior of these membranes using permeation measurements, rather than directly using sorption. The sorption rate of solvents into zeolite 4A was therefore checked as part of this work using the pressure decay sorption apparatus. Activated zeolites were dispersed in dichloromethane via sonication for 60 seconds followed by recovery using a vacuum filtration setup with PTFE filter paper. These zeolites were then dried in the TGA under nitrogen at 100°C for 12 hr. Both equilibrium and kinetic sorption are below that expected for a freshly activated sample, as shown in Figure 6.11. The half time for this sample (open diamonds in Figure 6.11) is ~8000 seconds, compared to less than 60 seconds for a freshly activated sample. Subsequently, these same zeolites were dried for an additional 12 hr at 250°C. Although the equilibrium sorption in this sample is essentially normal and the half time decreased to ~1000 seconds, the half time is still higher than for freshly activated samples. Thus, even dichloromethane, which was previously assumed too large to enter the zeolites, affects zeolite sorption. Such effects would also be expected to influence mixed matrix permeation, as discussed in the final section. A similar decrease in the sorption rate is observed for zeolites sonicated in toluene and dried at 250°C in nitrogen for 12 hours. Clearly, more rigorous drying conditions are necessary, but the silane stability limits the maximum drying temperature, so additional drying time is the main variable that should be altered.

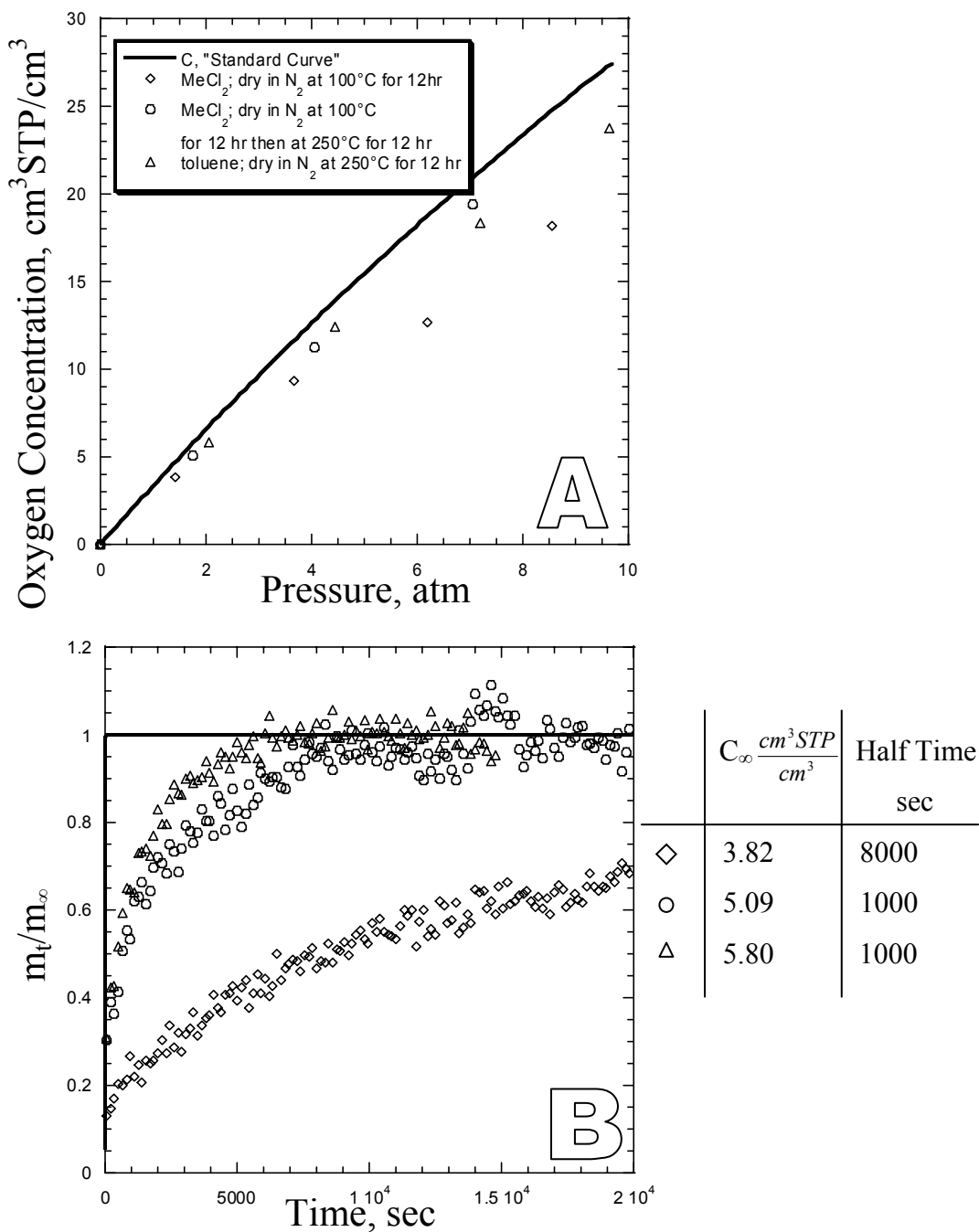


Figure 6.11: (a) Equilibrium and (b) transient oxygen sorption in activated zeolite 4A sonicated in various solvents followed by reactivation under different conditions. The transient curves are from the lowest equilibration pressure, ~2 atm. The maximum uptake and half time at that equilibration pressure for each transient sample are given.

The effect of silanation solvents on sorption in zeolites was also studied. Although Mahajan had used 95:5 ethanol : water successfully as a silanation solvent [6], a 95:5 isopropanol : water mixture was initially used here to match collaborators. Isopropanol was thought too large to enter the zeolite. Zeolites silanated in IPA : water with γ -aminopropyldimethylethoxysilane exhibit reduced equilibrium sorption and slower sorption rates. As shown in Figure 6.12, drying of the silanated zeolites at either 200°C (diamonds) or 250°C (circles) for 12 hr in nitrogen is insufficient to recover normal sorption. However, the half time for the 200°C dried sample is longer than for the 250°C dried sample, indicating the favorable effect of increased temperature. Recall, however, that weight loss still occurs in a sample that was sonicated in IPA : water, even after drying at 250°C for 8 hr in nitrogen (Figure 5.5). Other experiments, discussed in section 7.2.3, had already proven that water could be removed at 250°C, so the poor sorption must be a result of the silane or the isopropanol. Thus, processing steps in the silanation procedure were performed on freshly activated zeolites, *without the silane*. In the figure legend, this is indicated as a “sonicated” sample. This sample (open triangles) was then dried at 200°C for 12 hr in nitrogen. Sorption is significantly lower and slower than for freshly activated zeolites. Following these experiments, the effect of sonication was checked by using the 50 W sonicator (labeled “Sonicated; small”) instead of the 1000 W sonicator. Although both sonicators operate at the same frequency, it was thought the 1000 W sonicator may have damaged the surface of the sieves. The half time for sorption is significantly shorter than for the sample sonicated with the larger sonicator, but it is still too long compared to freshly activated samples. Finally, in order to check whether the reduction in equilibrium and kinetic sorption is reversible, the sample sonicated in IPA : water with the large sonicator (open triangles in Figure 6.12) was calcined for 30 min in air. Notably, the half time became too short to accurately measure with this technique, as for freshly activated samples, but the sample exhibits a significant tail. This may be caused by an external mass transfer resistance in this sample due to agglomeration, but this needs to be verified.

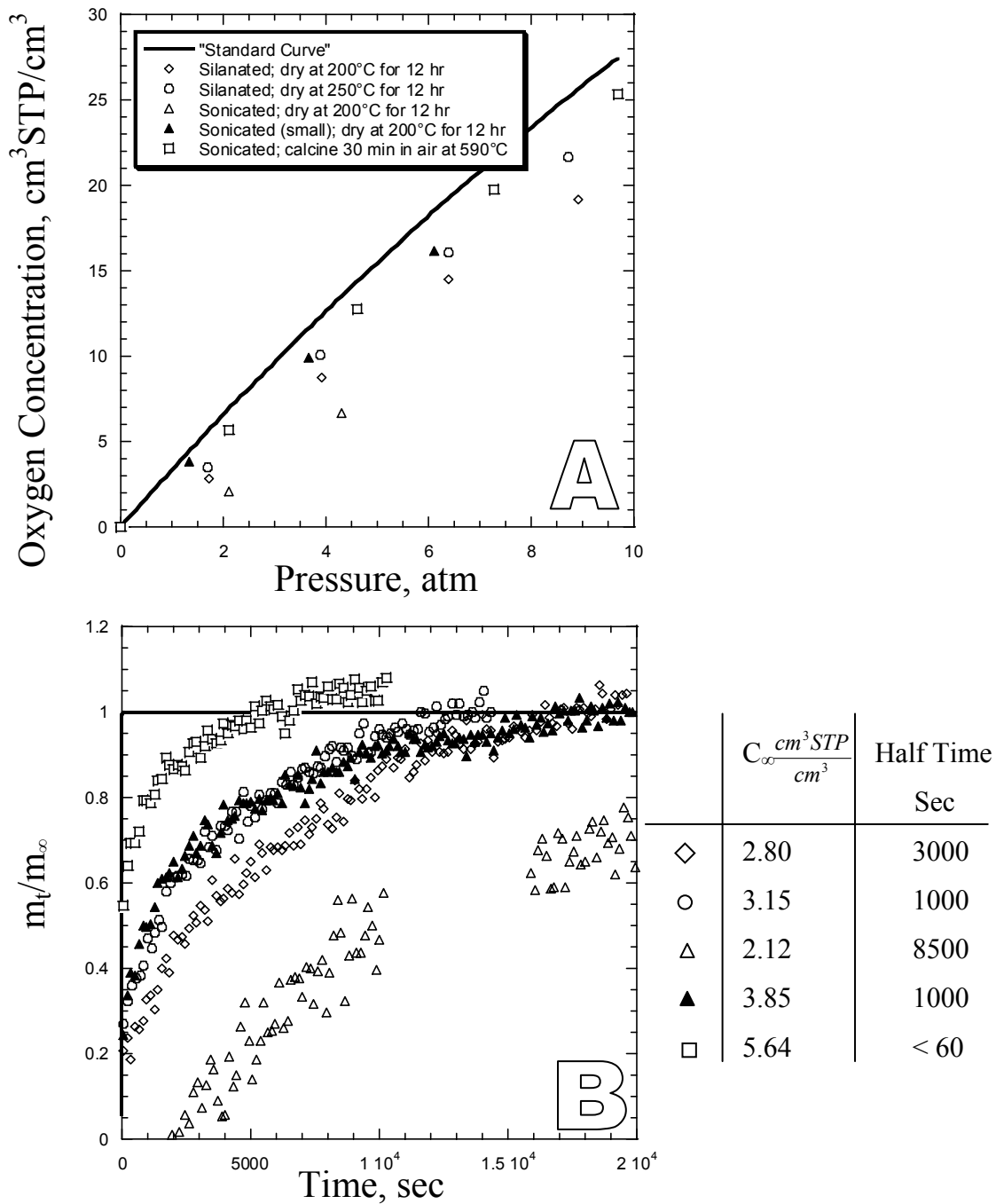


Figure 6.12: (a) Equilibrium and (b) transient oxygen sorption in activated zeolite 4A exposed to various conditions present during silanation in 95:5 isopropanol : water. The transient curves are from the lowest equilibration pressure, ~ 2 atm. The maximum uptake and half time at that equilibration pressure for each transient sample are given.

After the poor results with 95:5 IPA : water, 95:5 ethanol : water was reconsidered as a silanation solvent. The equilibrium and kinetic sorption for several samples exposed to various treatments in EtOH : water are shown in Figure 6.13. The silanation procedure was again performed on freshly activated zeolites, without adding the silane, followed by drying at 200°C for 12 hr in the TGA under nitrogen (open circles). This was insufficient to recover a normal sorption rate; however, this sample was stopped after 30000 seconds, before equilibrium was reached, so the half time is unknown. The TGA curve for this sample was still decreasing after the initial 12 hr of drying at 200°C, indicating residual solvent was present. Thus, this same sample was dried for an additional 12 hr at 250°C in nitrogen (open triangles). This significantly improved the sorption rate. In fact, about 90% of the sorption occurs before the first data point is taken, similar to the freshly activated samples shown in Figure 6.6. This indicates that EtOH can be removed from the zeolites using reasonable drying conditions, making 95:5 EtOH : water an acceptable silanation solvent. Notably, the sample sonicated in IPA : water and dried at 250° for 12 hr in nitrogen does not exhibit such rapid sorption indicating IPA is more difficult to remove from the zeolite. Unfortunately, this discovery was made after the bulk of the work done in Chapter 5 was completed.

Next, zeolites were silanated with γ -aminopropyltrimethylethoxysilane in EtOH : water, followed by drying at 250°C for 12 hr in nitrogen (open diamonds in Figure 6.13). This sample sorbs too slowly (half time \sim 1500 seconds) and equilibrium sorption is lower than the “standard curve” for unsilanated zeolite 4A. This slight reduction in equilibrium sorption in silanated zeolites was also noted for both zeolite 4A and HSSZ-13 silanated in IPA : water. One final possibility was checked: the silanation was performed without any sonication. Ramesh et al report that sonication causes condensation of silanol groups between silica particles and consequent agglomerate formation [7], and this could lead to slower kinetics. Instead of sonication, the silanation mixture was stirred at \sim 1600 rpm with periodic reversal to keep the zeolites suspended (filled triangles). In the absence of any sonication or heating, the intended

reaction between the zeolite and the silane may not have occurred. Nevertheless, this provides a method to test the effect of just the silane on the zeolite. However, the half time, ~1000 seconds, is not much better than the sample silanated with the sonicator. Therefore, the *silane must have caused the observed reductions in the sorption of zeolites silanated in ethanol.* As discussed in section 6.5.1, such reductions in the zeolite sorption rate may significantly reduce permeation through mixed matrix membranes. Longer drying times or drying under vacuum instead of in nitrogen should be considered to better activate the silanated zeolites.

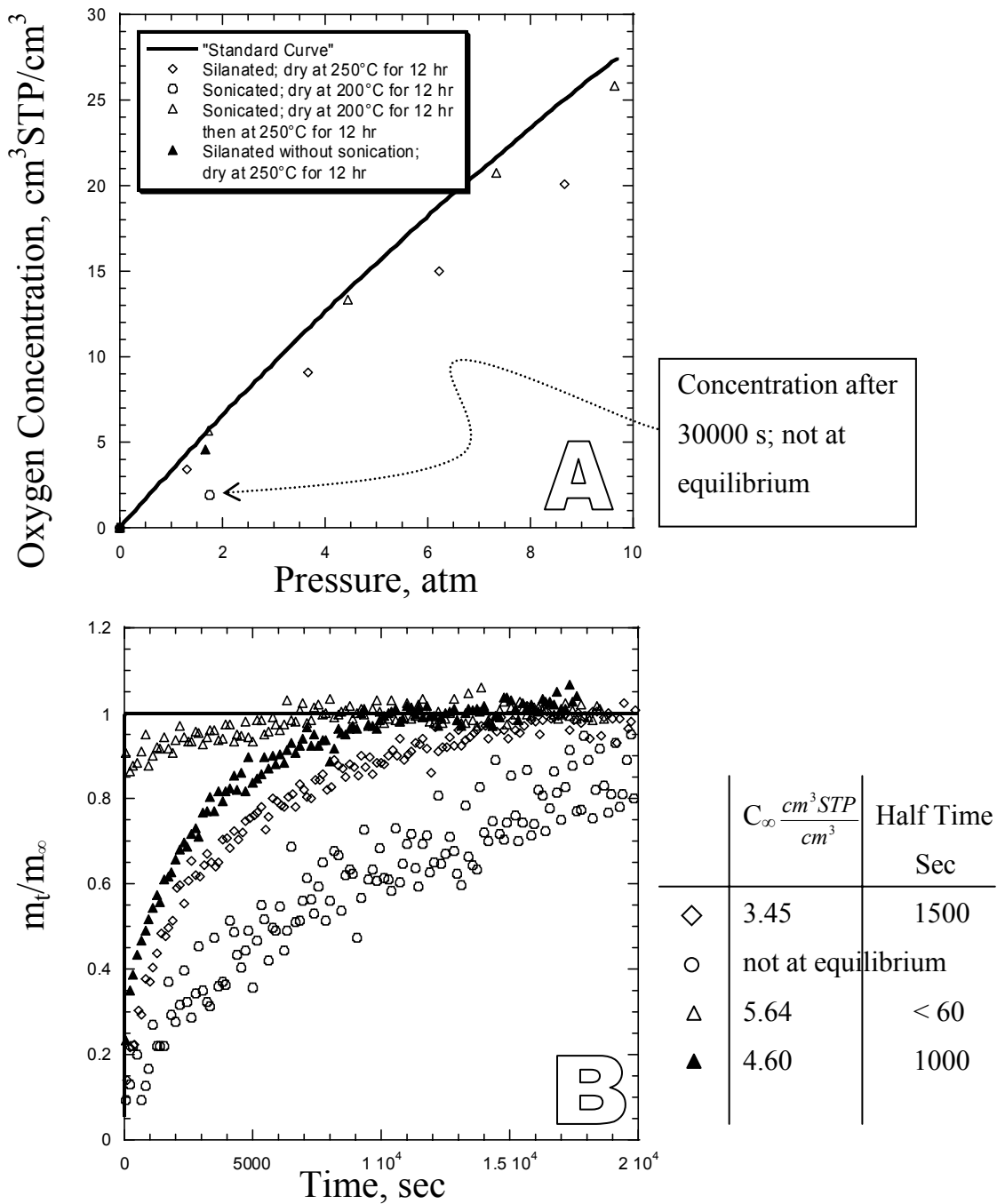
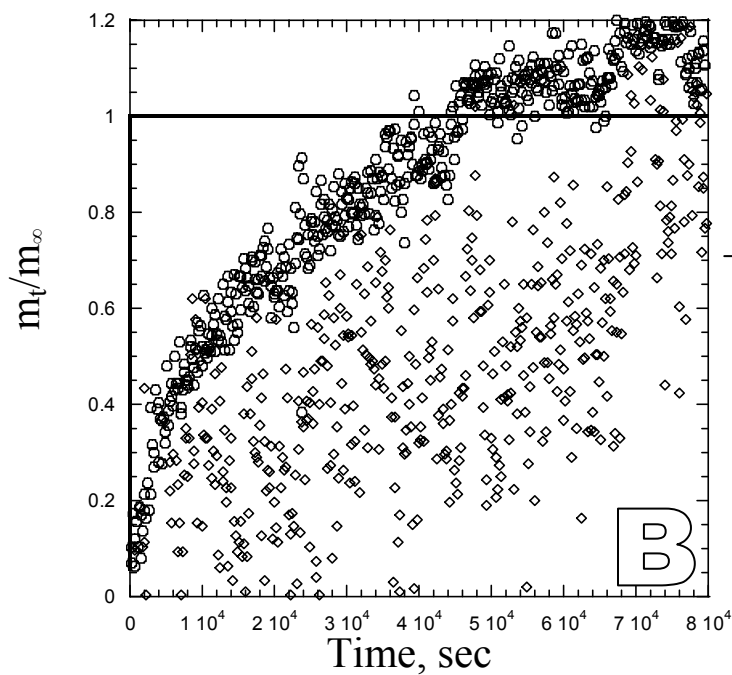
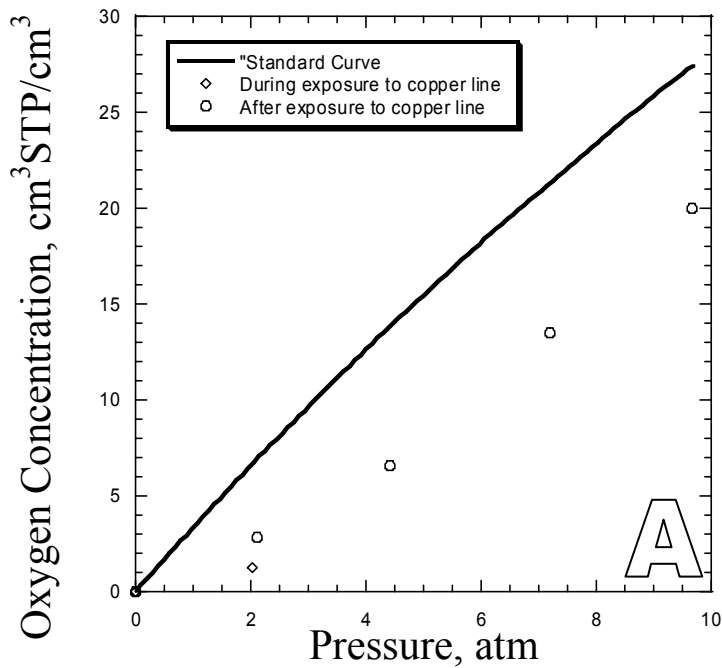


Figure 6.13: (a) Equilibrium and (b) transient oxygen sorption in activated zeolite 4A exposed to various conditions present during silanation in 95:5 ethanol : water. The transient curves are from the lowest equilibration pressure, ~ 2 atm. The maximum uptake and half time at that equilibration pressure for each transient sample are given.

6.3.3. Effect of Processing Equipment on Zeolite Sorption

Many instances were encountered of “processing equipment” affecting transport of gases through zeolites. Clearly, it is unlikely the equipment itself has physically altered the zeolites, but it is possible that the zeolites have sorbed a contaminant present in the processing equipment. In hindsight, this observation is not totally surprising given the highly receptive nature of zeolites toward sorbates.

Initially, the pressure decay sorption apparatus was connected through copper tubing that was built into the infrastructure of the labs when the research group relocated to Georgia Tech. After several preliminary *sorption* experiments, it became clear these lines, or something within them, were affecting the zeolites. *Permeation* through membranes in systems connected through similar copper lines also indicated that the zeolite 4A was impermeable or nearly so. The sample tested in the presence of the copper line (open diamonds in Figure 6.14) shows very low sorption, even after 2.5 days. Only the first 80000 seconds are shown. Recall that normal equilibrium should be reached in less than 1 minute. The significant scatter in the open diamonds Figure 6.14b is due to the very low equilibrium sorption (m_∞). After that, the sample was removed from the sorption system with the copper line and placed in one with a standard rubber vacuum tube (open circles). Although the amount of gas taken up by the sample improved, the sorption rate is still quite depressed compared to freshly activated samples. This indicates that the sample must have absorbed something from the copper line. These same systems (with copper lines) were used to measure sorption in polymer samples, and no deviations from the expected sorption were observed. This illustrates the extreme sensitivity of zeolites to certain contaminants.

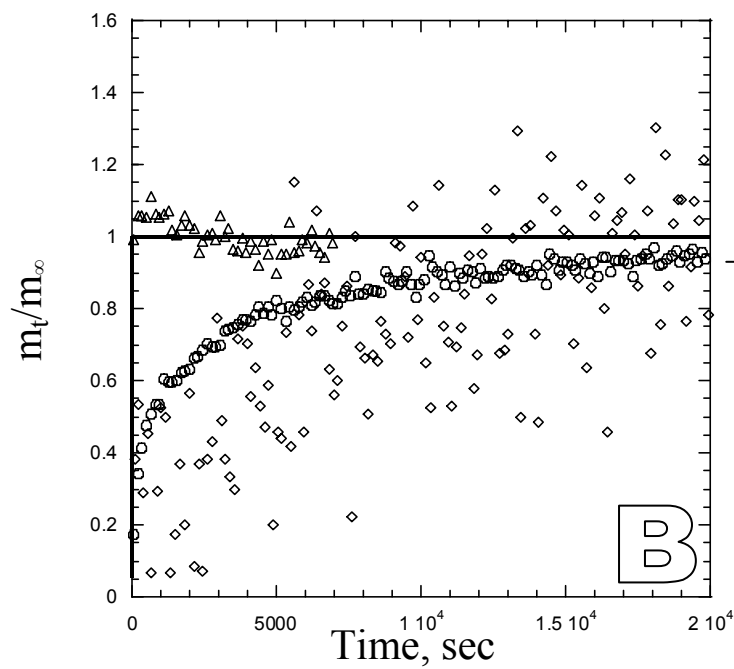
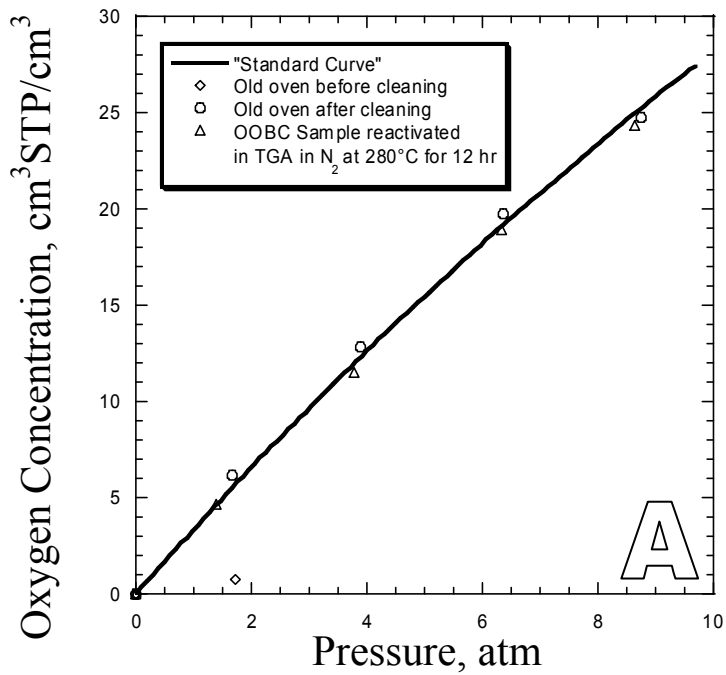


	$C_\infty \frac{cm^3 STP}{cm^3}$	Half Time Sec
◇	1.28	--
○	2.81	8000

Figure 6.14: (a) Equilibrium and (b) transient oxygen sorption in activated zeolite 4A during and after exposure to a “sweated” copper vacuum line. The transient curves are from the lowest equilibration pressure, ~2 atm. The maximum uptake and half time at that equilibration pressure for each transient sample are given.

Several methods were attempted to identify the contaminant(s) in the copper lines including: (i) direct identification of isolated compounds using attenuated total reflectance infrared spectroscopy (ATR-IR), (ii) sorption of potential vapors from the contaminant(s) in lines onto zeolite 4A followed by examination using ATR-IR, (iii) sorption of vapors onto zeolite 4A followed by heating in the TGA with IR analysis of the evolved gas, and (iv) analysis of vapors in the lines using a gas chromatograph with thermal conductivity and flame ionization detectors. A hydrocarbon-based grease and a perfluorinated polyether were isolated using method (i) and a third contaminant could be inferred based on smell alone. It is unclear how either of the identified components could directly affect sorption in the zeolites, especially given their very low vapor pressures (< 0.001 torr). However, it is possible that one or both components are slowly degrading to release a product that causes reduced sorption in the zeolites. Used vacuum lines were coated with a black residue, which provides support for this suggestion. Nevertheless, removing the lines from the system allowed normal sorption to be attained, so this was not deemed worth further study.

Various vacuum ovens also were able to activate zeolite 4A to seemingly different degrees. After all-purpose use by the research group, vacuum ovens become contaminated with a brown residue on the glass door and on inside surfaces of the ovens. Figure 6.15 shows sorption in samples exposed to one such oven before and after cleaning. Cleaning was performed by heating the oven to its maximum temperature, $\sim 285^{\circ}\text{C}$, in air, followed by a wipe-down with acetone, followed by heating again to the maximum temperature in air. Before cleaning, the oven exhibited very low sorption (open diamonds). After cleaning (open circles), the sorption rate increased significantly (half time ~ 750 seconds), although it still did not attain the rate of freshly activated samples in Figure 6.6. Finally, the sample tested before cleaning was reactivated in the TGA at 280°C for 12 hr under nitrogen (open triangles) and the sorption rate recovered. This indicates there must have been some small molecule sorbed on the inside of the oven or in its sealing gasket that enters the zeolite.



	$C_\infty \frac{cm^3 STP}{cm^3}$	Half Time Sec
◇	0.75	--
○	6.13	750
△	4.66	< 60

Figure 6.15: (a) Equilibrium and (b) transient oxygen sorption in activated zeolite 4A exposed to a vacuum oven, before and after cleaning. The transient curves are from the lowest equilibration pressure, ~2 atm. The maximum uptake and half time at that equilibration pressure for each transient sample are given.

After discovery of the poor sorption characteristics in the cleaned oven, a new oven was purchased for dedicated use drying zeolites. This new oven was used for the “new oven” samples in Figure 6.6. Collaborators at ChevronTexaco, report that it is nearly impossible to completely clean a contaminated oven for use with zeolites [8].

6.4. SORPTION OF GASES IN MIXED MATRIX MEMBRANES

Sorption of gases in mixed matrix membranes was studied to give additional information about their transport properties. It was hypothesized that sorption in mixed matrix membranes, S_{MM} , should be additive, within acceptable error limits:

$$S_{MM} = \phi_{POLY}S_{POLY} + \phi_{SIEVE}S_{SIEVE} \quad (6.1)$$

where ϕ is the appropriate volume fraction. This was valid for some mixed matrix membranes. Figure 6.16 compares oxygen and nitrogen sorption for 14.6 vol% HSSZ-13 in Ultem[®] with sorption calculated using Eq 6.1 and the Langmuir coefficients given in Table 6.1 and Table 6.2. Sorption is additive within the error of the measurements.

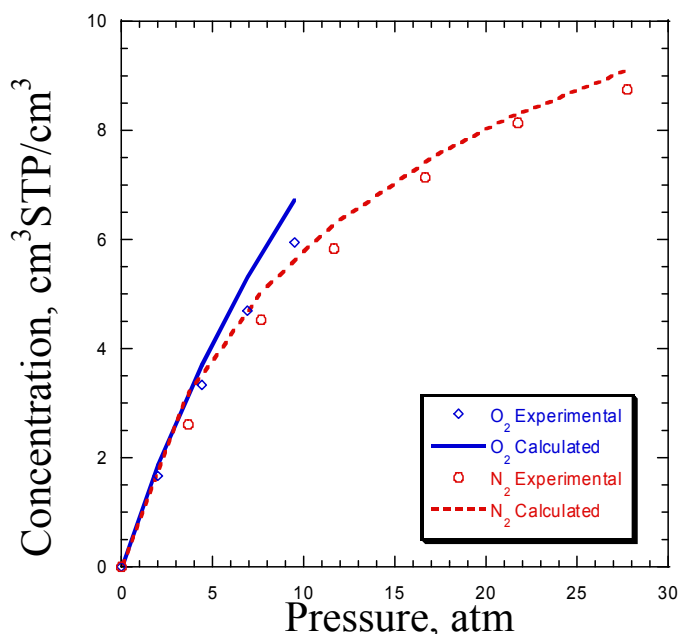


Figure 6.16: Demonstration of additivity of sorption in mixed matrix membranes. O₂ and N₂ sorption in 14.6 vol% HSSZ-13 dispersed in Ultem[®].

Because the sieves sorb much more gas than the same weight of polymer, approximately half the total sorption in a ~15 vol% sieve membrane can be attributed to the zeolite. This makes it easy to diagnose inactive zeolites even after they are incorporated into mixed matrix membranes. The polymer matrix may afford some protection from contaminants, since it is expected to slow their diffusion into the membrane, but if given enough time contaminants will still enter the zeolites. Of course, for the solvents used to process the dopes, the polymer matrix can afford no protection to the zeolites. A lesson learned in this work was the significant effects of immeasurable levels of residual components introduced during processing.

A common problem with membranes containing zeolite 4A is that they sorb significantly less gas than the additive assumption, indicating a problem with sorption in the zeolite. Figure 6.17 for 13.7 vol% zeolite 4A dispersed in Ultem[®] cast from dichloromethane is one such example. Oxygen sorption in this membrane is lower than the additive assumption, even after drying at 250°C for 12 hr. If the zeolite phase of the membrane does not sorb enough gas, the membrane will be expected to exhibit lower permeability. Moreover, the reduced diffusion coefficients observed in pure zeolites may cause an even more adverse effect on mixed matrix membrane permeability. The membrane dried at 100°C had permeabilities consistent with sieve-in-a-cage morphology; while the 250°C dried membrane appeared to suffer from impermeable zeolites. The zeolites may not be completely impermeable, but even a 50% reduction in the permeability of the zeolite can have a dramatic effect on the transport properties of the resulting mixed matrix membranes. This situation is modeled in section 6.5.1. The sorption rate of oxygen into the membrane is also significantly slower than expected, especially at higher equilibration pressures. This membrane was prepared without a silane coupling agent, eliminating the complications associated with silanation. However, it was also cast from dichloromethane, which according to Figure 6.11 could slow sorption into the zeolites enough to cause reduced transport properties.

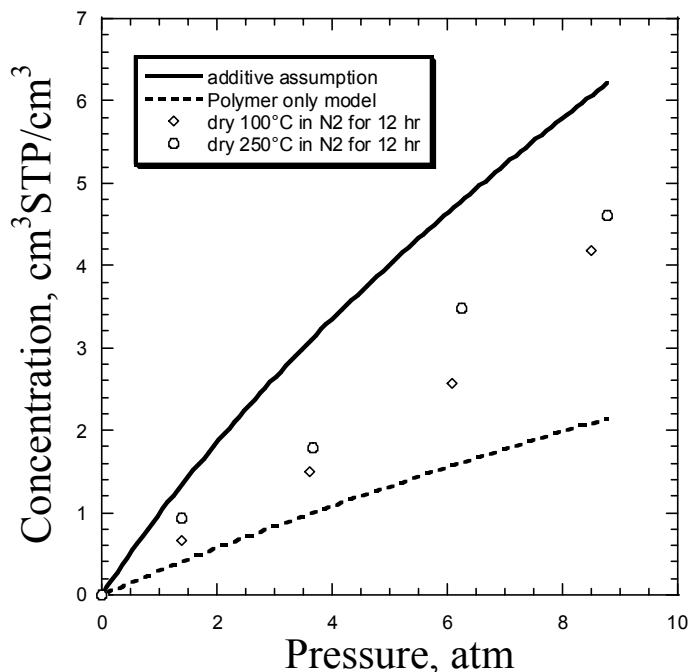


Figure 6.17: Oxygen sorption in 13.7 vol% zeolite 4A dispersed in Ultem[®] cast from dichloromethane dried under different conditions.

6.5. DISCUSSION

The implications of the data in the forgoing sections are discussed next. Mixed matrix membranes containing zeolites exhibiting reduced sorption or slow kinetics will have poorer transport properties than those prepared with fully sorbing zeolites. This is shown in the first subsection. The second subsection discusses methods to recover full sorption in poorly sorbing zeolites, including one that did not lead to improved sorption. In the final subsection, the behavior of zeolites toward contaminants is contrasted with carbon molecular sieves.

6.5.1. Effect of Poorly Sorbing Zeolites on the Transport Properties of Mixed Matrix Membranes

Permeation through mixed matrix membranes with poorly (slow kinetics or reduced equilibrium) sorbing zeolites is now considered. Recall that permeability is the product of the sorption and diffusion coefficients of a gas in a material. “Normal” or freshly

activated zeolite 4A has an oxygen permeability of 0.77 Barrer, a sorption coefficient of $1.44 \text{ cm}^3 \text{ STP/cm}^3$, and a diffusion coefficient of $4 \times 10^{-9} \text{ cm}^2/\text{s}$ at 35°C [9]. Figure 6.18 shows the theoretical kinetic sorption for zeolite 4A as the diffusion coefficient decreases. The solid black line is for a zeolite exhibiting a normal diffusion coefficient. If the diffusion coefficient is lowered by an order of magnitude, the half time is still estimated to be less than 100 seconds, which is difficult to detect with pressure decay sorption. A drop by two orders of magnitude or more is required before a significant reduction in the sorption kinetics is discernable. Even a three orders of magnitude decrease in the diffusion coefficient yields a half time of only 2000 seconds. The half times for oxygen sorption in samples exposed to solvents (Figure 6.11), various silanation conditions (Figure 6.12 and Figure 6.13), or processing equipment (Figure 6.14 and Figure 6.15) are in many cases 1000 seconds or more. This translates to a diffusion coefficient between 4×10^{-11} and $4 \times 10^{-12} \text{ cm}^2/\text{s}$. It is important to differentiate between these zeolites that exhibit increased half times and those that exhibit tailing (e.g. many of the freshly activated samples in Figure 6.6, the calcined sample in Figure 6.12, and the sample sonicated in ethanol and dried at 250°C for 12 hr in nitrogen in Figure 6.13.) The tailing may be caused by an external mass transfer resistance in some of the samples because of agglomeration, as mentioned previously. It may be easier to prevent agglomeration in mixed matrix membranes because the zeolites can be primed, so tailing may be an artifact of the measurement technique. Conversely, extended half times are believed to reflect effects occurring within individual zeolite crystals.

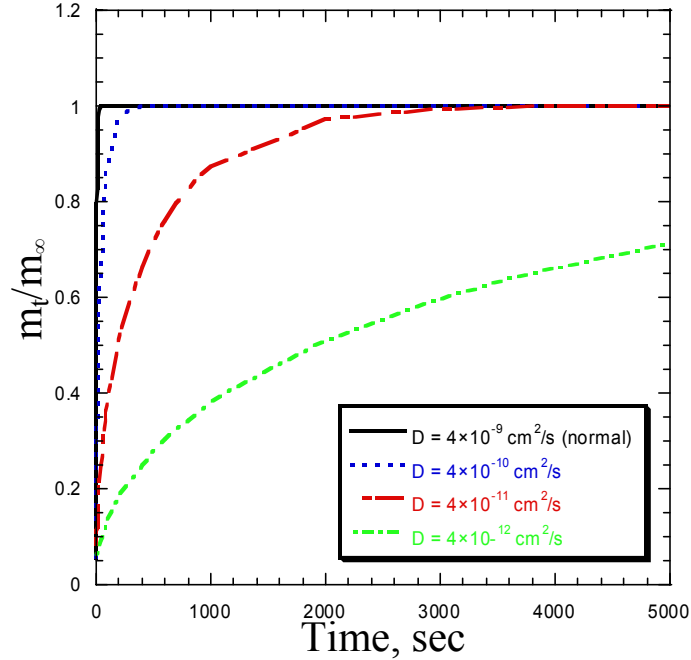


Figure 6.18: Effect of diffusion coefficient on the theoretical uptake over maximum uptake of oxygen in zeolite 4A.

Figure 6.19 shows the transport properties calculated for 15 vol% zeolite 4A dispersed in Ultem[®] for different values of the oxygen diffusion coefficient through the zeolite calculated using the Maxwell model. The sorption coefficient is assumed constant, and the permeability is calculated using Eq 2.1. The selectivity is also assumed unchanged in this simple calculation. A 50% drop in the diffusion coefficient of gas through zeolite 4A gives a small decrease in the expected performance of the mixed matrix membrane, to a selectivity of about 9.0. An order of magnitude drop in the diffusion coefficient of zeolite 4A makes the permeability of the mixed matrix membrane lower than Ultem[®] with only a modest increase in selectivity. Increasingly smaller diffusion coefficients make the zeolites in the mixed matrix membrane look impermeable to oxygen. The half times found for many of the zeolites samples in this chapter are consistent with diffusion coefficients that are decreased by two or more orders of magnitude. Figure 6.19 does not consider the effect of reduced equilibrium sorption,

which accompanied the slow kinetics in many of the zeolite 4A samples tested. A reduction in equilibrium sorption would further decrease the permeability of the zeolite.

Many of the Ultem[®] – zeolite 4A membranes prepared for this work have permeabilities lower than neat Ultem[®] with little or no improvement in selectivity (see Figure 5.14). The results presented in this chapter indicate this could be caused by exposure to contaminated processing equipment, silanation of the zeolites, or incomplete drying of the membranes after exposure to certain solvents. The next section discusses potential methods to recover full sorption in zeolites exhibiting poor sorption characteristics. These methods could then potentially be applied to mixed matrix membranes.

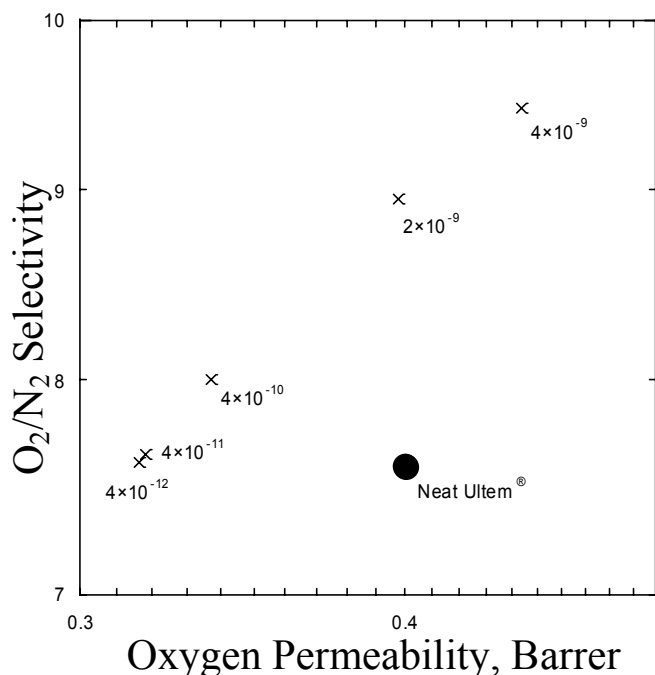


Figure 6.19: Effect of decreased diffusion coefficients (cm^2/s) on the theoretical transport properties of 15 vol% zeolite 4A dispersed in Ultem[®].

Although this chapter concentrated on zeolite 4A, similar effects on the transport properties are also possible in other zeolites. For example, although many of the membranes prepared with HSSZ-13 exhibit improved transport properties, most do not exhibit improvements as large as expected. This could potentially be attributed to the

sorption-related effects discussed in this chapter. Unfortunately, it is difficult to measure these effects in HSSZ-13. Most of the HSSZ-13 available for this work was submicron. These effects were sometimes difficult to measure with 5 μm zeolite 4A particles because sorption was too fast, and they could not be observed with submicron zeolite 4A. HSSZ-13 is estimated to have permeability an order of magnitude higher than zeolite 4A, but it exhibits similar sorption (compare Figure 6.3 and Figure 6.4). Thus, HSSZ-13 must have a diffusion coefficient an order of magnitude faster than zeolite 4A, making it more difficult to characterize reduced sorption rates in HSSZ-13 than in zeolite 4A.

6.5.2. Recovery of Sorption in Poorly Sorbing Zeolites

Work presented in this chapter demonstrated normal sorption could be recovered in some poorly sorbing samples by reactivating the zeolites with one of the activation methods used in Figure 6.6. Recovery in such cases is probably due to the presence of a small molecule that is easily removed (such as water or ethanol). In other zeolite samples (e.g. after exposure to isopropanol, dichloromethane, or toluene), sorption recovers after drying at 250°C, but not completely. A method for reactivating zeolites after silanation is also needed, since the silane was found to reduce sorption rates.

Clearly, more rigorous drying conditions should be considered. Extended drying times are possible with no damage to mixed matrix membrane morphology. A temperature of 250°C was used as a somewhat arbitrary upper drying temperature for silanated zeolites because the silane was observed to degrade *in air* at about 250°C. Drying is typically done in nitrogen or under vacuum, where the silane was observed to be more stable (see section 5.2.1.3), so higher temperatures may be possible. Nonetheless, evidence was presented that mixed matrix membranes are damaged when dried at 300°C (see section 5.4.3), so there is a ceiling on the drying temperature of mixed matrix membranes.

One reactivation method that was tried in several cases without success was to displace potential contaminant(s) with a strongly sorbing gas, such as CO₂. In such cases, CO₂ typically sorbed quickly into the samples at equilibrium or near equilibrium concentrations. The sample was then evacuated to try to extract potential contaminants, followed by retesting with oxygen. Unfortunately, the oxygen sorption did not improve after the CO₂ extraction.

6.5.3. Comparison of Contaminant Effects on Zeolites and Carbon Molecular Sieves

Although freshly prepared zeolite 4A-based membranes can be severely affected by levels of contamination that are too low to be identified, no problems were observed with carbon molecular sieve (CMS)-based mixed matrix membranes. Once a polymer-CMS combination has been identified that gives mixed matrix membranes with enhanced transport properties (e.g. Ultem[®] – CMS), they can generally be prepared with a reasonable success rate [10]. Furthermore, an Ultem[®] – CMS membrane had no change in properties (with 10/90 CO₂/CH₄) after three years in storage. Ambient storage included hot (90°F+) and cold (~45°F) conditions as well as high and low humidities. Thus, CMS-based membranes may represent a more robust mixed matrix platform. A similar experiment performed with an Ultem[®] – zeolite 4A (35 vol%) membrane prepared by Mahajan [11] indicated that the zeolites were impermeable. The following chapter will show that water absorbed from the atmosphere during storage could have caused the zeolites to become impermeable, even though they were not impermeable when originally tested by Mahajan.

6.6. REFERENCES

1. Barbari, T.A.; W.J. Koros; and D.R. Paul. J. Polym. Sci., Part B: Polym. Phys. 1988, 26, 709-27.
2. Barbari, T.A.; W.J. Koros; and D.R. Paul. J. Polym. Sci., Part B: Polym. Phys. 1988, 26, 729-44.

3. Breck, D.W., Zeolite molecular sieves: Structure, chemistry, and use. 1974, Malabar, FL: Robert E. Krieger Publishing Co, Inc.
4. Ruthven, D.M. and R.I. Derrah. J. Chem. Soc., Faraday Trans. 1 1975, 71, 2031-44.
5. Qin, J., Explorations of forming and characterizing mixed matrix gas separation membranes. Department of Chemical Engineering, University of Texas at Austin. 1999.
6. Mahajan, R., Formation, characterization and modeling of mixed matrix membrane materials. Department of Chemical Engineering, University of Texas at Austin. 2000.
7. Ramesh, S.; Y. Koltypin; and A. Gedanken. J. Matl. Res. 1997, 12, 3271-3277.
8. Miller, S., Personal communication. 2004.
9. Zimmerman, C.M., Advanced gas separation membrane materials: Hyper rigid polymers and molecular sieve-polymer mixed matrixes, Department of Chemical Engineering, University of Texas at Austin. 1998.
10. Vu, D.Q.; W.J. Koros; and S.J. Miller. J. Membr. Sci. 2003, 211, 311-334.
11. Mahajan, R. and W.J. Koros. Polym. Engr. and Sci. 2002, 42, 1432-1441.

Chapter 7. EFFECT OF FEED CONTAMINANTS ON MIXED MATRIX MEMBRANE TRANSPORT PROPERTIES

7.1. OVERVIEW

Many factors contribute to overall membrane performance. The permeability and selectivity can change appreciably with operating conditions. Temperature and pressure are obviously important, but one important factor that is sometimes overlooked is the effect of minor components in the feed gas. Condensable linear and aromatic hydrocarbons present in trace quantities in natural gas streams can have detrimental effects on many polymers [1], as can water [2]. Water is present in both air and natural gas feeds, which are among the applications mixed matrix membranes are particularly well suited to. Perhaps more important, especially based on the observations in Chapter 6, is the potential effect of contaminants on the sieving phases. Gas sorption in zeolite 4A is reduced by preadsorption of water, a strongly adsorbed molecule, at 1-2% relative humidity [3]. It is reasonable to hypothesize that water will dramatically affect the transport properties of mixed matrix membranes containing zeolite 4A. Funke et al report a 60% decrease in the nitrogen permeance of α -alumina supported silicalite membranes for humidified nitrogen feeds [4], even though silicalite is typically considered hydrophobic. Unfortunately, they do not report the humidity of the feed and they state their silicalite may have been contaminated by aluminum from the α -alumina support, making it more hydrophilic.

It is obviously not possible to measure the effect of every conceivable contaminant on mixed matrix membrane performance. The approach taken here is to couple careful studies using representative contaminants with detailed modeling. Provided the modeling results agree reasonably with experimental data, it should be possible to use the model to predict the behavior of other contaminants. The model is also useful for determining the effect of the contaminants on the zeolite phase.

The next section discusses the effect of water on the oxygen permeability of zeolite 4A filled membranes. Many simplifying assumptions can be made to the detailed modeling presented in section 2.2.3. The effects of a “typical” organic component, n-butane, on mixed matrix membrane transport properties are discussed in section 7.3 using the entire model as described in 2.2.3. Finally, section 7.4 discusses the implications of the results and modeling presented in this chapter.

7.2. EFFECT OF WATER ON MIXED MATRIX MEMBRANES

The effect of water, as a model hydrophilic contaminant, was determined on mixed matrix membranes. Both zeolite 4A and HSSZ-13 were dispersed in PVAc using dichloromethane as the solvent. The first step was to determine the effect of water on oxygen permeability through the neat polymer. This was done using the Oxtran apparatus discussed in section 3.4.1.4. Zeolite 4A filled PVAc was prepared and tested at 25°C by Trinh Vo at the University of Texas at Austin. This temperature was chosen to facilitate comparison of the results with zeolite 4A water sorption from the literature. Oxygen permeabilities for HSSZ-13 filled PVAc membranes were determined at 35°C. This slightly higher temperature was used so the results could be compared with other permeation data for HSSZ-13 filled PVAc.

7.2.1. Permeation through Pure Poly(vinyl acetate) with Humidified Oxygen

Knowledge of the permeability of pure poly(vinyl acetate) with humidified oxygen is needed to interpret mixed matrix performance. It was necessary to measure these data at both 25°C and 35°C to “subtract out” the behavior of the polymer phase in mixed matrix membranes to ascertain the behavior of the sieves. Figure 7.1 shows the oxygen permeability of PVAc as a function of relative humidity at both temperatures. Data for relative humidities greater than about 65% were not obtained at 35°C, because the water vapor partial pressures at these relative humidities exceed saturation at room temperature. Thus, it was difficult to prevent condensation in the system.

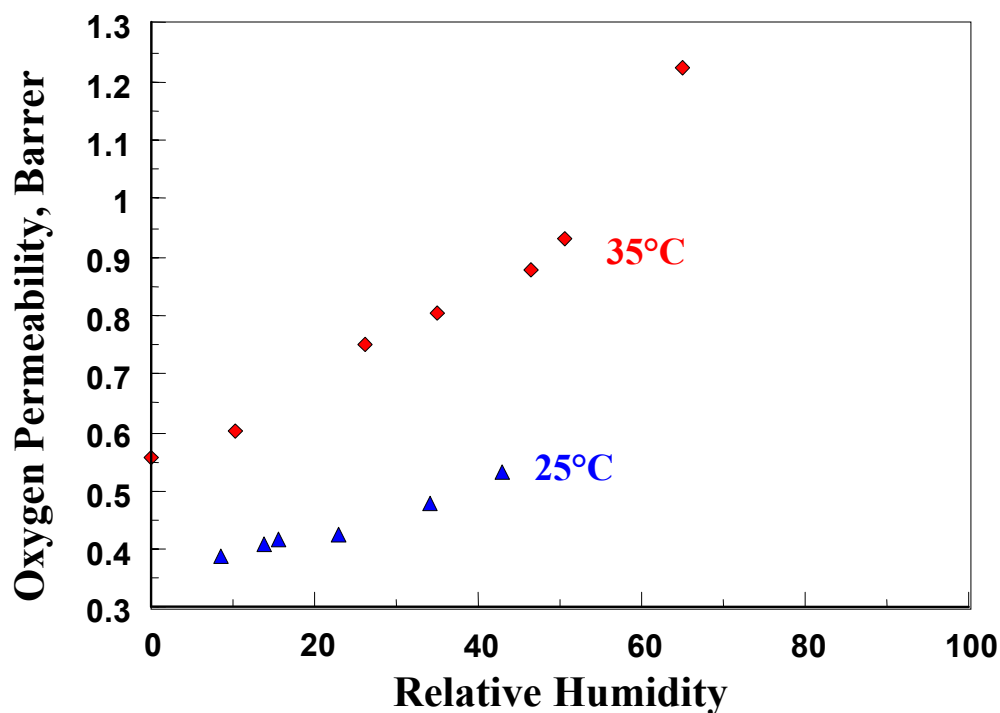


Figure 7.1: Oxygen permeability of neat poly(vinyl acetate) at 25°C and 35°C as a function of relative humidity.

The upswing in oxygen permeability measured at 35°C between 50% and 65% relative humidity can potentially be explained as swelling of the matrix by sorbed water [5], with concomitant increase in the oxygen permeability. This trend is also exhibited by the mixed matrix membranes discussed later. Although 25°C is below the T_g , swelling by water leads to a lower T_g in PVAc [6, 7], so it is likely the polymer phase is rubbery under most of the experimental conditions studied. Increased chain mobility caused by swelling allows for an increase in the diffusion coefficients of penetrants in many polymers, and the same is probably true of PVAc. Typically, such swelling causes plasticization and disproportionate increases in the diffusivities of the slower penetrants, such as nitrogen, so that the overall effect is decreased selectivity [8]. In more rigid glassy polymers, the major effect of water is the occupation of sorption sites usually available to other penetrants [2, 9], so the decline in selectivity may be less severe. Pye et al found only a small depression in the H_2/CH_4 selectivity [10] in several glassy polymers exposed to water. This provides another reason to use a glassy matrix.

7.2.2. Permeation through Mixed Matrix Membranes with Humidified Oxygen

Three cases for the potential behavior of zeolites within the membrane are considered. One case assumes the zeolites are unaffected by water (open model), and a second assumes the zeolites are rendered completely impermeable to oxygen by water (closed model). A third case (equilibrium adsorption model) assumes the zeolite permeability is proportional to the fraction of its Langmuir capacity unoccupied by water in the absence of competitive sorption, $x_W/x_{W,MAX}$. Mathematically:

$$P_{Sieve} = P_0 \left(1 - \frac{x_W}{x_{W,MAX}} \right) = P_0 \left(1 - \frac{b_W p_W}{1 + b_W p_W} \right) \quad (7.1)$$

where P_0 is the permeability of the sieve in a dehumidified feed, b is the Langmuir affinity constant, p is the partial pressure, and the subscript W is for water.

Table 7.1 shows the oxygen permeability at selected feed relative humidities for zeolite 4A filled PVAc, including model predictions for each of the three cases discussed above. Note that the experimental data and modeling predictions for 1.5% relative humidity are for a membrane with 40 vol% zeolite 4A, while the data at 10% relative humidity correspond to a 25 vol% zeolite 4A membrane. A higher zeolite loading was used at the lower humidity to increase the sensitivity of the zeolite to the measurement. The results clearly show that the “equilibrium adsorption” model most closely parallels the experimental observations for zeolite 4A. Because of the high affinity of water for zeolite 4A, the “equilibrium adsorption” model is similar to the “closed” model. This is consistent with Figure 6.5, which shows that zeolite 4A is nearly saturated with water at ~ 0.003 atm, corresponding to about 10% relative humidity. Based on these observations, it can be inferred that oxygen permeation in zeolite 4A is reduced by water adsorbed on the pore walls of the zeolite, even at very low relative humidities.

Table 7.1: Summary of experimental data and model predictions for zeolite 4A filled PVAc membranes tested at 25°C.

Relative Humidity	Zeolite Fraction	Permeability, Barrer			
		Open Model	Equilibrium Adsorption Model	Closed Model	Experimental Data
1.5%	40%	0.50	0.30	0.20	0.33
10%	25%	0.51	0.30	0.27	0.28

Essentially, water exhibits a selective surface flow effect (see section 2.1.4); it is strongly adsorbing within the zeolite and limiting oxygen sorption. The Oxtran apparatus can only measure oxygen permeability, so the O₂/N₂ selectivity could not be determined. Because the zeolite permeability is reduced, a lower selectivity is expected, since a higher fraction of oxygen normally permeates through the zeolites. This makes the use of zeolite 4A as a mixed matrix sieving phase less attractive in practical applications. A potential solution is to coat the membranes with a very hydrophobic layer such as Teflon[®] AF, which excludes water from membranes [11], but this adds complexity. Alternatively, a pretreatment stage can be added to remove water from the feed stream before it contacts membranes containing zeolite 4A. This pretreatment could potentially be accomplished with another membrane. However, both alternatives will increase the cost of a membrane separation system, and the sorption experiments discussed in the next subsection demonstrate that zeolite 4A is extremely sensitive to even small amounts of water.

A more desirable alternative is to utilize a molecular sieve that is not so adversely affected by water, such as HSSZ-13. Figure 7.2 shows that the experimental results for a 15 vol% HSSZ-13 in PVAc membrane are most closely approximated by the “open” case or the “equilibrium adsorption” case. The important difference between HSSZ-13 and zeolite 4A is that the “equilibrium adsorption” case for HSSZ-13 is more similar to

the “open” case, whereas in zeolite 4A it was more similar to the “closed” case. This indicates that HSSZ-13 is less affected by water.

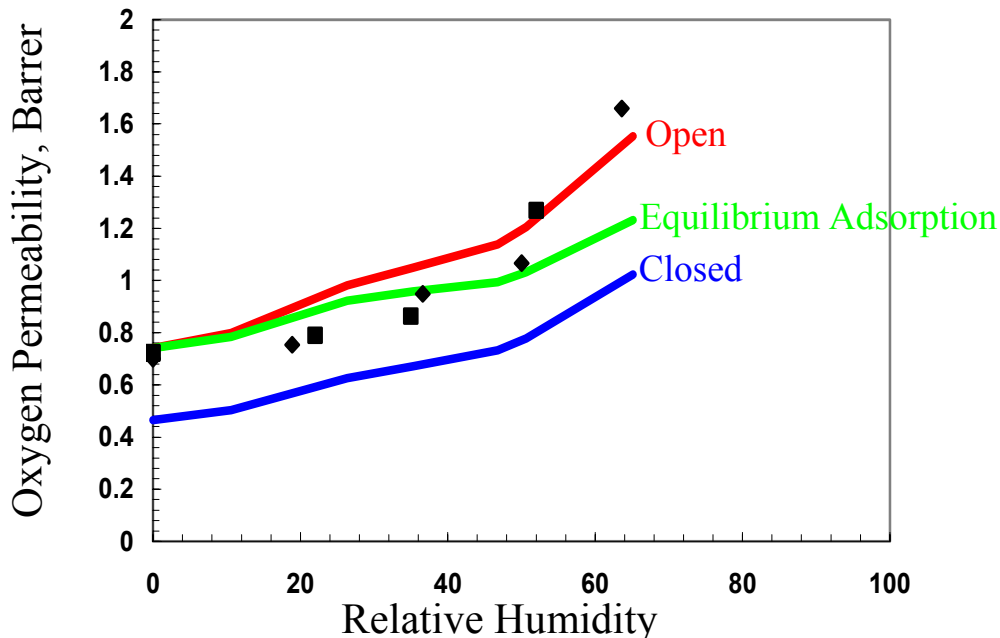


Figure 7.2: Effect of feed humidity on the oxygen permeability of a 14.2 vol% HSSZ-13 filled poly(vinyl acetate) membrane. Experiments were performed at 35°C. ♦, Membrane 1 data; ■ Membrane 2 data.

As stated earlier, the “equilibrium adsorption” model assumes the zeolite permeability is proportional to the fraction of the zeolite not occupied by water in the absence of competitive sorption. If this assumption is relaxed to allow for competitive sorption, this equation becomes:

$$P_{Steve} = P_0 \left(1 - \frac{x_w}{x_{w,MAX}} \right) = P_0 \left(1 - \frac{b_w p_w}{1 + b_w p_w + b_{O_2} P_{O_2}} \right) \quad (7.2)$$

Clearly, Eq 7.1 is equivalent to Eq 7.2 if $b_w p_w \gg b_{O_2} P_{O_2}$. Given the Langmuir affinity constants in Table 6.2, this assumption is quite valid for zeolite 4A despite the much smaller partial pressure of water in the otherwise pure oxygen feed. On the other hand, for HSSZ-13 at moderate relative humidities, this assumption breaks down; at about ten

percent relative humidity $b_{O_2}p_{O_2}$ is 0.056 and b_{WPW} is 0.141. Nevertheless, using the full multicomponent sorption model gives permeabilities between the open and equilibrium adsorption calculations, so the underlying conclusions are still valid.

7.2.3. Effect of Reactivation Conditions on Sorption in Zeolite 4A after Pre-adsorption of Water

The effect of water on oxygen transport through zeolite 4A was also probed using sorption experiments. Samples were activated using one of the proven activation methods from section 6.2. After loading into the zeolite holder (Figure 3.8), samples were put in a plastic cylindrical container with one open end, which floated on a few mL of water in an enclosed glass vial. They were kept in this manner overnight to ensure the zeolites were saturated with water. This was followed by one of five different reactivation treatments: (i) evacuation in the sorption cell overnight, or drying in the TGA under N_2 for 12 hours at (ii) 150°C, (iii) 200°C, (iv) 280°C, or (v) 590°C. Both transient and equilibrium oxygen sorption for these samples are shown in Figure 7.3. Transient sorption is not shown for case (ii) because it was taken at a higher pressure, but it exhibits slow kinetics. The figure shows that the highest three activation temperatures give full sorption and reasonable kinetics with half times less than 60 seconds. The two less severe reactivation conditions, (i) and (ii), give oxygen sorption lower and slower than for “normal” zeolite 4A.

Although the half time of the sample (iii) reactivated at 200°C is very small, it still exhibits a larger tail than the other samples, even though equilibrium oxygen sorption indicates very little adsorbed water. A small amount of adsorbed water may cause this effect. The simple model considered here neglects site energetic heterogeneity. The first water molecules preferentially sorb near the cations within the zeolite pore structure [12]. One of the cations partially blocks the pores of zeolite 4A, so water associated with that cation could significantly slow sorption into the zeolite. This effect would require only a small amount of water to occupy the cation sites.

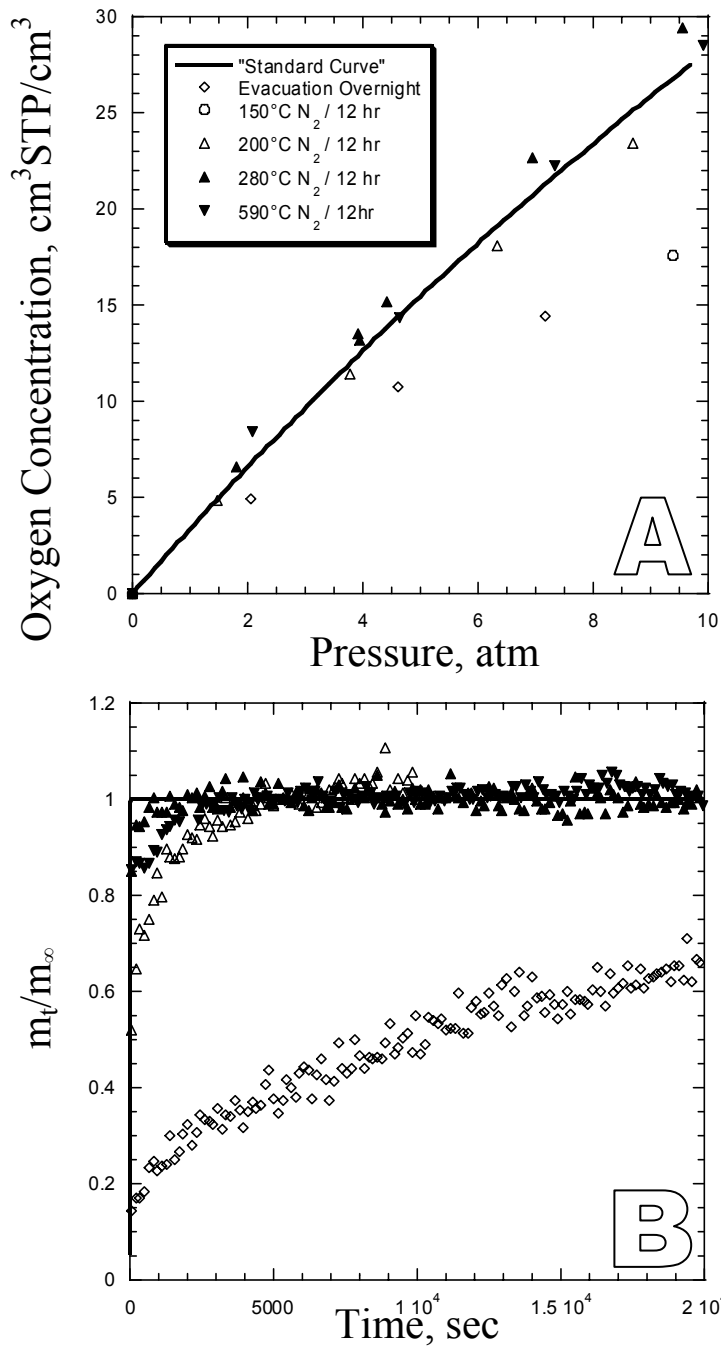


Figure 7.3: (a) Equilibrium and (b) transient oxygen sorption for activated zeolite 4A samples exposed to water and reactivated under different conditions. The “Standard Curve” on the equilibrium sorption plot is from section 6.2. The transient curves are from the lowest equilibrium pressure, ~ 2 atm.

Saturated zeolite 4A contains about 29 wt% adsorbed water. A dried sample was exposed to water in the gravimetric sorption apparatus (see section 3.4.2.1) at 35°C, followed by evacuation overnight to remove the water. Sorption of water was very rapid, with equilibrium reached in well under one hour. Desorption was much slower. In the first 4 hours of desorption, the amount of sorbed water decreased to ~5 wt%, and after 20 hours, the amount sorbed was 4.3 wt%. At this point, the temperature was increased to 70°C for four hours to see if additional water could be removed, but the amount of sorbed water was unchanged. Thus, evacuation overnight (activation method (i) in Figure 7.3) is expected to leave 4-5 wt% adsorbed water in zeolite 4A, which is enough to significantly slow sorption into the sample. It would also cause equilibrium oxygen sorption lower than the “standard curve”, because part of the available sorption capacity is occupied by water.

7.3. EFFECT OF N-BUTANE ON MIXED MATRIX MEMBRANES

This section discusses the effect of an organic contaminant on mixed matrix membranes prepared with a hydrophobic sieve. Specifically the Ultem[®] – HSSZ-13 system is studied. The behavior of the pure materials is first discussed. This is followed by detailed modeling of the transport properties expected of mixed matrix membranes. Finally, the predictions are compared with limited experimental data from collaborators.

7.3.1. Modeling Considerations

The transport properties of the polymer and sieve phase are first modeled separately, and then the Maxwell model is used to predict the permeability of mixed matrix membranes. The dual-mode model (section 2.2.3.1) is used for the polymer phase, and the multicomponent Langmuir equation is used to model sorption in the zeolites. The diffusion coefficients in the sieve are assumed constant in these calculations. Recall that the diffusion coefficient of oxygen in zeolite 4A was not a function of pressure (Figure 6.7), but it may be necessary to calculate D according to Eq 2.22 when the sieve is nearly saturated [13]. Nonetheless, the results obtained using diffusion coefficients

from Eq 2.22 were qualitatively similar to those for a constant diffusion coefficient, so they are not presented in detail. Allowing the diffusion coefficient to vary according to Eq 2.22 led to slightly lower zeolite permeabilities at low feed pressures with slightly higher permeabilities at higher feed pressures.

7.3.2. Effect of n-Butane on the CO₂ / CH₄ Transport Properties of Ultem[®]

Permeation data for n-butane in Ultem[®] are not available, so it was necessary to estimate the sorption and diffusion of this penetrant in Ultem[®]. It would be difficult to study this directly because of the long time lags and very low permeabilities expected. These calculations were done assuming n-butane *does not plasticize* Ultem[®] at the conditions studied. An empirical correlation for sorption in polymers has been given by van Amerongen [14]:

$$\ln (S) = k_1 + k_2 T_C \quad (7.3)$$

where k_1 and k_2 are empirical constants and T_C is the critical temperature of the penetrant. The Langmuir affinity constant, b , and the Henry's law sorption coefficient can both be correlated using similar expressions [15]. Based on affinity constants and Henry's law coefficients for N₂, CO₂, and CH₄ in Ultem[®] reported by Barbari et al [16], the Langmuir affinity and Henry's law coefficients for n-butane at 35°C are estimated as 1.22 atm⁻¹ and 4.25 cm³STP/cm³/atm, respectively. The Langmuir affinity constant is needed to approximate the effect of n-butane on the sorption of carbon dioxide and methane in the polymer using the multicomponent dual-mode model. The Henry's law coefficient and diffusion coefficient are needed to estimate the time lags in neat Ultem[®] and in HSSZ-13 filled Ultem[®]. The diffusion coefficient has been correlated to the Lennard-Jones collision diameter using the following correlation:

$$\ln (D) = k_3 + k_4 \sigma_{LJ} \quad (7.4)$$

where k_3 and k_4 are empirical constants and σ_{LJ} is the Lennard-Jones collision diameter [17]. Dissolved mode diffusion coefficients, D_D , for N_2 , CO_2 , and CH_4 in Ultem[®] measured by Barbari [18] are used in the correlation to estimate the diffusion coefficient of n-butane in Ultem[®] as $1 \times 10^{-13} \text{ cm}^2/\text{s}$.

Based on the estimated diffusion coefficient of n-butane in Ultem[®], the time lag for a 1000 Å thick neat Ultem[®] separation layer (in a hollow fiber membrane) is 3 minutes, so steady state is achieved quickly. On the other hand, for a 10 μm thick dense film, the time lag is ~19 days, so it is infeasible to study n-butane permeation in a dense film. Preparing defect-free dense films thinner than 10 μm is difficult.

The calculated effects of n-butane in an otherwise 10% CO_2 / 90% CH_4 mixture on the permeability and selectivity of neat Ultem[®] is minimal, so they are not shown. Addition of n-butane slightly reduces the carbon dioxide and methane permeabilities and CO_2/CH_4 selectivity. The gas permeabilities and CO_2/CH_4 selectivity both decrease with increasing pressure, exhibiting the typical response of glassy polymers. In neat Ultem[®], a significant fraction of the permeation occurs through the dissolved mode, where n-butane is expected to have less of an effect, rather than the Langmuir mode, where n-butane can out-compete the two gases. Thus, the effect of n-butane on the transport properties of Ultem[®] is expected to be minimal, *unless plasticization occurs*.

7.3.3. Effect of n-Butane on the CO_2 / CH_4 Transport Properties of HSSZ-13

The calculated effect of n-butane on the permeability of HSSZ-13 is more significant than the effect on neat Ultem[®]. Addition of 2% n-butane causes a drop greater than an order of magnitude in the carbon dioxide and methane permeabilities of HSSZ-13 except at very low total feed pressures, as shown in Figure 7.4. The permeability of HSSZ-13 is decreased by approximately 50% in the presence of 0.1% n-butane, but 0.01% n-butane (not shown) has little effect on the permeability. These effects reflect

competition of the more condensable n-butane versus the other feed gases for permeation pathways in the sieve.

The calculated CO₂/CH₄ selectivity of HSSZ-13 has a fixed value of $\frac{b_{CO_2} C_H'_{CO_2} D_{CO_2}}{b_{CH_4} C_H'_{CH_4} D_{CH_4}}$

for the model used here. Because the affinity constant of carbon dioxide in the sieve is so much greater than that of methane, the calculated selectivity is about 4400. The selectivity varies when the diffusion coefficient in the sieve is calculated according to Eq 2.22, but not significantly. Nevertheless, the calculated mixed matrix membrane methane permeabilities are not very sensitive to the CO₂/CH₄ selectivity of the sieve once it exceeds about 100 because most of the methane permeates through the polymer.

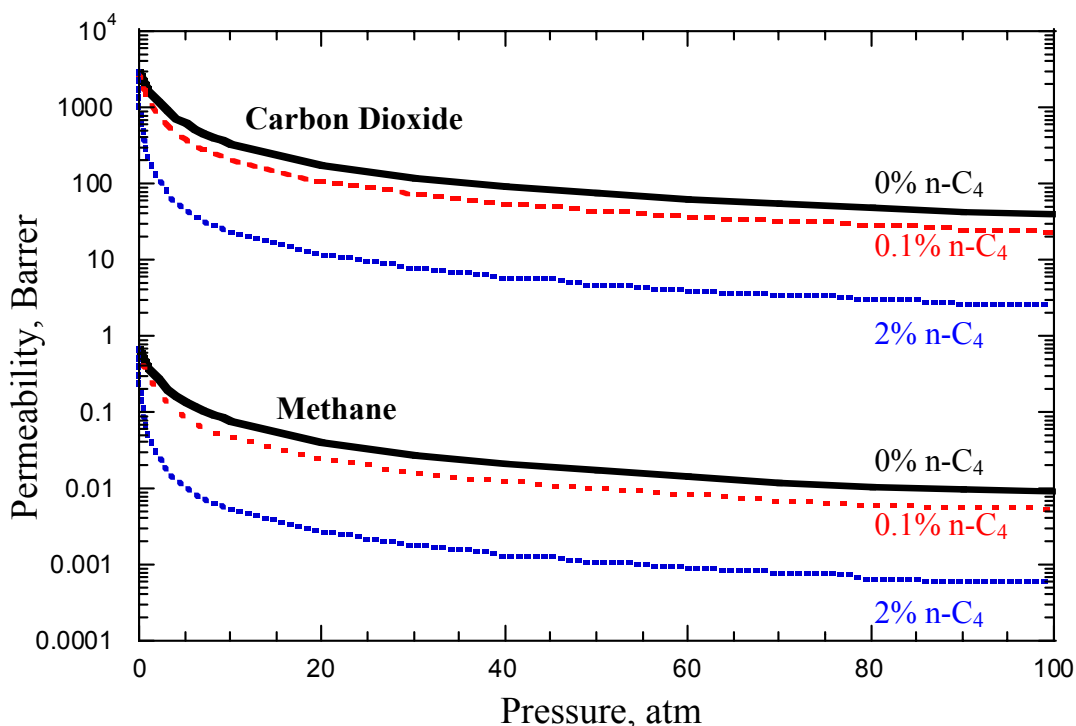


Figure 7.4: Calculated CO₂ and CH₄ permeabilities in HSSZ-13 at 35°C as a function of feed pressure for a synthetic natural gas mixture (10% CO₂ / 90% CH₄) with selected concentrations of n-butane as a model contaminant. Calculations assume constant diffusion coefficients in the sieve.

7.3.4. Effect of n-Butane on the CO₂/CH₄ Transport Properties of 15% HSSZ-13 Filled Ultem[®] Mixed Matrix Membranes

The calculated transport properties of mixed matrix membranes with n-butane contaminated feeds show some unexpected behavior. The carbon dioxide and methane permeabilities calculated assuming constant diffusion coefficients in the sieve are shown in Figure 7.5. As expected, the carbon dioxide and methane permeabilities decrease with both pressure and increasing n-butane concentration. However, the decrease in methane permeability is more precipitous at low pressures and high n-butane feed concentration. This is because n-butane is more likely to reduce methane sorption in the sieves, rather than carbon dioxide sorption, because methane has the weakest affinity for the sieve.

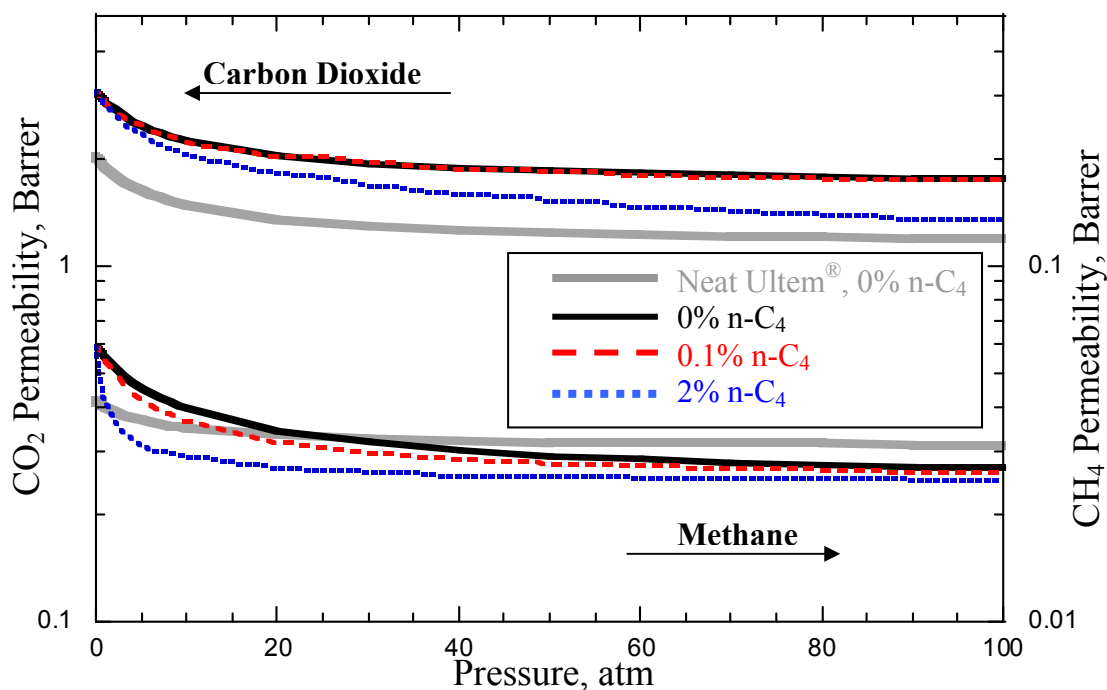


Figure 7.5: Calculated CO₂ and CH₄ permeabilities in 15 vol% HSSZ-13 filled Ultem[®] at 35°C as a function of feed pressure for a synthetic natural gas mixture (10% CO₂ / 90% CH₄) with selected concentrations of n-butane as a model contaminant. Calculations assume constant diffusion coefficients in the sieve. The permeabilities of neat Ultem[®] in the absence of n-butane are shown for comparison.

The most interesting behavior occurs in the CO_2/CH_4 selectivity of mixed matrix membranes. The selectivity is predicted to *increase* with the addition of n-butane under some conditions, as shown in Figure 7.6. This is contrary to the behavior of neat polymers or even pure molecular sieves. The increase in selectivity at low pressures and moderate n-butane contamination is a result of the precipitous decrease in methane permeability through the sieve mentioned above. This is explained in the context of matching of the permeabilities of the two phases (see section 2.3) with the help of Figure 7.7. Without n-butane, the permeability of the sieve is several orders of magnitude greater than neat Ultem[®]. Since methane permeates through the sieve faster than through Ultem[®] in this case, it incurs no tortuosity penalty in the mixed matrix membrane. The sieve permeability is reduced dramatically in the presence of n-butane, such that it becomes better matched to the Ultem[®] matrix. Thus, Ultem[®]-based mixed matrix membranes should show higher selectivities in the presence of n-butane (green diamonds) than in its absence (red diamonds). The *methane* permeability of the Ultem[®] matrix is then lower than the methane permeability of the sieve, causing a tortuosity penalty. However, at some pressure, carbon dioxide permeation through the sieve is also decreased by adsorbed n-butane to such an extent that the overall selectivity of the mixed matrix membrane is reduced. So, certain contaminants in the feed gas at moderate concentrations may actually be *beneficial* under some conditions.

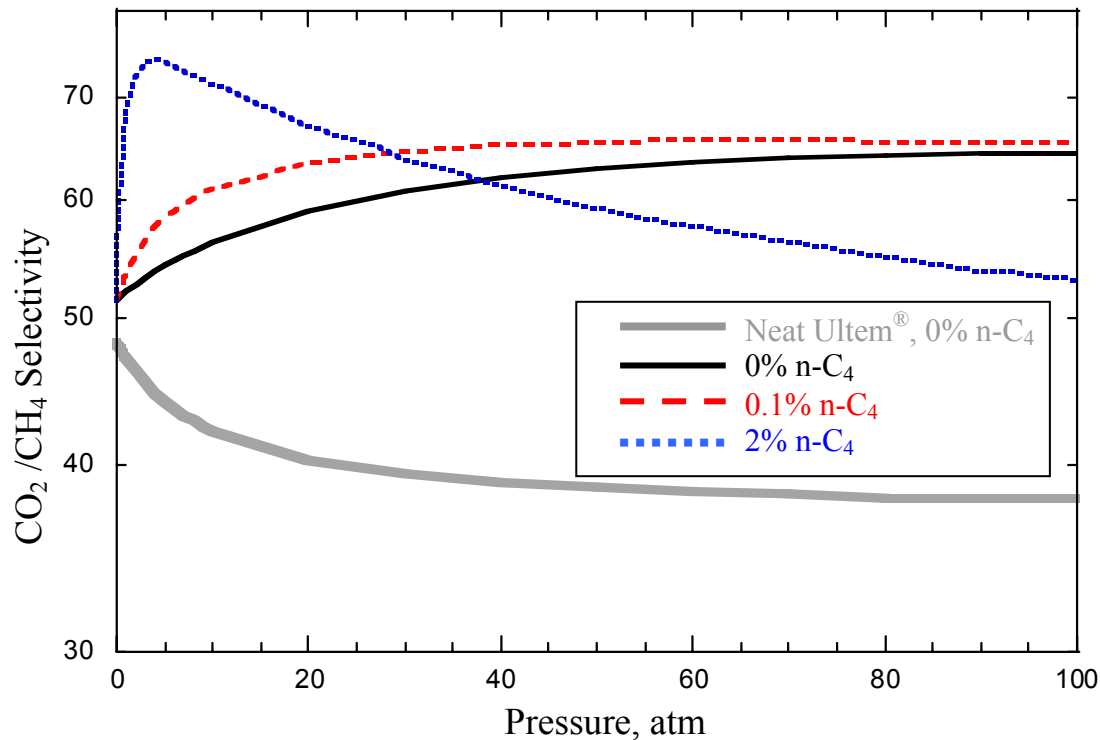


Figure 7.6 Calculated CO₂/CH₄ selectivity of 15 vol% HSSZ-13 filled Ultem[®] at 35°C as a function of feed pressure for a synthetic natural gas mixture (10% CO₂ / 90% CH₄) with selected concentrations of n-butane as a model contaminant. The selectivity of neat Ultem[®] in the absence of n-butane is shown for comparison.

Figure 7.7 also shows predicted transport properties for a hypothetical upper-bound polymer that is better “matched” to HSSZ-13 using the criteria in section 2.3, for convenience, with a CO₂ permeability of 100 Barrer. Mixed matrix membranes prepared with this polymer should exhibit significant improvement in selectivity in the absence of n-butane (red circles). However, adding n-butane decreases the sieve permeability, so only modest increases in the selectivity of mixed matrix membranes are predicted (green circles).

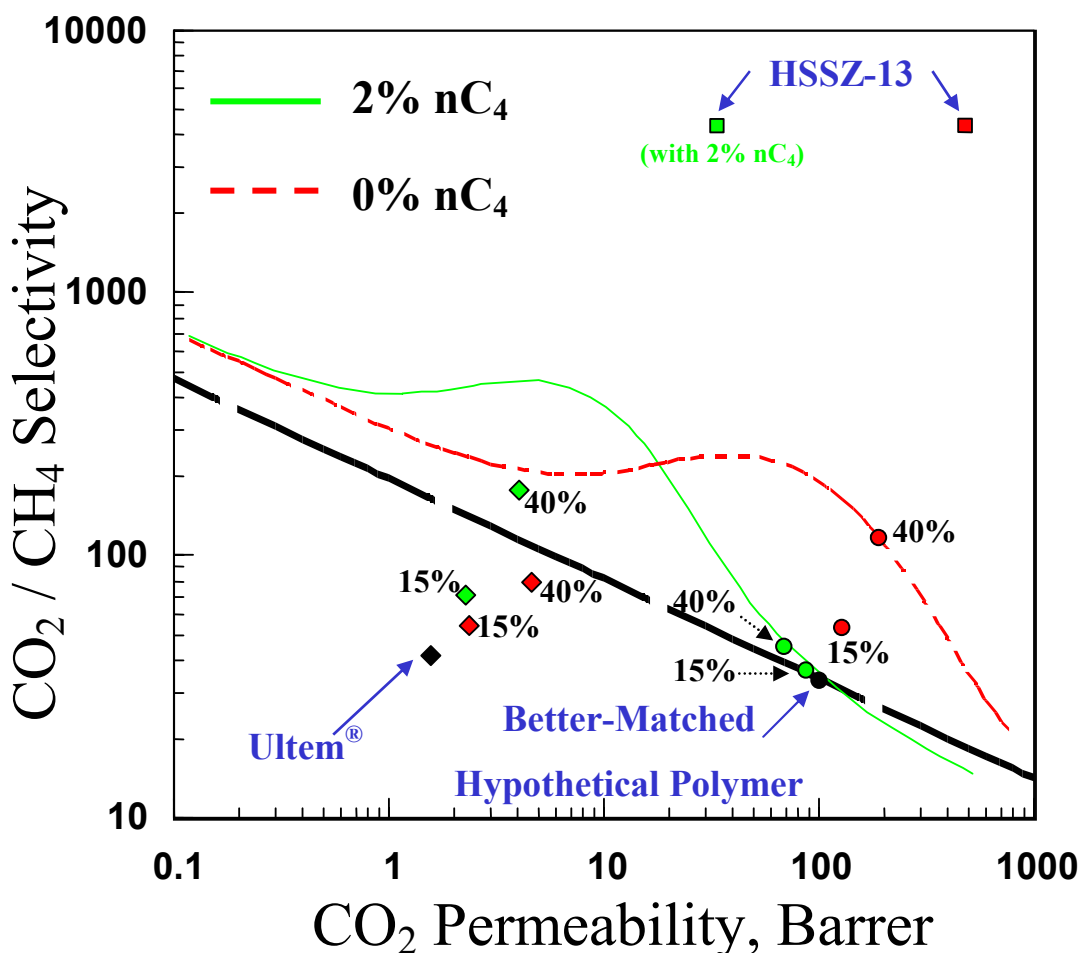


Figure 7.7: Upper-bound plot for Ultem[®] and a better-“matched” hypothetical polymer with dispersed HSSZ-13 for a 10% CO₂ / 90% CH₄ synthetic natural gas feed with and without 2% n-butane. Red markers indicate a pure feed, while green markers indicate 2% n-butane in the feed. The upper bound is given by the heavy dashed black line. The green and dashed red lines represent calculated transport properties for 40 vol% HSSZ-13 in polymers on the upper bound with and without n-butane in the feed, respectively.

7.3.5. Comparison with Permeation Data from 15% HSSZ-13 filled Ultem[®] Modules Prepared and Tested at Medal

Because of the difficulty in measuring permeabilities of feeds containing n-butane through dense films, hollow fiber mixed matrix membranes prepared by collaborators at Medal LP are used to validate the model. Table 7.2 summarizes measured and predicted CO₂/CH₄ selectivities for Ultem[®] and 15% HSSZ-13 filled Ultem[®]

membranes. Calculated permeabilities are not correlated against the permeances of the modules because of the difficulty in determining accurate skin thicknesses of hollow fibers. The modeling parameters at 35°C are regressed from experimental data. However, insufficient data is available at 50°C to regress all the parameters in the model. Thus, most were estimated using appropriate correlations from the known parameters at 35°C. The only parameters that are based on experimental data at 50°C are the Langmuir affinity and capacity constants of carbon dioxide and n-butane in HSSZ-13. The derivation of the required modeling parameters at 50°C is discussed in Appendix H. The Langmuir affinity and capacity constants of methane at 50°C were not measured and could not be reliably estimated, so they are assumed unchanged from 35°C. This should produce a lower bound on the selectivity since this assumption will over-predict the sorption of methane in the zeolites at 50°C.

Table 7.2: Comparison of selectivities calculated and measured using Medal modules versus n-butane loading in an otherwise 10% CO₂ / 90% CH₄ feed gas at ~100 psia.

n-butane Loading	Membrane	CO ₂ /CH ₄ Selectivity			
		Measured		Calculated	
		50°C	50°C	35°C	
0%	Ultem [®]	38	31	43	
	15% HSSZ-13 in Ultem [®]	50	39	55	
2%	Ultem [®]	45	31	43	
	15% HSSZ-13 in Ultem [®]	57	39	73	

As expected, the mixed matrix membranes show improved selectivities compared to neat Ultem[®] with and without n-butane in the feed, qualitatively in agreement with model predictions. The predicted mixed matrix enhancement is 26% with or without n-butane, and the measured enhancement is 32% and 27% without and with n-butane in

the feed, respectively. The model under-predicts the absolute selectivity at 50°C in both neat Ultem[®] and the mixed matrix membrane. This is probably because the parameters were extrapolated to 50°C as mentioned above. Another possibility is that n-butane is acts as an antiplasticizer for Ultem[®] under the conditions studied. Unfortunately, no methods exist to predict antiplasticization effects.

The model predicts a negligible enhancement in the selectivity of the mixed matrix membrane in the presence of n-butane. The results seem to support this since most of the mixed matrix selectivity enhancement with n-butane was attributable to the neat polymer selectivity enhancement. Thus, the shortcoming of the model appears to be with the prediction of pure polymer properties and not with the effect of n-butane.

The model predicts a significant improvement in selectivity of the mixed matrix membrane at 35°C in the presence of n-butane. The temperature dependence of this result is quite important. It was expected that raising the temperature would reduce the effect of n-butane, since raising the temperature lowers the amount of n-butane sorbed in the sieves. Although in this case, raising the temperature had the undesirable effect of lowering the selectivity, if n-butane had had a deleterious effect on mixed matrix performance, it should also have been ameliorated by raising the temperature.

An estimate of the maximum time lag of n-butane in the mixed matrix membrane was also made using an expression for the time lag with completely immobilized sorption in the Langmuir sites reported by Paul and Kemp [19]. Using the estimated diffusion coefficient of n-butane Ultem[®], 1×10^{-13} cm²/s, as a minimum for the average diffusion coefficient gives a maximum time lag of ~10000 seconds for a hollow fiber mixed matrix membrane, assuming a separation layer thickness of 1000 Å. For comparison, n-butane was earlier estimated to have a time lag of 3 minutes in a neat Ultem[®] hollow fiber. This indicates that the modules should have reached steady state during the experiments, which were run for several days. A more accurate estimate of the time lag could be made using the partial immobilization model reported by Paul and Koros [20],

but it will be necessary to modify the expression to account for the ratio of the polymer and sieve volume fractions.

7.4. DISCUSSION

The results presented in this chapter illustrate the importance of considering the effects of contaminants on mixed matrix membrane transport properties. In particular, the performance of zeolites can be changed appreciably by low concentrations of contaminant, because of their much larger affinities towards many penetrants compared to polymers. Because zeolites have a fixed number of permeation pathways, they are more prone to “clogging”, whereas polymers have an infinite number of permeation pathways. If the contaminant effect is similar to water on zeolite 4A, some provision such as pretreatment of the feed to remove the contaminant must be made to avoid reduced membrane performance.

Assuming no plasticization, the permeability and selectivity of *neat* Ultem[®] are both predicted to decrease slightly with the addition of small amounts of n-butane. Ultem[®] membranes actually seem to exhibit increased selectivity in the presence of 2% n-butane. This could be because n-butane is acting as an antiplasticizer. The model does not account for this, so it could explain why the model does not capture the behavior of the neat polymer. Also, the model at 50°C is not as accurate because its parameters were extrapolated to this temperature. Other polymers that do not plasticize or antiplasticize would be also expected to exhibit reductions in permeability. Rubbery polymers are more likely to plasticize than glassy polymers. This appears to be the case with water in PVAc, which has a Tg of 30°C. In any case, plasticization should be avoided since it may undermine the selectivity of the matrix; however, antiplasticization may be helpful.

Counter intuitively, n-butane is predicted to *increase* the selectivity of mixed matrix membranes composed of Ultem[®] and HSSZ-13 under some conditions. This is

achieved with a small penalty in permeability. Only at the highest n-butane concentration at elevated pressure is the selectivity of mixed matrix membranes predicted to decrease. Increases in CO₂/CH₄ selectivity are also expected for small amounts of water in the feed for HSSZ-13 in Ultem[®], but higher concentrations cause decreased selectivity. This effect is related to the poor matching of the Ultem[®] and HSSZ-13. For a better matched polymer and sieve, modeling predicts decreases in selectivity in the presence of n-butane because the sieve permeability is reduced. Nonetheless, it appears the potential deleterious effects of contaminants can be avoided by (i) pretreatment of the feed to remove or lower the contaminant concentration, or (ii) selection of a matrix with knowledge of the likely effect of contaminants so the effect will be neutral or positive as in the Ultem[®] – HSSZ-13 system.

The work with n-butane and water contaminants has demonstrated the utility of the modeling approach validated with limited testing. Although the model does not perfectly predict the performance of neat polymers or mixed matrix membranes, it does properly predict the kinds of effects that are observed in the presence of two contaminants. This is very promising considering that the parameters for the contaminants were estimated in most cases. Only the Langmuir affinity constants of the contaminant in the sieves were actually measured. Sorption measurements are relatively simple, and they can be quickly repeated for other contaminants, so their effect on mixed matrix membrane transport properties can also be predicted.

7.5. REFERENCES

1. Djoekita, G., Characterization and analysis of asymmetric hollow fiber membranes for natural gas purification in the presence of hydrocarbons. Department of Chemical Engineering, University of Texas at Austin. 2000.
2. Chern, R.T.; W.J. Koros; E.S. Sanders; and R. Yui. J. Membr. Sci. 1983, 15, 157-69.
3. Peterson, D. Zeolites 1981, 1, 105-12.

4. Funke, H.H.; K.R. Frender; K.M. Green; J.L. Wilwerding; B.A. Sweitzer; J.L. Falconer; and R.D. Noble. *J. Membr. Sci.* 1997, 129, 77-82.
5. Long, F.A. and L.J. Thompson. *J. Polymer Sci.* 1955, 15, 413-26.
6. Lindemann, M.K., Physical constants of poly(vinyl acetate), in *Polymer handbook*, J. Brandrup and E.H. Immergut, Editors. 1989, John Wiley & Sons: New York. p. V/71-5.
7. Blum, F.D.; J.E. Dickson; and W.G. Miller. *J. Polym. Sci., Polym. Phys. Ed.* 1984, 22, 211-21.
8. Paulson, G.T.; A.B. Clinch; and F.P. McCandless. *J. Membr. Sci.* 1983, 14, 129-37.
9. Koros, W.J.; R.T. Chern; V. Stannett; and H.B. Hopfenberg. *J. Polym. Sci., Polym. Phys. Ed.* 1981, 19, 1513-1530.
10. Pye, D.G.; H.H. Hoehn; and M. Panar. *J. Appl. Polym. Sci.* 1976, 20, 287-301.
11. Jones, C.W. and W.J. Koros. *Ind. Eng. Chem. Res.* 1995, 34, 164-7.
12. Breck, D.W.; W.G. Eversole; R.M. Milton; T.B. Reed; and T.L. Thomas. *J. Am. Chem. Soc.* 1956, 78, 5963-71.
13. Moreau, S., Personal communication. 2002.
14. van Amerongen, G.J. *J. Appl. Phys.* 1946, 17, 972-85.
15. Yampolskii, Y.; D. Wiley; and C. Maher. *J. Appl. Polym. Sci.* 2000, 76, 552-560.
16. Barbari, T.A.; W.J. Koros; and D.R. Paul. *J. Polym. Sci., Part B: Polym. Phys.* 1988, 26, 729-44.
17. Okamoto, K.; K. Noborio; J. Hao; K. Tanaka; and H. Kita. *J. Membr. Sci.* 1997, 134, 171-179.
18. Barbari, T.A.; W.J. Koros; and D.R. Paul. *J. Polym. Sci., Part B: Polym. Phys.* 1988, 26, 709-27.
19. Paul, D.R. and D.R. Kemp. *J. Polym. Sci., Polym. Symp.* 1973, No. 41, 79-93.
20. Paul, D.R. and W.J. Koros. *J. Polym. Sci., Polym. Phys. Ed.* 1976, 14, 675-85.

Chapter 8. CONCLUSIONS AND RECOMMENDATIONS

8.1. SUMMARY AND CONCLUSIONS

As stated in the first chapter, the overall objective of this work was to *develop the knowledge to allow subsequent researchers to create mixed matrix materials with desirable transport and mechanical properties for appropriate polymer – sieve combinations tailored to a specific gas pair*. This work achieved a number of significant advancements toward that goal. Each is listed below and then discussed in more detail in the following paragraphs. Conclusions drawn from this research are highlighted in this section in **bold** text.

1. Development of a unifying framework to explain how both matrix rigidification and sieve-in-a-cage morphologies are formed, giving rise to a better understanding of how preparation conditions lead to various membrane morphologies that each have signature transport properties
2. Optimization of dope preparation methods to minimize agglomerate formation, allowing the preparation of membranes with submicron zeolites
3. Application of sorption-based experiments to gain additional insights into transport through both zeolites and the resulting mixed matrix membranes
4. Development and preliminary validation of a model for the transport properties of mixed matrix membranes in the presence of contaminants in the feed gases

The understanding of the relationship between mixed matrix membrane morphologies and their resultant transport properties was well developed at the onset of this work. The fundamental causes of these morphologies were less well understood. Sieve-in-a-cage morphology was previously attributed to a combination of: poor flexibility of the polymer matrix, limiting its ability to conform to the sieve surface; unfavorable

interactions between the polymer and the sieve; and stresses caused by contraction of the polymer matrix away from the sieve surface as the solvent evaporates. Matrix rigidification was previously attributed to chain immobilization at the sieve surface, but the underlying cause of this phenomenon was identified as the interaction with the surface. Chapter four discussed how these two phenomena both arise from the same underlying cause; namely, stresses that accumulate at the interface as the solvent evaporates. The nature of these stresses determines which of these two seemingly opposite morphologies form. Contraction of the polymer matrix (e.g. via solvent loss) leads to *compressive* stresses on the interface. **Compressive stresses are believed to cause matrix rigidification. The stresses on the interface must be tensile normal to the sieve surface to cause sieve-in-a-cage morphology.** Tensile stresses acting normal to the interface can only occur if there is an external factor that causes them. For example, a membrane prepared on a substrate to which it strongly adheres will be unable to contract in the plane of the film, giving rise to normal tensile stresses at polymer – sieve interfaces. Removing the surface should eliminate tensile stresses, although this is difficult in practice. Instead, it is better to cast the membrane on a surface, and then to remove it before the nascent film loses enough solvent to become glassy. Thus, **tensile stresses at the interface can be avoided through the selection of proper membrane casting techniques**, as demonstrated in chapter five. Chapter five also demonstrated that high temperatures may damage mixed matrix membranes.

The Ultem[®] – HSSZ-13 system was used for extensive tests of selected silane treatments on the morphology and transport properties of mixed matrix membranes, as discussed in chapter five. The most significant difference was between silanated sieves and unsilanated sieves, while the particular silane coupling agent used produced little difference on either morphology or transport properties. **Dopes prepared with unsilanated submicron zeolites were inherently unstable**, resulting in mixed matrix membranes with many large sieve agglomerates. These agglomerates formed in the casting dope rather than during membrane formation, meaning they can be eliminated

form the membranes if the dopes are stabilized. **Stabilization of the casting dopes was achieved via silanation of the zeolites and through appropriate priming of the sieve surfaces** after silanation and before addition of the bulk polymer. Agglomerates that did form could be settled out or filtered from the casting dope before casting the membranes. Because of the highly viscous nature of the dopes, gravitational settling required long times (~months) and filtration required high pressure (~50 atm). Thus, these procedures are not practical on an industrial scale.

Although dope formulation and casting methods were developed that gave membranes with morphologies expected to have excellent transport properties, **many of the membranes appeared to suffer from impermeable or poorly permeable zeolites**. Measuring equilibrium and kinetic sorption of the zeolites provided important insights into these observations. These experiments illustrated the extreme sensitivity of zeolites to certain contaminants, even at levels where it was difficult to otherwise detect them. This was the case for samples exposed to used vacuum ovens or the vacuum lines through which equipment at Georgia Tech was initially connected, which both caused reduced permeability in the zeolites. **Assumptions regarding the ability to remove highly volatile solvents thought too large to enter the zeolites were also disproved**. This was demonstrated with dichloromethane and toluene, which were used in casting dopes, and with isopropanol, which was used as a silanation solvent. In some cases, full, normal sorption could be recovered in the zeolites after an appropriate reactivation treatment. **Nonetheless, some of the reactivation methods are clearly not valid for mixed matrix membranes** (e.g. calcination in air at 590°C for 30 min). More work is needed to better determine how to fully reactivate zeolites within mixed matrix membranes. The sorption-based technique developed in chapter six provides an important tool to accomplish this.

The preceding paragraph discussed the effect of contaminants that arise during processing, but mixed matrix membranes will also be exposed to numerous potential

contaminants in real feeds. Foremost among these is water, which is present in both air and natural gas feeds. Work in chapter seven demonstrated that **zeolite 4A becomes almost completely impermeable in the presence of very low concentrations of water, because of the extremely hydrophilic nature of this sieve.** Conversely, **the effect of water on HSSZ-13, with its more hydrophobic interior, was minimal, but the permeability of HSSZ-13 could be dramatically lowered by organic contaminants.** If dispersed in a matrix to which its permeability was well matched, such effects on the sieve could substantially reduce the performance of mixed matrix membranes. In the particular case studied here, Ultem[®] – HSSZ-13, the effect was increased selectivity. This is because the permeability of HSSZ-13, while lowered in the presence of the n-butane, became better matched to the Ultem[®] matrix. **The modeling work presented in chapter seven provides a convenient framework to approximate the types of effects potential contaminants may have on mixed matrix membranes.** Conveniently, the only information about the contaminant needed for this model that must be determined experimentally is the Langmuir affinity constant of the contaminant in the zeolite.

A big disappointment is the continuing inability to easily prepare mixed matrix membranes having improved transport properties commensurate with an appropriate model. The next section gives recommendations to resolve these issues and discusses additional areas requiring further study before the mixed matrix platform is economically and technologically viable.

8.2. RECOMMENDATIONS FOR FUTURE WORK

8.2.1. Further Investigations of Mixed Matrix Membranes in the Presence of Contaminants

The most pressing area of future research is to acquire a better understanding of how the zeolites can be reactivated after processing. Based on work presented here, it appears

some mixed matrix membranes are not realizing their full transport properties, because zeolites are not completely active after incorporation into membranes. Some problems can be easily fixed, for example avoiding contaminated processing equipment, while others are not so easily overcome. A number of potential solutions have been outlined in the text. Foremost among these is the consideration of more robust drying conditions. Longer drying times are certainly possible. Higher drying temperatures may also be permitted; however, care must be taken not to damage the intricate morphologies (i.e. silane coupling agents) at the interface.

Another approach may be to pre-adsorb a sorbate into the zeolite that prevents an undesirable processing solvent from accessing the internal structure. Such a sorbate could then be removed after processing. This is analogous to the concept of a protective group in organic chemistry reactions. One candidate for such a “protective sorbate” scheme is water. It is strongly held by zeolite 4A, which should make it difficult for other contaminants to displace it. Second, work has already demonstrated that water can be removed from zeolites using conditions that do not damage mixed matrix membranes. Nonetheless, this approach may be limited, as contaminants that are more difficult than water to remove are presumably more strongly held by the zeolite, and may displace water if given sufficient time. Because of the added complexity and potential unanticipated consequences of this route, it should only be considered if effective reactivation conditions for mixed matrix membranes can not be developed. Another potential approach would be to pre-adsorb a slowly diffusing, weakly held gas such as methane or nitrogen into the zeolite. Although these molecules are likely easily displaced by most potential contaminants, they diffuse through zeolite 4A quite slowly, so the replacement rate should be slow. This approach may allow longer handling times during short exposures to the atmosphere where zeolite 4A could potentially sorb water.

More research is also warranted to understand the effects of feed contaminants, including methods to maximize desirable effects and to minimize undesirable ones.

The work presented here for two model components, water and n-butane, demonstrated the types of effects feed contaminants may have on mixed matrix membranes. These two contaminants provided data to validate a simple model for permeation through mixed matrix membranes in the presence of contaminated feeds. Nevertheless, very limited experimental data were obtained. In particular, the selectivity of membranes in the presence of contaminants needs to be more rigorously tested against the model. In the case of humidified feeds through membranes containing zeolite 4A, the selectivity is expected to decrease to near that of the neat polymer because the zeolite phase becomes essentially impermeable. The equipment to test this hypothesis was not available, but it would not be too difficult to modify existing equipment for these measurements. A bubbler setup could be used to introduce water to a synthetic air feed using the permeation system in 3.4.1.1. The GC column currently used for the air analysis will not tolerate water, so water must be removed from the permeate before analysis, unless an alternative column can be located. Organic contaminants are more difficult to study in dense films because of their slower diffusion coefficients, but additional studies could be done with hollow fiber membranes. Contaminants with functional groups likely to be attractive toward the zeolite should certainly be considered, since they may affect permeation through the zeolites at even lower concentrations.

One potential advantageous effect of contaminants that should be studied in more detail is the expected *increase* in the selectivity of mixed matrix membranes in the presence of contaminants when the sieve is far more permeable than the polymer matrix. The model predicts that an optimal feed contaminant concentration exists, corresponding to the point where the reduced sieve permeability is best matched to the polymer matrix. In particular, it would be worthwhile to retest the hollow fiber modules at 35°C to see if such an increase in selectivity is observed in the presence of n-butane.

Another contaminant-related issue that was not studied as part of this work is the effect of plasticization on mixed matrix membranes. As discussed earlier, plasticization

causes increased permeabilities and reduced selectivities in mixed matrix membranes. Plasticization could be due to either low concentrations of condensable contaminants or higher concentrations of carbon dioxide [1, 2]. If the polymer phase of a mixed matrix membrane becomes plasticized, lower overall selectivities are expected, unless the polymer matrix permeability becomes better matched to that of the sieve. On the other hand, mixed matrix membranes may be inherently plasticization resistant. The zeolites should act as artificial crosslinks between the matrix when it is directly bonded to the zeolite surface, especially as the particle size decreases [3-5]. Crosslinking is one method frequently applied to reduce the effect of plasticizers on polymer membranes [6, 7]. This effect would be easy to study with the current permeation setup using high pressure carbon dioxide. Alternatively, plasticization induced swelling may be able to heal defects at polymer – sieve interfaces in membranes displaying sieve-in-a-cage morphology, especially for small interfacial void sizes. Such an effect may occur in mixed matrix membranes prepared with glassy matrices and used for pervaporation, where swelling is common. In particular, high pressure CO₂ should be investigated as a potential method to relax residual stresses in mixed matrix membranes. It is unclear whether such an effect would remain after exposure to the highly swelling conditions. This could be tested by comparing gas permeation properties of a mixed matrix membrane and the corresponding neat polymer before and after an appropriate swelling regimen. Alternatively, it may be possible to prepare a mixed matrix membrane containing residual solvent, as in the cast and remove before vitrification method, and then to use high pressure CO₂ to extract the remaining solvent. The high pressure CO₂ should confer increased flexibility on the matrix, allowing stresses to relax more easily.

8.2.2. Development of Methods to Repair Undesirable Mixed Matrix Membrane Morphologies

The “repair” of mixed matrix membranes exhibiting poor properties is another frontier that warrants additional research. There are two types of morphologies where repair is

desirable: excess matrix rigidification at the interface and sieve-in-a-cage morphology. Annealing is frequently used to relax residual stresses in the polymer. For sieve-in-a-cage morphologies, a stress relief mechanism has already occurred, so the residual stresses in the membranes should be small. It is therefore difficult to envision how annealing of sieve-in-a-cage morphologies would be helpful, especially if the voids between the polymer and sieves are large. Conversely, matrix rigidification is believed to be caused by residual stresses that exist at the polymer – sieve interface. Evidence of this was shown in the birefringence images in Figure 4.5. If the residual stresses caused by solvent evaporation are high, as for glassy matrices, careful annealing of the mixed matrix membranes above the T_g of the matrix may be helpful. After the membrane is heated above its T_g for a sufficiently long time, it should exist in a stress free state at that temperature. Cooling the membrane will induce a small residual stress at the polymer – sieve interface because of a larger contraction in the polymer matrix than the sieve. This stress may be smaller than that induced by solvent evaporation, especially in high T_g polymers where a lot of solvent is required to depress the T_g to ambient casting conditions. One complication is the stability of the silane at the interface. The ability of silanated interfaces to withstand annealing conditions needs to be carefully investigated. Preliminary experiments into annealing of mixed matrix membranes above the T_g of the polymer matrix have suggested very high temperatures can destroy the intricate interfacial morphologies. Furthermore, heating and cooling rates may be important, and they have not been studied.

Methods to repair sieve-in-a-cage morphology should also be developed. The swelling method mentioned above likely would only apply to sieve-in-a-cage morphologies exhibiting small voids between the polymer and the sieve, and may not be permanent. An alternative is to try to fill the voids with a low permeability polymer, as shown in Figure 8.1. This approach is similar to the caulking of hollow fiber membranes [8], which seals pinhole defects in the separation layer of hollow fiber membranes. Caulking polymer – sieve voids in mixed matrix membranes is complicated by two

factors: (i) the polymer matrix surrounding the zeolites will make it difficult for the caulking agent to reach the voids, and (ii) the permeability of this region must be such that it allows gas to access the zeolite. Essentially, the caulking polymer also needs to be matched to the zeolite in the same manner as the matrix polymer (see section 2.3). Problem (i) could be solved by imbibing a suitable monomer into the void and then polymerizing it in situ, but the product polymer should still satisfy criterion (ii) above. One possibility is to caulk the interfacial voids with nylon-6. The corresponding monomer, ϵ -caprolactam, should be able to permeate into the voids, especially if the membrane is swollen with an appropriate solvent. In the presence of a little bit of water, it should then be possible to polymerize the ϵ -caprolactam by heating to $\sim 250^\circ\text{C}$ for a few hours [9]. Importantly, this temperature will not damage the membranes. Less rigorous reaction conditions may also be possible. Also, because this is a ring opening polymerization, there is no byproduct to possibly cause problems. One potential problem is that the oxygen permeability of nylon-6 is ~ 0.01 Barrer [10], which would likely inhibit permeation into the zeolite. On the other hand, the nylon-6 may incompletely fill the voids such that its permeability is greater than bulk nylon-6, but not so great to allow bypassing of the sieves. If the permeability of nylon-6 is too low, it may be possible to use a substituted caprolactam to yield a poorly packing polymer with a higher permeability. Some hollow fibers are currently treated using another reactive caulking technique [11], and this technique may be valid to repair sieve-in-a-cage morphologies. This technique involves intercalating a reactive mixture of diethyltoluenediamine and trimesoyl chloride in an appropriate solvent (e.g. heptane) into defects in the hollow fibers. It was also used by Mahajan to repair similar pinhole defects (but not sieve-in-a-cage morphology) in thin (< 1 mil) mixed matrix membranes supported on porous ceramic substrates [12]. Clearly, there are a lot of technical issues to resolve before either of these techniques can be used to repair defective mixed matrix membranes.

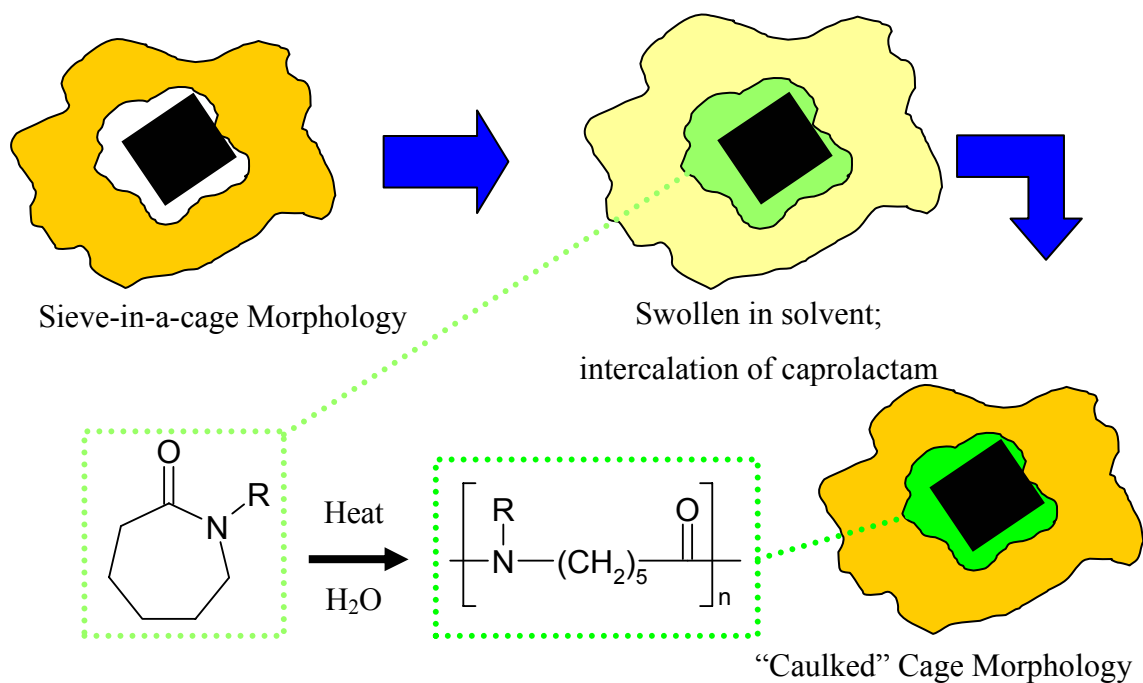


Figure 8.1: Scheme for the repair of mixed matrix membranes exhibiting sieve-in-a-cage morphology using a reactive intercalation scheme

8.2.3. Investigation of Developmental Issues Impeding Economic Feasibility of Mixed Matrix Membranes

This work focused on membranes with molecular sieving dispersed phases, but it should also be possible to use a zeolite that operates via a selective surface flow mechanism (see section 2.1.4). If such membranes could be developed, it would broaden the spectrum of separations possible with mixed matrix membranes. Selective surface flow-based mixed matrix membranes would allow for the selective permeation of more condensable (typically larger) penetrants or for separations where there is little size difference. If a method to measure the water permeability of a mixed gas feed can be devised, it should be simple to demonstrate a proof-of-concept selective surface flow membrane using either water/O₂ or water/N₂ through a membrane containing zeolite 4A. It may also be possible to develop this technology with a desirable gas pair, such as n-butane in hydrogen or n-butane in methane, using membranes containing HSSZ-13.

Finally, if mixed matrix membranes are to be economically feasible, they must be prepared as asymmetric hollow fibers. The preparation of hollow fibers differs significantly from that of dense films. The first major difference is encountered in dope formulation. Hollow fiber dopes contain some nonsolvent to assist in the spinodal decomposition that forms the underlying support layer. This adds to the number of components that can detrimentally affect transport through the zeolite. Hollow fiber dopes also tend to be more viscous, which makes dope preparation more difficult, but which should help stabilize the suspension once it is homogeneous. Another potential complication is that the dopes are subjected to significant shear stresses in the spinneret, which may lead to sieve agglomeration or migration. The biggest difference between dense films and hollow fibers is their corresponding formation methods. These will make the sieves within the matrix subject to different stresses during the formation process. First, the separation layer of the hollow fiber, which is equivalent to a dense film, forms in a fraction of a second. This allows less time for stresses that form in the matrix to relax, but it may also “freeze” the structure before debonding occurs. Which of these dominates must be determined. Another important difference is that hollow fibers are not prepared on a surface, so sieve-in-a-cage formation caused by inhibited in-plane contraction will be less of a concern. However, drawing of the fiber (to decrease its diameter) may cause tensile stresses on polymer – sieve interfaces, and this is potentially exacerbated by vitrification of the separation layer before the support layer. The support layer is formed by a phase separation process, and typically water is used to initiate phase separation. The drying conditions are also quite different, because the intricate hollow fiber morphology is typically considered too fragile to dry at elevated temperatures used for dense films. This will make it more difficult to completely remove solvents from the zeolites, especially with a hydrophilic zeolite if water is used to initiate phase separation. All of these complications need to be investigated, but this is not an exhaustive list. Nonetheless, spinning of mixed matrix hollow fibers is an important milestone that must be surpassed before mixed matrix technology can supplant some of the more traditional gas separation technologies.

8.3. REFERENCES

1. Okamoto, K.; K. Noborio; J. Hao; K. Tanaka; and H. Kita. *J. Membr. Sci.* 1997, 134, 171-179.
2. Ismail, A.F. and W. Lorna. *Seprn. Purification Tech.* 2002, 27, 173-194.
3. Sforca, M.L.; I.V.P. Yoshida; C.P. Borges; and S.P. Nunes. *J. Appl. Polym. Sci.* 2001, 82, 178-185.
4. Vankelecom, I.F.J.; E. Scheppers; R. Heus; and J.B. Uytterhoeven. *J. Phys. Chem.* 1994, 98, 12390-6.
5. Nunes, S.P.; J. Schultz; and K.V. Peinemann. *J. Matl. Sci. Lett.* 1996, 15, 1139-1141.
6. Staudt-Bickel, C. and W.J. Koros. *J. Membr. Sci.* 1999, 155, 145-154.
7. Wind, J.D.; C. Staudt-Bickel; D.R. Paul; and W.J. Koros. *Ind. Eng. Chem. Res.* 2002, 41, 6139-48.
8. Henis, J.M.S. and M.K. Tripodi. *J. Membr. Sci.* 1981, 8, 233-46.
9. Allcock, H.R. and F.W. Lampe, *Contemporary polymer chemistry*. 2nd ed. 1990, Englewood Cliffs, NJ: Prentice Hall.
10. Bianchi, F.; S. Cantagallo; G. Consolati; M. Laporta; M. Pegoraro; G. Tieghi; and L. Zanderighi. *J. Appl. Polym. Sci.* 2002, 86, 559-571.
11. Ekiner, O.M. and S.S. Kulkarni, Process for making hollow fiber mixed matrix membranes. US Patent No. 6,663,805. 2003.
12. Mahajan, R., Formation, characterization and modeling of mixed matrix membrane materials. Department of Chemical Engineering, University of Texas at Austin. 2000.

Appendix A. ESTIMATION OF THE CO₂/CH₄ TRANSPORT PROPERTIES OF ZEOLITE 4A

The calculation of the CO₂/CH₄ transport properties of zeolite 4A closely parallels the calculation of the O₂/N₂ transport properties by Zimmermann [1]. Data from the literature are used to determine the diffusion and sorption coefficients, which are multiplied to give the permeability. The activation energy for diffusion and preexponential factor are obtained from Yucel and Ruthven for CO₂ [2] and from Haq and Ruthven for CH₄ [3]. Sorption data for CO₂ in zeolite 4A at 50°C are reported by Yucel and Ruthven [2]. Sorption data near ambient temperatures for CH₄ are only available for the Henry's law region of the adsorption isotherm. Therefore, a Freundlich isotherm (50°C) reported by Harper et al is used to calculate CH₄ sorption [4]. The heats of sorption reported by Haq and Ruthven for CO₂ and CH₄ are used to scale the sorption isotherms to 35°C [3]. Sorption of pure CO₂ and pure CH₄ at 50°C in zeolite 4A from the aforementioned sources is shown in Figure A.1. These data compare well with experimental data shown in Figure 6.3. Note that the scale on the abscissa of this figure is only 0.4 atm, so CO₂ saturates the sieve at very low pressures.

It is necessary to pick a reference conditions for the calculation, since the sorption coefficient depends on pressure. A 50% CO₂ / 50% CH₄, each at 1 atm partial pressure is assumed, since this is the maximum pressure for the CH₄ sorption data. Using a higher reference pressure would result in a lower CO₂/CH₄ selectivity. Zimmermann used a mixed gas sorption isotherm to calculate the O₂/N₂ transport properties; however, this was not possible for the CO₂/CH₄ transport properties since a Langmuir fit of the CH₄ data is unavailable.

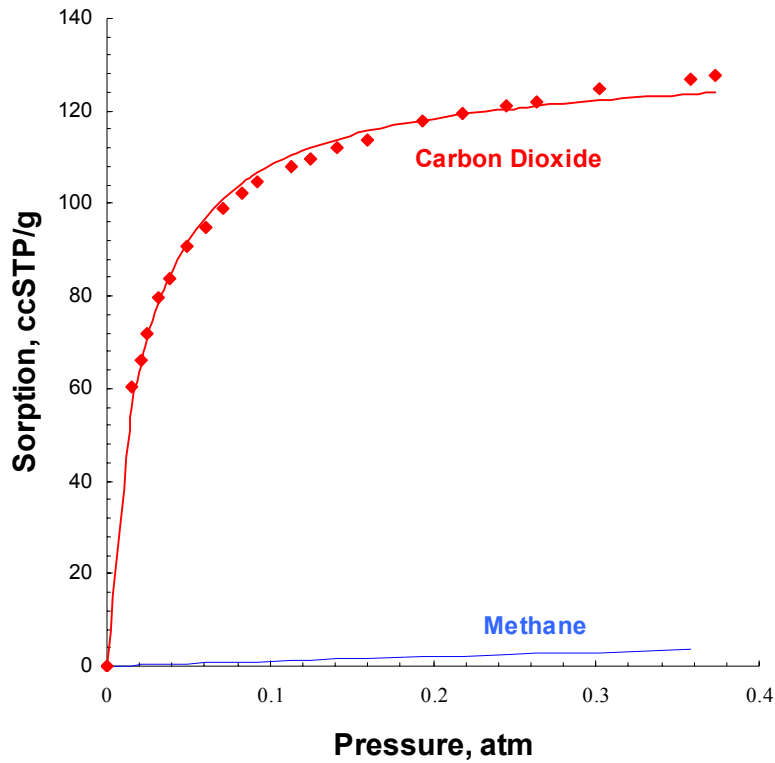


Figure A.1: Pure gas sorption isotherms for carbon dioxide and methane in zeolite 4A at 50°C. CO₂ isotherm is from [2] and CH₄ isotherm is from [4].

The calculated transport properties are summarized in Table A.1. As for the O₂/N₂ system, diffusion contributes more to the overall selectivity than sorption. There is some discrepancy in reported CH₄ diffusion coefficients, even within the same group. Using an alternative CH₄ diffusion coefficient reported by Yucel and Ruthven [5] gives a calculated selectivity of only 130.

Table A.1: Gas transport properties of zeolite 4A at 35°C (50/50 CO₂/CH₄ and 2 atm total pressure).

	P_{CO_2} Barrer	$\frac{P_{CO_2}}{P_{CH_4}}$	S_{CO_2} $\frac{cm^3STP}{cm^3 \cdot atm}$	$\frac{S_{CO_2}}{S_{CH_4}}$	D_{CO_2} $\frac{cm^2}{s}$	$\frac{D_{CO_2}}{D_{CH_4}}$
4A	15	340	100	7.8	1.2×10^{-9}	43

It is also possible to estimate the transport properties using the data measured for this work (Figure 6.3 and Table 6.2). Using the same assumption of a feed consisting of CO₂ at 1 atm of CH₄ at 1 atm, the calculated S_{CO₂}/S_{CH₄} using the experimental data is 8.5 (corresponding to a CO₂/CH₄ selectivity of 370). This is similar to the value derived from the literature in Table A.1. Allowing a more realistic 10% CO₂ / 90% CH₄ feed at 1000 psi total pressure, the calculated S_{CO₂}/S_{CH₄} is 4.3 (corresponding to a CO₂/CH₄ selectivity of 190), where the multicomponent Langmuir equation has been used to account for competition. This illustrates the significant effect of partial pressures on the selectivity of the CO₂/CH₄ system in zeolites. Nonetheless, for selectivities above ~100, most of the methane is already forced to permeate through the polymer phase (for a well matched polymer – sieve combination), so increasing sieve selectivities have little effect on the overall mixed matrix membrane selectivity.

REFERENCES

1. Zimmerman, C.M.; A. Singh; and W.J. Koros. *J. Membr. Sci.* 1997, 137, 145-154.
2. Yucel, H. and D.M. Ruthven. *J. Colloid Interface Sci.* 1980, 74, 186-95.
3. Haq, N. and D.M. Ruthven. *J. Colloid Interface Sci.* 1986, 112, 154-63.
4. Harper, R.J.; G.R. Stifel; and R.B. Anderson. *Can. J. Chem.* 1969, 47, 4661-9.
5. Yucel, H. and D.M. Ruthven. *J. Chem. Soc., Faraday Trans. 1* 1980, 76, 60-70.

Appendix B. REACTION OF SILANE COUPLING AGENTS WITH POLYMERS AND ZEOLITES

Silanation of the zeolite surface to improve adhesion with polyimides for membrane applications has been suggested by many researchers [1-6]. Silanation is a well known technique for improving the compatibility of organic – inorganic composites [7, 8]. This appendix reviews information regarding the reaction of silane coupling agents with zeolites or silica and of aminosilane coupling agents with polyimides, including work done by Alexis Hillock of the research group to prove the reaction between aminosilanes and polyimides. The reaction that occurs between silanol (or aluminol) groups on the zeolite surface and between the amine end of the silane and a polyimide is shown in Figure B.1.

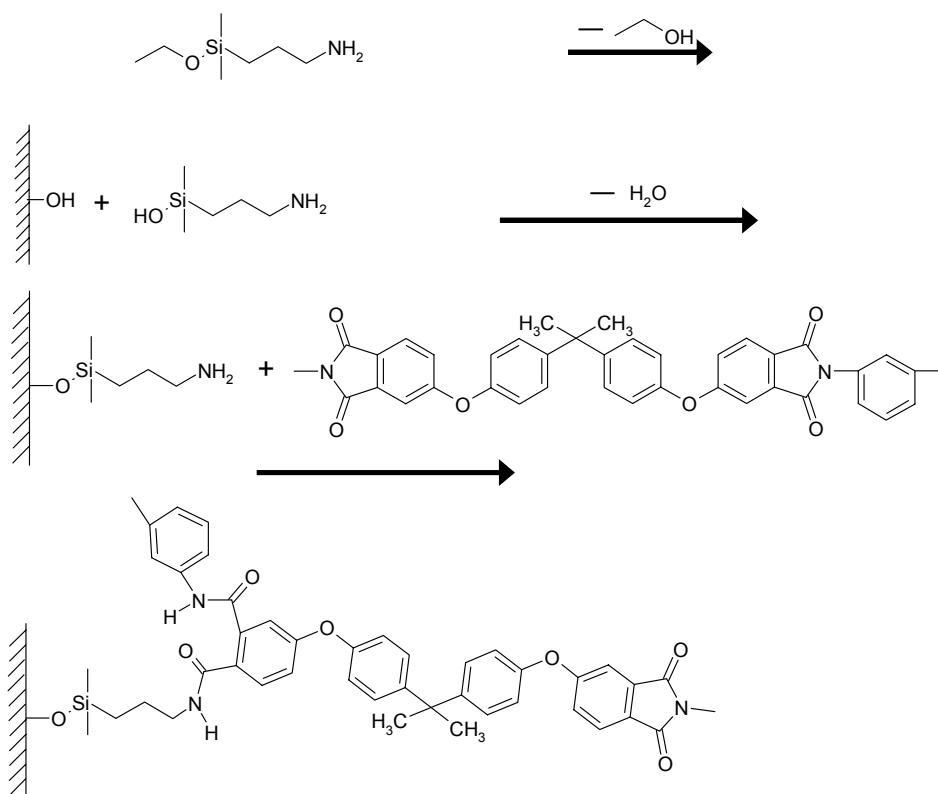


Figure B.1: Reaction of γ -aminopropyltrimethoxysilane with zeolite silanol groups and with imide groups (i.e. Ultem[®]).

The reaction of γ -aminopropyldimethylethoxysilane (APDMES), or its close analog, γ -aminopropyltriethoxysilane (APTES), has been studied extensively in the literature. Researchers have also used model compounds to probe this reaction. White and Tripp used methoxymethylsilanes to probe the reaction of silane coupling agents with silica surfaces [9]. At room temperature, these methoxymethylsilanes form hydrogen bonds with the surface, but even the most reactive species, $(\text{CH}_3\text{O})_4\text{Si}$, does not react with the surface at room temperature. At 150°C , the methoxy groups have reacted with the surface. These researchers also found that the amino end of APDMES competes with its ethoxy group to form hydrogen bonds with available silanols on the surface [10]. The amino group forms stronger hydrogen bonds with the surface than the alkoxy group. As chemisorption occurs, hydrogen bonded ethoxy groups are replaced with reacted species, but hydrogen bonded amine groups remain on the surface. They attempted to use a stronger base (triethanolamine) to prevent hydrogen bonding of the amine end, without success. Conversely, Kanan, Tze, and Tripp report that hydrogen bonding by the amine end can be prevented by preadsorbing ethylenediamine [11]. The EDA is then replaced as silane alkoxy groups react with the surface.

The pH of the silanation solution is also an important consideration when silanating from a solution. Work by the Tripp group detailed above was done in the gas phase. Plueddemann reports that the most favorable silanation condition is the isoelectric point of the zeolite [7]. This optimizes the attachment of the silane, while minimizing the interaction of the amine end of the silane. On the other hand, Suryanarayana and Mittal report that applying APTES to a silicon wafer at the “natural” pH of the aqueous silane solution (8.0) gives the best adhesion to polyimides [12], so there is some disagreement on the optimal silanation conditions.

The reaction between the polyimides and silanated surfaces is difficult to study directly, so probe molecules have been used to study various aspects of this reaction. Anshel and Murphy used ^{15}N labeled APTES to demonstrate that a bond forms between the amine

end of the silane and polyimides (as well as amic acids, amic esters, and isoimides) [13]. Linde reported that the presence of excess APTES caused chain scission of the polyimide because the alkyimide is the thermodynamically stable product (compared to the aromatic polyimide) [14]. It was unclear whether this also occurred on the surface since the polyimide is less flexible. Reacting the poly(amic acid) precursor of a polyimide with the silane is also possible [12-16]. This will result in chain scission of the polymer [14, 16], which can be beneficial or detrimental. The increased flexibility of the lower molecular weight scission products allow the interface to tolerate higher stress, but they also decrease its cohesive strength [16]. Chain scission can be prevented by using an N-methyl silane [16].

In the case of mixed matrix membranes, chain scission may be tolerable so long as the polymer remains on the surface. NMR spectroscopy performed by Alexis Hillock verified the reaction of Ultem[®] with APDMES. This was done by analyzing the peaks formed upon heating a solution of 15 wt% Ultem[®] and 2 wt% APDMES in deuterated NMP to 150°C for 4 hours. Two control samples of 15 wt% Ultem[®] in NMP and 2 wt% APDMES in NMP were also analyzed. The solution with both Ultem[®] and APDMES (Figure B.2) had peaks (at ~7.1 and 7.25 ppm) that were not present in either of the control samples (e.g. Figure B.3 for Ultem[®]). These peaks are attributed to shifting of the protons on the benzene ring attached to the reacted imide ring within Ultem[®]. Furthermore, new peaks also arise (highlighted in green of Figure B.3) that are attributed to newly formed N – H bonds in the imide and an altered N – H bond in APDMES. This is all evidence that APDMES has indeed reacted with Ultem[®] at 150°C.

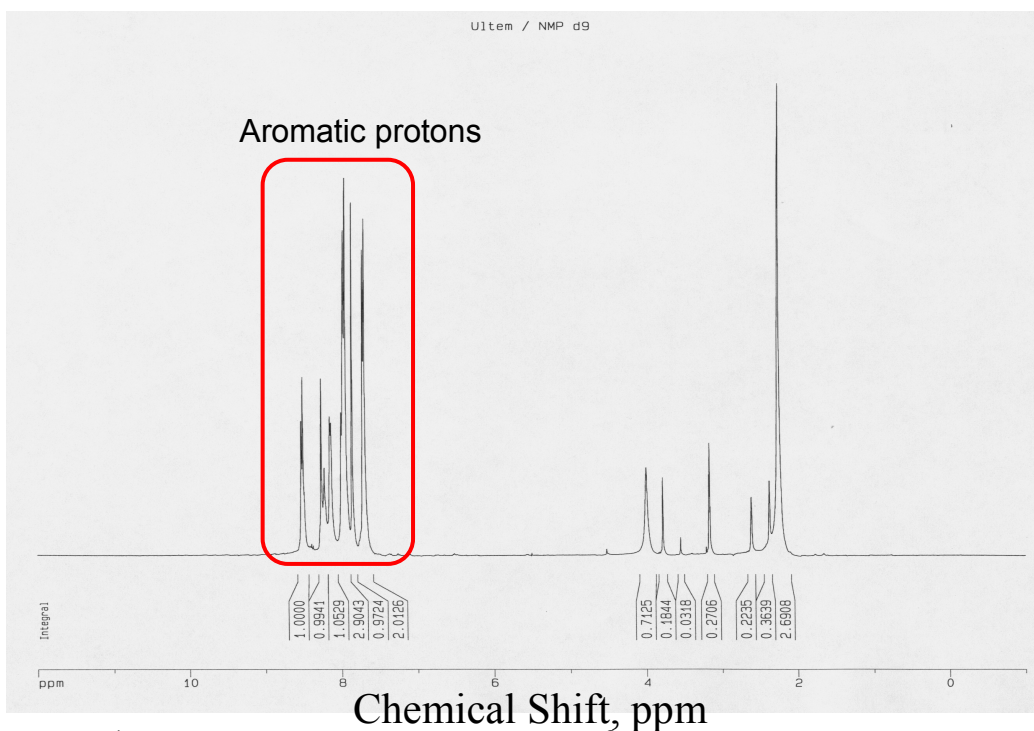


Figure B.2: ^1H -NMR spectrum of ~ 15 wt% Ultem[®] / 2 wt% APDMES in NMP.

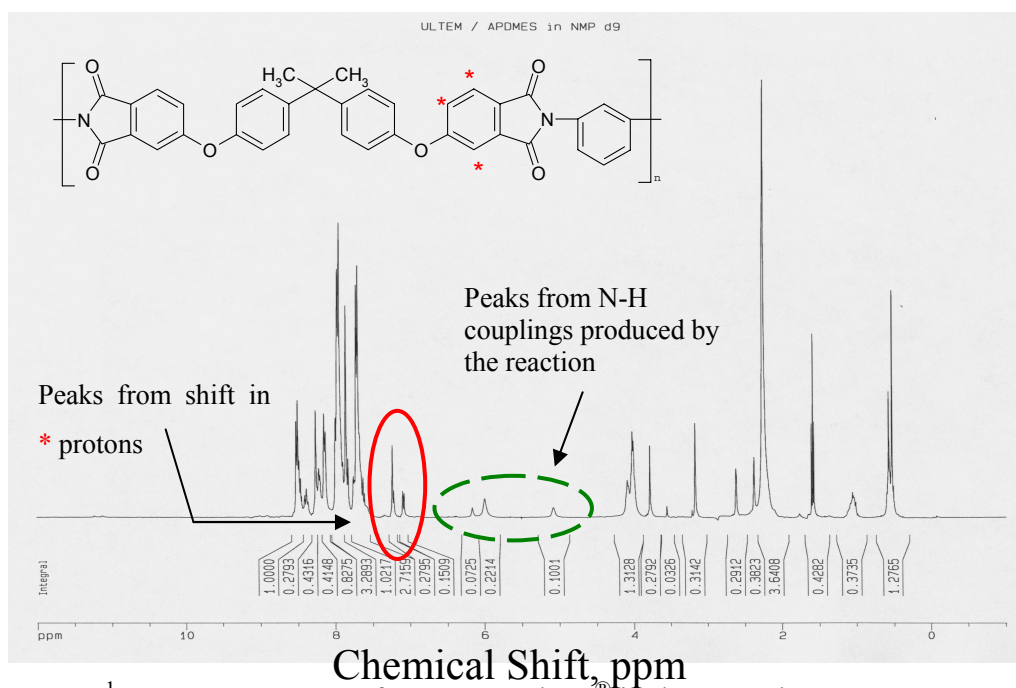


Figure B.3: ^1H -NMR spectrum of ~ 15 wt% Ultem[®] in deuterated NMP.

REFERENCES

1. Vankelecom, I.F.J.; S. Van den Broeck; E. Merckx; H. Geerts; P. Grobet; and J.B. Uytterhoeven. *J. Phys. Chem.* 1996, 100, 3753-8.
2. Marand, E.; C.J. Cornelius; P. Meakin; and A.J. Hill. *Polym. Matl. Sci. and Engr.* 2001, 85, 297-298.
3. Joly, C.; S. Goizet; J.C. Schrotter; J. Sanchez; and M. Escoubes. *J. of Membr. Sci.* 1997, 130, 63-74.
4. Sysel, P.; M. Frycova; R. Hobzova; V. Krystl; P. Harabanek; B. Bernauer; L. LBrabec; and M. Kocirik. Impact of zeolites and other porous materials on the new technologies at the beginning of the new millennium, part b. In: *Stud. Surf. Sci. Catal.*, 2002; 142b. in 2nd International FEZA (Federation of the European Zeolite Association) Conference. 2002. Taormina, Italy: Elsevier.
5. Mahajan, R. and W.J. Koros. *Polym. Engr. and Sci.* 2002, 42, 1420-1431.
6. Mahajan, R. and W.J. Koros. *Polym. Engr. and Sci.* 2002, 42, 1432-1441.
7. Plueddemann, E.P., *Silane coupling agents*. 1982, New York: Plenum Press. 235
8. Ahmad, Z. and J.E. Mark. *Chemistry of Materials* 2001, 13, 3320-3330.
9. White, L.D. and C.P. Tripp. *J. Colloid Interface Sci.* 2000, 224, 417-424.
10. White, L.D. and C.P. Tripp. *J. Colloid Interface Sci.* 2000, 232, 400-407.
11. Kanan, S.M.; W.T.Y. Tze; and C.P. Tripp. *Langmuir* 2002, 18, 6623-6627.
12. Suryanarayana, D. and K.L. Mittal. *J. of Appl. Polym. Sci.* 1984, 29, 2039-43.
13. Ansel, M. and P.D. Murphy. *J. Adhesion Sci. Tech.* 1994, 8, 787-806.
14. Linde, H.G. *J. Polym. Sci., Polym. Chem. Ed.* 1982, 20, 1031-41.
15. Xenopoulos, C.; L. Mascia; and S.J. Shaw. *Journal of Matl. Chem.* 2002, 12, 213-218.
16. Greenblatt, J.; C.J. Araps; and H.R. Anderson, Jr., Aminosilane-polyimide interactions and their implications in adhesion, in *Polyimides: Synthesis, characterization, and applications* [Proceedings of the technical conference on polyimides]. 1984. p. 573-88.

Appendix C. COMPRESSIBILITY FACTORS OF THE GASES USED IN THIS WORK

The compressibility factors are needed for the mole balance to determine the sorbed concentration using pressure decay sorption (section 3.4.2.2). The equations for compressibility factors at 35°C for the gases used in this work are given below. They were taken from Zimmerman [1], who used a least squares routine to fit compressibility factors calculated using the DDMIX program available from the National Institute of Standards and Technology.

$$\text{O}_2: z = 1 - \frac{3.635 \times 10^{-5}}{\text{psia}} P + \frac{4.757 \times 10^{-9}}{\text{psia}^2} P^2 + \frac{1.132 \times 10^{-12}}{\text{psia}^3} P^3 \quad (\text{C.1})$$

$$\text{N}_2: z = 1 - \frac{8.589 \times 10^{-6}}{\text{psia}} P + \frac{1.078 \times 10^{-8}}{\text{psia}^2} P^2 - \frac{1.066 \times 10^{-13}}{\text{psia}^3} P^3 \quad (\text{C.2})$$

$$\text{CO}_2: z = 1 - \frac{2.846 \times 10^{-4}}{\text{psia}} P - \frac{2.006 \times 10^{-7}}{\text{psia}^2} P^2 + \frac{2.60 \times 10^{-10}}{\text{psia}^3} P^3 - \frac{2.154 \times 10^{-13}}{\text{psia}^4} P^4 \quad (\text{C.3})$$

$$\text{CH}_4: z = 1 - \frac{1.049 \times 10^{-4}}{\text{psia}} P + \frac{3.818 \times 10^{-9}}{\text{psia}^2} P^2 + \frac{5.202 \times 10^{-12}}{\text{psia}^3} P^3 \quad (\text{C.4})$$

REFERENCE

1. Zimmerman, C.M., Advanced gas separation membrane materials: Hyper rigid polymers and molecular sieve-polymer mixed matrixes. Department of Chemical Engineering, University of Texas at Austin. 1998.

Appendix D. DISCUSSION OF A MORE RIGOROUS METHOD TO CHARACTERIZE POLYMER-SIEVE THERMODYNAMICS

In section 4.3.2, the importance of acid-base interactions between the polymer and the sieve is discussed. Polymer – sieve pairs with higher enthalpies of acid-base adduct formation (ΔH_{AB}) or works of adhesion (W_A) may be able to tolerate higher stresses, and therefore be less likely to form sieve-in-a-cage morphology. This appendix summarizes several equations that calculate these quantities. Unfortunately, tabulations of the parameters in these equations do not exist for the materials in this work, and in many cases they are nontrivial to measure.

Fowkes used a tabulation of parameters correlating acid-base strength prepared by Drago [1, 2]. These parameters correlate electrostatic (E_A and E_B) and covalent (C_A and C_B) contributions to the enthalpy of acid-base adduct formation, as given by the following equation:

$$-\Delta H^{AB} = C_A C_B + E_A E_B \quad (D.1)$$

These heats of interaction can be determined by calorimetry, ellipsometry, or contact angle measurements [3, 4]. However, these measurements are more suited to solutions rather than surface adhesion. Nonetheless, there are reports of E_A ($4.36 \text{ (kcal/mol)}^{1/2}$) and C_A ($1.08 \text{ (kcal/mol)}^{1/2}$) for silica surfaces [5] and for E_A ($2.1 \text{ (kcal/mol)}^{1/2}$), C_A ($0.27 \text{ (kcal/mol)}^{1/2}$), E_B ($1.6 \text{ (kcal/mol)}^{1/2}$) and C_B ($1.5 \text{ (kcal/mol)}^{1/2}$) for a “6F polyimide” surface [3]. This gives a ΔH^{AB} of -7.5 kcal/mol for 6F polyimide onto silica. The polymer shows both acidic and basic character. This has also been noted by Fowkes [5]. However, this absolute value is not particularly useful given in absence of comparative ΔH_{AB} values, which are not available for other polymers used here.

These ideas can also be expressed using the thermodynamic principle of the work of adhesion, which characterizes the work per unit area required to create new surface area

between two dissimilar materials [6]. Closely related is the work of cohesion, which characterizes the work per unit area required to create new surface area between two identical materials. The work of adhesion can be expressed in terms of surface energies, γ , using the DuPré equation:

$$W_A = \gamma_P + \gamma_S - \gamma_{PS} \quad (D.2)$$

where the subscript P refers to the polymer, S to the sieve, and PS to the polymer – sieve interface. Surface energies can be derived from contact angle measurements using the Young equation:

$$\gamma_{SL} = \gamma_S - \gamma_L \cos \theta + \pi_E \quad (D.3)$$

where the subscript S refers to a solid, L to a liquid, and SL to the solid – liquid interface. The equilibrium spreading pressure, π_E , is reportedly negligible for contact angles larger than 10° [7].

Typically, the work of adhesion has accounted for dispersive interactions only. This corresponds to the solubility parameter treatment of Hildebrand, where solubility occurs for materials with similar solubility parameters (i.e. like dissolves like). The solubility parameters of alumina and silica have both been estimated to be $32 \text{ mPa}^{1/2}$ [8]. This could be used as an approximate value for the two molecular sieves together with solubility parameters for the polymer, either experimental or from group contribution methods, to correlate with observed mixed matrix morphology. Based on solubility parameters, the most compatible of the polymers in Table 4.3 with the zeolites are Ultem[®] and Matrimid[®], while the least compatible is PVAc. In contrast, the observed transport properties and SEMs for membranes prepared with these materials indicate that PVAc is well adhered to the zeolite while Ultem[®] and Matrimid[®] are not. This may indicate the peril of neglecting specific interactions or simply the lesser importance of polymer – sieve affinity compared to flexibility during membrane formation.

Good, van Oss, and Chaudhury recognized that potential acid-base interactions need to be accounted for [9, 10], and it appears such strong interactions may be helpful for the formation of successful mixed matrix membranes. They proposed the following equation for the work of adhesion:

$$W_A = 2\left(\sqrt{\gamma_P^D \gamma_S^D} + \sqrt{\gamma_P^+ \gamma_S^-} + \sqrt{\gamma_P^- \gamma_S^+}\right) \quad (\text{D.4})$$

Here, γ^+ is a measure of the electron-acceptability and γ^- is a measure of the electron-donicity, *relative to water*. Water is assigned arbitrary γ^+ and γ^- of 25.5 mJ/m² [11]. Because these values are taken relative to an assumed reference state for water, the absolute values are meaningless, but the product $\gamma^+ \times \gamma^-$ is a measure of the contribution of acid-base interactions to the surface energy.

The parameters γ^+ and γ^- for polymers and sieves can be determined in several ways. These include the measurement of contact angles on surfaces with various probe liquids, inverse gas chromatography, determination of the change in binding energy with various adsorbed probe molecules using x-ray photoelectron spectroscopy, and microcalorimetry [3, 9, 12, 13]. However, these methods are nontrivial and some suffer from poor accuracy (i.e. the contact angle method), and there is no universally accepted method for determination of the parameters. Current research in this area seeks a viable method to accurately characterize acid-base interactions, so this can not yet serve as a predictive tool for mixed matrix membrane properties.

REFERENCES

1. Drago, R.S.; G.C. Vogel; and T.E. Needham. J. Am. Chem. Soc. 1971, 93, 6014-26.
2. Drago, R.S.; L.B. Parr; and C.S. Chamberlain. J. Am. Chem. Soc. 1977, 99, 3203-9.
3. Filippov, L. Colloid Polym. Sci. 1994, 272, 1043-55.

4. Dilsiz, N. and J.P. Wightman. *Colloids and Surfaces, A: Physicochemical and Engr. Aspects* 2000, 164, 325-336.
5. Fowkes, F.M. *Rubber Chem. Technol.* 1984, 57, 328-43.
6. Israelachvili, J.N., *Intermolecular and surface forces.* 2 ed. 1992, San Diego, CA: Academic Press Inc.
7. Chang, W. and X. Qin, "repulsive acid-base interactions": Fantasy or reality, in *Acid-base interactions*, K. Mittal, Editor. 2000, VSP: Utrecht, Netherlands. p. 3-53.
8. Schoenmakers, P.J.; H.A.H. Billiet; and L. De Galan. *Chromatographia* 1982, 15, 205-14.
9. Van Oss, C.J.; M.K. Chaudhury; and R.J. Good. *Chem. Rev.* 1988, 88, 927-41.
10. Good, R.J., On the acid/base theory of contact angles, in *Acid-base interactions*, K. Mittal, Editor. 2000, VSP: Utrecht, Netherlands. p. 167-171.
11. van Oss, C., Irrelevance of the ratio of the electron-acceptivity to the electron-donicity of water with respect to the determination of polar surface tension components, interfacial tensions and free energies of interaction of liquid and/or solids, in *Acid-base interactions*, K. Mittal, Editor. 2000, VSP: Utrecht, Netherlands. p. 181-196.
12. Chehimi, M.M.; E. Cabet-Deliry; A. Azioune; and M.-L. Abel. *Macromolecular Symposia* 2002, 178, 169-181.
13. Volpe, C.D. and S. Siboni, Troubleshooting of surface free energy acid-base theory applied to solid surfaces: The case of good, van oss and chaudhury theory, in *Acid-base interactions*, K. Mittal, Editor. 2000, VSP: Utrecht, Netherlands. p. 55-90.

Appendix E. PROOF OF HIGHER STRESS IN THE POLYMER AT THE CENTER OF TWO VERTICAL PARTICLES AFTER SOLVENT EVAPORATION

This appendix will show that a more compressive stress exists in the polymer at the central axis between two vertically adjacent particles that have moved toward one another during solvent evaporation. This will complicate the stress distribution on the surface of the particles. In a mixed matrix membrane, this will be manifested as a normal compressive stress on the particle perpendicular to the casting substrate. Coupled with the normal tensile stress on the particle parallel to the substrate, a shear stress will develop on the surface towards the plane parallel with the casting substrate through the center of the particle. This may cause a failure of the polymer – sieve interface earlier than predicted if only the tensile stress caused by inhibited contraction is considered.

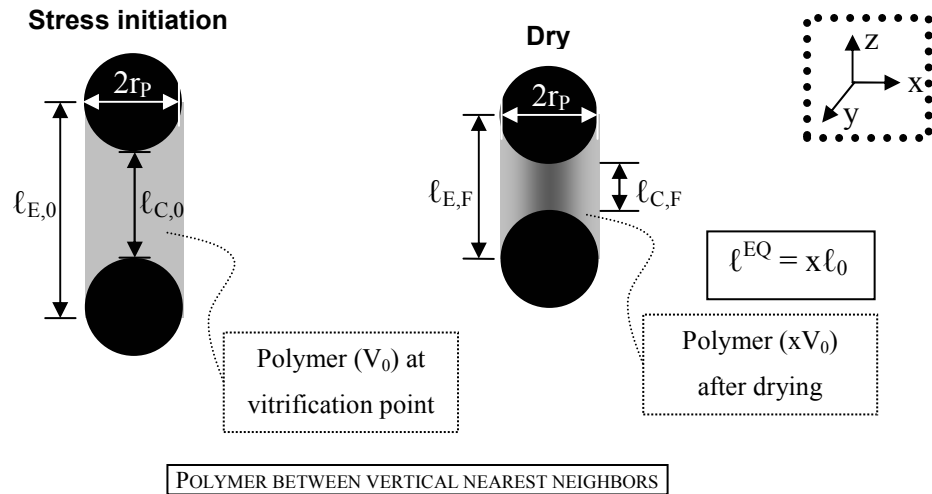


Figure E.1: Geometry of polymer between two vertically aligned particles before and after solvent evaporation for an initially vitrified state.

The following expressions are based on the geometry shown in Figure E.1:

- for the length of the polymer between the particles as a function of distance from the central axis between the two vertically adjacent particles

$$\ell(r) = \ell_E - 2\sqrt{(r_p^2 - r^2)} \quad (\text{E.1a})$$

$$\text{and at the center (r = 0)} \quad \ell_C = \ell_E - 2r_p \quad (\text{E.1b})$$

- for the volume before and after the polymer contracts (where 0 denotes “initial” and F denotes “final”)

$$V_0 = \pi r_p^2 \ell_{E,0} - \frac{4\pi r_p^3}{3} \quad (\text{E.2})$$

$$V_F = \pi r_p^2 \ell_{E,F} - \frac{4\pi r_p^3}{3} \quad (\text{E.3})$$

If the volume contracts by a factor (1-x) when the solvent evaporates, $V_F = xV_0$. Solving Eq E.2 and Eq E.3 for $\ell_{E,0}$ and $\ell_{E,F}$ and taking their ratio gives:

$$\frac{\ell_{E,F}}{\ell_{E,0}} = \frac{\frac{xV_0}{\pi r_p^2} + \frac{4r_p}{3}}{\frac{V_0}{\pi r_p^2} + \frac{4r_p}{3}} \quad (\text{E.4})$$

Further, using (E.1b):

$$\frac{\ell_{C,F}}{\ell_{C,0}} = \frac{\frac{xV_0}{\pi r_p^2} + \frac{4r_p}{3} - 2r_p}{\frac{V_0}{\pi r_p^2} + \frac{4r_p}{3} - 2r_p} = \frac{\frac{xV_0}{\pi r_p^2} - \frac{2r_p}{3}}{\frac{V_0}{\pi r_p^2} - \frac{2r_p}{3}} \quad (\text{E.5})$$

Comparing (E.4) and (E.5), it is clear that $\frac{\ell_{E,F}}{\ell_{E,0}} \neq \frac{\ell_{C,F}}{\ell_{C,0}}$ unless $V_0 = 0$, $V_0 = \infty$, $r_p = 0$, $r_p =$

∞ , or $x = 1$. The cases of $V_0 = 0$, $V_0 = \infty$, and $r_p = \infty$ are physically unrealistic. The case of $r_p = 0$ is uninteresting since this indicates the absence of particles. Finally $x = 1$ means that no contraction occurred.

It can be shown mathematically that $\frac{\ell_{E,F}}{\ell_{E,0}} > \frac{\ell_{C,F}}{\ell_{C,0}}$ for $(0 \leq x < 1)$, indicating the polymer at the central axis of the particles will be compressed more than polymer at the edge.

The stress in the material will be proportional to the difference between the actual length after contraction and the equilibrium length after contraction. The equilibrium length, ℓ^{EQ} , will be $x\ell_0$. If the material is Hookean, the stress will be proportional to $\Delta\ell/\ell$ where $\Delta\ell$ is the difference between the final and *equilibrium* lengths (and not between the final and initial lengths). Then, one can look at the inequality between the stresses at the center versus the edge of the polymer cylinder between the two spheres:

$$\begin{aligned} K\left(\frac{\ell_{E,F}}{\ell^{EQ}} - 1\right) &= K\left(\frac{\ell_{C,F}}{\ell^{EQ}} - 1\right) \\ \left(\frac{\ell_{E,F}}{x\ell_{E,0}}\right) &= \left(\frac{\ell_{E,F} - 2r_p}{x(\ell_{E,0} - 2r_p)}\right) \\ x\ell_{E,F}(\ell_{E,0} - 2r_p) &= x(\ell_{E,F} - 2r_p)\ell_{E,0} \\ -2xr_p\ell_{E,F} &> -2xr_p\ell_{E,0} \text{ since } \ell_{E,F} < \ell_{E,0} \end{aligned}$$

This means that the polymer at the central axis between the two particles will be more compressed than the polymer connecting the outside edges of the two particles.

Appendix F. DEVELOPMENT OF MORE COMPLEX MIXED MATRIX MEMBRANE TRANSPORT PROPERTY MAPS

In Chapter 5, transport property maps were developed for the O₂/N₂ separation through Ultem[®] – zeolite 4A and Ultem[®] – HSSZ-13 membranes. The simple transport property maps shown in Figure 5.1 and Figure 5.2 assume constant selectivities in the nonideal morphology regions. These assumptions are relaxed in this appendix. The potential for two different nonideal morphologies is also modeled.

It is quite plausible that both permeability and selectivity of zeolites are reduced as contaminants sorb into them. The primary selective mechanism of the zeolites used in this work is diffusion through the pore windows. Thus, any molecule that selectively sorbs into this window could significantly affect the selectivity. In section 7.2.3, it was suggested that water may preferentially associate with the sodium ions in zeolite 4A. The effects of subtle changes in the pore window caused by different counterions are well known. In zeolite 4A, sodium ions partially occlude the pores [1]. If the ion is exchanged to calcium (zeolite 5A), less of the pore window is occluded, and the selectivity decreases significantly. On the other hand, if the larger potassium ion is used (zeolite 3A), the zeolites are impermeable to both oxygen and nitrogen. A sorbed contaminant associated with an ion in the pore window could also cause a subtle change in the pore size or shape that may significantly affect the transport properties.

The energetic and entropic contribution to the selectivity of oxygen over nitrogen in zeolite 4A was analyzed by Singh [2, 3]. Oxygen diffuses faster through the pore because it has two rotational degrees of freedom in the window, whereas nitrogen can not rotate in the pore. If the size of the pore window is altered slightly, the entropic selectivity of diffusion may change appreciably. The entropic selectivity of diffusion for penetrant A over penetrant B is given by the following equation:

$$\frac{D_A}{D_B} = \mathbf{exp}\left(\frac{S_{DA}^\ddagger - S_{DB}^\ddagger}{R}\right) = \left(\frac{F_A^\ddagger / F_A}{F_B^\ddagger / F_B}\right) \quad (\text{F.1})$$

where S_D^\ddagger is the activation energy of diffusion and F^\ddagger and F are the total partition functions in the transition and normal states, respectively. The partition functions are related to the number of allowed states for the molecule (i.e. more allowed states equate to a higher partition function). The total partition function is the product of the translational, rotational, vibrational, and electronic partition functions. The electrons all exist in the ground state except at elevated temperatures, so the electronic partition function is one. Equations for the other three partition functions are given below.

$$F_{trans} = \left(\frac{2\pi mkT}{h^2}\right)^{\frac{n_{trans}}{2}} a^{n_{trans}} \quad (\text{F.2})$$

$$F_{rot} = \left(\frac{8\pi^2 IkT}{h^2}\right)^{\frac{n_{rot}}{2}} \quad (\text{F.3})$$

$$F_{vib} = \left(\frac{\mathbf{exp}\left(-h\nu/2kT\right)}{1 - \mathbf{exp}\left(-h\nu/kT\right)}\right)^{n_{vib}} \quad (\text{F.4})$$

The parameters in these three equations are explained in Table F.1. Values compiled by Singh [2] are also duplicated. The degrees of freedom in the normal and transition states are discussed in the following paragraph.

Table F.1: Parameters and values used to calculate the partition functions in Eq F.2 Eq F.3, and Eq F.4 [2, 4-6].

Variable	Definition	Value
m	Molecule mass	O ₂ : 5.31×10^{-23} g N ₂ : 4.65×10^{-23} g
k	Boltzmann's constant	1.38×10^{-23} J/K
T	Temperature	308 K
h	Plank's constant	6.626×10^{-34} J-s
n_{trans}	Translational degrees of freedom	O ₂ , normal: 3 O ₂ , transition: 0 N ₂ , normal: 3 N ₂ , transition: 0
n_{rot}	Rotational degrees of freedom	O ₂ , normal: 2 O ₂ , transition: 0 to 2 N ₂ , normal: 2 N ₂ , transition: 0
n_{vib}	Vibrational degrees of freedom	O ₂ , normal: 1 O ₂ , transition: 1 to 3 N ₂ , normal: 1 N ₂ , transition: 3
a	Length of cubic cavity in which the particle is confined	Normal state: 11.2 Å Transition state: 3.8 Å
I	Moment of inertia	Lumped with θ_{rot}
ν	Frequency of vibration (at 300 K)	O ₂ : 2.0×10^{-12} s ⁻¹ N ₂ : 2.6×10^{-12} s ⁻¹
$\theta_{rot} = h^2/8\pi^2Ik$	Lumped Parameter	O ₂ : 2.07 K N ₂ : 2.88 K

A molecule comprised of N atoms has 3N degrees of freedom. These correspond to the number of coordinates (i.e. x, y, and z) required to specify the position of each atom. Every molecule in the normal state has 3 translational degrees of freedom (i.e. x-, y-,

and z-directions). Polyatomic molecules have 3 rotational degrees of freedom, while linear molecules have only 2 because of symmetry. This leaves $3N-5$ and $3N-6$ vibrational modes for linear and nonlinear polyatomic molecules, respectively. Therefore, oxygen and nitrogen each have 3 translational, 2 rotational, and 1 vibrational degrees of freedom in the normal state. The position of the center of mass of the molecule is fixed in the transition state, so the molecule has no translational degrees of freedom. (Also, translations in the y- and z-directions are not allowed because of the pore structure.) Vibration of both oxygen and nitrogen is unhindered in the transition state, so they each retain the vibrational degree of freedom from their respective normal states. In zeolite 4A, the pore is unable to hinder the rotation of oxygen, so it also retains both rotational degrees of freedom in the transition state. On the other hand, the pore hinders complete rotation of nitrogen in the transition state, so these modes become additional vibrational modes. Thus, oxygen has 0, 2, and 1, while nitrogen has 0, 0, and 3 translational, rotational, and vibrational degrees of freedom in the transition state for a “normal” zeolite 4A pore.

If there is a small molecule associated with the sodium ion in zeolite 4A that further occludes the pore, the number of rotational degrees of freedom for oxygen would decrease to 1 or 0, adding 1 and 2 vibrational degrees of freedom. However, the small molecule may not saturate all the available ion sites until it reaches a certain concentration. Thus, there would be a distribution of pores, with and without the additional occlusion of the small molecule. Therefore, while it is not possible for an individual pore to have a noninteger number of degrees of freedom, it is possible for the zeolite as a whole, to have *on average* a noninteger number of degrees of freedom. The permeability and selectivity in a “reduced oxygen permeability zeolite” would then both decrease continuously as the rotational degrees of freedom of oxygen in the pore decrease from 2 to 0 (with commensurate increase in the associated vibrational degrees of freedom.) There is no change in the degrees of freedom of nitrogen caused by this additional small molecule occlusion, so its degrees of freedom remain the same as in the

transition state of “normal” zeolite 4A. When the number of rotational degrees of freedom of oxygen reaches zero, the zeolite has oxygen permeability of 0.053 Barrer and O₂/N₂ selectivity of 2.54. This low selectivity is the result of the limited ability of the pore to discriminate between two molecules with the same number of translational, rotational, and vibrational degrees of freedom. Furthermore, zeolite 4A is actually sorption selective for nitrogen, and this further hampers the O₂/N₂ selectivity. The O₂/N₂ selectivity was assumed constant as the oxygen permeability decreases beyond 0.053 Barrer. This explains the minimum in the “reduced oxygen permeability zeolite” curve on Figure 5.16.

There may be an important difference between the case above, where a small molecule modifies the pore size of zeolite 4A, and the effect of larger penetrants. Larger penetrants, such as n-butane, may not significantly affect the diffusion selectivity of two gases (i.e. CO₂/CH₄ selectivity). First, such molecules may be more likely to predominantly occupy the cage rather than the pore, and this would not affect the transition state in the manner discussed above. Second, if such a large molecule occludes the pore, it is unlikely that either gas can diffuse around it, so this would not cause reduced selectivity either. Thus, the primary effect of larger contaminants on the sieve may simply be reduced permeability.

For regions of the matrix that exhibit decreased (matrix rigidification) or increased permeability (stress dilated), the selectivity is likely different than the bulk matrix. The underlying cause of altered permeability in the matrix rigidification and stress dilated regions is believed to be a difference in fractional free volumes from the bulk polymer. Gas permeabilities are a function of the fractional free volume (FFV) of a polymer. Park and Paul developed correlations for the gas permeabilities of polymers as a function of their fractional free volume [7]. These correlations take the form shown in the following equation:

$$P = A \exp\left(\frac{-B}{FFV}\right) \quad (\text{F.5})$$

where A and B are empirical constants. This correlation is plotted as the red curve on Figure F.1. For oxygen, A and B are 397 and 0.839, respectively, while these quantities are 112 and 0.914 for nitrogen. Thus, one possibility is to use this correlation to estimate the dependence of the matrix rigidification and stress dilated regions (i.e. when $\beta \neq 1$ in Eq 2.14). However, the properties of neat Ultem[®] are not fit well by this curve. In order to account or the permeability of Ultem[®] as its FFV changes slightly, it seems reasonable to force to Park-Paul correlation to go through the transport properties corresponding to neat Ultem[®], assuming the slope is unchanged. This is shown as the dashed red curve on Figure F.1, and has the functional form given below:

$$\alpha_{O_2/N_2} = \frac{P_{O_2}}{\frac{\frac{P_{O_2}^{\circ}}{a_{O_2/N_2}^{\circ}}}{\exp\left(\frac{-B_{N_2}}{FFV^{\circ}}\right)} \exp\left[\frac{-B_{N_2}}{-B_{O_2}} \ln\left(\frac{P_{O_2}}{\frac{P_{O_2}^{\circ}}{\exp\left(\frac{-B_{O_2}}{FFV^{\circ}}\right)}}\right)\right]} \quad (\text{F.6})$$

where the “^o” superscript indicates the properties of neat Ultem[®]. There is one problem with using this modified Park-Paul FFV dependent curve. Neat Ultem[®] has a FFV of 0.150 [7]. Above ~25 Barrer (O₂ permeability), the O₂/N₂ selectivity predicted by this modified Park-Paul curve (Eq F.6) exceeds the upper bound. This corresponds to an FFV of 0.575. Conversely, decreasing the permeability of by two orders of magnitude from Ultem[®] can be done by decreasing the FFV to 0.082. It may be easier to add FFV to a polymer than to decrease it. Thus, it may be more important to properly capture the behavior of the higher FFV region. An alternative to the modified Park-Paul correlation is to assume the transport properties of the affected region of polymer parallel the

upper-bound trade-off curve [8], again passing through neat Ultem[®]. This modified curve is given by the following equation:

$$P_{O_2} = \frac{P_{O_2}}{\left(\frac{P_{O_2}}{\alpha_{O_2/N_2}} \right)^{-5.8}} \quad (F.7)$$

where the -5.8 is the slope of the upper bound curve given by Robeson. The standard and modified upper-bound trade-off curves are plotted as solid and dashed black lines on Figure F.1. Nonideal morphology regions derived using this functional dependence for the selectivity of the affected polymer matrix are outlined on the transport property map in Figure 5.16 and Figure 5.17. The upper and lower limits for the transport property regions calculated using the modified Park-Paul correlation (Eq F.6) are between the corresponding upper and lower limits calculated using constant selectivity or using the modified upper-bound (Eq F.7).

Nonetheless, the upper limits of these nonideal morphology regions may be unrealistic since they require the entire polymer matrix to exhibit the nonideal morphology (matrix rigidification or stress dilated). Therefore, the assumption of $(\ell/r_s)_{MAX} = 0.3$ was made to derive the “experimentally accessible” transport property maps of Figure 5.15c. This is admittedly somewhat arbitrary, but perhaps less arbitrary than other values, for two reasons. First, it is the smallest ℓ/r_s that can explain most of the experimental data. Assuming a larger value of ℓ/r_s will not explain any additional points on Figure 5.16 or Figure 5.17. Second, $\ell/r_s \approx 0.3$ gave a reasonable fit to experimental transport properties for several different polymer – sieve systems at different zeolite loadings [9].

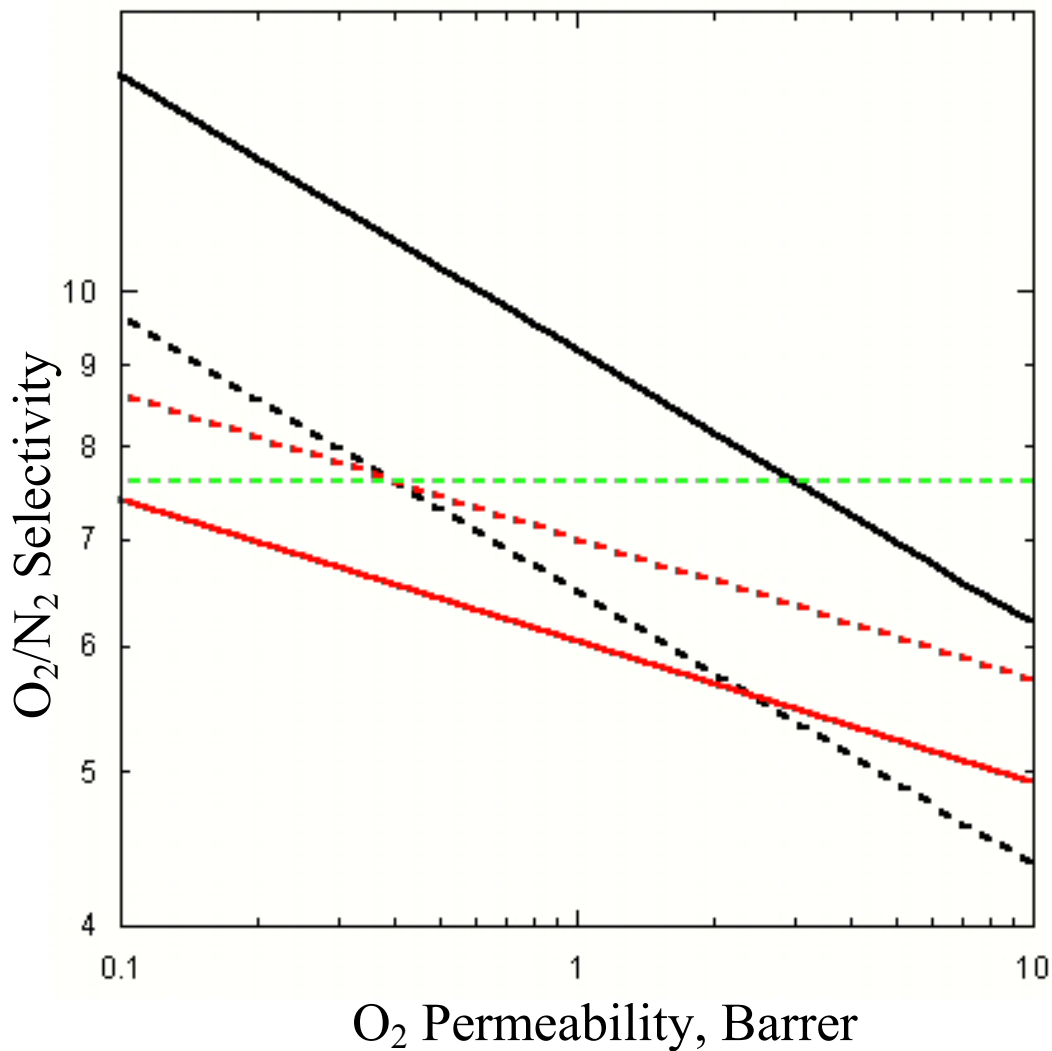


Figure F.1: Potential functional dependence of selectivity on the permeability of the matrix rigidification and stress dilated regions. Black, upper-bound trade-off curve; red, Park-Paul correlation; green, constant selectivity. Dashed lines were modified to go through the transport properties of neat Ultem[®].

The final case that was not included on the simple transport property maps in Figure 5.1 and Figure 5.2 is the possibility that fractions of sieves within the same membrane exhibit different nonideal morphologies at the polymer – sieve interface. This appears to be the case in Figure 5.3 or for any membrane containing sieve agglomerates. A cartoon of such morphology is shown in Figure F.2. A fraction of the zeolite is well dispersed (dispersed phase 1), while the rest exist as agglomerates (dispersed phase 2).

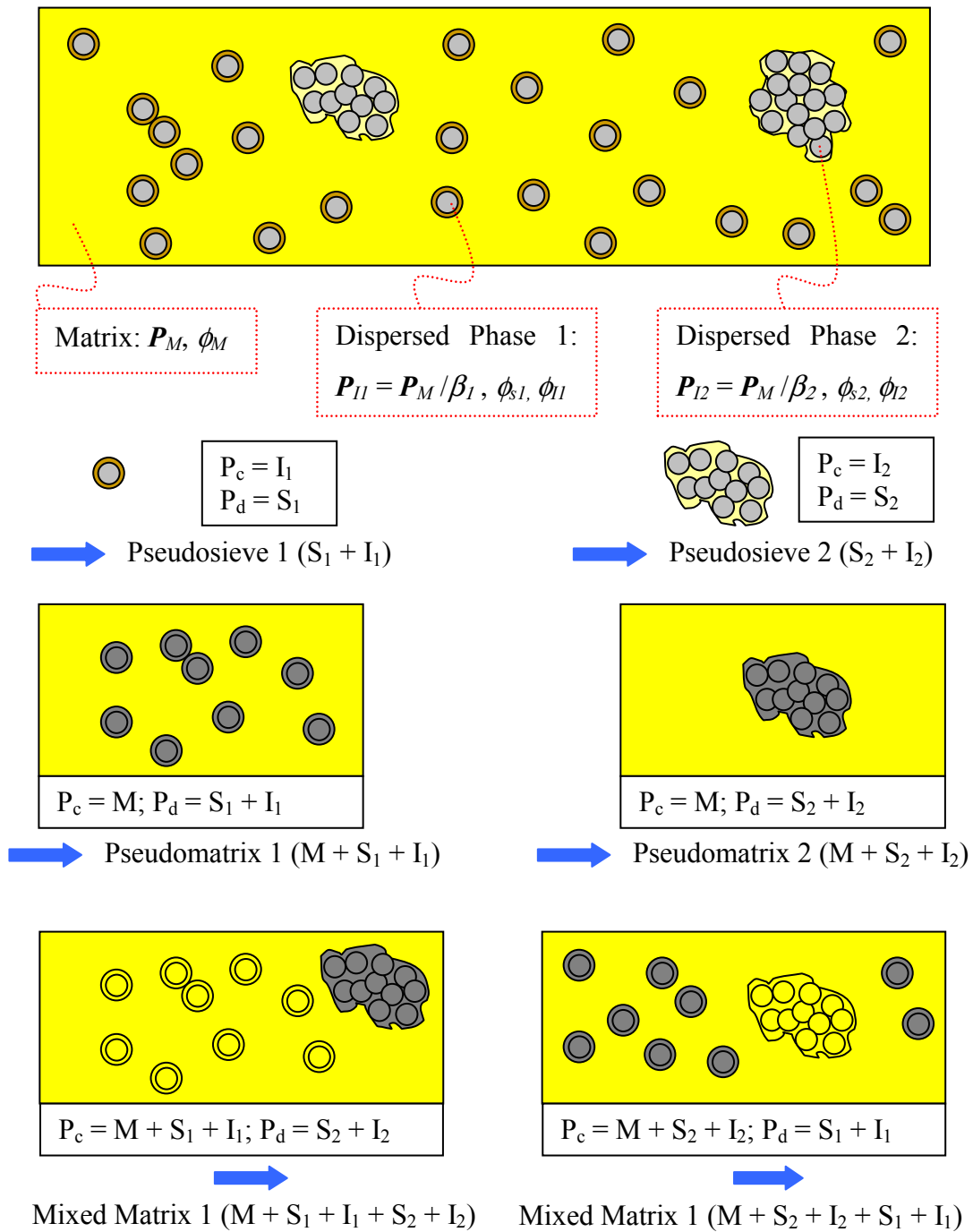


Figure F.2: Cartoon shown multiple nonideal morphologies for different fractions of sieve at the polymer – sieve interface and the modeling strategy.

Three methods were considered to model this system, and all gave similar results. The first two involve 3 applications of the Maxwell model, as outlined in Figure F.2. In each case, the Maxwell model was used to calculate the properties of two “pseudosieve” phases, as in section 2.2.2, one each for dispersed phase 1 and its associated interphase (pseudosieve 1) and for dispersed phase 2 with its associated interphase (pseudosieve 2). Then, the properties of a “pseudomatrix” phase, comprised of either the matrix and pseudosieve 1 phase (pseudomatrix 1), or the matrix and pseudosieve 2 phase (pseudomatrix 2) were calculated using the Maxwell model a second time. Finally, a third application of the Maxwell model is used to calculate the properties of the overall mixed matrix membrane with the pseudomatrix and remaining pseudosieve phases (i.e. pseudomatrix 1 + pseudosieve 2 and pseudomatrix 2 + pseudosieve 1). These two separate calculations give slightly different, but similar transport properties. A third method used the effective medium theory (Table 2.1) for three phases (matrix, pseudosieve 1, and pseudosieve 2) to calculate the properties of a “multiple nonideal morphology” membrane. It also gave predictions similar to the two Maxwell model predictions. Several predictions for selected values of the parameters detailed in Figure F.2 are given in Table F.2. They were calculated using the third method (effective medium theory) described above.

Table F.2: Calculation of O₂/N₂ transport properties for 15 vol% zeolite 4A in Ultem[®] containing fractions of sieves exhibiting multiple nonideal morphologies. The variables in the first 5 columns are shown in Figure F.2. ($\phi_{s1} + \phi_{s2} = 0.15$)

ϕ_{s1}	$(\ell_1/r_s)_1 \sim \phi_{11}$	$(\ell_1/r_s)_2 \sim \phi_{12}$	β_1	β_2	O ₂ Permeability, Barrer	O ₂ /N ₂ Selectivity
0.15	0.3	0.3	3	0.0001	0.360	9.49
0.14	0.3	0.3	3	0.0001	0.388	9.08
0.10	0.3	0.3	3	0.0001	0.552	8.63
0.075	0.3	0.3	3	0.0001	0.745	8.36
0.15	0.3	0.3	10	0.0001	0.284	8.31
0.14	0.3	0.3	10	0.0001	0.310	8.24
0.12	0.3	0.3	10	0.0001	0.378	8.12
0.10	0.3	0.3	10	0.0001	0.473	8.00
0.12	0.3	0.5	10	0.0001	0.432	8.11
0.12	0.3	0.3	10	0.0001	0.377	8.12
0.12	0.3	0.1	10	0.0001	0.345	8.12
0.12	0.3	0.3	10	0.1	0.348	8.20
0.12	0.3	0.3	10	0.01	0.372	8.12
0.12	0.3	0.3	10	0.001	0.377	8.12
0.12	0.3	0.3	10	0.0001	0.378	8.12

REFERENCES

1. Breck, D.W., Zeolite molecular sieves: Structure, chemistry, and use. 1974, Malabar, FL: Robert E. Krieger Publishing Co, Inc.
2. Singh, A. and W.J. Koros. Ind. Eng. Chem. Res. 1996, 35, 1231-4.
3. Singh, A., Membrane materials with enhanced selectivity: An entropic interpretation. Department of Chemical Engineering, University of Texas at Austin. 1997.

4. Barrer, R., Zeolites and clay minerals as sorbents and molecular sieves. 1978, New York: Academic Press Inc.
5. McQuarrie, D., Statistical thermodynamics. 1973, New York: Harper & Row Publishers, Inc.
6. Karger, J. and D. Ruthven, Diffusion in zeolites. 1992, New York: John Wiley and Sons.
7. Park, J.Y. and D.R. Paul. Journal of Membrane Science 1997, 125, 23-39.
8. Robeson, L.M. J. Membr. Sci. 1991, 62, 165-85.
9. Moore, T.T.; R. Mahajan; D.Q. Vu; and W.J. Koros. AIChE J. 2004, 50, 311-21.

Appendix G. POLYMERS CONTAINING DIAMINOBENZOIC ACID (DABA) FOR ENHANCED INTERACTION WITH THE ZEOLITES

G.1. 6FDA-6FpDA:4MPD:DABA (2:2:1) {6-64D} BASED MEMBRANES

Mahajan had used 6FDA-6FpDA:4MPD:DABA (2:2:1) to demonstrate the feasibility of forming covalent bonds between polymers with reactive pendant groups and zeolites, thereby avoiding sieve-in-a-cage morphology [1]. The carboxylic acid in DABA is believed to react with silanol groups ubiquitous on the surface of zeolites. The structure of 6FDA-6FpDA:4MPD:DABA is given in section 3.2.1; henceforth, it will be called 6-64D. This polymer has an oxygen permeability of 22 Barrer, compared to 0.77 Barrer in zeolite 4A. Because of the poor matching of these two permeabilities, the O₂/N₂ selectivity for a mixed matrix membrane with 15 vol% zeolite 4A is only predicted to increase from 4.2 to 4.25. Nonetheless, the Maxwell model predicts a significant decrease in the permeability of this membrane. 6-64D is used here for three reasons: (i) to repeat the results of Mahajan before extension to other polymers with reactive pendant groups, (ii) to test 6-64D – zeolite 4A membranes for the CO₂/CH₄ separation, and (iii) to determine the transport properties of 6-64D – HSSZ-13 membranes.

The procedures used for preparing mixed matrix membranes from DABA containing polymers are outlined in Figure G.. After the priming step, which requires evaporation of dimethylacetamide (DMAc) to obtain a primed polymer-sieve mass, the polymer-sieve mass is dried in the vacuum oven (drying II step). Mahajan did not record the detailed drying II procedures [2]. Hence, the primed polymer – sieve mass was broken in half, with half dried in the vacuum oven at ambient temperature and half at 260°C. The resulting mixed matrix membranes were then dried at 50°C. The results from these membranes (A and C in Figure G.1) are summarized on the transport property map for 15% zeolite 4A in 6-64D given in Figure G.2, which also shows the data of Mahajan. Membrane A, prepared by drying the primed polymer – sieve mass under vacuum at

ambient temperature (drying II step), most closely matches the results of Mahajan. Although it may appear that the membrane prepared by Mahajan was more selective, the difference in *selectivity* between the least (4.2) and most (4.5) selective membranes of Figure G.2 is similar to the experimental error in these measurements.

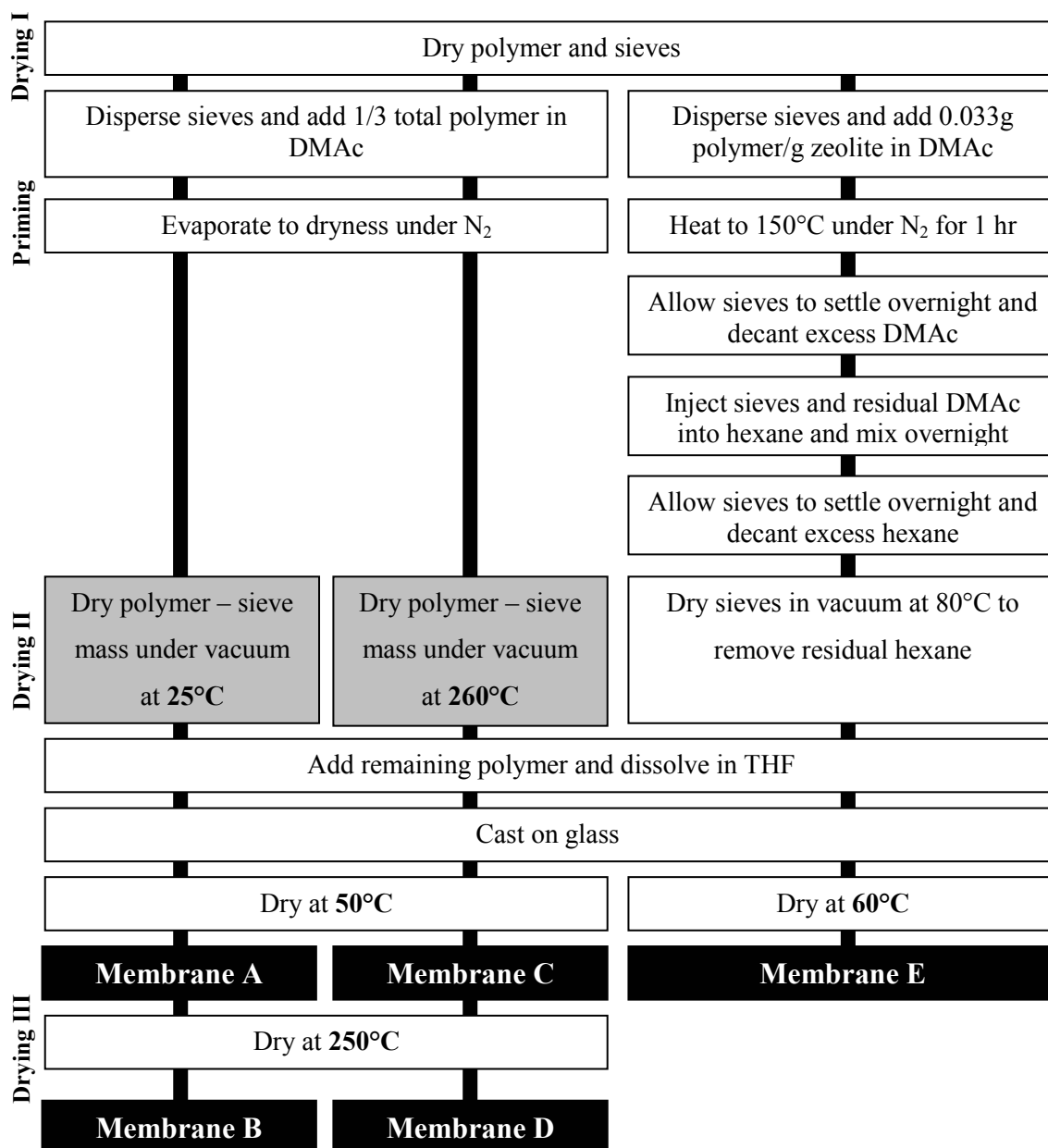


Figure G.1: Preparation procedures used for mixed matrix membranes from polymers containing diaminobenzoic acid (DABA) in their backbones.

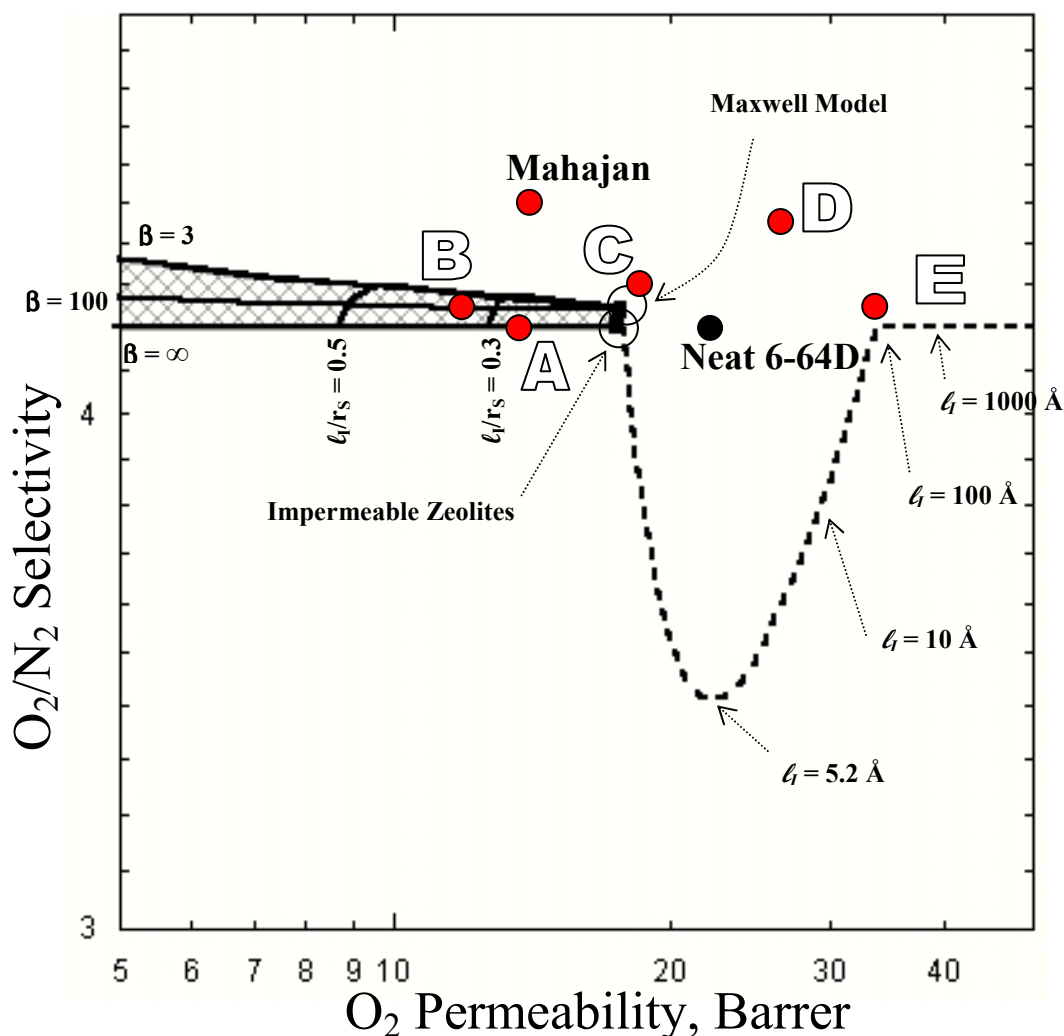


Figure G.2: Summary of 6FDA-6FpDA:4MPD:DABA (2:2:1) mixed matrix membranes with 15 vol% zeolite 4A on an O₂/N₂ transport property map. The membranes were prepared as shown in Figure G.1. Tested at 35°C and 65 psia.

Interestingly, there is a significant difference in the *permeabilities* of the membranes prepared using the different drying II temperatures. Membrane C, prepared from the primed polymer – sieve mass dried at 260°C, exhibits transport properties near the Maxwell model prediction. The dissolution time of the primed polymer-sieve mass is also greatly affected by the drying II temperature. The primed polymer – sieve mass dried at ambient temperature had dissolved within one day, whereas three weeks were needed for the other, which was dried at 260°C. Charge transfer complexes (CTCs)

may have formed in the heated portion of the primed polymer – sieve mass to cause slower dissolution. Matrimid[®] that has been treated at high temperatures (350°C) displays additional plasticization resistance, attributed to the formation of charge transfer complexes [3]. These CTCs tighten the matrix, so they would be expected to cause the polymer dissolve more slowly. Because both portions of the primed polymer – sieve mass are exposed to additional solvent (THF) after they are dried, it is unclear why there should be a significant difference in apparent rigidification of the interface. This may merit additional investigation, but the extended dissolution time of the 260°C primed polymer-sieve mass makes this procedure impractical. Furthermore, another DABA containing polymer was unable to dissolve after a similar heat treatment, making the high temperature drying II step even less desirable. Thus, the 25°C drying II step was used for future mixed matrix membranes prepared in this manner.

Membranes A and C were then further dried at 250°C to see if the apparent rigidification (i.e. stress) in the lower permeability membrane (membrane A) could be relaxed. These results are also shown on Figure G.2 as membranes B and D, respectively. Membrane B exhibits a slightly *lower* permeability than membrane A, which may indicate a small increase in rigidification caused by the heat treatment. Conversely, membrane D exhibits increased permeability compared to membrane C. The higher permeability of membrane D is most consistent with sieve-in-a-cage morphology, both for O₂/N₂ and, as shown later, for CO₂/CH₄. Although membrane D appears to exhibit higher selectivity than membrane C, recall that any selectivity changes for this system are negligible compared to experimental error.

As discussed in section 4.4.4, drying at an elevated temperature should cause the polymer matrix to expand (away from the sieve surface) upon heating and then to contract (toward the sieve surface) during cooling. For a matrix that exhibits rigidified regions near the sieve surface (membrane A), high temperatures may be able to release some of the rigidification, especially if the membrane is annealed above the T_g of the

matrix. However, 6-64D has a T_g of 368°C [4], so drying at 250°C may not have given the matrix sufficient flexibility, and a slight decrease in permeability was observed (compare membranes A and C). On the other hand, for a matrix that exhibits a well bonded interface with no rigidification (membrane C), thermal expansion may cause the polymer – sieve bond to fail. If a new bond can not form as the matrix is cooled, sieve-in-a-cage morphology may arise (as in membrane D).

The membranes (B and D) that underwent additional drying at 250°C were also tested with CO₂ and CH₄. Their CO₂/CH₄ transport properties, shown in Figure G.3, are consistent with the morphologies inferred based on their O₂/N₂ transport properties. Membrane B has CO₂ permeability lower than the Maxwell prediction consistent with matrix rigidification. Membrane D has CO₂ permeability most consistent with sieve-in-a-cage morphology. As in Figure G., the small differences in *selectivities* between the mixed matrix membranes and neat 6-64D on Figure G. are probably insignificant compared to experimental error, but differences in permeabilities are quite significant.

As discussed later, problems were encountered getting another DABA containing polymer to dissolve after the higher temperature drying II step. Thus, a new procedure (used for membrane E of Figure G.1) was developed to circumvent this problem. This procedure was also done using 6-64D to see if results equivalent to membrane A were obtained. There are two differences in the preparation of membrane E: (i) the priming step is performed in a dilute polymer solution (DMAc) and (ii) the primed sieves are precipitated into a nonsolvent (hexane) to try to force the polymer onto the zeolite surface. This latter approach was successfully applied by Mahajan to prepare PVAc – zeolite 4A membranes at higher sieve loadings [5]. The dilute priming conditions were used to alleviate problems getting the other polymer (in section G.3) to dissolve after priming. The results for the 6-64D – zeolite 4A membrane prepared with this modified reaction procedure are also shown on Figure G.2 and Figure G.3, labeled as membrane E. The transport properties of this membrane are consistent with sieve-in-a-cage

morphology, so the modified reaction procedure does not appear to yield favorable results.

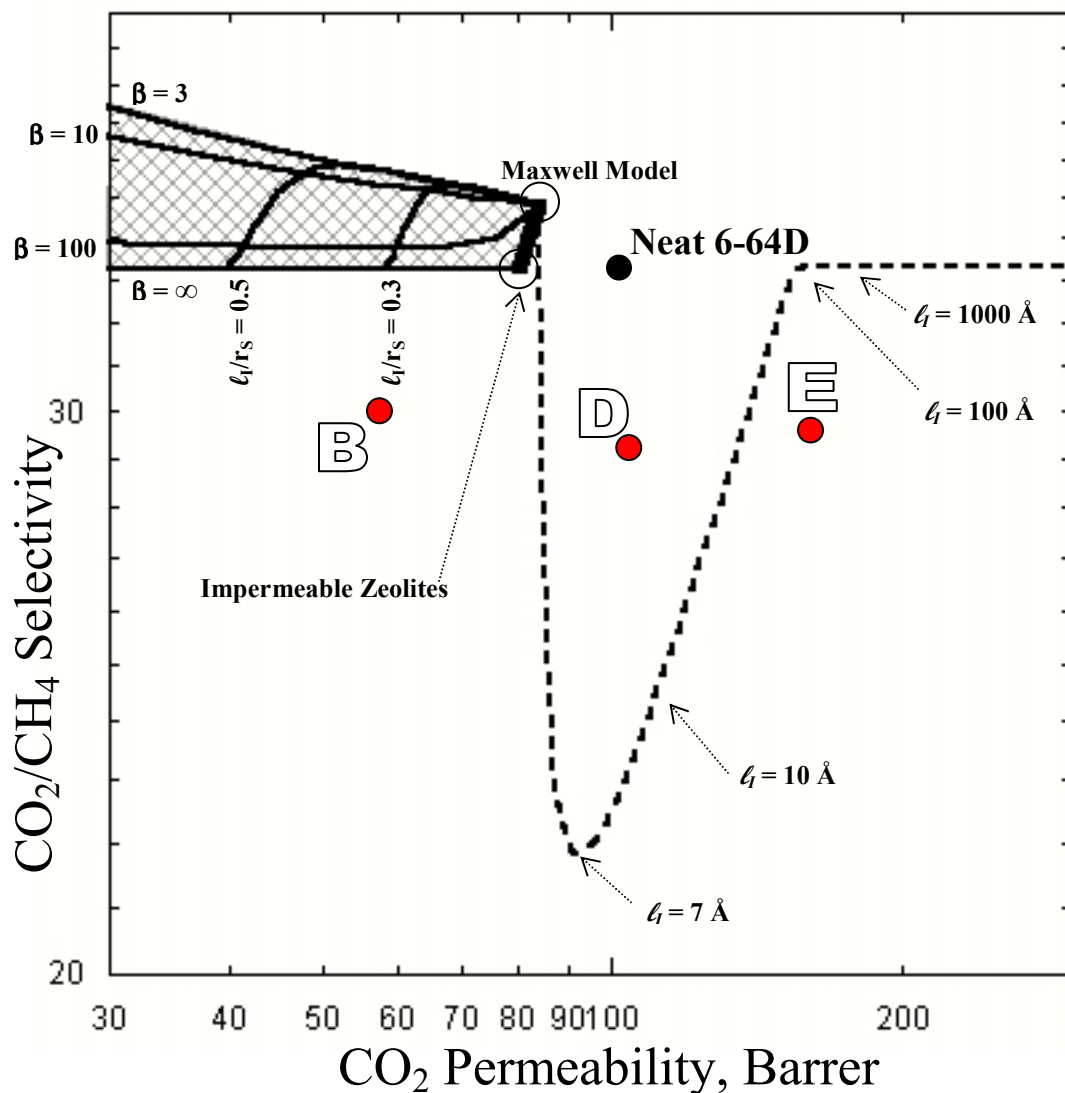


Figure G.3: Summary of 6FDA-6FpDA:4MPD:DABA (2:2:1) mixed matrix membranes with 15 vol% zeolite 4A on a CO₂/CH₄ transport property map. The membranes were prepared as shown in Figure G.1. Tested at 35°C and 65 psia.

The selectivity improvement expected of the 6-64D – zeolite 4A system is minimal because of the poorly matched permeabilities of these materials. On the other hand, HSSZ-13 is better matched than zeolite 4A, and a significant improvement in the

CO₂/CH₄ selectivity (from 33 to 46) is expected. A membrane was prepared with HSSZ-13 using the preparation procedure for membrane A outlined in Figure G.1. However, as shown in Table G.1, this membrane exhibits greater decreases in permeability compared to the neat polymer than predicted by the Maxwell model. The transport properties of these membranes are best matched by a prediction assuming the zeolites are impermeable. There are two possible explanations for this: (1) the HSSZ-13 received during this period was known to be less active because of a synthesis problem, and (2) these membranes were among the first tested after the research group relocated to new labs, and the built-in vacuum lines were later found to cause reduced permeabilities in the zeolites (see section 6.3.3). This may also have affected the membranes prepared with zeolite 4A (Figure G.2 and Figure G.3), but the transport property difference expected for mixed matrix membranes with permeable and impermeable zeolites is less than the experimental error.

Table G.1: Transport properties for ~15 vol% HSSZ-13 in 6FDA-6FpDA:4MPD:DABA membranes. Tested at 35°C and 65 psia.

	O ₂ Permeability, Barrer	O ₂ /N ₂ Selectivity	CO ₂ Permeability, Barrer	CO ₂ /CH ₄ Selectivity
Neat 6FDA-6FpDA:4MPD:DABA	22	4.2	100	33
Maxwell Model	20	4.7	110	46
Maxwell Model, Impermeable HSSZ-13	17	4.2	80	33
Observed	15	4.3	80	30

G.2. 6FDA-mPDA:DABA (2:1) {6-MD} BASED MEMBRANES

In contrast to 6-64D, 6FDA-mPDA:DABA has transport properties that are well matched to zeolite 4A. Henceforth, 6FDA-mPDA:DABA is referred to as 6-mD. 6-mD mixed matrix membranes were prepared with both zeolite 4A and HSSZ-13 using the procedure that gave good properties for 6-64D – zeolite 4A (membrane A of Figure

G.1). Unfortunately, neither of the resulting mixed matrix membranes displays increased selectivity relative to neat 6-mD. The transport properties of the zeolite 4A membrane (“Dried at 50°C”) are reported in Table G.2. This membrane has O₂/N₂ and CO₂/CH₄ selectivities below the neat polymer. Several methods were attempted to improve the selectivity of this membrane. The transport properties for these experiments are also given in Table G.2. Heating the membrane to 250°C under vacuum overnight improves the selectivities to nearer those of neat 6-mD, but the permeabilities still indicate a sieve-in-a-cage morphology. Annealing this membrane was also tried at 350°C under vacuum, but the membrane became black. A neat 6-mD membrane annealed at the same time in the same tube furnace became somewhat discolored, but not black. It is possible that the zeolite 4A has catalyzed the pyrolysis of the polymer matrix. The properties of this blackened membrane were tested, but the transport properties still indicate sieve-in-a-cage morphology. A membrane comprised of HSSZ-13 dispersed in 6-mD also shows poor selectivities indicative of sieve-in-a-cage morphology, as shown in Table G.2. Drying of this membrane at 350°C also appears to further damage the morphology.

Table G.2: Transport properties for ~15 vol% zeolite 4A or HSSZ-13 in 6FDA-mPDA:DABA dried at selected temperatures. Tested at 35°C and 65 psia.

		O ₂ Permeability, Barrer	O ₂ /N ₂ Selectivity	CO ₂ Permeability, Barrer	CO ₂ /CH ₄ Selectivity
Neat 6FDA-mPDA:DABA		2.1	7.0	7.6	74
Maxwell Model		1.8	7.8	8.5	92
Zeolite 4A	Dried at 50°C	3.6	4.9	20	35
	Dried at 250°C	3.9	6.4	14	62
	Dried at 350°C	9.2	5.8	35	51
HSSZ-13	Dried at 50°C	5.9	4.7	32	37
	Dried at 250°C	9.7	3.2	36	59

The 6-mD – zeolite 4A mixed matrix membrane was used to probe the strength of the attraction of the polymer for zeolite 4A. A piece of this membrane was dissolved in and washed with excess THF to see if any polymer remained on the surface. Any residual polymer would indicate a strong attraction or covalent bond between the polymer and the zeolite. After this process, the zeolites were collected and x-ray photoelectron spectroscopy (XPS) was used to see if any polymer remained on the surface. This is a surface sensitive technique that probes $\sim 1 \mu\text{m}$ into the sample. Nitrogen and fluorine are not present in zeolite 4A, so they indicate the presence of polymer. Two control samples were also tested: (i) pure zeolite 4A (negative control) and (ii) zeolite 4A with 6-mD (0.02 g/g zeolite) precipitated onto the zeolite surface (positive control). The elemental compositions determined using XPS are shown in Table G.3. Both the sample recovered from the membrane and the positive control have significant nitrogen and fluorine, indicating that the polymer is strongly held by the zeolite. Thus, there appears to be a strong attraction between 6-mD and zeolite 4A. A potential explanation of the poor transport properties of these membranes, despite the favorable polymer – sieve affinity is discussed in section G.4.

Table G.3: Elemental composition obtained by XPS of the zeolite 4A samples.

Element	4A recovered from 6-mD – zeolite 4A membrane	Pure zeolite 4A	Zeolite 4A with precipitated 6-mD
C	31	15	43
N	4.4	†	5.0
O	30	45	22
F	11	†	17
Na	4.8	16	3.8
Al	11	12	5.0
Si	7.0	12	4.5

† These peaks were indiscernible from the background noise.

G.3. BPADA-DAPI:DABA (1:1) {B-DD} BASED MEMBRANES

BPADA-DAPI:DABA also has transport properties well matched to zeolite 4A. This polymer, henceforth abbreviated B-DD, should allow the preparation of mixed matrix membranes with improved selectivity compared to the polymer matrix. However, a number of problems were encountered preparing mixed matrix membranes from this polymer. Initially, B-DD – zeolite 4A membranes were prepared using the high temperature drying II step in Figure G.1, but the primed polymer – sieve mass would not dissolve in either THF or NMP, which both dissolve neat B-DD. One potential explanation is the B-DD may have a higher molecular weight than the 6-64D. Another potential explanation is the higher DABA content (50%) of B-DD versus 6-64D (20%) creates increased interchain interactions in B-DD, making it more difficult to dissolve. Recall that drying the primed 6-64D – zeolite 4A mass at 260°C caused slower dissolution (21 days) than the corresponding 6-64D – zeolite 4A mass dried at ambient temperature (1 day). Thus, the priming procedure for membrane A in Figure G.1 was repeated with B-DD. NMP was found to dissolve neat B-DD dried at 250°C about twice as quickly as THF, so NMP was used as the casting solvent instead of THF. These two modifications allowed preparation of a B-DD – zeolite 4A membrane. Nonetheless, this membrane is twice as permeable as the neat polymer with no increase in selectivity, indicating sieve-in-a-cage morphology, as shown in Table G.4 (“concentrated priming”). Potential reasons for this performance are discussed later.

The dilute priming procedure (membrane E of Figure E.1) was also tried with B-DD before the importance of performing the drying II step at ambient temperature was realized. The membrane prepared using the dilute priming procedure is characterized by large sieve agglomerates (visible with a 50× magnification microscope). Transport properties for this membrane given in Table G.4 indicate that the agglomerates allow nonselective permeation through the membrane. No agglomerates are present in the 6-64D membrane prepared in the same manner, so perhaps B-DD has a lower affinity for the zeolite surface compared to other DABA containing polymers.

Table G.4: Transport properties for ~15 vol% zeolite 4A in BPADA-DAPI:DABA membranes. Tested at 35°C and 65 psia feed pressure.

	O ₂ Permeability, Barrer	O ₂ /N ₂ Selectivity	CO ₂ Permeability, Barrer	CO ₂ /CH ₄ Selectivity
Neat BPADA- DAPI:DABA	0.65	6.8	2.7	33
Maxwell Model	0.67	8.2	3.5	46
Concentrated priming	1.2	6.7	4.6	30
Dilute priming	21	1.0	Not tested	

G.4. DISCUSSION OF POLYMERS WITH REACTIVE GROUPS AS A GENERAL METHOD FOR AVOIDING SIEVE-IN-A-CAGE MORPHOLOGY

Given the results presented in this subsection, it does not appear that adding DABA to a polymer backbone is a *general* method allowing membranes to be prepared without sieve-in-a-cage morphology. Representative SEMs of membranes prepared with the three DABA containing polymers used in the previous subsections are shown in Figure G.4 to compare with the morphologies diagnosed from the membrane transport properties. 6-64D and 6-mD both produce SEMs free of large voids at polymer – sieve interfaces; however, large interfacial voids are clearly present in the B-DD matrix. B-DD has flexible ether linkages, so it is likely the most flexible of these three polymers. Thus, it was initially hypothesized that this polymer would be most likely to form good polymer – sieve interfaces.

There is one critical observation regarding these membranes that may explain why 6-64D gives the best morphologies and why B-DD gives the worst morphologies. When the 6-64D – zeolite 4A membrane (A in Figure G.1) was cast, it delaminated from the substrate (glass) during casting, although a crack did form in the membrane. If the nascent membrane was not adhered to the casting substrate, sieve-in-a-cage morphology would be unlikely according to the analysis presented in section 4.4.2. This is

consistent with the transport properties and the SEM for the 6-64D mixed matrix membrane. On the other hand, a number of membranes spontaneously shattered when they were touched after initial solvent removal, indicating large stresses in the plane of the membrane. These stresses may have caused sieve-in-a-cage morphology based on the analysis in section 4.4.2. One of these samples was the 6-64D – zeolite 4A membrane prepared using the dilute priming procedure of Figure G.1 (membrane E), which has poor transport properties. B-DD mixed matrix membranes were also cast on glass since they were prepared from NMP. These membranes were well adhered to the glass substrate after initial drying at 160°C under vacuum for ~36 hours and they had to be floated off the surface using distilled water. These membranes would have been subjected to considerable in-plane stresses that may have caused the sieve-in-a-cage morphology observed in Figure G. G.4. This was done before the “cast and remove before vitrification” procedure of section 5.4.1 was developed. The significant chemical difference (fluorine) between B-DD and 6-64D may explain why 6-64D delaminates from glass while B-DD is strongly adhered, but the different casting solvents used for these two materials make this speculative

This work with DABA polymers was performed before any experiments reported in chapters 5, 6, and 7. In fact, the unanticipated performance of these DABA containing membranes prompted the switch to Ultem[®] and the experiments in Chapter 5. With the additional understanding developed in these later chapters, it may be worth revisiting using polymers with DABA. Certainly, if methods to unclog the zeolites are developed, it is worthwhile to repeat the experiments with HSSZ-13 in 6-64D. It is probably also useful to use the casting techniques in section 5.4.1 with B-DD. The poor 6-mD transport properties contradict the morphology observed in the SEM, so this system also requires additional study. The transport properties are consistent with pinhole defects in the membranes or interconnected cages from overlapping sieve-in-a-cage regions, but the SEMs do not indicate sieve-in-a-cage. Finally, using silane treated sieves with these polymers should be considered, since the silanes can also interact with DABA.

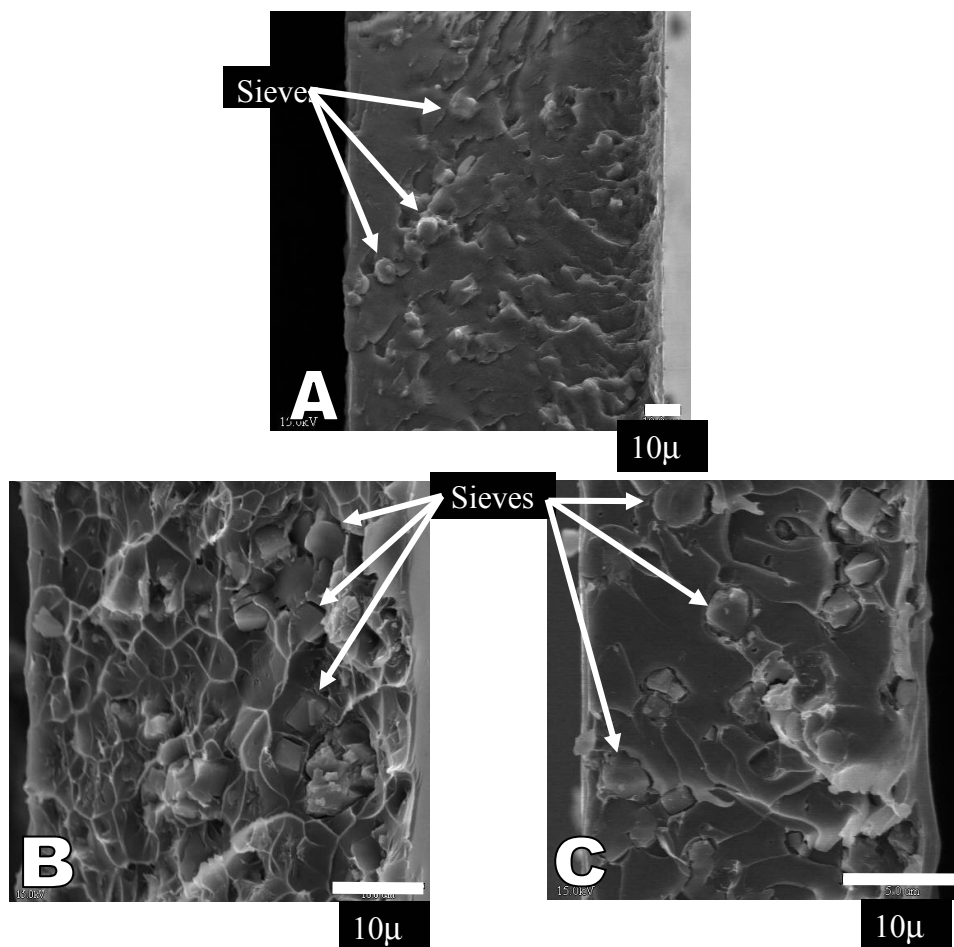


Figure G.4: SEM of mixed matrix membranes prepared with zeolite 4A in selected DABA containing polymers. a) 6FDA-6FpDA:4MPD:DABA b) 6FDA-mPDA:DABA c) BPADA-DAPI:DABA.

REFERENCES

1. Mahajan, R. and W.J. Koros. *Polym. Engr. and Sci.* 2002, 42, 1432-1441.
2. Mahajan, R., Personal communication. 2004.
3. Bos, A.; I.G.M. Punt; M. Wessling; and H. Strathmann. *Sepr. Purification Tech.* 1998, 14, 27-39.
4. Ren, J.; C. Staudt-Bickel; and R.N. Lichtenthaler. *Sepr. Purification Tech.* 2001, 22 and 23, 31-43.
5. Mahajan, R. and W.J. Koros. *Ind. Eng. Chem. Res.* 2000, 39, 2692-2696.

Appendix H. EFFECT OF N-BUTANE ON THE TRANSPORT PROPERTIES OF MIXED MATRIX MEMBRANES AT 50°C

Modeling of the transport properties of mixed matrix membranes using natural gas feeds containing n-butane is discussed in section 7.3. The modeling parameters are based on experimental data at 35°C. Since hollow fiber permeation was measured at 50°C, it was necessary to estimate the transport properties at 50°C. The only parameters that could not be estimated reliably were the Langmuir affinity and capacity constants of methane in HSSZ-13. They were assumed unchanged from 35°C to 50°C; although both would be expected to decrease with increasing temperature. This assumption likely gives Langmuir constants that are too high, leading to a lower limit on the selectivity. The parameters necessary to model permeation in Ultem[®] – HSSZ-13 membranes are listed in Table H.1 (on the following page), together with the method used to obtain or estimate them.

REFERENCES

1. Karger, J. and D. Ruthven, Diffusion in zeolites. 1992, New York: John Wiley and Sons.
2. Yampolskii, Y.; D. Wiley; and C. Maher. J. Appl. Polym. Sci. 2000, 76, 552-560.
3. Koros, W.J. and D.R. Paul. J. Polym. Sci., Polym. Phys. Ed. 1978, 16, 1947-63.
4. Zoller, P. and P. French. J. Thermal Anal. 1996, 47, 993-1012.
5. van Amerongen, G.J. J. Appl. Phys. 1946, 17, 972-85.
6. Koros, W. and D. Paul. Polym. Engr. Sci. 1980, 20, 14-9.
7. Rezac, M.E. and B. Schoberl. J. Membr. Sci. 1999, 156, 211-222.

Table H.1: Method used or assumption made to estimate the parameters necessary to model gas transport in mixed matrix membranes at 50°C with synthetic natural gas feeds contaminated with n-butane.

Parameter	Estimation method / Assumption
b_{CO_2} , b_{nC_4} , $C_{H'CO_2}$, $C_{H'nC_4}$ in HSSZ-13	Least squares fit to sorption data provided by ChevronTexaco ETC
b_{CH_4} , $C_{H'CH_4}$ in HSSZ-13	Assumed the same as at 35°C
D_{CO_2} , D_{CH_4} in HSSZ-13	Assume the activation energy is the average of the values reported for 4A by Karger [1] since the pore sizes of HSSZ-13 and zeolite 4A are similar
b_{CO_2} , b_{CH_4} , b_{nC_4} in Ultem®	In the literature, the following correlation is reported for b : $b = b_0 \exp\left(\frac{-\Delta H_s}{RT}\right)$ $\ln(b) = k_1 + k_2 T_c$ [2]. Also, $\ln(b) = k_1 + k_2(T_c/T)$. Since b_0 is not a function of temperature, and $\Delta H_s \sim T_c$, the correlation $\ln(b) = k_1 + k_2(T_c/T)$ should be equally valid. This assumption was checked by plotting the available Langmuir affinity constant data for the penetrants CO ₂ , CH ₄ , n-C ₄ , and water in HSSZ-13 at both 35°C and 50°C. A reasonably linear curve was obtained, although the b_{nC_4} point at 35°C was an outlier.
$C_{H'CO_2}$, $C_{H'CH_4}$ in Ultem®	$(C_{H'})_{50^\circ C} = \frac{\left(\frac{\hat{V}_G - \hat{V}_L}{\hat{V}_G} \rho^*_{CO_2}\right)_{50^\circ C}}{\left(\frac{\hat{V}_G - \hat{V}_L}{\hat{V}_G} \rho^*_{CO_2}\right)_{35^\circ C}} (C_{H'})_{35^\circ C}$; [3, 4]
k_{D,CO_2} , k_{D,CH_4} in Ultem®	Van Amerongen reports a correlation of the form $\ln(k_D) = k_1 + k_2(T_c)$ [5]. Assume k_1 and k_2 are independent of temperature so that $\ln(k_D) = k_1 + k_2(T_c/T)$ is valid.
F_{CO_2} , F_{CH_4} in Ultem® ($F = D_H/D_D$)	Assume the difference in the energy of activation for diffusion in the “hole” and “dissolved” modes is similar to that in poly(ethylene terephthalate): 2000 cal/mol [6]
D_{D,CO_2} , D_{D,CH_4} in Ultem®	Use the known energy of activation for permeation [7] with the known / estimated dual mode parameters above to calculate D_D

Bibliography

- Matrimid Product Data Sheet*. 2000, Vantico, Inc.: Brewster, NY.
- Standard test methods for measuring adhesion by tape test (D 3359-97)*. 1997, American Society for Testing and Materials: West Conshohocken, PA.
- Udel Product Data Sheet*. 1993, Amoco Performance Products, Inc.: Alpharetta, GA.
- Ultem Product Data Sheet*. 1997, GE Plastics: Pittsfield, MA.
- Affolter, S.; A. Ritter; and M. Schmid, *Interlaboratory tests on polymers by differential scanning calorimetry (DSC): determination of glass transition temperature (T_g)*. *Macro.Matl. Engr.*, 2001. **286**(10): p. 605-610.
- Aharoni, S.M., *On entanglements of flexible and rodlike polymers*. *Macromolecules*, 1983. **16**(11): p. 1722-8.
- Ahmad, Z. and J.E. Mark, *Polyimide-Ceramic Hybrid Composites by the Sol-Gel Route*. *Chemistry of Materials*, 2001. **13**(10): p. 3320-3330.
- Allcock, H.R. and F.W. Lampe, *Contemporary Polymer Chemistry*. 2nd ed. 1990, Englewood Cliffs, NJ: Prentice Hall.
- Anschel, M. and P.D. Murphy, *Hydrothermal degradation and thermal regeneration of an aminosilane interface used to couple polyimide to alumina*. *J.Adhesion Sci. Tech.*, 1994. **8**(7): p. 787-806.
- Bader, R.F.W.; W.H. Henneker; and P.E. Cade, *Molecular charge distributions and chemical binding*. *J. Chem. Phys.*, 1967. **46**(9): p. 3341-63.
- Baerlocher, C.; W.M. Meier; and D.H. Olson, *Atlas of zeolite framework types*. 5 ed. 2001, New York: Elsevier. 302.
- Barbari, T.A.; W.J. Koros; and D.R. Paul, *Gas sorption in polymers based on bisphenol-A*. *J. Polym. Sci., Part B: Polym. Phys.*, 1988. **26**(4): p. 729-44.
- Barbari, T.A.; W.J. Koros; and D.R. Paul, *Gas transport in polymers based on bisphenol A*. *J. Polym. Sci., Part B: Polym. Phys.*, 1988. **26**(4): p. 709-27.
- Barrer, R., *Zeolites and Clay Minerals as Sorbents and Molecular Sieves*. 1978, New York: Academic Press Inc.

- Barrer, R.M. and S.D. James, *Electrochemistry of crystal-polymer membranes. I. Resistance measurements*. J. Phys. Chem., 1960. **64**: p. 417-21.
- Barrer, R.M. and S.D. James, *Electrochemistry of crystal-polymer membranes. II. Membrane potentials*. J. Phys. Chem., 1960. **64**: p. 421-7.
- Barrer, R.M. and W.M. Meier, *Structural and ion sieve properties of a synthetic crystalline exchanger*. Trans. Faraday Soc., 1958. **54**: p. 1074-85.
- Bartels-Caspers, C.; E. Tusel-Langer; and R.N. Lichtenthaler, *Sorption isotherms of alcohols in zeolite-filled silicone rubber and in PVA-composite membranes*. J. Membr. Sci., 1992. **70**(1): p. 75-83.
- Barton, A.F.M., *CRC Handbook of Solubility Parameters and Other Cohesion Parameters*. 1983, Boca Raton, FL: CRC Press Inc.
- Bianchi, F.; S. Cantagallo; G. Consolati; M. Laporta; M. Pegoraro; G. Tieghi; and L. Zanderighi, *Properties of bioriented nylon 6 films related to film production technology*. J. Appl. Polym. Sci., 2002. **86**(3): p. 559-571.
- Blum, F.D.; J.E. Dickson; and W.G. Miller, *Effect of diluents on poly(vinyl acetate) dynamics*. J. Polym. Sci., Polym. Phys. Ed., 1984. **22**(2): p. 211-21.
- Bos, A.; I.G.M. Punt; M. Wessling; and H. Strathmann, *Plasticization-resistant glassy polyimide membranes for CO₂/CH₄ separations*. Sepn. Purification Tech., 1998. **14**(1-3): p. 27-39.
- Bouma, R.H.B.; A. Checchetti; G. Chidichimo; and E. Drioli, *Permeation through a heterogeneous membrane: the effect of the dispersed phase*. J. Membr. Sci., 1997. **128**(2): p. 141-149.
- Breck, D.W., *Zeolite Molecular Sieves: Structure, Chemistry, and Use*. 1974, Malabar, FL: Robert E. Krieger Publishing Co, Inc. 771.
- Breck, D.W.; W.G. Eversole; R.M. Milton; T.B. Reed; and T.L. Thomas, *Crystalline zeolites. I. Properties of a new synthetic zeolite, type A*. J. Am. Chem. Soc., 1956. **78**: p. 5963-71.
- Bruggemann, D.A.G., *Berechnung verschiedener physikalischer Konstanten von heterogenen Substanzen. I. Dielektrizitätskonstanten und Leitfähigkeiten der Mischkörper aus isotropen Substanzen (The calculation of various physical constants of heterogeneous substances. I. The dielectric constants and conductivities of mixtures composed of isotropic substances*. Annalen der Physik V, 1935. **24**: p. 636.

- Bussery, B. and M. Aubert-Frecon, *Semiempirical investigation of the angular dependence of the interaction energy between two ground-state oxygen molecules*. Chem. Phys. Lett., 1991. **179**(4): p. 393-7.
- Caro, J.; M. Noack; P. Kolsch; and R. Schafer, *Zeolite membranes - state of their development and perspective*. Microporous and Mesoporous Materials, 2000. **38**(1): p. 3-24.
- Cauvel, A.; D. Brunel; F. Di Renzo; P. Moreau; and F. Fajula, *Functionalization of Y zeolites with organosilane reagents*, in *Catalysis by Microporous Materials*. 1995, Elsevier. p. 286-93.
- Chang, W. and X. Qin, *"Repulsive acid-base interactions": Fantasy or reality*, in *Acid-Base Interactions*, K. Mittal, Editor. 2000, VSP: Utrecht, Netherlands. p. 3-53.
- Chehimi, M.M.; E. Cabet-Deliry; A. Azioune; and M.-L. Abel, *Characterization of acid-base properties of polymers and other materials: relevance to adhesion science and technology*. Macromolecular Symposia, 2002. **178**(Polymer Characterization and Materials Science): p. 169-181.
- Chen, Y.D.; R.T. Yang; and L.M. Sun, *Further work on predicting multicomponent diffusivities from pure-component diffusivities for surface diffusion and diffusion in zeolites*. Chem. Engr. Sci., 1993. **48**(15): p. 2815-16.
- Chern, R.T.; W.J. Koros; E.S. Sanders; and R. Yui, *"Second component" effects in sorption and permeation of gases in glassy polymers*. J. Membr. Sci., 1983. **15**(2): p. 157-69.
- Chiou, J.S.; J.W. Barlow; and D.R. Paul, *Plasticization of glassy polymers by carbon dioxide*. J. Appl. Polym. Sci., 1985. **30**(6): p. 2633-42.
- Chow, T.S., *Molecular interpretation of glass transition temperature of polymer-diluent systems*. Macromolecules, 1980. **13**(2): p. 362-4.
- Costello, L.M. and W.J. Koros, *Comparison of pure and mixed gas carbon dioxide and methane permeabilities in polycarbonate: effect of temperature*. Ind. Eng. Chem. Res., 1993. **32**(10): p. 2277-80.
- Costello, L.M. and W.J. Koros, *Temperature dependence of gas sorption and transport properties in polymers: measurement and applications*. Ind. Eng. Chem. Res., 1992. **31**(12): p. 2708-14.
- Cotts, P.M.; T.M. Swager; and Q. Zhou, *Equilibrium Flexibility of a Rigid Linear Conjugated Polymer*. Macromolecules, 1996. **29**(23): p. 7323-7328.

- Croll, S.G., *Effect of titania pigment on the residual strain, glass transition, and mechanical properties of a PMMA coating*. *Polymer*, 1979. **20**(11): p. 1423-30.
- Croll, S.G., *The origin of residual internal stress in solvent-cast thermoplastic coatings*. *J. Appl. Polym. Sci.*, 1979. **23**(3): p. 847-58.
- Croll, S.G., *An overhanging beam method for measuring internal stress in coatings*. *J. Oil Colour Chem. Assoc.*, 1980. **63**(7): p. 271-5.
- Cussler, E.L.; S.E. Hughes; W.J. Ward, III; and R. Aris, *Barrier membranes*. *J. Membr. Sci.*, 1988. **38**(2): p. 161-74.
- Daniels, W.A., *Vinyl Ester Polymers*, in *Concise encyclopedia of polymer science and engineering*, J.I. Kroschwitz, Editor. 1990, John Wiley & Sons: New York. p. 1264-7.
- Davis, H.T., *The effective medium theory of diffusion in composite media*. *J. Am. Ceram. Soc.*, 1977. **60**(11-12): p. 499-501.
- Denkinger, P. and W. Burchard, *Determination of chain stiffness and polydispersity from static light-scattering*. *J. Polym. Sci., Part B: Polym. Phys.*, 1991. **29**(5): p. 589-600.
- Di Marzio, E.A.; C. Castellano; and A. Yang, *Glass temperature depression of polymer by use of mixed solvents: a colligative property*. *J. Polym. Sci., Part B: Polym. Phys.*, 1996. **34**(3): p. 535-43.
- Dilsiz, N. and J.P. Wightman, *Effect of acid-base properties of unsized and sized carbon fibers on fiber/epoxy matrix adhesion*. *Colloids and Surfaces, A: Physicochemical and Engr. Aspects*, 2000. **164**(2-3): p. 325-336.
- Djoekita, G., *Characterization and analysis of asymmetric hollow fiber membranes for natural gas purification in the presence of hydrocarbons*. Department of Chemical Engineering, University of Texas at Austin. 2000.
- Dotremont, C.; I.F.J. Vankelecom; M. Morobe; J.B. Uytterhoeven; and C. Vandecasteele, *Zeolite-Filled PDMS Membranes. 2. Pervaporation of Halogenated Hydrocarbons*. *J. Phys. Chem. B*, 1997. **101**(12): p. 2160-2163.
- Drago, R.S.; L.B. Parr; and C.S. Chamberlain, *Solvent effects and their relation to the E and C equation*. *J. Am. Chem. Soc.*, 1977. **99**(10): p. 3203-9.
- Drago, R.S.; G.C. Vogel; and T.E. Needham, *Four-parameter equation for predicting enthalpies of adduct formation*. *J. Am. Chem. Soc.*, 1971. **93**(23): p. 6014-26.

- Duval, J.M.; B. Folkers; M.H.V. Mulder; G. Desgrandchamps; and C.A. Smolders, *Adsorbent-filled membranes for gas separation. Part 1. Improvement of the gas separation properties of polymeric membranes by incorporation of microporous adsorbents*. J. Membr. Sci., 1993. **80**: p. 189-98.
- Duval, J.M.; A.J.B. Kemperman; B. Folkers; M.H.V. Mulder; G. Desgrandchamps; and C.A. Smolders, *Preparation of zeolite filled glassy polymer membranes*. J. Appl. Polym. Sci., 1994. **54**(4): p. 409-18.
- Echt, W. *Hybrid systems; combining technologies leads to more efficient gas conditioning*. in *Laurance Reid gas Conditioning Conference*. 2002.
- Eisenberg, A.; B. Hird; and R.B. Moore, *A new multiplet-cluster model for the morphology of random ionomers*. Macromolecules, 1990. **23**(18): p. 4098-107.
- Ekiner, O.M. and S.S. Kulkarni, *Process for making hollow fiber mixed matrix membranes*. US Patent 6,663,805.
- Fedors, R.F., *Method for estimating both the solubility parameters and molar volumes of liquids*. Polym. Engr. Sci., 1974. **14**(2): p. 147-54.
- Fedors, R.F., *Method for estimating both the solubility parameters and molar volumes of liquids. Addendum*. Polym. Engr. Sci., 1974. **14**(6): p. 472.
- Ferry, J.D., *Statistical evaluation of sieve constants in ultrafiltration*. Journal of General Physiology, 1936. **20**: p. 95-104.
- Fick, A., *Uber diffusion*. Poggendorff's Annalen der Physik and Chemie, 1855. **94**: p. 59-86.
- Filippov, L., *Comparative study of adsorption and heats of adsorption on planar and particulate polymer surfaces*. Colloid Polym. Sci., 1994. **272**(9): p. 1043-55.
- Flanigen, E.M.; J.M. Bennett; R.W. Grose; J.P. Cohen; R.L. Patton; R.M. Kirchner; and J.V. Smith, *Silicalite, a new hydrophobic crystalline silica molecular sieve*. Nature, 1978. **271**(5645): p. 512-16.
- Flory, P.J., *Principles of Polymer Chemistry*. 1953, Ithaca, NY: Cornell University Press.
- Fontana, B.J. and J.R. Thomas, *The configuration of adsorbed alkyl methacrylate polymers by infrared and sedimentation studies*. J. Phys. Chem., 1961. **65**: p. 480-7.

- Fowkes, F.M., *Acid-base contributions to polymer-filler interactions*. Rubber Chem. Technol., 1984. **57**(2): p. 328-43.
- Fowkes, F.M. and M.A. Mostafa, *Acid-base interactions in polymer adsorption*. Ind. Eng. Chem. Prod. Res. Dev., 1978. **17**(1): p. 3-7.
- Frank, B.P. and G. Belfort, *Intermolecular Forces between Extracellular Polysaccharides Measured Using the Atomic Force Microscope*. Langmuir, 1997. **13**(23): p. 6234-6240.
- Freeman, B.D., *Basis of Permeability/Selectivity Tradeoff Relations in Polymeric Gas Separation Membranes*. Macromolecules, 1999. **32**(2): p. 375-380.
- Fricke, H., *The electric conductivity and capacity of disperse systems*. Physica (The Hague), 1931. **1**: p. 106-15.
- Funke, H.H.; K.R. Frender; K.M. Green; J.L. Wilwerding; B.A. Sweitzer; J.L. Falconer; and R.D. Noble, *Influence of adsorbed molecules on the permeation properties of silicalite membranes*. J. Membr. Sci., 1997. **129**(1): p. 77-82.
- Galperin, I. and T.K. Kwei, *Dynamic mechanical properties of titanium dioxide-filled poly(vinyl acetate) at 0-40.degree*. J. Appl. Polym. Sci., 1966. **10**(5): p. 673-80.
- Ganesh, K.; R. Nagarajan; and J.L. Duda, *Rate of gas transport in glassy polymers: a free volume based predictive model*. Ind. Eng. Chem. Res., 1992. **31**(3): p. 746-55.
- Good, R.J., *On the acid/base theory of contact angles*, in *Acid-Base Interactions*, K. Mittal, Editor. 2000, VSP: Utrecht, Netherlands. p. 167-171.
- Graham, T., *On the absorption and dialytic separation of gases by colloid septa: Part I - Action of a septum of caoutchouc*. The London, Edinburgh, and Dublin Philosophical Magazine and Journal of Science, 1866. **XXXII**: p. 401-20.
- Greenblatt, J.; C.J. Araps; and H.R. Anderson, Jr., *Aminosilane-polyimide interactions and their implications in adhesion*, in *Polyimides: Synthesis, Characterization, and Applications [Proceedings of the Technical Conference on Polyimides]*. 1984. p. 573-88.
- Gür, T.M., *Permselectivity of zeolite filled polysulfone gas separation membranes*. J. Membr. Sci., 1994. **93**(3): p. 283-9.
- Hahn, K.; J. Kaerger; and V. Kukla, *Single-file diffusion observation*. Phys. Rev. Lett., 1996. **76**(15): p. 2762-5.

- Haq, N. and D.M. Ruthven, *Chromatographic study of sorption and diffusion in 4A zeolite*. J. Colloid Interface Sci., 1986. **112**(1): p. 154-63.
- Harding, P.H. and J.C. Berg, *The adhesion promotion mechanism of organofunctional silanes*. J. Appl. Polym. Sci., 1998. **67**(6): p. 1025-1033.
- Harding, P.H. and J.C. Berg, *The characterization of interfacial strength using single-particle composites*. J. Adhesion Sci. Tech., 1997. **11**(8): p. 1063-1076.
- Harding, P.H.; S.A. Page; J.A.E. Maanson; and J.C. Berg, *Measurement of residual stress effects by means of single-particle composite tests*. J. Adhesion Sci. Technol., 1998. **12**(5): p. 497-506.
- Harper, R.J.; G.R. Stifel; and R.B. Anderson, *Adsorption of gases on 4A synthetic zeolite*. Can. J. Chem., 1969. **47**(24): p. 4661-9.
- Henis, J.M.S. and M.K. Tripodi, *Composite hollow fiber membranes for gas separation: the resistance model approach*. J. Membr. Sci., 1981. **8**(3): p. 233-46.
- Higuchi, W.I., *A new relation for the dielectric properties of two-phase mixtures*. J. Phys. Chem., 1958. **62**: p. 649-53.
- Higuchi, W.I. and T. Higuchi, *Theoretical analysis of diffusional movement through heterogeneous barriers*. J. Am. Pharm. Assoc., Sci. Ed., 1960. **49**: p. 598-606.
- Hirschfelder, J.O.; C.F. Curtiss; and R.B. Bird, *Molecular Theory of Gases and Liquids*. 1954, New York: John Wiley & Sons, Inc.
- Iler, R.K., *The Chemistry of Silica: Solubility, Polymerization, Colloid and Surface Properties and Biochemistry*. 1979, New York: John Wiley & Sons. 892 pp.
- Inoue, T. and K. Osaki, *Role of Polymer Chain Flexibility on the Viscoelasticity of Amorphous Polymers around the Glass Transition Zone*. Macromolecules, 1996. **29**(5): p. 1595-9.
- Ismail, A.F. and L.I.B. David, *A review on the latest development of carbon membranes for gas separation*. J. Membr. Sci., 2001. **193**(1): p. 1-18.
- Ismail, A.F. and W. Lorna, *Penetrant-induced plasticization phenomenon in glassy polymers for gas separation membrane*. Sepn. Purification Tech., 2002. **27**(3): p. 173-194.
- Israelachvili, J.N., *Intermolecular and surface forces*. 2 ed. 1992, San Diego, CA: Academic Press Inc. 450.

- Jacques, C.H.M. and H.B. Hopfenberg, *Vapor and liquid equilibriums in glassy polyblends of polystyrene and poly(2,6-dimethyl-1,4-phenylene oxide)*. Polym. Eng. Sci., 1974. **14**(6): p. 441-8.
- Jaroniec, C.P.; R.K. Gilpin; and M. Jaroniec, *Adsorption and Thermogravimetric Studies of Silica-Based Amide Bonded Phases*. J. Phys. Chem. B, 1997. **101**(35): p. 6861-6866.
- Jia, M.; K.V. Peinemann; and R.D. Behling, *Molecular sieving effect of the zeolite-filled silicone rubber membranes in gas permeation*. J. Membr. Sci., 1991. **57**(2-3): p. 289-96.
- Joly, C.; S. Goizet; J.C. Schrotter; J. Sanchez; and M. Escoubes, *Sol-gel polyimide-silica composite membrane: gas transport properties*. J. of Membr. Sci., 1997. **130**(1-2): p. 63-74.
- Jones, C.W. and W.J. Koros, *Carbon Composite Membranes: A Solution to Adverse Humidity Effects*. Ind. Eng. Chem. Res., 1995. **34**(1): p. 164-7.
- Jordan, S.S. and W.J. Koros, *A Free Volume Distribution Model of Gas Sorption and Dilution in Glassy Polymers*. Macromolecules, 1995. **28**(7): p. 2228-35.
- Kamaruddin, H.D. and W.J. Koros, *Some observations about the application of Fick's first law for membrane separation of multicomponent mixtures*. J. Membr. Sci., 1997. **135**(2): p. 147-159.
- Kanan, S.M.; W.T.Y. Tze; and C.P. Tripp, *Method to Double the Surface Concentration and Control the Orientation of Adsorbed (3-Aminopropyl)dimethylethoxysilane on Silica Powders and Glass Slides*. Langmuir, 2002. **18**(17): p. 6623-6627.
- Kang, S.; S.I. Hong; C.R. Choe; M. Park; S. Rim; and J. Kim, *Preparation and characterization of epoxy composites filled with functionalized nanosilica particles obtained via sol-gel process*. Polymer, 2000. **42**(3): p. 879-887.
- Karger, J. and D. Ruthven, *Diffusion in Zeolites*. 1992, New York: John Wiley and Sons.
- Kayser, H., Wied. Annalen der Physik, 1891. **43**: p. 544.
- Kazarian, S.G.; M.F. Vincent; F.V. Bright; C.L. Liotta; and C.A. Eckert, *Specific Intermolecular Interaction of Carbon Dioxide with Polymers*. J. Am. Chem. Soc., 1996. **118**(7): p. 1729-36.

- Kesting, R. and A. Fritzsche, *Polymeric Gas Separation Membranes*. 1993, New York: John Wiley & Sons.
- Knudsen, M., *The Law of the Molecular Flow and Viscosity of Gases Moving through Tubes*. Annalen der Physik (Weinheim, Germany), 1909. **28**: p. 75-130.
- Ko, F.K. and P. Fang, *Inorganic Fibers*, in *Concise Encyclopedia of Polymer Science and Engineering*, J.I. Kroschwitz, Editor. 1990, John Wiley & Sons: New York. p. 472-7.
- Koros, W. and D. Paul, *Sorption and transport of CO₂ above and below the glass transition of poly(ethylene terephthalate)*. Polym. Engr. Sci., 1980. **20**(1): p. 14-9.
- Koros, W.J.; R.T. Chern; V. Stannett; and H.B. Hopfenberg, *Model For Permeation of Mixed Gases and Vapors in Glassy Polymers*. J. Polym. Sci., Polym. Phys. Ed., 1981. **19**(10): p. 1513-1530.
- Koros, W.J.; M.R. Coleman; and D.R.B. Walker, *Controlled permeability polymer membranes*. Annu. Rev. Mater. Sci., 1992. **22**: p. 47-89.
- Koros, W.J. and G.K. Fleming, *Membrane-based gas separation*. J. Membr. Sci., 1993. **83**(1): p. 1-80.
- Koros, W.J.; G.K. Fleming; S.M. Jordan; T.H. Kim; and H.H. Hoehn, *Polymeric membrane materials for solution-diffusion based permeation separations*. Prog. Polym. Sci., 1988. **13**(4): p. 339-401.
- Koros, W.J. and D.R. Paul, *Carbon dioxide sorption in poly(ethylene terephthalate) above and below the glass transition*. J. Polym. Sci., Polym. Phys. Ed., 1978. **16**(11): p. 1947-63.
- Koros, W.J. and D.R. Paul, *Design considerations for measurement of gas sorption in polymers by pressure decay*. J. Polym. Sci., Polym. Phys. Ed., 1976. **14**(10): p. 1903-7.
- Kraus, G. and J.T. Gruver, *Thermal expansion, free volume, and molecular mobility in a carbon black-filled elastomer*. J. Polym. Sci., Part A-2, 1970. **8**: p. 571-81.
- Krishna, R., *Diffusion of binary mixtures across zeolite membranes: Entropy effects on permeation selectivity*. Intl. Comm. in Heat and Mass Transfer, 2001. **28**(3): p. 337-346.

- Krishna, R. and D. Paschek, *Separation of hydrocarbon mixtures using zeolite membranes: a modelling approach combining molecular simulations with the Maxwell-Stefan theory*. Sepn. Purification Tech., 2000. **21**(1-2): p. 111-136.
- Kuhn, W., *The shape and properties of threadlike molecules in solution (and in the elastic solid state)*. Angew. Chem., 1936. **49**: p. 858-62.
- Kulprathipanja, S.; R.W. Neuzil; and N.N. Li, *Separation of fluids by means of mixed matrix membranes*, US Patent No. 697,990. 1988.
- Kwei, T.K. and C.A. Kumins, *Polymer-filler interaction: vapor sorption studies*. J. Appl. Polymer Sci., 1964. **8**(3): p. 1483-90.
- Landauer, R., *The electrical resistance of binary metallic mixtures*. J. Appl. Phys., 1952. **23**: p. 779-84.
- Lee, A.L.; H.L. Feldkirchner; S.A. Stern; A.Y. Houde; J.P. Gamez; and H.S. Meyer, *Field tests of membrane modules for the separation of carbon dioxide from low-quality natural gas*. Gas Sepn. Purification, 1995. **9**(1): p. 35-43.
- Lee, E.K. and W.J. Koros, *Membranes, Synthetic, Applications*, in *Encyclopedia of Polymer Science and Technology*. 2002, Academic Press: New York. p. 279-344.
- Lee, S.H. and Y.C. Bae, *Thermal stress analysis for polyimide thin film: the effect of solvent evaporation*. Macromolecular Theory and Simulations, 2000. **9**(5): p. 281-286.
- Linde, H.G., *Adhesive interface interactions between primary aliphatic amine surface conditioners and polyamic acid/polyimide resins*. J. Polym. Sci., Polym. Chem. Ed., 1982. **20**(4): p. 1031-41.
- Lindemann, M.K., *Physical constants of poly(vinyl acetate)*, in *Polymer Handbook*, J. Brandrup and E.H. Immergut, Editors. 1989, John Wiley & Sons: New York. p. V/71-5.
- Long, F.A. and L.J. Thompson, *Diffusion of water vapor in polymers*. J. Polymer Sci., 1955. **15**: p. 413-26.
- Maeda, Y. and D.R. Paul, *Effect of antiplasticization on selectivity and productivity of gas separation membranes*. J. Membr. Sci., 1987. **30**(1): p. 1-9.

- Mahajan, R., *Formation, characterization and modeling of mixed matrix membrane materials*. Department of Chemical Engineering, University of Texas at Austin. 2000.
- Mahajan, R., *Personal Communication*. 2004.
- Mahajan, R.; R. Burns; M. Schaeffer; and W.J. Koros, *Challenges in forming successful mixed matrix membranes with rigid polymeric materials*. J. Appl. Polym. Sci., 2002. **86**(4): p. 881-890.
- Mahajan, R. and W.J. Koros, *Factors Controlling Successful Formation of Mixed-Matrix Gas Separation Materials*. Ind. Eng. Chem. Res., 2000. **39**(8): p. 2692-2696.
- Mahajan, R. and W.J. Koros, *Mixed matrix membrane materials with glassy polymers. Part 1*. Polym. Engr. and Sci., 2002. **42**(7): p. 1420-1431.
- Mahajan, R. and W.J. Koros, *Mixed matrix membrane materials with glassy polymers. Part 2*. Polym. Engr. and Sci., 2002. **42**(7): p. 1432-1441.
- Manson, J.A. and E.H. Chiu, *Permeation of liquid water in a filled epoxy resin*. J. Polym. Sci., Polym. Symp., 1973. **No. 41**: p. 95-108.
- Manson, J.A. and L.H. Sperling, *Polymer Blends and Composites*. 1976, New York: Plenum Press.
- Marand, E.; C.J. Cornelius; P. Meakin; and A.J. Hill, *Hybrid organic-inorganic membranes*. Polym. Matl. Sci. and Engr., 2001. **85**: p. 297-298.
- Marmo, M.J.; M.A. Mostafa; H. Jinnai; F.M. Fowkes; and J.A. Manson, *Acid-base interaction in filler-matrix systems*. Ind. Eng. Chem., Prod. Res. Dev., 1976. **15**(3): p. 206-11.
- Maxwell, J.C., *A treatise on electricity and magnetism*. Vol. 1. 1873, Oxford: Clarendon press.
- McBain, J.W., *The Sorption of Gases and Vapours by Solids*. Twentieth-Century Chemistry, ed. J.C. Philip. 1932, London: George Routledge & Sons, Ltd.
- McHattie, J.S.; W.J. Koros; and D.R. Paul, *Gas transport properties of polysulfones. 1. Role of symmetry of methyl group placement on bisphenol*. Polymer, 1991. **32**(5): p. 840-50.

- McQuarrie, D., *Statistical Thermodynamics*. 1973, New York: Harper & Row Publishers, Inc.
- Merkel, T.C.; B.D. Freeman; R.J. Spontak; Z. He; I. Pinnau; P. Meakin; and A.J. Hill, *Ultrapermearable, reverse-selective nanocomposite membranes*. *Science*, 2002. **296**(5567): p. 519-522.
- Michaels, A.S. and H.J. Bixler, *Flow of gases through polyethylene [and rubbery polymers]*. *J. Polym. Sci.*, 1961. **50**: p. 413-39.
- Michaels, A.S. and H.J. Bixler, *Solubility of gases in polyethylene [and rubbery polymers]*. *J. Polym. Sci.*, 1961. **50**: p. 393-412.
- Michaels, A.S. and R.B. Parker, Jr., *Sorption and flow of gases in polyethylene*. *J. Polym. Sci.*, 1959. **41**: p. 53-71.
- Michaels, A.S.; W.R. Vieth; and J.A. Barrie, *Diffusion of gases in poly(ethylene terephthalate)*. *J. Appl. Phys.*, 1963. **34**: p. 13-20.
- Miller, A.C. and J.C. Berg, *The prediction of adhesion between polymer matrices and silane-treated glass surfaces in filled composites*. *J. Adhesion Sci. Tech.*, 2002. **16**(5): p. 495-507.
- Miller, S., *Personal Communication*. 2004.
- Mitchell, J.K., *On the penetrativeness of fluids (Part I)*. *J. Royal Institution of Great Britain*, 1831. **IV**: p. 101-118.
- Mitchell, J.K., *On the penetrativeness of fluids (Part II)*. *J. Royal Institution of Great Britain*, 1831. **V**: p. 307-321.
- Monk, D.J.; Y. He; and D.S. Soane, *Stresses in polyimide films during cure and thermal cycling*, in *Manufacturing Processes and Materials Challenges in Microelectronic Packaging*. 1991, ASME: New York. p. 87-93.
- Moore, T.T.; S. Damle; J. Williams; and W.J. Koros, *Characterization of Low Permeability Gas Separation Membranes and Barrier Materials: Design and Operation Considerations*. *J. Membr. Sci.*, 2004. **Accepted**.
- Moore, T.T.; R. Mahajan; D.Q. Vu; and W.J. Koros, *Hybrid Membrane Materials Comprising Organic Polymers with Rigid Dispersed Phases*. *AIChE J.*, 2004. **50**(2): p. 311-21.
- Moreau, S., *Personal Communication*. 2002.

- Nielsen, L.E., *Models for the permeability of filled polymer systems*. J. Macromol. Sci., Part A, 1967. **1**(5): p. 929-42.
- Nielsen, L.E. and T.B. Lewis, *Temperature dependence of relative modulus in filled polymer systems*. J. Polym. Sci., Part A-2, 1969. **7**(10): p. 1705-19.
- Nunes, S.P.; J. Schultz; and K.V. Peinemann, *Silicone membranes with silica nanoparticles*. J. Matl. Sci. Lett., 1996. **15**(13): p. 1139-1141.
- O'Brien, K.C.; W.J. Koros; T.A. Barbari; and E.S. Sanders, *A new technique for the measurement of multicomponent gas transport through polymeric films*. J. Membr. Sci., 1986. **29**(3): p. 229-38.
- Ohya, H.; V.V. Kudryavtsev; and S.I. Semenova, *Polyimide Membranes: Applications, Fabrications, and Properties*. 1996, Tokyo, Japan: Gordon and Breach Publishers. 324 pp.
- Okamoto, K.; K. Noborio; J. Hao; K. Tanaka; and H. Kita, *Permeation and separation properties of polyimide membranes to 1,3-butadiene and n-butane*. J. Membr. Sci., 1997. **134**(2): p. 171-179.
- Park, J.Y. and D.R. Paul, *Correlation and prediction of gas permeability in glassy polymer membrane materials via modified free volume based group contribution method*. Journal of Membrane Science, 1997. **125**(1): p. 23-39.
- Patel, K.S.; P.A. Kohl; and S.A.B. Allen, *Dual capacitor technique for measurement of through-plane modulus of thin polymer films*. J. Polym. Sci., Part B: Polym. Phys., 2000. **38**(12): p. 1634-1644.
- Paul, D.R. and D.R. Kemp, *Diffusion time lag in polymer membranes containing adsorptive fillers*. J. Polym. Sci., Polym. Symp., 1973. **No. 41**: p. 79-93.
- Paul, D.R. and W.J. Koros, *Effect of partially immobilizing sorption on permeability and the diffusion time lag*. J. Polym. Sci., Polym. Phys. Ed., 1976. **14**(4): p. 675-85.
- Paulson, G.T.; A.B. Clinch; and F.P. McCandless, *The effects of water vapor on the separation of methane and carbon dioxide by gas permeation through polymeric membranes*. J. Membr. Sci., 1983. **14**(2): p. 129-37.
- Pavlov, A.V.; O.M. Karanyan; A.G. Morozov; G.S. Matvelashvili; G.V. Kazakova; and N.A. Anissimova, *Molecular properties of poly(ether imide) in solution*, in *Polyimides and Other High Temperature Polymers; Proceedings of the 2nd. European Technical Symposium*. 1991. p. 173-7.

- Perera, D.Y., *Internal stress and film formation in emulsion paints*. J. Oil Colour Chem. Assn., 1985. **68**(11): p. 275-81.
- Perera, D.Y., *On adhesion and stress in organic coatings*. Prog. Organic Coatings, 1996. **28**(1): p. 21-23.
- Perera, D.Y. and D. Vanden Eynde, *Effect of pigmentation on internal stress in latex coatings*. J. Coatings Tech., 1984. **56**(717): p. 47-53.
- Perera, D.Y. and D. Vanden Eynde, *Internal stress in pigmented thermoplastic coatings*. J. Coatings Tech., 1981. **53**(678): p. 40-5.
- Peterson, D., *Influence of presorbed water on the sorption of nitrogen by zeolites at ambient temperatures*. Zeolites, 1981. **1**(2): p. 105-12.
- Petropoulos, J.H., *A comparative study of approaches applied to the permeability of binary composite polymeric materials*. J. Polym. Sci., Polym. Phys. Ed., 1985. **23**(7): p. 1309-24.
- Petropoulos, J.H., *Plasticization effects on the gas permeability and permselectivity of polymer membranes*. J. Membr. Sci., 1992. **75**(1-2): p. 47-59.
- Peysers, P., *Glass transition temperatures of polymers*, in *Polymer Handbook*, J. Brandrup and E. Immergut, Editors. 1989, John Wiley & Sons: New York. p. VI209-VI212.
- Piirma, I., *Polymeric Surfactants*. Surfactant Science Series. Vol. 42. 1992, New York, NY: Marcel Dekker, Inc. 289 pp.
- Plueddemann, E.P., *Silane Coupling Agents*. 1982, New York: Plenum Press. 235 pp.
- Porod, G., *The mean separation of chain-ends in threadlike molecules*. Monatshefte fuer Chemie, 1949. **80**: p. 251-5.
- Pye, D.G.; H.H. Hoehn; and M. Panar, *Measurement of gas permeability of polymers. I. Permeabilities in constant volume/variable pressure apparatus*. J. Appl. Polym. Sci., 1976. **20**(7): p. 1921-31.
- Pye, D.G.; H.H. Hoehn; and M. Panar, *Measurement of gas permeability of polymers. II. Apparatus for determination of permeabilities of mixed gases and vapors*. J. Appl. Polym. Sci., 1976. **20**(2): p. 287-301.

- Qin, J., *Explorations of forming and characterizing mixed matrix gas separation membranes*. Department of Chemical Engineering, University of Texas at Austin. 1999.
- Ramesh, S.; Y. Koltypin; and A. Gedanken, *Ultrasound driven aggregation and surface silanol modification in amorphous silica microspheres*. J. Matl. Res., 1997. **12**(12): p. 3271-3277.
- Rao, M.B. and S. Sircar, *Nanoporous carbon membranes for separation of gas mixtures by selective surface flow*. J. Membr. Sci., 1993. **85**(3): p. 253-64.
- Ren, J.; C. Staudt-Bickel; and R.N. Lichtenthaler, *Separation of aromatics/aliphatics with crosslinked 6FDA-based copolyimides*. Sepn. Purification Tech., 2001. **22** and **23**(1-3): p. 31-43.
- Rezac, M.E. and B. Schoberl, *Transport and thermal properties of poly(ether imide)/acetylene-terminated monomer blends*. J. Membr. Sci., 1999. **156**(2): p. 211-222.
- Rice, G.L. and S.L. Scott, *Characterization of Silica-Supported Vanadium(V) Complexes Derived from Molecular Precursors and Their Ligand Exchange Reactions*. Langmuir, 1997. **13**(6): p. 1545-1551.
- Rice, G.L. and S.L. Scott, *Site-specific oxygen-18 labeling of silica-supported vanadium(V) complexes: Implications for oxidation catalysis*. J. Molecular Catalysis A: Chem., 1997. **125**(1): p. 73-79.
- Robeson, L.M., *Correlation of separation factor versus permeability for polymeric membranes*. J. Membr. Sci., 1991. **62**(2): p. 165-85.
- Ruthven, D.M. and R.I. Derrah, *Diffusion of monoatomic and diatomic gases in 4A and 5A zeolites*. J. Chem. Soc., Faraday Trans. 1, 1975. **71**(10): p. 2031-44.
- Schmitz, L. and M. Ballauff, *Characterization of a stiff-chain polyimide in solution*. Polymer, 1995. **36**(4): p. 879-82.
- Schoenmakers, P.J.; H.A.H. Billiet; and L. De Galan, *The solubility parameter as a tool in understanding liquid chromatography*. Chromatographia, 1982. **15**(3): p. 205-14.
- Sforca, M.L.; I.V.P. Yoshida; C.P. Borges; and S.P. Nunes, *Hybrid membranes based on SiO₂/polyether-b-polyamide: morphology and applications*. J. Appl. Polym. Sci., 2001. **82**(1): p. 178-185.

- Shang, X.-y.; Z.-k. Zhu; J. Yin; and X.-d. Ma, *Compatibility of Soluble Polyimide/Silica Hybrids Induced by a Coupling Agent*. Chem. Matr., 2002. **14**(1): p. 71-77.
- Shelekhin, A.B.; A.G. Dixon; and Y.H. Ma, *Theory of gas diffusion and permeation in inorganic molecular-sieve membranes*. AIChE J., 1995. **41**(1): p. 58-67.
- Sholl, D.S. and K.A. Fichthorn, *Normal, single-file, and dual-mode diffusion of binary adsorbate mixtures in AlPO₄-5*. J. Chem. Phys., 1997. **107**(11): p. 4384-4389.
- Simha, R. and R.F. Bayer, *General relation involving the glass temperature and coefficients of expansion of polymers*. J. Chem. Phys., 1962. **37**: p. 1003-7.
- Singh, A., *Membrane materials with enhanced selectivity: an entropic interpretation*. Department of Chemical Engineering, University of Texas at Austin. 1997.
- Singh, A. and W.J. Koros, *Significance of Entropic Selectivity for Advanced Gas Separation Membranes*. Ind. Eng. Chem. Res., 1996. **35**(4): p. 1231-4.
- Sircar, S.; M.B. Rao; and C.M.A. Thaeron, *Selective surface flow membrane for gas separation*. Sepn. Sci. and Tech., 1999. **34**(10): p. 2081-2093.
- Smith, L.J.; A. Davidson; and A.K. Cheetham, *A neutron diffraction and infrared spectroscopy study of the acid form of the aluminosilicate zeolite, chabazite (H-SSZ-13)*. Catal. Lett., 1998. **49**(3,4): p. 143-146.
- Staudt-Bickel, C. and W.J. Koros, *Improvement of CO₂/CH₄ separation characteristics of polyimides by chemical crosslinking*. J. Membr. Sci., 1999. **155**(1): p. 145-154.
- Süer, M.G.; N. Ba; and L. Yilmaz, *Gas permeation characteristics of polymer-zeolite mixed matrix membranes*. J. Membr. Sci., 1994. **91**(1-2): p. 77-86.
- Suh, S.H. and J.M.D. MacElroy, *Molecular dynamics simulation of hindered diffusion in microcapillaries*. Mol. Phys., 1986. **58**(3): p. 445-73.
- Suryanarayana, D. and K.L. Mittal, *Effect of pH of silane solution on the adhesion of polyimide to a silica substrate*. Journal of Applied Polymer Science, 1984. **29**(6): p. 2039-43.
- Sysel, P.; M. Frycova; R. Hobzova; V. Krystl; P. Harabaneck; B. Bernauer; L. LBrabec; and M. Kocirik. *Impact of Zeolites and Other Porous Materials on the New Technologies at the Beginning of the New Millennium, Part B*. In: Stud. Surf. Sci. Catal., 2002; 142B. in 2nd International FEZA (Federation of the European Zeolite Association) Conference. 2002. Taormina, Italy: Elsevier.

- Tabe-Mohammadi, A., *A review of the applications of membrane separation technology in natural gas treatment*. Sep. Sci. Tech., 1999. **34**(10): p. 2095-2111.
- Te Hennepe, H.J.C.; C.A. Smolders; D. Bargeman; and M.H.V. Mulder, *Exclusion and tortuosity effects for alcohol/water separation by zeolite-filled PDMS membranes*. Sep. Sci. Tech., 1991. **26**(4): p. 585-96.
- van Amerongen, G.J., *Permeability of different rubbers to gases and its relation to diffusivity and solubility*. J. Appl. Phys., 1946. **17**: p. 972-85.
- van Krevelen, D., *Properties of polymers; their correlation with chemical structure, their numerical estimation and prediction from additive group contributions*. 3 ed. 1990, New York: Elsevier.
- van Oss, C., *Irrelevance of the ratio of the electron-acceptivity to the electron-donicity of water with respect to the determination of polar surface tension components, interfacial tensions and free energies of interaction of liquid and/or solids*, in *Acid-base interactions*, K. Mittal, Editor. 2000, VSP: Utrecht, Netherlands. p. 181-196.
- Van Oss, C.J.; M.K. Chaudhury; and R.J. Good, *Interfacial Lifshitz-van der Waals and polar interactions in macroscopic systems*. Chem. Rev., 1988. **88**(6): p. 927-41.
- Vankelecom, I.F.J.; S. De Beukelaer; and J.B. Uytterhoeven, *Sorption and Pervaporation of Aromatic Compounds Using Zeolite-Filled PDMS Membranes*. J. Phys. Chem. B, 1997. **101**(26): p. 5186-5190.
- Vankelecom, I.F.J.; J. De Kinderen; B.M. Dewitte; and J.B. Uytterhoeven, *Incorporation of Hydrophobic Porous Fillers in PDMS Membranes for Use in Pervaporation*. J. Phys. Chem. B, 1997. **101**(26): p. 5182-5185.
- Vankelecom, I.F.J.; E. Merckx; M. Luts; and J.B. Uytterhoeven, *Incorporation of Zeolites in Polyimide Membranes*. J. Phys. Chem., 1995. **99**(35): p. 13187-92.
- Vankelecom, I.F.J.; E. Scheppers; R. Heus; and J.B. Uytterhoeven, *Parameters Influencing Zeolite Incorporation in PDMS Membranes*. J. Phys. Chem., 1994. **98**(47): p. 12390-6.
- Vankelecom, I.F.J.; S. Van den Broeck; E. Merckx; H. Geerts; P. Grobet; and J.B. Uytterhoeven, *Silylation To Improve Incorporation of Zeolites in Polyimide Films*. J. Phys. Chem., 1996. **100**(9): p. 3753-8.
- Volpe, C.D. and S. Siboni, *Troubleshooting of surface free energy acid-base theory applied to solid surfaces: The case of Good, van Oss and Chaudhury theory*, in

- Acid-Base Interactions*, K. Mittal, Editor. 2000, VSP: Utrecht, Netherlands. p. 55-90.
- von Wroblewski, S., *Wied. Annalen der Physik*, 1879. **8**: p. 29.
- Vrancken, K.C.; P. Van Der Voort; K. Possemiers; and E.F. Vansant, *Surface and structural properties of silica gel in the modification with gamma-aminopropyltriethoxysilane*. *J. Colloid Interface Sci.*, 1995. **174**(1): p. 86-91.
- Vrentas, J.S. and C.M. Vrentas, *Sorption in glassy polymers*. *Macromolecules*, 1991. **24**(9): p. 2404-12.
- Vu, D.Q., *Formation and characterization of asymmetric carbon molecular sieve and mixed matrix membranes for natural gas purification*. Department of Chemical Engineering, University of Texas at Austin. 2001.
- Vu, D.Q.; W.J. Koros; and S.J. Miller, *High pressure CO₂/CH₄ separation by using carbon molecular sieve hollow fiber membranes*. *Ind. Engr. Chem. Res.*, 2002. **41**(3): p. 367-380.
- Vu, D.Q.; W.J. Koros; and S.J. Miller, *Mixed matrix membranes using carbon molecular sieves. I. Preparation and experimental results*. *J. Membr. Sci.*, 2003. **211**(2): p. 311-334.
- Vu, D.Q.; W.J. Koros; and S.J. Miller, *Mixed matrix membranes using carbon molecular sieves. II. Modeling permeation behavior*. *J. Membr. Sci.*, 2003. **211**(2): p. 335-348.
- Wang, H.; B.A. Holmberg; and Y. Yan, *Homogeneous polymer-zeolite nanocomposite membranes by incorporating dispersible template-removed zeolite nanocrystals*. *J. Matl. Chem.*, 2002. **12**(12): p. 3640-3643.
- Wessling, M.; S. Schoeman; T. Van der Boomgaard; and C.A. Smolders, *Plasticization of gas separation membranes*. *Gas Sep. Purif.*, 1991. **5**(4): p. 222-8.
- White, L.D. and C.P. Tripp, *A low-frequency infrared study of the reaction of methoxymethylsilanes with silica*. *J. Colloid Interface Sci.*, 2000. **224**(2): p. 417-424.
- White, L.D. and C.P. Tripp, *Reaction of (3-Aminopropyl)dimethylethoxysilane with Amine Catalysts on Silica Surfaces*. *J. Colloid Interface Sci.*, 2000. **232**(2): p. 400-407.

- Wijmans, J.G. and R.W. Baker, *The solution-diffusion model: a review*. J. Membr. Sci., 1995. **107**(1-2): p. 1-21.
- Wind, J.D.; C. Staudt-Bickel; D.R. Paul; and W.J. Koros, *The effects of crosslinking chemistry on CO₂ plasticization of polyimide gas separation membranes*. Ind. Eng. Chem. Res., 2002. **41**(24): p. 6139-48.
- Xenopoulos, C.; L. Mascia; and S.J. Shaw, *Polyimide-silica hybrids derived from an iso-imide oligomer precursor*. J. of Matl. Chem., 2002. **12**(2): p. 213-218.
- Yampolskii, Y.; D. Wiley; and C. Maher, *Novel correlation for solubility of gases in polymers: effect of molecular surface area of gases*. J. Appl. Polym. Sci., 2000. **76**(4): p. 552-560.
- Yong, H.H.; H.C. Park; Y.S. Kang; J. Won; and W.N. Kim, *Zeolite-filled polyimide membrane containing 2,4,6-triaminopyrimidine*. J. Membr. Sci., 2001. **188**(2): p. 151-163.
- Yucel, H. and D.M. Ruthven, *Diffusion in 4A zeolite. Study of the effect of crystal size*. J. Chem. Soc., Faraday Trans. 1, 1980. **76**(1): p. 60-70.
- Yucel, H. and D.M. Ruthven, *Diffusion of carbon dioxide in 4A and 5A zeolite crystals*. J. Colloid Interface Sci., 1980. **74**(1): p. 186-95.
- Zhang, J.; H. Chen; Y. Li; R. Suzuki; T. Ohdaira; and Y.C. Jean, *Variation of glass transition temperature in a thin polystyrene film studied by positron annihilation spectroscopy*. Polym. Preprints, 2004. **45**(1): p. 9-10.
- Zimmerman, C.M., *Advanced gas separation membrane materials: hyper rigid polymers and molecular sieve-polymer mixed matrixes*. Department of Chemical Engineering, University of Texas at Austin. 1998.
- Zimmerman, C.M.; R. Mahajan; and W.J. Koros, *Fundamental and practical aspects of mixed matrix gas separation membranes*. Polym. Mater. Sci. Engr., 1997. **77**: p. 328-329.
- Zimmerman, C.M.; A. Singh; and W.J. Koros, *Tailoring mixed matrix composite membranes for gas separations*. J. Membr. Sci., 1997. **137**(1-2): p. 145-154.
- Zoller, P. and P. French, *The thermal analysis of polymers at high pressures*. J. Thermal Anal., 1996. **47**(4): p. 993-1012.

Vita

Theodore Thomas Moore was born in Madison, Wisconsin on May 9, 1978, the son of Timothy John Moore and Susan Irene Moore. After completing his studies at Manhattan High School, Manhattan, Kansas, in 1995, he entered Kansas State University in Manhattan. In 1996, he transferred to Iowa State University of Science and Technology, from where he received a Bachelor of Science degree in Chemical Engineering in May 1999. In August 1999, he enrolled in the graduate school at the University of Texas at Austin. In October 2001, he physically relocated to the Georgia Institute of Technology in Atlanta, GA with his advisor, William J. Koros, to complete his research, while remaining academically at the University of Texas at Austin. In December 2004, he fulfilled the requirements for the Doctor of Philosophy degree in Chemical Engineering. Thereafter, he began working at Solvay Advanced Polymers, LLC in Alpharetta, GA

Permanent address: 120 Cinnabar Trail
San Antonio, TX 78109

This dissertation was typed by the author.